AWARD NUMBER: W81XWH-20-1-0132

TITLE: Anti-Inflammatory Viral Proteins to Treat Sepsis

PRINCIPAL INVESTIGATOR: Amelia K. Pinto Ph.D.

CONTRACTING ORGANIZATION: Saint Louis University
1 North Grand
Saint Louis, Missouri
63103-2006

REPORT DATE: October 2022

TYPE OF REPORT: Final Report

PREPARED FOR: U.S. Army Medical Research and Development Command
Fort Detrick, Maryland 21702-5012

REPORT DOCUMENTATION PAGE

Form Approved
OMB No. 0704-0188

1. REPORT DATE	2. REPORT TYPE	3. DATES COVERED *(From - To)*
OCTOBER 2022	Final Technical Report	01 July 2020 - 30 June 2022

4. TITLE AND SUBTITLE

Anti-Inflammatory Proteins to treat Viral Sepsis

5a. CONTRACT NUMBER
W81XWH-20-1-0132

5b. GRANT NUMBER
PR192269

5c. PROGRAM ELEMENT NUMBER

6. AUTHOR(S)

Amelia Pinto PhD

E-Mail:amelia.pinto@health.slu.edu

5d. PROJECT NUMBER

5e. TASK NUMBER

5f. WORK UNIT NUMBER

7. PERFORMING ORGANIZATION NAME(S) AND ADDRESS(ES)

Saint Louis University
1 North Grand
Saint Louis, Missouri
63103-2006

8. PERFORMING ORGANIZATION REPORT NUMBER

9. SPONSORING / MONITORING AGENCY NAME(S) AND ADDRESS(ES)

U.S. Army Medical Research and Development Command
Fort Detrick, Maryland 21702-5012

10. SPONSOR/MONITOR'S ACRONYM(S)

11. SPONSOR/MONITOR'S REPORT NUMBER(S)

12. DISTRIBUTION / AVAILABILITY STATEMENT

Approved for Public Release; Distribution Unlimited.

13. SUPPLEMENTARY NOTES

14. ABSTRACT

Viral sepsis is a preventable cause of morbidity and mortality for the United States military. Sepsis is caused by a dysregulation of the host response to a pathogen. One third of those who develop sepsis die. One factor often overlooked in our response to sepsis is that the diseases they have striking similarities. Our proposal focuses on the similarities in the inflammation associated with sepsis to rapidly target the symptoms by using anti-inflammatory viral proteins encoded by poxviruses to controlling sepsis induced inflammation. To date we have shown that the administration of the poxvirus protein chemokine response modifier D (CrmD) during severe dengue in our mouse model prolongs survival. This result is significant as it suggests that administration of CrmD can increase the time to diagnosis and treat disease which can save lives. We have also shown that the vaccinia virus complement control protein (VCP) can reduce compliment activation caused by severe dengue in our model. This results is significant as it demonstrates that the administration of VCP can block complement activation which is though to be a major contributor of inflammation.

15. SUBJECT TERMS

NONE LISTED

16. SECURITY CLASSIFICATION OF:			17. LIMITATION OF ABSTRACT	18. NUMBER OF PAGES	19a. NAME OF RESPONSIBLE PERSON
a. REPORT	b. ABSTRACT	c. THIS PAGE			USAMRDC
Unclassified	Unclassified	Unclassified	Unclassified	157	19b. TELEPHONE NUMBER *(include area code)*

TABLE OF CONTENTS

	Page
1. Introduction	4
2. Keywords	4
3. Accomplishments	4-10
4. Impact	10-11
5. Changes/Problems	11-12
6. Products	12-15
7. Participants & Other Collaborating Organizations	15-16
8. Special Reporting Requirements	17
9. Appendices	17-157

1. **INTRODUCTION:** *Narrative that briefly (one paragraph) describes the subject, purpose and scope of the research.*

   The high mortality associated with sepsis is caused by immune inflammation. Our approach is to reduce the inflammation by administering novel virally derived anti-inflammatories. Our goal is to target the inflammation to "buy the time" needed for diagnosis and administer effective treatments against the infection. The murine model will be used to mimic the clinical features of sepsis including rapid mortality following the administration of a viral infection. We will test anti-inflammatory treatments after the onset of sepsis to determine if we can prolong survival.

2. **KEYWORDS:** *Provide a brief list of keywords (limit to 20 words).*

   Viral sepsis, dengue shock, anti-inflammatory, TNF-alpha inhibition, complement blockade, poxvirus immune evasion, cytokine storm

3. **ACCOMPLISHMENTS:** *The PI is reminded that the recipient organization is required to obtain prior written approval from the awarding agency grants official whenever there are significant changes in the project or its direction.*

   What were the major goals of the project?
   List the major goals of the project as stated in the approved SOW. If the application listed milestones/target dates for important activities or phases of the project, identify these dates and show actual completion dates or the percentage of completion.

	Timeline	**Percent completion**
Major Task 1: Therapeutic treatment of DENV2	1-12	100%
Major Task 2: Determine if the administration of CrmD prolongs survival	4-8	100%
Major Task 3- Identify if the cells making the cytokine are also the infected cells	6-10	40%
Major Task 4- Determine efficacy of VCP administration with DENV2	10-18	100%
Major Task 5- Determine if the administration of VCP prolongs survival	16-22	100%

   What was accomplished under these goals?
   For this reporting period describe: 1) major activities; 2) specific objectives; 3) significant results or key outcomes, including major findings, developments, or conclusions (both positive and negative); and/or 4) other achievements. Include a discussion of stated goals not met. Description shall include pertinent data and graphs in sufficient detail to explain any significant results achieved. A succinct description of the methodology used shall be provided. As the project progresses to completion, the emphasis in reporting in this section should shift from reporting activities to reporting accomplishments.

1. MAJOR ACTIVITIES:

Use of poxvirus proteins to improve Dengue-virus induced sepsis disease outcomes.

We hypothesized that targeting TNF-α and C' activation would serve as a viable therapeutic intervention in the treatment of DENV-induced viral sepsis. More specifically, we hypothesized that the poxvirus proteins CrmD and VCP could effectively inhibit the hypercytokinemia and excess complement activation that contributes to septic shock. The proposed studies attempt to establish the potential of poxvirus immunomodulatory proteins in mitigating viral sepsis by (1) demonstrating the ability of these immunomodulatory proteins to reduce systemic inflammatory cytokine levels and impact viral titer (2) describing the impact of reducing systemic inflammation in our mouse model of DENV-induced sepsis and (3) examining the contribution of monocytes to the inflammatory cytokine milieu.

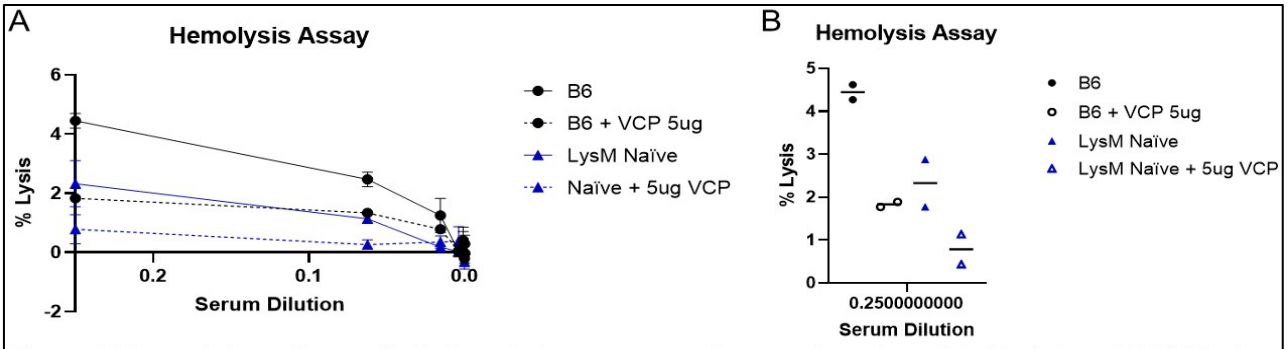

Figure 1: Figure 1 shows the result of a hemolysis assay comparing complement mediated lysis from C57BL/6 mice (n = 3) or LysM Cre^{+} IFNAR1 $^{fl/fl}$ mice (n = 3). Sera was collected by submandibular bleed and clarified by centrifugation at 12,000 x g for 15 minutes. Sera from each group was pooled into a tube and used to perform four-fold serial dilutions in PBS. To wells containing VCP, 5µg was added directly to wells containing sera and PBS. To the plate of serially diluted sera, 50µL/well of 10% packed sheep red-blood cells (SRBC) sensitized with 1µg/mL of α-SRBC antibody by incubating for 60 minutes at 30°C. The sera+sensitized SRBC was then allowed to incubate at 37°C for 30 minutes before centrifugation at 500 x g for 10 minutes. The resulting supernatant was mixed 1:1 with PBS and absorbance measured at 540nm. The results were normalized to a blank (PBS only, no lysis) control or total lysis (NH_4Cl) control to determine % lysis and the results plotted for each dilution (A) or only the highest dilution (B).

2. SPECIFIC OBJECTIVES:

Demonstrate the ability of immunomodulatory proteins to reduce systemic inflammatory cytokine levels.

a) <u>Produce and verify the function and specificity of CrmD for TNF-α</u>

In order to determine whether poxviral proteins targeting TNF-α are viable therapeutic options for DENV-induced viral sepsis, we first must be able to produce and rigorously demonstrate that CrmD is capable of inhibiting TNF-α in our model. To this end, we use an Expi293-based expression system for the production of his-tagged CrmD protein, which is purified using a nickel affinity column. In order to measure reduction in TNF-α levels, we examined TNF-α gene expression via qPCR and ELISA.

b) <u>Produce and verify the function and specificity of VCP and C' activation</u>

In order to determine whether poxviral proteins targeting C' are viable therapeutic options for DENV-induced viral-sepsis, we expressed and purify VCP in the same manner as CrmD. Using the hemolysis assays, which relies on the lysis of red blood cells sensitized with a standard quantity of antibody to determine the lytic capabilities of complement components of mouse sera we have quantified the lytic activity of both C57BL/6 mouse sera as well as LysM Cre^{+} IFNAR1 $^{fl/fl}$ sera in the presence and absence of VCP. The addition of VCP (5 µg) *in vitro* showed a slight reduction in the lysis of RBC

in hemolysis assays (**Fig 1**). However, we have not been able to show a reduction in the lytic capacity of C' by administering VCP intraperitoneally (i.p.) due to the limited sensitivity of the assay.

Describe the impact of reducing systemic inflammation in our more immunocompetent model of DENV-induced viral sepsis

a) Validate our approach using West Nile Virus (WNV) induced sepsis

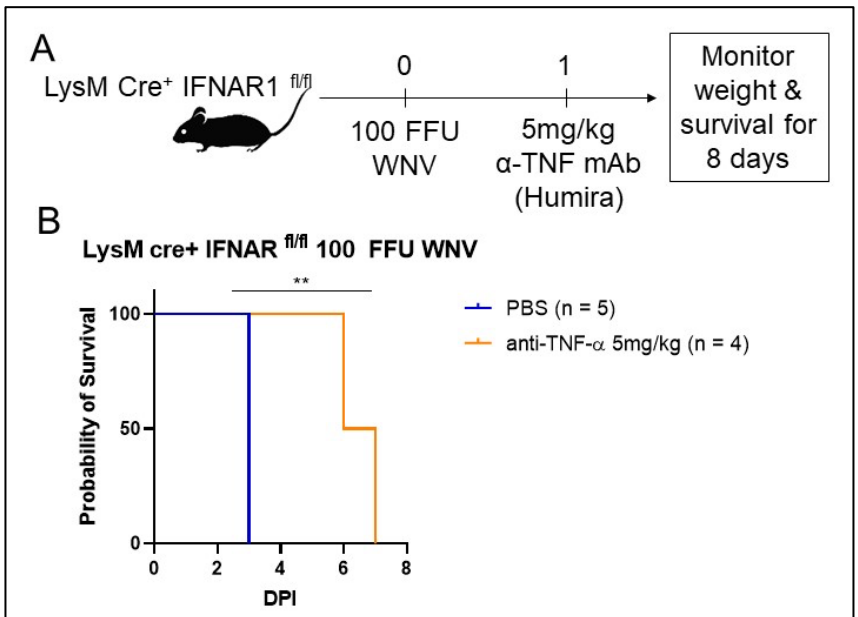

Figure 2: Figure 2 shows the experiment design (A) and survival outcome (B) as a result of challenging LysM Cre+ IFNAR1 fl/fl mice with 100 FFU WNV at time t = 0 followed by 5mg/kg of a TNF-α blocking monoclonal antibody (Humira) or PBS control at time t = 1 day post infection (DPI) via intraperitoneal (i.p.) injection.

Before determining whether reducing systemic inflammation by targeting TNF-α and C' activation improves outcomes of DENV-induced viral sepsis, we first wanted to validate that targeting TNF-α and C' activation can ameliorate severe disease observed in our mouse model. For this purpose, we utilized WNV infection in our LysM Cre^{+} $IFNAR1^{fl/fl}$ mouse model. WNV, although not known to cause sepsis, results in uniform mortality in our model, and is therefore a good system to monitor improvements in disease burden or mean time to death (MTD). To this end, we challenged LysM Cre^{+} $IFNAR1^{fl/fl}$ mice with 100 FFU of WNV. One day post challenge, we administered 5mg/kg of a TNF-α blocking monoclonal antibody (mAb, Humira) or a PBS control. (**Fig 2**) Consistent with previous studies done by our lab, blocking TNF-α extended survival time from a MTD of 3 DPI to a MTD of 7.5 MTD. This study serves as a strong proof-of-concept that TNF-α targeting can be a viable strategy for improving outcomes in our sepsis model.

b) Validate our approach using dengue virus (DENV)-induced sepsis

In order to determine whether reducing systemic inflammation by targeting TNF-α and C' activation improves outcomes of DENV-induced viral sepsis, we must first validate our mouse model of DENV-induced viral sepsis. In addition to its utility in recapitulating ablated type I IFN signaling in flavivirus infection, we have also observed that this model shares many features of DENV-induced viral sepsis, including thrombocytopenia, vascular leakage, and high hematocrit levels. To this end, we challenged 3-4 week old LysM Cre^{+} $IFNAR1^{fl/fl}$ mice with varying doses of D2S20, a mouse adapted variant of DENV2 **(Fig 3).** We found that only at two infectious doses (5×10^4 FFU, 1×10^5 FFU) tested in combination with 4G2 mAb that recapitulates prior flavivirus exposure, did we see appreciable weight

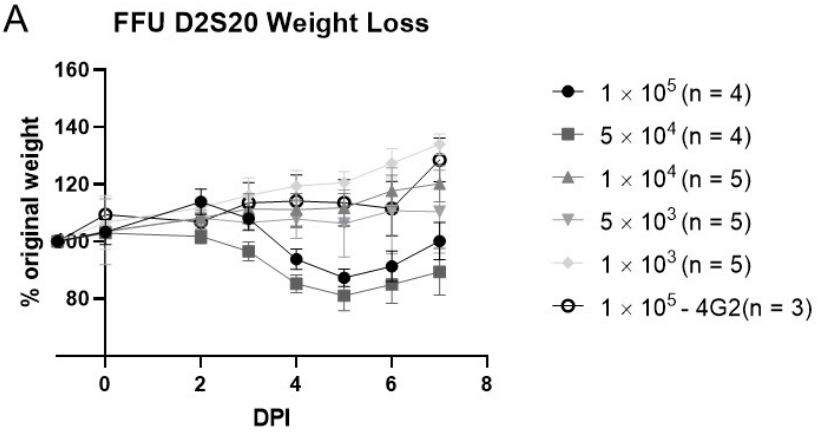

Figure 3: Figure 3 shows the result of challenging 3-4 week old LysM Cre+ IFNAR1 fl/fl mice with 20 µg of monoclonal antibody specific to the flavivirus fusion loop (4G2) at time t = -1 day prior to infection. At time t = 0, mice were challenged with various infectious doses of D2S20 and monitored for survival and weight loss for 8 days.

loss in our model. At lower doses, or notably in the absence of 4G2 mAb, we see no appreciable weight change. While these mice do appear to show some clinical signs of disease (data not shown) and display delayed weight gain relative to naïve mice of the same age, there is a more pronounced phenotype resembling DENV-induced viral sepsis at the higher doses tested in combination with the mAb 4G2.

3. MAJOR FINDINGS, DEVELOPMENTS, and CONCLUSIONS

Since beginning of this project, significant time has been devoted to these studies. While some of progress regarding this project was hampered by our lab's pivot to study SARS-CoV-2 beginning in March 2020, We made considerable progress in the completion of the proposed aims. We have produced and purified recombinant his-tagged CrmD and VCP using the Expi293 expression system (Fig 4a). We have an assay optimized for validating our CrmD protein in vivo (Fig 4b). We have been able to confirm via hemolysis assay that we can inhibit and detect complement activation (Fig 4c). We demonstrated that our concept of targeting TNF-α in the context of virus-induced sepsis was sound by challenging our mice with WNV and treating with mAb Humira following infection (Fig 4d). We demonstrated that DENV-2 infection, when preceded by prior flavivirus exposure (e.g. 4G2) causes morbidity and signs of disease in our LysM Cre IFNAR1 fl/fl. We tested the efficacy of the CrmD and VCP proteins in our mouse model with DENV-induced sepsis however did not see measurable improvements in disease severity associated with DENV infection (Fig 4e).

While we were able to evaluate the role of VCP and CrmD in our murine model of viral sepsis we did have stated goals that were not met. Specifically, the identification of the cell types producing the cytokines associated with the cytokine storm. To address this we attempted to determine the contribution of IFNAR1-deficient monocytes to the cytokine milieu by qPCR, ELISA, and flow cytometry. For qPCR analysis of cytokine and chemokine expression, we cultured bone-marrow-derived macrophages (BMM) in the presence and absence of DV2 and performed qPCR to look for expression of cytokines of interest (IL-1β, TNF-α, IL-6) and chemokines of interest (i.e. CX3CL1). We then planned to also perform these assays in the presence and absence of CrmD and VCP to examine how cytokine profiles are altered by the addition of these immunomodulatory proteins. However, we were unable to detect differences in cytokine levels in the cultured BMM with and without DENV2 preventing the determination of these cells in cytokine production. We also attempted an ELISA analysis, using the same cultured BMM approach in the presence and absence of DV2 examining similar targets as in our qPCR-based approach. As with the qPCR-based approach,

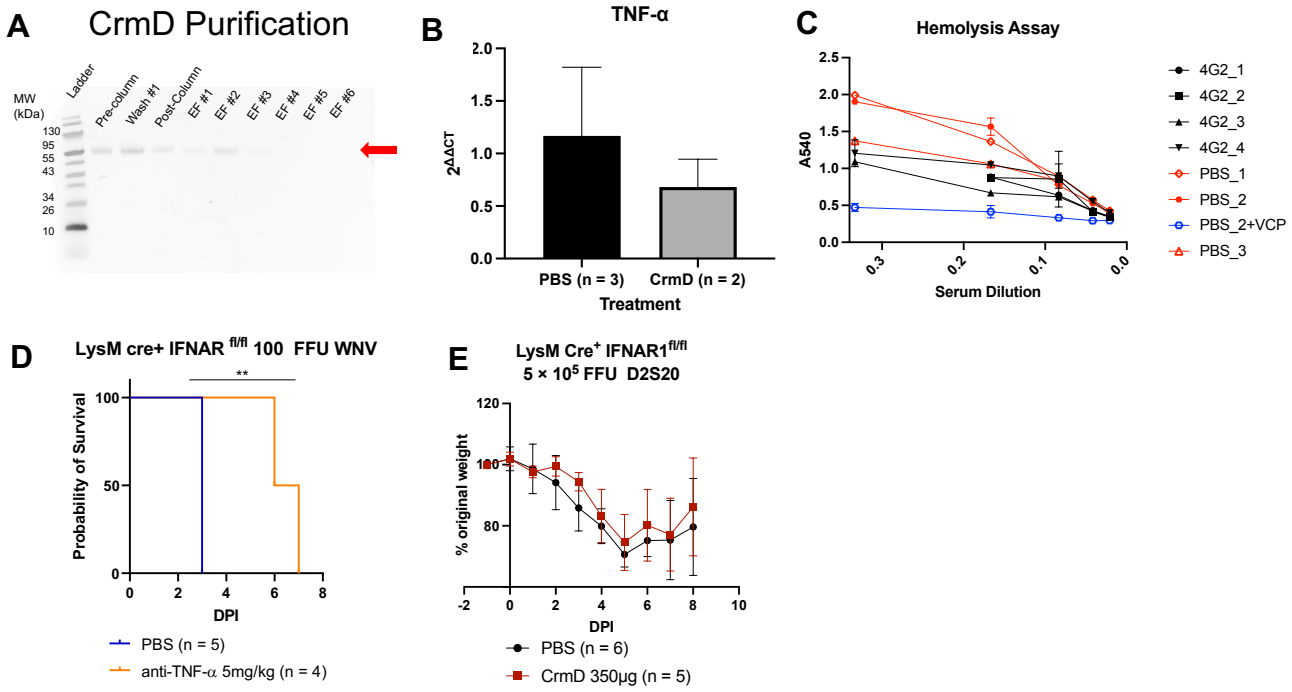

Figure 4 4A. Evidence of CrmD purification from a Nickle column. **4B.** Evidence that the administration of CrmD was able to moderately inhibit TNF-alpha production in vivo. **4C.** Evidence that VCP was able to inhibit hemolysis in vitro. **4D.** Evidence that blocking TNF-alpha in vivo prolongs survival of West Nile infected mice. **4E**. Demonstration that administration of CrmD does not impact the morbidity of mice infected with DENV**.**

we were unable to see differences that prevented further progress on this aim using this approach. We had also hoped to examine how cytokines produced by monocytes impact innate immune cell extravasation by performing *in vitro* cell migration assays with murine monocytes in the context of DENV infection, as well as in the presence and absence of CrmD and VCP. However, the lack of differences associated with our in vitro culture system prevented further investigation of these parameters.

What opportunities for training and professional development has the project provided?
If the project was not intended to provide training and professional development opportunities or there is nothing significant to report during this reporting period, state "Nothing to Report."

Describe opportunities for training and professional development provided to anyone who worked on the project or anyone who was involved in the activities supported by the project. "Training" activities are those in which individuals with advanced professional skills and experience assist others in attaining greater proficiency. Training activities may include, for example, courses or one-on-one work with a mentor. "Professional development" activities result in increased knowledge or skill in one's area of expertise and may include workshops, conferences, seminars, study groups, and individual study. Include participation in conferences, workshops, and seminars not listed under major activities.

Training: I was invited to join the Sigma Xi honors scientific society at Saint Louis University. This group is a community of science, technology, engineering, and mathematical professionals dedicated

to research excellence, promoting public engagement with science, and fostering the next generation of researchers. The work completed on this project provided me with the invitation only opportunity to join this group. Future studies beyond the work covered under this Discovery Award will come from collaborations with this group.

I am a course director for the graduate Virology course offered at Saint Louis University. I have taught the graduate student Virology and Immunology classes in the fall of 2021. I have used data generated as part of this project to explain poxvirus immune evasion, dengue severe disease, cytokine chemokine and complement contributions to inflammation and to contrast viral sepsis with bacterial sepsis. I used the knowledge we gained from protein production and regulation of cytokine responses toward understanding disease pathology associated with the related flavivirus Powassan. In doing so I was able to invited to submit a full application to the DoD as part of a Department of Defense (DOD) Tick-Borne Disease Research Program (TBDRP) Idea Development Award for developing a POWV vaccine

E. Taylor Stone is a PhD candidate whose training is being supported by this project. The project supported a portion of Taylor's dissertation research and through work generated by this project Taylor applied for and was recently awarded an NIH F31 fellowship to continue her graduate training. I have mentored Taylor one-on-one on these studies in our individual meetings to discuss the development of this project. The goals and milestones and to analyze the reported data. Taylor has participated in four RCR trainings, through interactive Zoom and in-person sessions culminating in 8 hours of training on ethical conduct of research practices. These trainings covered topics on intellectual property law in the research setting and conflicts of interest in the research setting, and resulted in the completion of her required 8 hours of RCR training for anyone funded by an NIH grant.

Professional Development: As this project is being completed during the SARS-CoV-2 pandemic some of the professional development has been completed virtually.

Our current research on viral sepsis was presented to the Sepsis and Immunology working group at Saint Louis University. A virtually presented our current studies on Viral Sepsis during the Virology Seminar series at Oregon Health and Sciences University. Additional courses in Responsible Conduct in Research and CITI training to expand these studies beyond the murine model to understand the parallels in human sepsis. I present portions of this work as part of an invited talk at The 2022 Immunology conference sponsored by the American Association of Immunologists. Additionally, Taylor also has presented at seven research conferences over the past year listed in the activities section below. As part of her participation Taylor present posters and talks at most of these conferences. Additionally, Taylor has received multiple abstract awards for the presentation at these conferences.

How were the results disseminated to communities of interest?
If there is nothing significant to report during this reporting period, state "Nothing to Report."

Describe how the results were disseminated to communities of interest. Include any outreach activities that were undertaken to reach members of communities who are not usually aware of these project activities, for the purpose of enhancing public understanding and increasing interest in learning and careers in science, technology, and the humanities.

Nothing to Report

What do you plan to do during the next reporting period to accomplish the goals?
If this is the final report, state "Nothing to Report."

Nothing to Report.

Describe briefly what you plan to do during the next reporting period to accomplish the goals and objectives.

Nothing to Report. This is the final report for this project.

4. **IMPACT:** D*escribe distinctive contributions, major accomplishments, innovations, successes, or any change in practice or behavior that has come about as a result of the project relative to:*

What was the impact on the development of the principal discipline(s) of the project?
If there is nothing significant to report during this reporting period, state "Nothing to Report."

Describe how findings, results, techniques that were developed or extended, or other products from the project made an impact or are likely to make an impact on the base of knowledge, theory, and research in the principal disciplinary field(s) of the project. Summarize using language that an intelligent lay audience can understand (Scientific American style).

Worldwide sepsis contributes to one in every five deaths and the current treatment for sepsis includes antibiotics and fluids. To make an impact on sepsis other treatments are needed. This project impacts the field of sepsis by providing evidence that controlling inflammation can improve disease.

What was the impact on other disciplines?
If there is nothing significant to report during this reporting period, state "Nothing to Report."

Describe how the findings, results, or techniques that were developed or improved, or other products from the project made an impact or are likely to make an impact on other disciplines.

Nothing to Report

What was the impact on technology transfer?
If there is nothing significant to report during this reporting period, state "Nothing to Report."

Describe ways in which the project made an impact, or is likely to make an impact, on commercial technology or public use, including:

- *transfer of results to entities in government or industry;*
- *instances where the research has led to the initiation of a start-up company; or*
- *adoption of new practices.*

Nothing to Report

What was the impact on society beyond science and technology?

If there is nothing significant to report during this reporting period, state "Nothing to Report."

Describe how results from the project made an impact, or are likely to make an impact, beyond the bounds of science, engineering, and the academic world on areas such as:

- *improving public knowledge, attitudes, skills, and abilities;*
- *changing behavior, practices, decision making, policies (including regulatory policies), or social actions; or*
- *improving social, economic, civic, or environmental conditions.*

Nothing to Report

5. **CHANGES/PROBLEMS:** *The PD/PI is reminded that the recipient organization is required to obtain prior written approval from the awarding agency grants official whenever there are significant changes in the project or its direction. If not previously reported in writing, provide the following additional information or state, "Nothing to Report," if applicable:*

Changes in approach and reasons for change
Describe any changes in approach during the reporting period and reasons for these changes. Remember that significant changes in objectives and scope require prior approval of the agency.

Nothing to Report.

Actual or anticipated problems or delays and actions or plans to resolve them
Describe problems or delays encountered during the reporting period and actions or plans to resolve them.

Nothing to Report.

Changes that had a significant impact on expenditures
Describe changes during the reporting period that may have had a significant impact on expenditures, for example, delays in hiring staff or favorable developments that enable meeting objectives at less cost than anticipated.

Nothing to Report.

Significant changes in use or care of human subjects, vertebrate animals, biohazards, and/or select agents
Describe significant deviations, unexpected outcomes, or changes in approved protocols for the use or care of human subjects, vertebrate animals, biohazards, and/or select agents during the reporting period. If required, were these changes approved by the applicable institution committee (or equivalent) and reported to the agency? Also specify the applicable Institutional Review Board/Institutional Animal Care and Use Committee approval dates.

Significant changes in use or care of human subjects

Not Applicable-Nothing to report

Significant changes in use or care of vertebrate animals

No changes-Nothing to report

Significant changes in use of biohazards and/or select agents

No changes-nothing to report

6. **PRODUCTS:** *List any products resulting from the project during the reporting period. If there is nothing to report under a particular item, state "Nothing to Report."*

- **Publications, conference papers, and presentations**
  Report only the major publication(s) resulting from the work under this award.

  Journal publications. *List peer-reviewed articles or papers appearing in scientific, technical, or professional journals. Identify for each publication: Author(s); title; journal; volume: year; page numbers; status of publication (published; accepted, awaiting publication; submitted, under review; other); acknowledgement of federal support (yes/no).*

Stone ET, Hirsch AJ, Smith JL, Brien JD, Pinto AK. Titration and neutralizing antibody quantification by focus forming assay for Powassan virus. STAR Protoc. 2022 Jun 17;3(3):101473. doi: 10.1016/j.xpro.2022.101473. eCollection 2022 Sep 16. PMID: 35755126 *acknowledgement of federal support -yes.*

Stone ET, Hassert M, Geerling E, Wagner C, Brien JD, Ebel GD, Hirsch AJ, German C, Smith JL, Pinto AK Balanced T and B cell responses are required for immune protection against Powassan virus in virus-like particle vaccination. Cell Rep. 2022 Feb 15;38(7):110388. doi: 10.1016/j.celrep.2022.110388. PMID: 35172138 *acknowledgement of federal support -yes*

Nasr MC, Geerling E, and Pinto AK. Impact of Obesity on Vaccination to SARS-CoV-2 Front. Endocrinol., 20 June 2022 | https://doi.org/10.3389/fendo.2022.898810 *acknowledgement of federal support -yes*

Wollner CJ, Richner M, Hassert MA, Pinto AK, Brien JD, Richner JM.J A Dengue Virus Serotype 1 mRNA-LNP Vaccine Elicits Protective Immune Responses. Virol. 2021 May 24;95(12):e02482-20. DOI: 10.1128/JVI.02482-20. Print 2021 May 24.PMID: 33762420 *acknowledgement of federal support -yes*

Hassert M, Steffen TL, Scroggins S, Coleman AK, Shacham E, Brien JD, Pinto AK Prior Heterologous Flavivirus Exposure Results in Reduced Pathogenesis in a Mouse Model of Zika Virus Infection. .J Virol. 2021 Jul 26;95(16):e0057321. DOI: 10.1128/JVI.00573-21. Epub 2021 Jul 26.PMID: 34076486 *acknowledgement of federal support -yes*

Geerling E, Stone ET, Steffen TL, Hassert M, Brien JD, Pinto AK. Obesity Enhances Disease Severity in Female Mice Following West Nile Virus Infection. Front Immunol. 2021;12:739025. Epub 2021/09/18. doi: 10.3389/fimmu.2021.739025. PubMed PMID: 34531877; PMCID: PMC8439568 *acknowledgement of federal support -yes*

Pike DP, McGuffee RM, Geerling E, Albert CJ, Hoft DF, Shashaty MGS, Meyer NJ, Pinto AK, Ford DA. Plasmalogen Loss in Sepsis and SARS-CoV-2 Infection. Front Cell Dev Biol. 2022 Jun 6;10:912880. doi: 10.3389/fcell.2022.912880. eCollection 2022. PMID: 35784479 *acknowledgement of federal support -no*

- **Books or other non-periodical, one-time publications.** *Report any book, monograph, dissertation, abstract, or the like published as or in a separate publication, rather than a periodical or series. Include any significant publication in the proceedings of a one-time conference or in the report of a one-time study, commission, or the like. Identify for each one-time publication: author(s); title; editor; title of collection, if applicable; bibliographic information; year; type of publication (e.g., book, thesis or dissertation); status of publication (published; accepted, awaiting publication; submitted, under review; other); acknowledgement of federal support (yes/no).*

Nothing to report

- **Other publications, conference papers and presentations**. *Identify any other publications, conference papers and/or presentations not reported above. Specify the status of the publication as noted above. List presentations made during the last year (international, national, local societies, military meetings, etc.). Use an asterisk (*) if presentation produced a manuscript.*

Stone ET, Hassert M, Geerling EL, Pham C, Schwetye K, Hirsch AJ, Smith JL, and **Pinto, A.K** The role of CD8+ T cells in immunopathogenesis in murine models of Powassan virus infection Annual Meeting of the American Society of Tropical Medicine and Hygiene (Oral & poster presentation)

Stone ET, Hassert M, Geerling EL, Pham C, Schwetye K, Hirsch AJ, Smith JL, and **Pinto, A.K** The role of CD8+ T cells in immunopathogenesis in murine models of Powassan virus infection Viral Immunity: Basic Mechanisms and Therapeutic Applications Keystone Symposia (Poster)

Stone ET, Hassert M, Geerling EL, Pham C, Schwetye K, Hirsch AJ, Smith JL, and **Pinto, A.K** The role of T cells in immunopathogenesis in murine models of Powassan virus infection 41st Annual Meeting of the American Society for Virology—Madison, WI (Oral & poster presentation)

Stone ET, Hassert M, Geerling EL, Pham C, Schwetye K, Hirsch AJ, Smith JL, and Pinto AK Balanced T and B Cell Responses are Required for Immune Protection against Powassan Virus in Virus-Like Particle Vaccination The American Association for Immunologists IMMUNOLOGY2022 Annual Meeting; Portland, OR 2022 (oral and poster presentations)

Stone ET, Hassert M, Geerling EL, Pham C, Schwetye K, Hirsch AJ, Smith JL, and **Pinto, A.K** Balanced T and B Cell Responses are Required for Immune Protection against Powassan Virus in Virus-Like Particle Vaccination Saint Louis University Graduate Research Symposium; Saint Louis, MO (oral presentation)

Stone ET, Hassert M, Geerling E, Pham C, Schwetye K, Hirsch AJ, Smith JL, and **Pinto, A.K** Balanced T and B Cell Responses are Required for Immune Protection against Powassan Virus in Virus-Like Particle Vaccination Saint Louis University Sigma Xi Research Symposium Virtual (oral presentation)

Stone ET, Hassert M, Geerling E, Pham C, Schwetye K, Hirsch AJ, Smith JL, and **Pinto, A.K** Balanced T and B Cell Responses are Required for Immune Protection against Powassan Virus in Virus-Like Particle Vaccination Core Graduate Student Poster Session—Saint Louis, MO (Poster)

Stone ET, Geerling E, Hassert M, Steffen TL, Brien JD, **Pinto, A.K**. Innate immunomodulation by virally-encoded cytokine response modifiers as a strategy to mitigate virus-induced cytokine release syndrome Cytokine & Interferon Society Virtual Meeting of the 9th Annual International Cytokine & Interferon Society (oral presentation)

Stone ET, Hassert M, Geerling E, Brien JD, **Pinto, A.K**. Correlates of protection for Powassan virus in mouse models of infection Core Graduate Student Poster Session Saint Louis, MO (Poster)

- **Website(s) or other Internet site(s)**
  List the URL for any Internet site(s) that disseminates the results of the research activities. A short description of each site should be provided. It is not necessary to include the publications already specified above in this section.

  Nothing to report

- **Technologies or techniques**
  Identify technologies or techniques that resulted from the research activities. Describe the technologies or techniques were shared.

- **Inventions, patent applications, and/or licenses**
  Identify inventions, patent applications with date, and/or licenses that have resulted from the research. Submission of this information as part of an interim research performance progress report is not a substitute for any other invention reporting required under the terms and conditions of an award.

  Nothing to report

- **Other Products**

  Identify any other reportable outcomes that were developed under this project. Reportable outcomes are defined as a research result that is or relates to a product, scientific advance, or research tool that makes a meaningful contribution toward the understanding, prevention, diagnosis, prognosis, treatment and /or rehabilitation of a disease, injury or condition, or to improve the quality of life. Examples include:

  - *data or databases;*
  - *physical collections;*
  - *audio or video products;*
  - *software;*
  - *models;*
  - *educational aids or curricula;*
  - *instruments or equipment;*
  - *research material (e.g., Germplasm; cell lines, DNA probes, animal models);*
  - *clinical interventions;*
  - *new business creation; and*
  - *other.*

  Research material:

  mRNA constructs that express either CrmD or VCP.
  Plasmids that express either CrmD or VCP

7. PARTICIPANTS & OTHER COLLABORATING ORGANIZATIONS

What individuals have worked on the project?

Provide the following information for: (1) PDs/PIs; and (2) each person who has worked at least one person month per year on the project during the reporting period, regardless of the source of compensation (a person month equals approximately 160 hours of effort). If information is unchanged from a previous submission, provide the name only and indicate "no change".

Name:	Amelia Kahler Pinto PhD
Project Role:	Principal Investigator
Researcher Identifier:	ORCID:0000-0002-7147-3978 ResearcherID: O-6658-2018 Loop profile: 637549 Scopus Author ID: 12445714500
Nearest person month worked:	2.4
Contribution to Project:	Dr. Pinto has authored the approved ACURO and animal protocols, directed Taylor Stone's progress on the animal and in vitro studies. Dr. Pinto has mentor Ms. Stone's and aided in experimental design and data analysis.
Name:	Emily Taylor Stone
Project Role:	Graduate Student

Researcher Identifier:	ORCID:0000-0001-6742-1270
Nearest person month worked:	8
Contribution to Project:	Taylor Stone has performed work in the area viral infection of murine model. Sepsis monitoring and delivery of anti-inflammatories. Ms. Stone has also contributed to data analysis and protocol development.

Has there been a change in the active other support of the PD/PI(s) or senior/key personnel since the last reporting period?
If there is nothing significant to report during this reporting period, state "Nothing to Report."

If the active support has changed for the PD/PI(s) or senior/key personnel, then describe what the change has been. Changes may occur, for example, if a previously active grant has closed and/or if a previously pending grant is now active. Annotate this information so it is clear what has changed from the previous submission. Submission of other support information is not necessary for pending changes or for changes in the level of effort for active support reported previously. The awarding agency may require prior written approval if a change in active other support significantly impacts the effort on the project that is the subject of the project report.

Nothing to Report.

What other organizations were involved as partners?
If there is nothing significant to report during this reporting period, state "Nothing to Report."

Describe partner organizations – academic institutions, other nonprofits, industrial or commercial firms, state or local governments, schools or school systems, or other organizations (foreign or domestic) – that were involved with the project. Partner organizations may have provided financial or in-kind support, supplied facilities or equipment, collaborated in the research, exchanged personnel, or otherwise contributed.

Provide the following information for each partnership:
Organization Name:
Location of Organization: (if foreign location list country)
Partner's contribution to the project (identify one or more)

- *Financial support;*
- *In-kind support (e.g., partner makes software, computers, equipment, etc., available to project staff);*
- *Facilities (e.g., project staff use the partner's facilities for project activities);*
- *Collaboration (e.g., partner's staff work with project staff on the project);*
- *Personnel exchanges (e.g., project staff and/or partner's staff use each other's facilities, work at each other's site); and*
- *Other.*

Nothing to Report.

8. SPECIAL REPORTING REQUIREMENTS

COLLABORATIVE AWARDS: *For collaborative awards, independent reports are required from BOTH the Initiating Principal Investigator (PI) and the Collaborating/Partnering PI. A duplicative report is acceptable; however, tasks shall be clearly marked with the responsible PI and research site. A report shall be submitted to* ***https://ebrap.org/eBRAP/public/index.htm*** *for each unique award.*

QUAD CHARTS: *If applicable, the Quad Chart (available on https://www.usamraa.army.mil/Pages/Resources.aspx) should be updated and submitted with attachments.*

9. APPENDICES:

Attach all appendices that contain information that supplements, clarifies or supports the text. Examples include original copies of journal articles, reprints of manuscripts and abstracts, a curriculum vitae, patent applications, study questionnaires, and surveys, etc.

Curriculum Vitae
Amelia Kahler Pinto Ph.D.
Assistant Professor

Personal Information

Professional Address:

Saint Louis University Department of Molecular Microbiology and Immunology
Saint Louis University School of Medicine
Doisy Research Center
Room 703
1100 S. Grand Blvd.,
St. Louis, MO 63104
314-977-8897
amelia.pinto@health.slu.edu

Current Position, Institution

Assistant Professor, Saint Louis University School of Medicine, Molecular Microbiology & Immunology,	12/15-current
Director Biosafety Level 3 Facility	06/17-current
Co-Director Graduate Virology	06/17-current

Education

Postgraduate training:

Postdoctoral Research Associate Department of Medicine Washington University School of Medicine,	01/10-11/13
Postdoctoral Research Fellow Department of Pathology Washington University School of Medicine,	11/07-12/09

Graduate degree:

Graduate Research Fellow Ph.D. Molecular Microbiology and Immunology Oregon Health & Science University, Portland, OR, Trained with Ann B. Hill, M.D., Ph.D.	06/00-08/07

Thesis title: Inhibition of T cell effector function by Murine cytomegalovirus immune evasion genes.

Undergraduate degree:

B.S. Molecular Biology, 09/94-05/97
University of Portsmouth
Portsmouth, England

Previous Professional experience

Research Faculty, Instructor, 12/13-10/15
Department of Microbiology
Washington University School of Medicine

Postdoctoral Associate, 01/10-11/13
Department of Medicine
Washington University School of Medicine

Postdoctoral Fellow 11/07-12/09
Department of Pathology
Washington University School of Medicine

Graduate Student 06/00-08/07
Department of Molecular Microbiology and Immunology
Oregon Health & Science University

Research Technician II, 03/98-06/00
Department of Pathology
University of Massachusetts Medical School

Professional Society memberships

National

Member, Serological Sciences Network **(**SeroNet) 2021- current

Member, EpiCenter for Emerging infectious Diseases (EEID) 2020-current

Member, Center research in emerging infectious diseases (CREID) 2020-current

Member, EMERGE 2020-current

Member, American Society of Tropical Medicine and Hygiene 2010-current

Member, American Committee on Arthropod-Borne Viruses 2010-current

Member, American Committee on Global Heath	2008-2012
Member, American Society for Virology	2006-current
Member, American Association of Immunologists	2004-current
Member, American Association for the Advancement of Science	2002-2018

Regional

SLU, Sepsis Immunology Research Group	2021
WASHU SOM, Infectious Disease Center (IDC)	2019
SLU, Institute for Drug and Biotherapeutic Innovation (IDBI)	2018
WASHU SOM, Institute of Clinical and Translational Science (ICTS)	2017
SLU, Vaccine and Treatment Evaluation Unit (VTEU)	2016

Honorary Societies, Honors, and Awards

Faculty

Sponsor: E. Taylor Stone F31AI172229 – 01	2022
Saint Louis University Seed Grant for COVID-19 studies	2020
Saint Louis University Scholarly Works Award	2020
Sponsor: Mariah Hassert F31 AI152460-01	2020
Saint Louis University Presidential Research Fund Award	2017

Postgraduate

Travel grant: V Pan American Dengue Network Meeting	2016
Travel grant: IV Pan American Dengue Network Meeting	2014
Global Health World Health Interest Group Honoraria	2013
Travel grant: American Society for Virology	2009
W.M. Keck Postdoctoral Fellowship	2007-08

Graduate

Tartar Fellowship	2005
30th Annual International Herpesvirus Workshop Honoraria	2005
Travel grant: American Society for Virology	2005
Abstract Award: The American Association of Immunologists	2004
Travel grant: Keystone Symposia Taos New Mexico	2004
National Eye Institute Training Grant ACAEI0071	2004-07
Abstract Award: The American Association of Immunologists	2003
American Heart Association Fellowship 0215188Z2002-04	2002-04
Tartar Fellowship	2002

Professional Services

Committee Membership and Administrative roles

National

Chair 2022
Emerging viral infections
The American Association of Immunologists Annual Meeting
Immunology 2022
Portland, OR

Reviewer 2022
Burroughs Welcome Trust
Dengue Disease Models

Reviewer 2022
Wisconsin Regional Primate Center grants
Arboviruses in Non-human Primates

Chair 2021
Host Pathogen responses
The American Association of Immunologists Annual Meeting
Immunology 2021 (virtual)

Reviewer 2021
Burroughs Welcome Trust
Flavivirus infections

Chair 2019
Immune response to pathogens
Autumn Immunology Conference Annual Meeting
Chicago, IL

Membership review board 2017-19
American Society for Virology

Reviewer 2018
Military Infectious Diseases Research Program (MIDRP)
Congressionally directed medical research programs (CDMRP)
Department of Defense
Baltimore, MD

Reviewer 2018
Emerging Infectious Diseases Panel (EID)
Congressionally directed medical research programs (CDMRP)
Department of Defense
Baltimore, MD

Reviewer 2017
Pre-application Emerging Infectious Diseases (PRE-EID)
Congressionally directed medical research programs (CDMRP)
Department of Defense

Reviewer 2017
NIH Special Emphasis Panel PAR-16-106
Rapid Assessment of Zika Virus Complications (R21)

Reviewer 2017
Emerging Infectious Diseases Panel (EID)
Congressionally directed medical research programs (CDMRP)
Department of Defense

Reviewer 2016
Vaccine Development for Infectious Diseases (VDID)
Congressionally directed medical research programs (CDMRP)
Department of Defense
Baltimore, MD

University Service

Graduate School Admissions Committee 2020-current
Saint Louis School of Medicine

Director of the Biosafety level 3 facility 2017- current
Saint Louis School of Medicine

Co-Director Graduate Virology Course 2017- current
Saint Louis School of Medicine

Editorial and Journal Board review

Section Editor
Associate Editor 2022-current
Topics in Viral Immunology
Frontiers in Immunology

Associate Editor 2021-current
Vaccines and Antivirals
Frontiers in Virology

Associate Editor 2020-2021
Special topics: Obesity Infection and Vaccination
Frontiers in Immunology:

Board of Reviewers 2019-current
Vaccines

Board of Reviewers 2019-current
Viruses

Associate Editor 2019-2020
Special topics: Vaccines against (re)emerging and Tropical Infectious Diseases
Viruses

Ad Hoc manuscript reviewer:

Frontiers in Virology 2021-Current

Cell 2020-Current

Cell Host Microbe	2020-Current
Cell Reports	2020-Current
iScience	2020-Current
Frontiers in Immunology	2019-Current
Science Immunology	2018-Current
Lancet	2018-Current
Lancet Microbiology	2018-Current
Nature Immunology	2018-Current
Nature Medicine	2018-Current
Nature Communications	2017-Current
Plos Biology	2017-Current
Virology	2017-Current
Vaccines	2017-Current
Viruses	2017-Current
Plos, Neglected Tropical Diseases	2017-Current
Scientific Reports	2016-Current
Emerging Infectious Diseases	2016-Current
PLoS Pathogens	2016-Current
Journal of Virology	2016-Current
Journal of Immunology	2016-Current
Ebio Medicine	2016-Current
mBio	2016-Current

Current and Past Teaching Responsibilities

Administrative

Co-Course Director — 2017-current
Graduate Virology Course
Department of Molecular Microbiology and Immunology
Saint Louis University School of Medicine

Courses and Lectures

Lecture: Viruses associated with human cancers — 2022-current
BBSC 5030 Viral oncogenesis and cell signaling

Discussion: Viral oncogenes — 2022- current
Cell cycle control and cellular transformation
BBSC 5030 Viral oncogenesis and cell signaling

Discussion: Viral oncogenes — 2022- current
Extracellular viral oncogene
BBSC 5030 Viral oncogenesis and cell signaling

Discussion: Viral oncogenes — 2022- current
Plasma membrane-associated viral oncogenes
BBSC 5030 Viral oncogenesis and cell signaling

Discussion: Viral oncogenes — 2022- current
Nuclear and Cytoplasmic viral oncogenes
BBSC 5030 Viral oncogenesis and cell signaling

Lecture: Alpha/beta herpes viruses — 2021-current
MBG-6350 Virology
Department of Molecular Microbiology and Immunology
Saint Louis University School of Medicine

Lecture: Gamma herpes viruses — 2021-current
MBG-6350 Virology
Department of Molecular Microbiology and Immunology
Saint Louis University School of Medicine

Lecture: Virus Control Cell cycle — 2021-current
Department of Molecular Microbiology and Immunology
Saint Louis University School of Medicine
MBG-6350 Virology

Lecture: Virus Vectors & Gene Transfer 2021-current
MBG-6350 Virology
Department of Molecular Microbiology and Immunology
Saint Louis University School of Medicine

Lecture: Virus Control of Apoptosis 2021-current
MBG-6350 Virology
Department of Molecular Microbiology and Immunology
Saint Louis University School of Medicine

Lecture: Secondary Effector T cell functions 2021-current
MBG-6650 Immunobiology
Department of Molecular Microbiology and Immunology
Saint Louis University School of Medicine

Discussion: Flavivirus 2020-current
MBG-6350 Virology
Department of Molecular Microbiology and Immunology
Saint Louis University School of Medicine

Lecture: Primary Immune Response to Pathogens 2017-current
MBG-6650 Immunobiology
Department of Molecular Microbiology and Immunology
Saint Louis University School of Medicine

Lecture: Adaptive Immune Response to Pathogens 2017-current
MBG-6650 Immunobiology
Department of Molecular Microbiology and Immunology
Saint Louis University School of Medicine

Lecture: Immune Evasion Strategies 2017-current
MBG-6650 Immunobiology
Department of Molecular Microbiology and Immunology
Saint Louis University School of Medicine

Lecture: The Red Queen Hypothesis 2017-current
MBG-6650 Immunobiology
Department of Molecular Microbiology and Immunology
Saint Louis University School of Medicine

Lecture: Vaccine immunobiology 2017-current
MBG-6650 Immunobiology
Department of Molecular Microbiology and Immunology

Saint Louis University School of Medicine

Lecture: Vaccines 2017-current
MBG-6650 Immunobiology
Department of Molecular Microbiology and Immunology
Saint Louis University School of Medicine

Lecture: Vaccines 2017-current
MBG-6350 Virology
Department of Molecular Microbiology and Immunology
Saint Louis University School of Medicine

Lecture: Antivirals 2017-current
MBG-6350 Virology
Department of Molecular Microbiology and Immunology
Saint Louis University School of Medicine

Lecture: Orthomyxoviruses 2017-current
MBG-6350 Virology
Department of Molecular Microbiology and Immunology
Saint Louis University School of Medicine

Lecture: Bunyaviruses 2017-current
MBG-6350 Virology
Department of Molecular Microbiology and Immunology
Saint Louis University School of Medicine

Discussion: Student mini lectures 2017-current
MBG-6350 Virology
Department of Molecular Microbiology and Immunology
Saint Louis University School of Medicine

Thesis Exam Committees

Elizabeth Geerling 2019-current
Chair, SLU Thesis Exam Committee
Department of Molecular Microbiology and Immunology
Saint Louis University School of Medicine

E. Taylor Stone 2019-current
Chair, SLU Thesis Exam Committee
Department of Molecular Microbiology and Immunology
Saint Louis University School of Medicine

Christine Noto 2019-2022
Member, SLU Thesis Exam Committee,
Department of Molecular Microbiology and Immunology
Saint Louis University School of Medicine

Mariah Hassert 2018-2021
Chair SLU Thesis Exam Committee Chair
Department of Molecular Microbiology and Immunology
Saint Louis University School of Medicine

Major Exam Committees

E. Taylor Stone 2022
Chair, Major Exam Committee
Department of Molecular Microbiology and Immunology
Saint Louis University School of Medicine

Stella Hoft, 2021
Member, Major Exam Committee,
Department of Molecular Microbiology and Immunology
Saint Louis University School of Medicine

Elizabeth Geerling. 2021
Chair, Major Exam Committee
Department of Molecular Microbiology and Immunology
Saint Louis University School of Medicine

Christine Noto 2020
Member, Major Exam Committee,
Department of Molecular Microbiology and Immunology
Saint Louis University School of Medicine

Nilofar Khojandi 2020
Member, Major Exam Committee
Department of Molecular Microbiology and Immunology
Saint Louis University School of Medicine

Lindsey Koehm 2019
Member, Major Exam Committee,
Department of Molecular Microbiology and Immunology
Saint Louis University School of Medicine

Mariah Hassert 2019
Chair, Major Exam Committee
Department of Molecular Microbiology and Immunology
Saint Louis University School of Medicine

Minor Exam Committees

Katie Hunt 2022
Virology Member, Minor Exam Committee
Department of Molecular Microbiology and Immunology
Saint Louis University School of Medicine

Alexander Piening 2021
Virology Member, Minor Exam Committee
Department of Molecular Microbiology and Immunology
Saint Louis University School of Medicine

Stella Hoft 2021
Virology Member, Minor Exam Committee
Department of Molecular Microbiology and Immunology
Saint Louis University School of Medicine

E. Taylor Stone 2020
Mentor Member, Minor Exam Committee
Department of Molecular Microbiology and Immunology
Saint Louis University School of Medicine

Elizabeth Geerling 2020
Mentor Member, Minor Exam Committee
Department of Molecular Microbiology and Immunology
Saint Louis University School of Medicine

Courtney Iberg 2019
Virology Member, Minor Exam Committee
Department of Molecular Microbiology and Immunology
Saint Louis University School of Medicine

Mariah Hassert 2018
Mentor Member, Minor Exam Committee
Department of Molecular Microbiology and Immunology
Saint Louis University School of Medicine

Protégé

Graduate Students

Elizabeth Geerling, 2019-current

Awards
Conference Award Second Place 2022

Saint Louis University Graduate Student Symposium

Abstract Award 2022
The American Association of Immunologists Annual Meeting

Abstract Award 2021
The American Association of Immunologists Annual Meeting

Conference Award Second Place 2021
Saint Louis University Graduate Student Association

Conference Award Third Place 2021
Saint Louis University Graduate Student Association

Conference Award Second Place 2021
Saint Louis University Sigma Xi Research Symposium

Conference Award 2021
Saint Louis University Graduate Student Association

Abstract Award 2021
Obesity: From Cell to Patient Keystone

Conference Award 2020
Saint Louis University Graduate Student Association

Excellence in Research Award 2020
Endocrine Society

Conference Award 2019
Saint Louis University Graduate Student Association

Presentations

2022

Geerling E., Stone E.T., Carpenter D., Schwetye K., **Pinto, A.K**. Metabolic syndrome enhances viral disease severity and reduces vaccine efficacy in mice. The American Association for Immunologists IMMUNOLOGY2022 Annual Meeting; Portland, OR 2022 (oral and poster presentations)

Geerling E., Stone E.T., Carpenter D., Schwetye K., **Pinto A.K.** Metabolic syndrome enhances viral disease severity and reduces vaccine efficacy in mice Saint Louis University Graduate Research Symposium; Saint Louis, MO (oral

presentation)

Geerling E., Stone E.T., Carpenter D., Schwetye K., **Pinto, A.K.** Obesity enhances viral disease severity and reduces vaccine efficacy in mice Saint Louis University Sigma Xi Research Symposium Virtual (oral presentation)

2021

Geerling E., Stone E.T., Hassert M., Carpenter D., Schwetye K., DeBosch B. and **Pinto, A.K.** Obesity enhances viral disease severity and reduces vaccine efficacy in mice Autumn Immunology Conference (AIC); Chicago, IL (oral and poster presentations)

Geerling E., Steffen T.L., Stone E.T., Hassert M., DeBosch B. and **Pinto, A.K.** Abnormal Cytokine levels in obese mice induce dysfunctional virus-specific immune responses. Cytokines 2021 9th Annual Meeting of the International Cytokine & Interferon Society (ICIS); virtual (poster presentation)

Geerling E., Steffen T.L., Stone E.T., Hassert M, **Pinto, A.K.** Female obese mice have a higher mortality rate and altered immune responses following viral infection in comparison to wild-type mice. The American Association for Immunologists IMMUNOLOGY2021 Annual Meeting Virtual (oral presentation and poster presentation)

Geerling E., Steffen T.L., Stone E.T., Hassert M, **Pinto, A.K.** Female obese mice have a higher mortality rate and aberrant immune responses following viral infection in comparison to wild-type mice. Saint Louis University Graduate Research Symposium; Virtual (oral presentation)

Geerling E., Steffen T.L., Stone E.T., Hassert M, **Pinto, A.K.** Female obese mice have a higher mortality rate and aberrant immune responses following viral infection in comparison to wild-type mice. Saint Louis University Sigma Xi Research Symposium. Virtual (oral presentation)

Geerling E., Hassert M., Stone E.T. and **Pinto, A.K.** Female obese mice have a higher mortality rate and altered immune responses following flavivirus infection in comparison to wild-type mice. Obesity: From Cell to Patient Keystone Symposia; Virtual l (poster presentation)

2020

Geerling E., Hassert M., Stone E.T., and **Pinto, A.K.** Obese mice have a higher mortality rate and altered immune responses following flavivirus infection in comparison to wild-type mice. American Society of Tropical Medicine & Hygiene; Virtual (oral presentation)

Geerling E., Hassert M., Stone E.T., and **Pinto, A.K.** Obese mice have a higher mortality rate and altered immune responses following flavivirus infection in comparison to wild-type mice. American Society for Virology Annual Meeting. Virtual (oral presentation and poster presentation)

Geerling, E., Hassert, M., Stone, E.T., and **Pinto, A.K.** Immune response differences between wild type and obese mice in the context of vaccination. Endocrine Society Annual Meeting San Francisco, CA. Virtual/canceled (oral presentation and poster presentation)

2019

Geerling, E., Hassert, M., Stone, E.T., and **Pinto, A.K**. Immune response differences between wild type and obese mice in the context of vaccination. Autumn Immunology Conference; Chicago, IL (oral presentation and poster presentation)

E. Taylor Stone 2019- current

Awards

NIH NIAID F31 Fellowship 1 F31AI172229 - 01 2022-2024

Student Travel Award 2022
American Society for Virology

Abstract Award 2022
The American Association of Immunologists Annual Meeting

Travel Scholarship 2022
Labroots

First Place Oral Presentation 2022
Saint Louis University Graduate Student Symposium:

Abstract Award 2021
Milstein

Abstract Award 2021
The American Association of Immunologists Annual Meeting

Travel Award 2021
American Committee Arthropod-borne viruses

Student Travel Award 2021
American Society for Virology

Conference Award 2020
Saint Louis University Graduate Student Association

Young Investigator Award 2019
The American Association of Immunologists AIC

Presentations

2022

Stone ET, Hassert M, Geerling EL, Pham C, Schwetye K, Hirsch AJ, Smith JL, and **Pinto, A.K** The role of CD8+ T cells in immunopathogenesis in murine models of Powassan virus infection Annual Meeting of the American Society of Tropical Medicine and Hygiene (Oral & poster presentation)

Stone ET, Hassert M, Geerling EL, Pham C, Schwetye K, Hirsch AJ, Smith JL, and **Pinto, A.K** The role of CD8+ T cells in immunopathogenesis in murine models of Powassan virus infection Viral Immunity: Basic Mechanisms and Therapeutic Applications Keystone Symposia (Poster)

Stone ET, Hassert M, Geerling EL, Pham C, Schwetye K, Hirsch AJ, Smith JL, and **Pinto, A.K** The role of T cells in immunopathogenesis in murine models of Powassan virus infection 41st Annual Meeting of the American Society for Virology—Madison, WI (Oral & poster presentation)

Stone ET, Hassert M, Geerling EL, Pham C, Schwetye K, Hirsch AJ, Smith JL, and Pinto AK Balanced T and B Cell Responses are Required for Immune Protection against Powassan Virus in Virus-Like Particle Vaccination The American Association for Immunologists IMMUNOLOGY2022 Annual Meeting; Portland, OR 2022 (oral and poster presentations)

Stone ET, Hassert M, Geerling EL, Pham C, Schwetye K, Hirsch AJ, Smith JL, and **Pinto, A.K** Balanced T and B Cell Responses are Required for Immune Protection against Powassan Virus in Virus-Like Particle Vaccination Saint Louis University Graduate Research Symposium; Saint Louis, MO (oral presentation)

Stone ET, Hassert M, Geerling E, Pham C, Schwetye K, Hirsch AJ, Smith JL, and **Pinto, A.K** Balanced T and B Cell Responses are Required for Immune Protection against Powassan Virus in Virus-Like Particle Vaccination Saint Louis University Sigma Xi Research Symposium Virtual (oral presentation)

Stone ET, Hassert M, Geerling E, Pham C, Schwetye K, Hirsch AJ, Smith JL, and **Pinto, A.K** Balanced T and B Cell Responses are Required for Immune Protection against Powassan Virus in Virus-Like Particle Vaccination Core Graduate Student Poster Session—Saint Louis, MO (Poster)

2021

Stone ET, Geerling E, Hassert M, Steffen TL, Brien JD, **Pinto, A.K**. Innate immunomodulation by virally-encoded cytokine response modifiers as a strategy

to mitigate virus-induced cytokine release syndrome Cytokine & Interferon Society Virtual Meeting of the 9th Annual International Cytokine & Interferon Society (oral presentation)

Stone ET, Hassert M, Geerling E, Brien JD, **Pinto, A.K**. Correlates of protection for Powassan virus in mouse models of infection Core Graduate Student Poster Session Saint Louis, MO (Poster)

2020

Stone ET, Hassert M, Geerling E, Brien JD, **Pinto, A.K**. Correlates of protection for Powassan virus in mouse models of infection Virtual Meeting of the American Society of Tropical Medicine and Hygiene. Virtual (oral presentation)

Stone ET, Hassert M, Geerling E, Brien JD, **Pinto, A.K**. Correlates of protection for Powassan virus in mouse models of infection Core Graduate Student Poster Session—Saint Louis, MO (Poster)

Stone ET, Hassert M, Geerling E, Brien JD, **Pinto, A.K**. Correlates of protection for Powassan virus in mouse models of infection 39th Annual Meeting of the American Society for Virology. Mini-Virtual (Poster presentation)

2019

Stone ET, Hassert M, Geerling E, Brien JD, **Pinto, A.K**. Correlates of protection for Powassan virus in mouse models of infection Core Graduate Student Poster Session—Saint Louis, MO (Poster)

Stone ET, Hassert M, Geerling E, Brien JD, **Pinto, A.K**. Correlates of protection for Powassan virus in mouse models of infection Autumn Immunology Conference—Chicago, IL (oral and poster presentations)

Mariah Hassert (Co-Mentor) 2017-2021

Awards

Graduate Student of the Year 2021
Saint Louis University (MMI Dept.)

Best Poster Presentation 2021
Saint Louis University Graduate Research Symposium

Trainee Abstract Award 2021
American Association of Immunologists

Young Investigator Award 2020
American Society of Tropical Medicine and Hygiene

Travel Award 2020
American Committee on Arthropod-Borne Viruses (ACAV)
American Society of Tropical Medicine and Hygiene

Graduate Student of the Year 2020
Saint Louis University (MMI Dept.)

Student Travel Award 2020
American Society for Virology

Travel for Techniques Fellowship 2019
American Association of Immunologists

Graduate Student of the Year 2019
Saint Louis University (MMI Dept.)

Best Poster Presentation 2019
Saint Louis University Graduate Research Symposium

Best Poster Presentation 2018
Saint Louis University Graduate Research Symposium

Alpha Sigma Nu Jesuit Honor Society 2018
Saint Louis University

Student Fellowship 2017
Saõ Paulo School of Advanced Science in Arbovirology

Course completion 2017
American Association of Immunologists

Presentations

2021

Hassert, M., Schwetye, K.E., Geerling, E., Steffen, T.L., Stone, E.T., Brien, J.D., **Pinto, A.K.** T cell cross-reactivity during heterologous infection results in enhanced cytolytic capacity but enhanced Zika virus disease. Immunology 2021; Virtual (Oral and Poster presentation).

Hassert, M., Schwetye, K.E., Geerling, E., Steffen, T.L., Stone, E.T., Brien, J.D., **Pinto, A.K.** T cell cross-reactivity during heterologous infection results in enhanced cytolytic capacity but enhanced Zika virus disease. Saint Louis University Graduate Research Symposium 2021; Virtual (Poster presentation).

2020

Hassert, M., Brien, J.D., **Pinto, A.K.** CD8+ T cell cross-reactivity during heterologous flavivirus infection results in cross-reactive immunodomination and enhanced cytolytic capacity at the expense of virus-specific responses, driving differences in protective capacity. American Society of Tropical Medicine and Hygiene 2020 Annual Meeting; Virtual (Poster Presentation).

Hassert, M., Steffen, T.L., Dorflinger, B.G., Dayton, J., Coleman, A., Cruz-Orengo, L., Brien, J.D., **Pinto, A.K.** Heterologous flavivirus exposure provides varying degrees of cross-protection from Zika virus infection in a mouse model of disease. American Society of Tropical Medicine and Hygiene 2020 Annual Meeting; Virtual (Oral Presentation).

Hassert, M., Weiss, C.M., Coffey, L.L., **Pinto, A.K.,** Brien, J.D. T cells restrict Zika virus replication and viral swarm diversity during infection. American Society of Tropical Medicine and Hygiene 2020 Annual Meeting; Virtual (Oral Presentation).

Hassert, M., Weiss, C.M., Feldman, M.S., Coffey, L.L., **Pinto, A.K.,** Brien, J.D. Altered T cell responses during heterologous flavivirus infection and the potential consequences for viral genome diversity. American Society for Virology 2020 Annual Meeting; Virtual (Oral Presentation).

2019

Hassert, M., **Pinto, A. K.,** Brien, J.D., Implications of altered immune restriction during heterologous flavivirus infection: Viral diversity, dissemination, and fitness. UC-Davis; Davis, CA. 2019 (Visiting Scientist Lecture).

Hassert, M., Brien, J.D., **Pinto, A.K.** Prior heterologous flavivirus exposure impacts virus-specific and cross-reactive T cell populations and their functions during Zika virus infection. Gordon Research Conference- Cells and Viruses; Lucca, Italy. 2019 (Poster Presentation).

Hassert, M., Brien, J.D., **Pinto, A.K.** Prior heterologous flavivirus exposure impacts virus-specific and cross-reactive T cell populations and their functions during Zika virus infection. SLU Graduate Research Symposium; St. Louis, MO. 2019 (Poster Presentation).

2018

Hassert, M., Brien, J.D**., Pinto, A.K**. Heterologous flavivirus immunity impacts Zika virus pathogenesis in a mouse model of infection. 47th Annual Autumn Immunology Conference; Chicago, IL. 2018 (Oral Presentation and Poster Presentation).

Hassert, M., Wolf, K. J., Schwetye, K. E., DiPaolo, R. J., Brien, J. D., & **Pinto, A. K.** CD4+ T cells mediate protection against severe Zika disease in a mouse model of infection. 47th Annual Autumn Immunology Conference; Chicago, IL. 2018 (Oral Presentation and Poster Presentation).

Hassert, M., Brien, J.D., **Pinto, A.K.** Heterologous flavivirus immunity impacts Zika virus pathogenesis in a mouse model of infection. American Society of Tropical Medicine and Hygiene 67th Annual Meeting; New Orleans, LA. 2018 (Poster Presentation).

Hassert, M., Wolf, K. J., Schwetye, K. E., DiPaolo, R. J., Brien, J. D., & Pinto, A. K. CD4+ T cells mediate protection against severe Zika disease in a mouse model of infection. American Society of Tropical Medicine and Hygiene 67th Annual Meeting; New Orleans, LA. 2018 (Poster Presentation).

Hassert, M., Brien, J.D., **Pinto, A.K.** Mapping the CD4+ T cell response in a mouse model of Zika virus infection. 6th Pan-American Dengue Research Network Meeting; Galveston, TX. 2018. (Poster Presentation).

Hassert, M., Brien, J.D., **Pinto, A.K**. Heterologous flavivirus immunity impacts Zika virus pathogenesis in a mouse model of infection. SLU Graduate Research Symposium; St. Louis, MO. 2018 (Poster Presentation).

2017

Hassert, M., Brien, J.D., **Pinto, A.K**. Mapping the CD4+ T cell response in a mouse model of Zika virus infection. SPSAS International Advanced Arbovirology Course and Meeting; Saõ Josè do Rio Preto, Saõ Paulo, Brazil. 2017. (Poster Presentation).

Scott Grady,

Graduate Student (Dr. Arnett, Chemistry), 2019-2021
Collaborative project Dr. Arnett on South Campus

Graduate Rotations:

Valarie Murphy, 2022

Emily Ebert, 2022

Rachel Wiess, 2020

Katie Phelps, 2019

Stella Hoft, M.D./Ph.D. 2018

Medical Student:

Samantha Zavertnik 2018
Awarded a Saint Louis University School of Medicine Research Fellowship

Post-Doctoral Research Associates:

June Ann D'Angelo 2016-2017

Undergraduate Students:

Current:

Bryson Mahari Undergraduate Biology Pre-Med	2022-current
Taneesh Makkena Undergraduate-Med Scholar Biology Pre-Med	2022-current
Srinidhi Karlapalem Undergraduate Biology-Pre-Med	2022-current
Maria Mai Undergraduate McNair Research Scholar Biology	2022-current
Christinia Pham Undergraduate Biology-Pre-Med	2021-current

Past:

Areeb Shah PreMed	2021
Derek Nguyen Summer, PreMed	2016-2017
Spreet Amar PreMed	2016-2018
Eunice Yeo PreMed	2016
Abigail Coleman, Biology	2016-2020

Research Support

ACTIVE

Federally Funded Studies

Title: Cellular and antibody responses to SARS-CoV-2 mRNA vaccination in the haemapoietic stem cell
Project Number:
Name of PD/PI: James Brien, PhD
Source of Support: NCI
Primary Place of Performance: Saint Louis University,

Project/Proposal Start and End Date: 09/2022 – 08/2023
Total Award Amount (including Indirect Costs):

Project Year	Person Months
09/22 – 08/23	1.2 CM

Title: Anti-Inflammatory Viral Proteins to Treat Sepsis
Project Number: PR192269
Name of PD/PI: Amelia K. Pinto, PhD
Source of Support: Department of Defense
Primary Place of Performance: Saint Louis University,
Project/Proposal Start and End Date: 07/2020 – 06/2023
Total Award Amount (including Indirect Costs):

Project Year	Person Months
09/20 – 08/21	2.4 CM
09/21 – 08/22	2.4 CM

Title: Vaccine and Treatment Evaluation Units (VTEU)
Project Number: HHSN27220130021
Name of PD/PI: Sarah George, MD
Source of Support: NIAID
Primary Place of Performance: Saint Louis University
Project/Proposal Start and End Date: 09/2013 – 09/2023
Total Award Amount (including Indirect Costs):

Project Year	Person Months
09/17 - 09/18	.24 CM
09/18 09/19	.24 CM
09/19 - 09/20	.24 CM
09/20 09/21	.24 CM
09/21 - 09/22	.24 CM
09/22 09/23	.24 CM

Title: Development of a Virus-Like Particle Vaccine for Powassan Virus
Project Number: 1 R01 AI15192
Name of PD/PI: Alec Hirsch, PhD
Source of Support: NIAID
Primary Place of Performance: Oregon Health & Sciences University,
Project/Proposal Start and End Date: 06/2020 – 05/2025
Subaward PD/PI: Amelia K. Pinto, PhD.
Place of Performance: Saint Louis University, Saint Louis, MO
Total Award Amount (including Indirect Costs):

Project Year	Person Months
06/21 – 05/22	1.8 CM
06/22 – 05/23	1.8 CM
06/23 – 05/24	2.4 CM
06/24 – 05/25	2.4 CM

Title: Dengue-Zika: correlates of cross-protection in non-human Primates
Project Number: R01 AI48264
Name of PD/PI: Carlos A. Sariol, MD
Source of Support: NIAID
Primary Place of Performance: University of Puerto Rico Med Sciences
Project/Proposal Start and End Date: 01/2020 – 12/2024
Subaward PD/PI: Amelia K. Pinto, PhD.
Place of Performance: Saint Louis University, Saint Louis, MO
Total Award Amount (including Indirect Costs):

Project Year	Person Months
01/22 - 12/22	0.6 CM
01/23 – 12/23	0.6 CM
01/24 – 12/24	0.6 CM

Title: Dengue virus mRNA lipid nanoparticle vaccine
Project Number: 1 R01 AI15067 01A1
Name of PD/PI: Justin Richner, PhD
Source of Support: NIAID
Primary Place of Performance: University of Illinois at Chicago
Project/Proposal Start and End Date: 08/2021 – 07/2025
Subaward PD/PI: Amelia K. Pinto PhD
Place of Performance: Saint Louis University, Saint Louis, MO
Total Award Amount (including Indirect Costs):

Project Year	Person Months
08/21 – 07/22	1.2 CM
08/22 – 07/23	2.4 CM
08/23 – 07/24	2.4 CM
08/24 – 07/25	2.4 CM

Title: SARS-CoV-2 correlates of protection in a Latino-origin population
Project Number: 1 U01 CA260541
Name of PD/PI: Carlos A. Sariol, MD
Source of Support: NCI
Primary Place of Performance: University of Puerto Rico Med Sciences
Project/Proposal Start and End Date: 09/2020 – 08/2024
Subaward PD/PI: James D. Brien, PhD
Role: Co-Investigator, Dr. Pinto
Subaward Place of Performance: Saint Louis University
Total Award Amount (including Indirect Costs):

Project Year	Person Months
09/20 – 08/21	1.2 CM
09/21 – 08/22	1.2 CM
09/22 – 08/23	1.2 CM
09/23 – 08/24	1.2 CM

Title: Evaluation of Antibody Responses Elicited by Zika Vaccination in Flavivirus-naïve and -experienced Individuals
Project Number: 1 R01 AI155983 01
Name of PD/PI: Shelly J Krebs (contact), Ph.D. Kayvon Modjarrad, MD
Source of Support: NIAID
Subaward PD/PI: James D. Brien, PhD
Role: Co-Investigator, Dr. Pinto
Primary Place of Performance: The Henry M. Jackson Foundation for the Advancement of Military Medicine, Inc, Bethesda, MD
Project/Proposal Start and End Date: 04/2021 – 03/2026
Total Award Amount (including Indirect Costs):

Project Year	Person Months
04/21 – 03/22	0.24 CM
04/23 – 03/24	0.24 CM
04/24 – 03/25	0.24 CM
04/25 – 03/26	0.24 CM

Contract Studies

Title: The use of humanized mice for SARS CoV-2 Research
Major Goals: The goal of this project is to study animal models for viral disease x.
Status of Support: Active
Project Number: A-01170
Name of PD/PI: Amelia K. Pinto, PhD
Source of Support: Jackson Labs (Bar Harbor, ME)
Primary Place of Performance: Saint Louis University, St. Louis, MO
Project/Proposal Start and End Date: 01/2021 – 04/2023
Total Award Amount (including Indirect Costs):

Project Year	Person Months
01/21 – 12/21	0.72 CM
01/22 – 12/22	0.72 CM
01/23 – 04/23	0.72 CM

Title: Preclinical Challenge Studies and Correlates of Protection for AdCOVID and mRNA-LNP COVID-19 vaccines in mice
Major Goals: Pre-clinical evaluation of Adenovirus SARS-CoV-2 vaccine in adult K18-hACE2 mice.
Status of Support: Active
Project Number: A-01255
Name of PD/PI: James D. Brien, PhD
Source of Support: Altimune (Gaithersburg, MD)
Primary Place of Performance: Saint Louis University, St. Louis, MO
Project/Proposal Start and End Date: 10/2020 – 09/2022
Total Award Amount (including Indirect Costs):

Project Year	Person Months
10/20 – 09/21	4.8 CM
10/21 – 09/22	4.8 CM

COMPLETED

Title: Transcriptional and functional profiling of cross-reactive T cells to understand outcomes for the pathogen and host during heterologous infection
Award Type: F31
Role: Mentor
Funding Amount: year
SLU grant total:
Start and End Date: 3/1/20-2/28/22

Title: *Vaccine and Treatment Evaluations Units Task 16-0033.D1.0086*
Award Type: NIH/NIAID HHSN 272201300014-16
PI: George,
Role: Co-investigator
Pinto lab total directs: year
SLU grant total: 1,020,609
Project Start and End: 09/25/17 – 02/28/22

Title: Novel humanized mouse models to study SARS-CoV-2 infection and pathogenesis
Award Type: Subcontract
Role: Co-Investigator
Funding Amount: year
SLU Contract total:
Start and End Date: 6/1/20-8/31/20

Title: In Vivo Safety Evaluation of Human Zika IVIG,
Award Type: Contract
Funder: Emergent Biosolutions
P.I.: Pinto
Role: Principal Investigator
Pinto lab total directs:
SLU grant total::
Project Start and End: 10/01/17-03/31/19

Title: Identification of Novel Zika Virus-specific HLA-A*02 T cell epitopes
Award Type: PRF
Funder: Saint Louis University
PI: Pinto
SLU grant total:
Project Start and End: 01/17/2017-01/18/2018

Title: In Vitro Safety Evaluation of Human Zika IVIG
Contract: Emergent Biosolutions
Role: Co-Investigator
Pinto lab total directs:
SLU grant total:
Start and End: 07/01/17-12/31/17

Title: Rapid Research Response to Zika Virus Infection in US Residents: Role Humoral and Cellular Immune Responses.
Award Type: HHSN 272201300021
P.I: Patel
Pinto lab total directs:year
Role: Co-Investigator
SLU grant total:
Start and End 04/13/16-03/09/22

Title: Development of a ribonucleoside analog to treat VEEV infections
Award Type: Subcontract
Funder Defense Threat Reduction Agency
PI: Emory University
Role: Co-Investigator
Pinto lab total directs:
SLU grant total:
Project Start and End: 12/11/14-6/30/17

Title: The Development/Optimization of a Drug for the Prophylaxis and Treatment of Alphavirus and Coronavirus Infections
Award Type: Subcontract
Funder: National Institutes of Health Proposal
PI: Emory University
Role: Co-Investigator
Pinto total directs:
SLU grant total:
Project Start and End: 7/30/14-6/29/17

PENDING

Title: Evaluation of an Adjuvanted Powassan Vaccine
Project Number: TB220056
Name of PD/PI: Amelia K. Pinto, PhD
Source of Support: Department of Defense
Primary Place of Performance: Saint Louis University,
Project/Proposal Start and End Date: 07/2023 – 06/2026
Total Award Amount (including Indirect Costs):

Project Year	Person Months
07/23 – 06/24	1.2 CM
07/24 – 06/25	2.4 CM
07/25 – 06/26	2.4 CM

Title: ACE2 inhibition and SARS-CoV-2 cognitive impairment -long-term implications for accelerated Alzheimer's Disease and related Dementias.
Status of Support: Pending
Project Number: 1 R21 AG 075449-01A1
Name of PD/PI: Amelia K. Pinto, PhD
Source of Support: NIH/Institute on Aging

Primary Place of Performance: Saint Louis University, Saint Louis, MO
Project/Proposal Start and End Date: 09/2022 – 08/2024
Total Award Amount

Project Year	Person Months
09/22 – 08/23	.6 CM
09/23 – 08/24	.6 CM

Title: Research into human disease-causing bunyaviruses using patient-derived xenografts (PDX) in vitro and in vivo
Status of Support: Pending
Project Number: 1 R01 AI 171433 01
Name of PD/PI: Amelia K. Pinto, PhD
Source of Support: NIAID
Primary Place of Performance: Saint Louis University, Saint Louis, MO
Project/Proposal Start and End Date: 07/2022 – 06/2027
Total Award Amount

Project Year	Person Months
07/22 – 06/23	3.6 CM
07/23 – 06/24	3.6 CM
07/24 – 06/25	3.6 CM
07/25 – 06/26	3.6 CM
07/26 – 06/27	3.6 CM

Title: Metabolic Syndrome's influence on the adaptive immune response to infection and vaccination
Status of Support: Pending
Project Number: 1 R01AI173196
Name of PD/PI: Amelia K. Pinto, PhD
Source of Support: NIAID
Primary Place of Performance: Saint Louis University, Saint Louis, MO
Project/Proposal Start and End Date: 12/2022 – 11/2027
Total Award Amount

Project Year	Person Months
12/22 – 11/23	6 CM
12/23 – 11/24	6 CM
12/24 – 11/25	6 CM
12/25 – 11/26	6 CM
12/26 – 11/27	6 CM

Title: Lipid Biology of SARS-CoV-2 Infection
Status of Support: Pending
Project Number: 1 R01 HL 161214-01A1
Name of PD/PI: David A Ford, PhD
Role: Co-Investigator
Source of Support: NHL
Primary Place of Performance: Saint Louis University, Saint Louis, MO
Project/Proposal Start and End Date: 09/2022 – 08/2027

Total Award Amount

Project Year	Person Months
09/22 – 08/23	1.2 CM
09/23 – 08/24	1.2 CM
09/24 – 08/25	1.2 CM
09/25 – 08/26	1.2 CM
09/26 – 08/27	1.2 CM

Publications

	Cited by	
	All	**Since 2017**
Citations	3319	1750
h-index	30	24
i10-index	45	40
Last Author	16	16

2022

Geerling E, Murphy V, Mai MC, Stone ET, Casals AG, Hassert M, O'Dea AT, Cao F, Donlin MJ, Elagawany M, Elgendy B, Pardali V, Giannakopoulou E, Zoidis G, Schiavone DV, Berkowitz AJ, Agyemang NB, Murelli RP, Tavis JE, Pinto AK, Brien JD. Metal coordinating inhibitors of Rift Valley fever virus replication PLoS One. 2022 Sep 16;17(9):e0274266. doi: 10.1371/journal.pone.0274266. eCollection 2022. PMID: 36112605

Marzan-Rivera N, Serrano-Collazo C, Cruz L, Pantoja P, Ortiz-Rosa A, Arana T, Martinez MI, Burgos AG, Roman C, Mendez LB, Geerling E, Pinto AK, Brien JD, Sariol CA. Infection order outweighs the role of CD4+ T cells in tertiary flavivirus exposure. iScience. 2022 Jul 16;25(8):104764. doi: 10.1016/j.isci.2022.104764. eCollection 2022 Aug 19. PMID: 35982798

Pike DP, McGuffee RM, Geerling E, Albert CJ, Hoft DF, Shashaty MGS, Meyer NJ, Pinto AK, Ford DA. Plasmalogen Loss in Sepsis and SARS-CoV-2 Infection. Front Cell Dev Biol. 2022 Jun 6;10:912880. doi: 10.3389/fcell.2022.912880.

Stone ET, Hirsch AJ, Smith JL, Brien JD, Pinto AK. Titration and neutralizing antibody quantification by focus forming assay for Powassan virus. STAR Protoc. 2022 Jun 17;3(3):101473. doi: 10.1016/j.xpro.2022.101473. eCollection 2022 Sep 16. PMID: 35755126

Karger AB, Brien JD, Christen JM, Dhakal S, Kemp TJ, Klein SL, Pinto LA, Premkumar L, Roback JD, Binder RA, Boehme KW, Boppana S, Cordon-Cardo C, Crawford JM, Daiss JL, Dupuis AP 2nd, Espino AM, Firpo-Betancourt A, Forconi C, Forrest JC, Girardin RC, Granger DA, Granger SW, Haddad NS, Heaney CD, Hunt DT, Kennedy JL, King CL, Krammer F, Kruczynski K, LaBaer J, Lee FE, Lee WT, Liu SL, Lozanski G, Lucas T, Mendu DR, Moormann AM,

Murugan V, Okoye NC, Pantoja P, Payne AF, Park J, Pinninti S, Pinto AK, Pisanic N, Qiu J, Sariol CA, Simon V, Song L, Steffen TL, Stone ET, Styer LM, Suthar MS, Thomas SN, Thyagarajan B, Wajnberg A, Yates JL, Sobhani K.The Serological Sciences Network (SeroNet) for COVID-19: Depth and Breadth of Serology Assays and Plans for Assay Harmonization. mSphere. 2022 Jun 15:e0019322. doi: 10.1128/msphere.00193-22. Online ahead of print. PMID: 35703544

Stone ET, Hassert M, Geerling E, Wagner C, Brien JD, Ebel GD, Hirsch AJ, German C, Smith JL, Pinto AK Balanced T and B cell responses are required for immune protection against Powassan virus in virus-like particle vaccination. Cell Rep. 2022 Feb 15;38(7):110388. doi: 10.1016/j.celrep.2022.110388. PMID: 35172138

Geerling E, Pinski AN, Stone TE, DiPaolo RJ, Zulu MZ, Maroney KJ, Brien JD, Messaoudi I, Pinto AK Roles of antiviral sensing and type I interferon signaling in the restriction of SARS-CoV-2 replication. iScience. 2022 Jan 21;25(1):103553. doi: 10.1016/j.isci.2021.103553. Epub 2021 Dec 3. PMID: 34877479

2021

Pinski AN, Steffen TL, Zulu MZ, George SL, Dickson A, Tifrea D, Maroney KJ, Tedeschi N, Zhang Y, Scheuermann RH, Pinto AK, Brien JD, Messaoudi I. Corticosteroid treatment in COVID-19 modulates host inflammatory responses and transcriptional signatures of immune dysregulation. J Leukoc Biol. 2021 Dec;110(6):1225-1239. DOI: 10.1002/JLB.4COVA0121-084RR. Epub 2021 Nov 3.PMID: 34730254

Sariol CA, Pantoja P, Serrano-Collazo C, Rosa-Arocho T, Armina-Rodrguez A, Cruz L, Stone ETT, Arana T, Climent C, Latoni G, Atehortua D, Pabon-Carrero C, Pinto AK, Brien JD, Espino AM. Function Is More Reliable than Quantity to Follow Up the Humoral Response to the Receptor-Binding Domain of SARS-CoV-2-Spike Protein after Natural Infection or COVID-19 Vaccination. Viruses. 2021 Sep 30;13(10):1972. DOI: 10.3390/v13101972.PMID: 34696403

Pinto AK, Hassert M, Han X, Barker D, Carnelley T, Branche E, Steffen TL, Stone ET, Geerling E, Viramontes KM, Nykiforuk C, Toth D, Shresta S, Kodihalli S, Brien JD. The Ability of Zika virus Intravenous Immunoglobulin to Protect From or Enhance Zika Virus Disease. Front Immunol. 2021 Sep 6;12:717425. DOI: 10.3389/fimmu.2021.717425. eCollection 2021.PMID: 34552587

Geerling E, Stone ET, Steffen TL, Hassert M, Brien JD, Pinto AK. Obesity Enhances Disease Severity in Female Mice Following West Nile Virus Infection. Front Immunol. 2021 Aug 31;12:739025. DOI: 10.3389/fimmu.2021.739025. eCollection 2021.PMID: 34531877

King RG, Silva-Sanchez A, Peel JN, Botta D, Dickson AM, Pinto AK, Meza-Perez S, Allie SR, Schultz MD, Liu M, Bradley JE, Qiu S, Yang G, Zhou F, Zumaquero E, Simpler TS, Mousseau B, Killian JT Jr, Dean B, Shang Q, Tipper JL, Risley CA, Harrod KS, Feng T, Lee Y, Shiberu B, Krishnan V, Peguillet I, Zhang J, Green TJ, Randall TD, Suschak JJ, Georges B, Brien JD, Lund FE, Roberts MS. Single-Dose Intranasal Administration of AdCOVID Elicits Systemic and Mucosal Immunity against SARS-CoV-2 and Fully Protects Mice from Lethal Challenge. Vaccines (Basel). 2021 Aug 9;9(8):881. DOI: 10.3390/vaccines9080881.PMID: 34452006

Grady SF, Pinto AK, Hassert M, D'Angelo JA, Brien JD, Arnatt CK. Selective estrogen receptor modulator, tamoxifen, inhibits Zika virus infection J Med Virol. 2021 Nov;93(11):6155-6162. DOI: 10.1002/jmv.27230. Epub 2021 Aug 4. PMID: 34314058

Hassert M, Steffen TL, Scroggins S, Coleman AK, Shacham E, Brien JD, Pinto AK Prior Heterologous Flavivirus Exposure Results in Reduced Pathogenesis in a Mouse Model of Zika Virus Infection. .J Virol. 2021 Jul 26;95(16):e0057321. DOI: 10.1128/JVI.00573-21. Epub 2021 Jul 26.PMID: 34076486

Wollner CJ, Richner M, Hassert MA, Pinto AK, Brien JD, Richner JM.J A Dengue Virus Serotype 1 mRNA-LNP Vaccine Elicits Protective Immune Responses. Virol. 2021 May 24;95(12):e02482-20. DOI: 10.1128/JVI.02482-20. Print 2021 May 24.PMID: 33762420

Khojandi N, Kuehm LM, Piening A, Donlin MJ, Hsueh EC, Schwartz TL, Farrell K, Richart JM, Geerling E, Pinto AK, George SL, Albert CJ, Ford DA, Chen X, Kline J, Teague RM Oxidized Lipoproteins Promote Resistance to Cancer Immunotherapy Independent of Patient Obesity.Cancer Immunol Res. 2021 Feb;9(2):214-226. DOI: 10.1158/2326-6066.CIR-20-0358. Epub 2020 Dec 10.PMID: 33303575

2020

Hassert M, Geerling E, Stone ET, Steffen TL, Feldman MS, Dickson AL, Class J, Richner JM, Brien JD, Pinto AK. mRNA induced expression of human angiotensin-converting enzyme 2 in mice for the study of the adaptive immune response to severe acute respiratory syndrome coronavirus 2.PLoS Pathog. 2020 Dec 16;16(12):e1009163. DOI: 10.1371/journal.ppat.1009163. Online ahead of print. PMID: 33326500.

Patra T, Meyer K, Geerling L, Isbell TS, Hoft DF, Brien J, Pinto AK, Ray RB, Ray R. SARS-CoV-2 spike protein promotes IL-6 trans-signaling by activation of angiotensin II receptor signaling in epithelial cells. PLoS Pathog. 2020 Dec 7;16(12):e1009128. DOI. eCollection 2020 Dec.PMID: 33284859 .

Hassert M, Wolf KJ, Rajeh A, Schiebout C, Hoft SG, Ahn TH, DiPaolo RJ, Brien JD, Pinto AK. Diagnostic differentiation of Zika and dengue virus exposure by analyzing T cell receptor sequences from peripheral blood of infected HLA-A2 transgenic mice. PLoS Negl Trop Dis. 2020 Dec 3;14(12):e0008896. DOI: 10.1371/journal.pntd.0008896. eCollection 2020 Dec.PMID: 33270635

Vijayalingam S, Ezekiel UR, Xu F, Subramanian T, Geerling E, Hoelscher B, San K, Ganapathy A, Pemberton K, Tycksen E, Pinto AK, Brien JD, Beck DB, Chung WK, Gurnett CA, Chinnadurai G. Human iPSC-Derived Neuronal Cells From CTBP1-Mutated Patients Reveal Altered Expression of Neurodevelopmental Gene Networks. Front. Neurosci. 2020 Oct 27;14:562292. doi: 10.3389/fnins.2020.562292. eCollection 2020.PMID: 33192249

Serrano-Collazo C, Perez-Guzman EX, Pantoja P, Hassert MA, Rodriguez IV, Giavedoni L, Hodara V, Parodi L, Cruz L, Arana T, Martinez MI, White L, Brien JD, de Silva A, Pinto AK, Sariol CA. Effective control of early Zika virus replication by Dengue immunity is associated to the length of time between the 2 infections but not mediated by antibodies. PLoS Negl Trop Dis. 2020;14(5):e0008285. Epub 2020/05/29. doi: 10.1371/journal.pntd.0008285. PubMed PMID: 32463814; PMCID: PMC7255596.

Steffen T, Hassert M, Hoft SG, Stone ET, Zhang J, Geerling E, Grimberg BT, Roberts MS, Pinto AK, Brien JD. Immunogenicity and Efficacy of a Recombinant Human Adenovirus Type 5 Vaccine against Zika Virus. Vaccines (Basel). 2020;8(2). Epub 2020/04/11. doi: 10.3390/vaccines8020170. PubMed PMID: 32272595; PMCID: PMC7349816.

Dussupt V, Sankhala RS, Gromowski GD, Donofrio G, De La Barrera RA, Larocca RA, Zaky W, Mendez-Rivera L, Choe M, Davidson E, McCracken MK, Brien JD, Abbink P, Bai H, Bryan AL, Bias CH, Berry IM, Botero N, Cook T, Doria-Rose NA, Escuer AGI, Frimpong JA, Geretz A, Hernandez M, Hollidge BS, Jian N, Kabra K, Leggat DJ, Liu J, Pinto AK, Rutvisuttinunt W, Setliff I, Tran U, Townsley S, Doranz BJ, Rolland M, McDermott AB, Georgiev IS, Thomas R, Robb ML, Eckels KH, Barranco E, Koren M, Smith DR, Jarman RG, George SL, Stephenson KE, Barouch DH, Modjarrad K, Michael NL, Joyce MG, Krebs SJ. Potent Zika and dengue cross-neutralizing antibodies induced by Zika vaccination in a dengue-experienced donor. Nat Med. 2020 Feb;26(2):228-235. doi: 10.1038/s41591-019-0746-2. Epub 2020 Feb 3. PMID: 32015557

de Oliveira LC, Ribeiro AM, Albarnaz JD, Torres AA, Guimarães LFZ, Pinto AK, Parker S, Doronin K, Brien JD, Buller MR, Bonjardim CA.The small molecule AZD6244 inhibits dengue virus replication in vitro and protects against lethal

challenge in a mouse model.Arch Virol. 2020 Mar;165(3):671-681. doi: 10.1007/s00705-020-04524-7. Epub 2020 Jan 16. PMID: 31942645

2019

Pérez-Guzmán EX, Pantoja P, Serrano-Collazo C, Hassert MA, Ortiz-Rosa A, Rodríguez IV, Giavedoni L, Hodara V, Parodi L, Cruz L, Arana T, White LJ, Martínez MI, Weiskopf D, Brien JD, de Silva A, Pinto AK, Sariol CA. Time elapsed between Zika and dengue virus infections affects antibody and T cell responses. Nat Commun. 2019 Sep 20;10(1):4316. doi: 10.1038/s41467-019-12295-2. PMID: 31541110

Brien JD, Hassert M, Stone ET, Geerling E, Cruz Orengo L, Pinto AK, Isolation and quantification of Zika virus from multiple organs in a mouse. JOVE J Vis Exp. 2019 Aug 15;(150). doi: 10.3791/5963

Hassert M, Harris MG, Brien JD, Pinto AK Identification of a Protective CD8 T Cell Responses in a Mouse Model of Zika Virus Infection. Front Immunol. 2019 July: doi: 10.3389/fimmu.2019.01678

2018

Hassert H, Wolf KJ, Schwetye KE, DiPaolo RJ, Brien JD, Pinto AK, $CD4^{+}$T cells mediate protection against Zika-associated severe disease in a mouse model of infection. PLoS Pathogens 2018 Sept2018 Sep 13;14(9):e1007237. doi: 10.1371/journal.ppat.1007237. eCollection 2018 Sep. PubMed PMID: 30212537

2017

Pantoja P, Pérez-Guzmán EX, Rodríguez IV, White LJ, González O, Serrano C, Giavedoni L, Hodara V, Cruz L, Arana T, Martínez MI, Hassert MA, Brien JD, Pinto AK, de Silva A, Sariol CA. Zika virus pathogenesis in rhesus macaques is unaffected by pre-existing immunity to dengue virus. Nat Commun. 2017 Jun 23;8:15674. doi: 10.1038/ncomms15674. PMID: 28643775

2016

Williams GD, Pinto AK, Doll B, Boon AC. A North American H7N3 Influenza Virus Supports Reassortment with 2009 Pandemic H1N1 and Induces Disease in Mice without Prior Adaptation. Journal of Virology 2016 Apr 14;90(9):4796-806. PMID: 26937034

DesRochers BL, Chen RE, Gounder AP, Pinto AK, Bricker T, Linton CN, Rogers CD, Williams GD, Webby RJ, Boon AC. Residues in the PB2 and PA genes contribute to the pathogenicity of avian H7N3 influenza A virus in DBA/2 mice. Virology. 2016 Apr 19;494:89-99 PMID: 27105450

2015

Proenca-Modena JL, Hyde JL, Sesti-Costa R, Lucas T, Pinto AK, Richner JM, Gorman MJ, Lazear HM, Diamond MS. IRF-5-dependent signaling restricts

Orthobunyavirus dissemination to the central nervous system. J Virol. 2015 Oct 14;90(1):189-205. doi: 10.1128/JVI.02276-15. Print 2016 Jan 1. PMID: 26468541

Pinto AK*, Brien JD*, Chia-Ying KL, Johnson S, Chiang C, Hiscott J, Sarathy VV, Barett AD, Shresta S, Diamond MS. 2015. Defining New Therapeutics Using a More Immunocompetent Mouse Model of Antibody-Enhanced Dengue Virus Infection. mBio. 2015 Sep 15;6(5):e01316-15. doi: 10.1128/mBio.01316-15. PMID: 26374123

Pinto AK, Williams G, Szretter K, White J, Proenca-Modena J, Liu G, Olejnik J, Brien JD, Ebihara H, Mühlberger E, Amarasinghe G, Diamond MS, and Boon A, 2015. Human and murine IFIT1 do not restrict infection of negative-sense RNA viruses of the orthomyxoviridae, bunyaviridae, and filoviridae families. J Virol. 2015 Sep;89(18):9465-76. doi: 10.1128/JVI.00996-15. Epub 2015 Jul 8. PMID: 26157117

Proenca-Modena JL, Sesti-Costa R, Pinto AK, Richner JM, Lazear HM, Lucas T, Hyde JL, Diamond MS. Oropouche virus infection and pathogenesis is restricted by MAVS, IRF-3, IRF-7, and type I IFN signaling pathways in non-myeloid cells. J Virol. 2015 May;89(9):4720-37. doi: 10.1128/JVI.00077-15. Epub 2015 Feb 25. PMID: 25717109

Lazear HM, Daniels BP, Pinto AK, Albert Huang A, Vick SC, Gale M., Klein RS, and Diamond MS. Interferon lambda restricts West Nile virus neuroinvasion by enhancing integrity of the blood-brain barrier. Sci Transl Med. 2015 Apr 22;7(284):284ra59. doi: 10.1126/scitranslmed.aaa4304. PMID: 25904743

2014

Thackray LB, Shrestha B, Richner JM, Miner JJ, Pinto AK, Lazear HM, Gale M Jr, Diamond MS. Interferon regulatory factor 5 (IRF5)-dependent immune responses in the draining lymph node protect against West Nile virus infection. J Virol. 2014 Oct;88(19):11007-21. doi: 10.1128/JVI.01545-14. Epub 2014 Jul 16. PMID: 25031348

Chou C, Pinto AK, Curtis JD, Persaud SP, Cella M, Lin CC, Edelson BT, Allen PM, Colonna M, Pearce EL, Diamond MS, Egawa T. c-Myc-induced transcription factor AP4 is required for host protection mediated by CD8+ T cells. Nat Immunol. 2014 Sep;15(9):884-93. doi: 10.1038/ni.2943. Epub 2014 Jul 13. PMID: 25029552

Kim, S*, Pinto, AK*, Myers, NB, Weidanz, JA, Hildebrand, WH, Diamond, MS, and Hansen, TH, Use of a novel T cell receptor mimic to define cells that cross-present an immunodominant West Nile virus epitope in mice. European Journal of Immunology 2014 Jul;44(7):1936-46. (*co-first author)

Pinto, AK, Ramos, HJ, Wu, X, Aggarwal, S, Shrestha, B, Gorman, M, Kristin Y. Kim, KY, Suthar, MS, Atkinson, JP, Gale, M, and Diamond, MS, A loss of IFN signaling in myeloid cells results in a MAVS-dependent sepsis after viral infection. PLoS Pathog. 2014 Apr 17;10(4):e1004086. doi: 10.1371/journal.ppat.1004086. eCollection 2014 Apr. PMID: 24743949

2013

Lazear HM, Pinto AK, Ramos HJ, Vick S, Shrethsa B, Suthar MS, Gale M Jr., and Diamond MS, Pattern recognition receptor MDA5 modulates CD8+T cell-dependent clearance of West Nile virus from the central nervous system. J Virol. 2013 Nov;87(21):11401-15. doi: 10.1128/JVI.01403-13. Epub 2013 Aug 21. PMID: 23966390

Nelson AM, Elftman MD, Pinto AK, Baldridge M, Hooper P, Kuczynski J, Petrosino JF, Young VB, Wobus CE. Murine norovirus infection does not cause major disruptions in the murine intestinal microbiota. Microbiome. Microbiome. 2013 Feb 18;1(1):7. doi: 10.1186/2049-2618-1-7. PMID: 24451302

Pinto AK, Richner J, Poore E, Patil P, Amanna I, Slifka M, and Diamond MS A hydrogen peroxide-inactivated virus vaccine elicits humoral and cellular immunity and protects against lethal West Nile virus infection in aged mice. J Virol. 2013 Feb;87(4):1926-36. doi: 10.1128/JVI.02903-12. Epub 2012 Dec 5. PMID: 23221549

2012

Shrestha B, Pinto AK, Green S, Bosch I, Diamond MS. CD8+ T cells use TRAIL to restrict West Nile virus pathogenesis by controlling infection in neurons. J Virol. 2012 Sep;86(17):8937-48. doi: 10.1128/JVI.00673-12. Epub 2012 Jun 27. PMID: 22740407

Markiewicz MA, Wise EL, Buchwald ZS, Pinto AK, Zafirova B, Polic B, and Shaw AS. RAE1 ligand expressed on pancreatic islets recruits NKG2D receptor-expressing cytotoxic T cells independent of T cell receptor recognition. Immunity. 2012 Jan 27;36(1):132-41. doi: 10.1016/j.immuni.2011.11.014. Epub 2012 Jan 12. PMID: 22244846

2011

Pinto AK, Daffis S, Brien JD, Gainey MD, Yokoyama WM, Sheehan KCF, Murphy KM, Schreiber RD, Diamond MS. A temporal role of type I interferon signaling in CD8+ T cell maturation during acute West Nile virus infection PLoS Pathog. 2011 Dec;7(12):e1002407. doi: 10.1371/journal.ppat.1002407. Epub 2011 Dec 1. PMID: 22144897

Schlub TE, Sun JC, Walton SM, Robbins SH, Pinto AK, Munks MW, Hill AB, Brossay L, Oxenius A, Davenport MP. Comparing the Kinetics of NK Cells, CD4, and CD8 T Cells in Murine Cytomegalovirus Infection. J Immunol. 2011 Aug

1;187(3):1385-92. doi: 10.4049/jimmunol.1100416. Epub 2011 Jun 22. PMID: 21697462

Lazear HM, Pinto AK, Vogt MR, Gale M Jr, Diamond MS. Interferon-{beta} controls West Nile virus infection and pathogenesis in mice. J Virol. 2011 Jul;85(14):7186-94. doi: 10.1128/JVI.00396-11. Epub 2011 May 4. PMID: 21543483

Fuchs A, Pinto AK, Schwaeble WJ, Diamond MS. The lectin pathway of complement activation contributes to protection from West Nile virus infection. Virology. 2011 Mar 30;412(1):101-9. doi: 10.1016/j.virol.2011.01.003. Epub 2011 Jan 26. PMID: 21269656

2009

Ammann CG, Messer RJ, Varvel K, Debuysscher BL, Lacasse RA, Pinto AK, Hasenkrug KJ. Effects of acute and chronic murine norovirus infections on immune responses and recovery from Friend retrovirus infection. J J Virol. 2009 Dec;83(24):13037-41. doi: 10.1128/JVI.01445-09. Epub 2009 Oct 7. PMID: 19812147.

Hensley SE, Pinto AK, Hickman HD, Kastenmayer RJ, Bennink JR, Virgin HW, Yewdell JW. Murine norovirus infection has no significant effect on adaptive immunity to vaccinia virus or influenza A virus. J Virol. 2009 Jul;83(14):7357-60. DOI: 10.1128/JVI.00623-09. Epub 2009 Apr 29. PMID: 19403665

2007

Pinto AK, Jamieson AM, Raulet DH, Hill AB. The role of NKG2D signaling in inhibition of CTL lysis of murine cytomegalovirus infected cells by m152/gp40. J Virol. 2007 Nov;81(22):12564-71. DOI: 10.1128/JVI.01328-07. Epub 2007 Sep 12. PMID: 17855532

Munks MW, Pinto AK, Doom CM, Hill AB. Viral interference with antigen presentation does not alter acute or chronic CD8 T cell immunodominance in murine cytomegalovirus infection. J Immunol. 2007 Jun 1;178(11):7235-41. DOI: 10.4049/jimmunol.178.11.7235. PMID: 17513772

2006

Pinto AK, Munks MW, Koszinowski UH, Hill AB. Coordinated function of murine cytomegalovirus genes completely inhibits CTL lysis. J Immunol. 2006 Sep 1;177(5):3225-34. DOI: 10.4049/jimmunol.177.5.3225. PMID: 16920962

Munks MW, Cho KS, Pinto AK, Sierro S, Klenerman P, Hill AB. Four distinct patterns of memory CD8 T cell responses to chronic murine cytomegalovirus infection. J Immunol. 2006 Jul 1;177(1):450-8. DOI: 10.4049/jimmunol.177.1.450. PMID: 16785542

Lu X, Pinto AK, Kelly AM, Cho KS, Hill AB. Murine cytomegalovirus interference with antigen presentation contributes to the inability of CD8 T cells to control virus in the salivary gland. J Virol. 2006 Apr;80(8):4200-2. DOI: 10.1128/JVI.80.8.4200-4202.2006. PMID: 16571839.

2000-2002

Brehm MA, Pinto AK, Daniels KA, Schneck JP, Welsh RM, Selin LK. T cell immunodominance and maintenance of memory regulated by unexpectedly cross-reactive pathogens. Nat Immunol. 2002 Jul;3(7):627-34. DOI: 10.1038/ni806. Epub 2002 Jun 3. PMID: 12055626.

Selin LK, Santolucito PA, Pinto AK, Szomolanyi-Tsuda E, Welsh RM. Innate immunity to viruses: control of vaccinia virus infection by gamma delta T cells. J Immunol. 2001 Jun 1;166(11):6784-94. DOI: 10.4049/jimmunol.166.11.6784 PMID: 11359837

Selin LK, Lin MY, Kraemer KA, Pardoll DM, Schneck JP, Varga SM, Santolucito PA, Pinto AK, Welsh RM. Attrition of T cell memory: selective loss of LCMV epitope-specific memory CD8 T cells following infections with heterologous viruses. Immunity. 1999 Dec;11(6):733-42. DOI: 10.1016/s1074-7613(00)80147-8. PMID: 10626895

Reviews:

Nasr MC, Geerling E, and Pinto AK. Impact of Obesity on Vaccination to SARS-CoV-2 Front. Endocrinol., 20 June 2022 | https://doi.org/10.3389/fendo.2022.898810

Geerling E, Steffen TL, Brien JD, Pinto AK. Current Flavivirus Research Important for Vaccine Development. Vaccines (Basel). 2020 Aug 27;8(3):477. DOI. PMID: 32867038

Hassert M, Brien JD, Pinto AK. Mouse Models of Heterologous Flavivirus Immunity: A Role for Cross-Reactive T Cells. Front Immunol. 2019 May 9;10:1045. Doi 10.3389/fimmu.2019.01045. PMID: 31143185

Hassert H, Brien JD, Pinto AK, The Temporal Role of Cytokines in Flavivirus Protection and Pathogenesis Curr Clin Micro Rpt (2018).

Pinto AK, Hill AB. Viral interference with antigen presentation to CD8+ T cells: lessons from cytomegalovirus. Viral Immunol. 2005;18(3):434-44. DOI: 10.1089/vim.2005.18.434.PMID: 16212522

Abstracts and Commentaries

Grady, S., Pinto, AK., Hassert, M., Brien, JD. and Arnatt, C. (2021), Tamoxifen as a Zika Virus Therapeutic. The FASEB Journal, 35:. https://doi.org/10.1096/fasebj.2021.35.S1.04991

Perez-Guzman, E.X., Pantoja, P., Serrano-Collazo, C., Hassert, M.A., Ortiz, A., Rodriguez, I.V., Giavedoni, L., Hodara, V., Parodi, L., Cruz, L. and Arana, T. White, L, Martinez, ML, Weiskopf D., Brien J.D., de Silva A., Pinto A.K., Sariol, C.A. Previous Zika exposure improves immune response against dengue without pathogenesis enhancement in rhesus macaques." in American journal of tropical medicine and hygiene, vol. 101, pp. 419-419. 2019.

Serrano-Collazo C., Pantoja, P., Cruz, L. A., Perez, E. X., Rodriguez, I. V., Arana, T., Martinez M., Hassert M., White LJ, Brien J.D., Hodara V., Giavedoni L., de Silva A., Pinto A.K., Sariol, C. A Primary Dengue infection modulates Zika pathogenesis in a time-dependent manner American Journal of Tropical Medicine and Hygiene, 2019.

Brien JB and Pinto AK, First case of Zika sexual transmission from female to male reported. Genetic Experts News Services, July 15, 2016

Pinto AK, First primate model of Zika virus infection allows scientists to study new treatments. Genetic Experts News Services, June 28, 2016

Pinto AK, Antibody protects mice against Zika infection. Genetic Experts News Services, May 2, 2016

Pinto AK, Zika virus infects lab-grown brain cells, suggests link to birth defects. Genetic Experts News Services, March 4, 2016

Hill AB, Munks M, C Doom, C, Pinto AK Immunodominance hierarchy and the effect of immune evasion in the CD8T cell response to murine cytomegalovirus Faseb Journal 19 (4), a392-a392

Pinto AK, Slifka MK Hidden death gene in 'flu Trends in Microbiology, v10, i2, p65, February 1, 2002, DOI:https://doi.org/10.1016/S0966-842X(02)02304-1

Selin LK, Lin MY, Santolucito PA, Pinto AK, Welsh RM Selective alterations in viral epitope-specific CD8 T cell responses as a consequence of infections with heterologous viruses. 2000 FASEB JOURNAL 14 (6), A978-A978 2000

Brehm M, Pinto AK, Satolucito PA, Welsh RM, Selin LK Cross-reactive CTL epitopes between heterologous viruses. 1999 FASEB JOURNAL 14 (6), A979-A979

Selin LK, Santolucito P, Pinto AK, Welsh RM. Early natural immunity mediated by gamma delta T cells in vaccinia virus (VV) infection. Faseb Journal 13 (4), A638-A638

SARS-CoV-2 studies not peer-reviewed

To aid in the immediate sharing of information during the SARS-CoV-2 pandemic, I was involved in multiple studies where data was published before peer review. These studies were referenced and used to inform the scientific community. Publications with an asterisk* contain some data that was then used in peer-reviewed publications. Other non-peer-reviewed published studies are ongoing, and some of the data may be used in future peer-reviewed journals.

*Karger AB, Brien JD, Christen JM, Dhakal S, Kemp TJ, Klein SL, Pinto LA, Premkumar L, Roback JD, Binder RA, Boehme KW, Boppana S, Cordon-Cardo C, Crawford JM, Daiss JL, Dupuis AP, Espino AM, Firpo-Betancourt A, Forconi C, Forrest JC, Girardin RC, Granger DA, Granger SW, Haddad NS, Heaney CD, Hunt DT, Kennedy JL, King CL, Krammer F, Kruczynski K, LaBaer J, Lee FE, Lee WT, Liu SL, Lozanski G, Lucas T, Mendu DR, Moormann AM, Murugan V, Okoye NC, Pantoja P, Payne AF, Park J, Pinninti S, Pinto AK, Pisanic N, Qiu J, Sariol CA, Simon V, Song L, Steffen TL, Stone ET, Styer LM, Suthar MS, Thomas SN, Thyagarajan B, Wajnberg A, Yates JL, Sobhani K. The Serological Sciences Network (SeroNet) for COVID-19: Depth and Breadth of Serology Assays and Plans for Assay Harmonization. medRxiv. 2022 Mar doi: 10.1101/2022.02.27.22271399. Preprint. PMID: 35262095

*Sariol CA, Pantoja P, Serrano-Collazo C, Rosa-Arocho T, Armina A, Cruz L, Stone ET, Arana T, Climent C, Latoni G, Atehortua D, Pabon-Carrero C, Pinto AK, Brien JD, Espino AM. Function is more reliable than quantity to follow up the humoral response to the Receptor Binding Domain of SARS- CoV-2 Spike protein after natural infection or COVID-19 vaccination. medRxiv. 2021 Aug 10:2021.06.02.21257975. Doi: 10.1101/2021.06.02.21257975. Preprint.PMID: 34100029

*Stone ET, Geerling E, Steffen TL, Hassert M, Dickson A, Spencer JF, Toth K, DiPaolo RJ, Brien JD, Pinto AK. Characterization of cells susceptible to SARS-COV-2 and methods for detection of neutralizing antibody by focus forming assay. bioRxiv. 2020:2020.08.20.259838. Doi: 10.1101/2020.08.20.259838.

Steffen TL, Stone ET, Hassert M, Geerling E, Grimberg BT, Espino AM, Pantoja P, Climent C, Hoft DF, George SL, Sariol CA, Pinto AK, Brien JD. The receptor-binding domain of SARS-CoV-2 spike is the key target of neutralizing antibody in human polyclonal sera. bioRxiv. 2020:2020.08.21.261727. DOI. (Co-corresponding)

*Hassert M, Geerling E, Stone ET, Steffen TL, Dickson A, Feldman MS, Class J, Richner JM, Brien JD, Pinto AK. mRNA induced expression of human angiotensin-converting enzyme 2 in mice for the study of the adaptive immune response to severe acute respiratory syndrome coronavirus 2.bioRxiv. 2020 Aug 7:2020.08.07.241877. Doi: 10.1101/2020.08.07.241877. Preprint. PMID: 32793909

Supplemental Material

Invited Speaker:	
American Association of Virologists Annual Meeting	2022
Western Carolina University	2021
Oregon Health and Sciences University	2021
COVID research at Saint Louis University	2020
Cortex Venture Café series, Emerging Infections	2020
University of Massachusetts School of Medicine, Pathology lecture	2019
University of Missouri S&T, Metabolic Systems Lecture Series	2018
American Association of Virologists Annual Meeting, New Faculty	2017
Saint Louis University, Graduate Symposium	2017
Southern Illinois University, Carbondale	2016
Washington University SOM, Immunology Series	2015
University of California Davis, Virology Lecture	2015
Boston University: National Emerging Infectious Disease Laboratory	2015
Imperial College, London,	2014
University of Alabama Birmingham School of Medicine	2014
American Association of Virologists Annual Meeting, Emerging Viruses	2014
University of Colorado School of Medicine, Immunology lecture	2014
University of California Riverside Mammalian Virology lecture	2014
Cold Spring Harbor, New Investigator lecture-Emerging Viral infections	2014

PATENTS

Full US patent submitted: Arnatt, C., Pinto, A., Brien, J., US 17/290,400. *Tamoxifen as a treatment for zika virus infection and uses thereof*.

Full US patent submitted: Tavis, J.E., Zoidis, G., Pinto, A., Brien, J., Murelli, R. US 63/023,576. *Inhibitors of Bunyaviridae and uses thereof*.

Intellectual Property Disclosure Patent for Inhibitors of SARS-CoV-2 virus Andy Nguyen, James Brien, and Amelia Pinto 2020

Full US patent submitted: Roberts, S. Pinto, A., Brien, J., Patent Number: 62/985,672 *Zika virus Immunogenic compositions and their use.*

Provisional US patent submitted: Bonjardim, C.A., Oliveira, L.C., Ribeiro, A.M., Pinto, A., Buller, R.M., Parker, S. Patent Number: USTL.P0078US.P1*Treatment for Flavivirus Infection.*

AMERICAN SOCIETY FOR MICROBIOLOGY | Journal of Virology®

VACCINES AND ANTIVIRAL AGENTS

A Dengue Virus Serotype 1 mRNA-LNP Vaccine Elicits Protective Immune Responses

Clayton J. Wollner,[a] Michelle Richner,[a] Mariah A. Hassert,[b] Amelia K. Pinto,[b] James D. Brien,[b] Justin M. Richner[a]

[a]Department of Microbiology and Immunology, University of Illinois College of Medicine, Chicago, Illinois, USA
[b]Department of Molecular Microbiology and Immunology, St. Louis University College of Medicine, St. Louis, Missouri, USA

ABSTRACT Dengue virus (DENV) is the most common vector-borne viral disease, with nearly 400 million worldwide infections each year concentrated in the tropical and subtropical regions of the world. Severe dengue complications are often associated with a secondary heterotypic infection of one of the four circulating serotypes. In this scenario, humoral immune responses targeting cross-reactive, poorly neutralizing epitopes can lead to increased infectivity of susceptible cells via antibody-dependent enhancement (ADE). In this way, antibodies produced in response to infection or vaccination are capable of contributing to enhanced disease in subsequent infections. Currently, there are no available therapeutics to combat DENV disease, and there is an urgent need for a safe and efficacious vaccine. Here, we developed a nucleotide-modified mRNA vaccine encoding the membrane and envelope structural proteins from DENV serotype 1 encapsulated in lipid nanoparticles (prM/E mRNA-LNP). Vaccination of mice elicited robust antiviral immune responses comparable to viral infection, with high levels of neutralizing antibody titers and antiviral $CD4^+$ and $CD8^+$ T cells. Immunocompromised AG129 mice vaccinated with the prM/E mRNA-LNP vaccine were protected from a lethal DENV challenge. Vaccination with either a wild-type vaccine or a vaccine with mutations in the immunodominant fusion loop epitope elicited equivalent humoral and cell-mediated immune responses. Neutralizing antibodies elicited by the vaccine were sufficient to protect against a lethal challenge. Both vaccine constructs demonstrated serotype-specific immunity with minimal serum cross-reactivity and reduced ADE in comparison to a live DENV1 viral infection.

IMPORTANCE With 400 million worldwide infections each year, dengue is the most common vector-borne viral disease. Forty percent of the world's population is at risk, with dengue experiencing consistent geographic spread over the years. With no therapeutics available and vaccines performing suboptimally, the need for an effective dengue vaccine is urgent. Here, we develop and characterize a novel mRNA vaccine encoding the dengue serotype 1 envelope and premembrane structural proteins that is delivered via a lipid nanoparticle. Our DENV1 prM/E mRNA-LNP vaccine induces neutralizing antibody and cellular immune responses in immunocompetent mice and protects an immunocompromised mouse from a lethal DENV challenge. Existing antibodies against dengue can enhance subsequent infections via antibody-dependent enhancement (ADE). Importantly our vaccine induced only serotype-specific immune responses and did not induce ADE.

KEYWORDS dengue fever, mRNA vaccine, vaccines

Dengue virus (DENV) is the most common vector-borne viral disease affecting humans (1–3). Its region of endemicity now includes 100 countries in Asia, the Pacific, the Americas, and the Middle East (3), with 40% of the world's population at risk. Disease states during dengue infection manifest as a range of severities, from a

Citation Wollner CJ, Richner M, Hassert MA, Pinto AK, Brien JD, Richner JM. 2021. A dengue virus serotype 1 mRNA-LNP vaccine elicits protective immune responses. J Virol 95:e02482-20. https://doi.org/10.1128/JVI.02482-20.

Editor Mark T. Heise, University of North Carolina at Chapel Hill

Address correspondence to Justin M. Richner, richner@uic.edu.

Received 5 January 2021
Accepted 18 March 2021
Accepted manuscript posted online 24 March 2021
Published 24 May 2021

self-limiting, febrile illness to more severe cases with life-threatening vascular leakage that can lead to multiorgan failure associated with a virus-driven cytokine storm (4, 5).

DENV is a member of the family *Flaviviridae* of which Zika virus, West Nile virus, yellow fever virus, and Japanese encephalitis virus are also members. It is spread by the arthropod vector *Aedes aegypti* and, to a much lesser extent, *Aedes albopictus* (2, 3). The virus contains a single-stranded, positive-sense RNA genome which codes for a single polypeptide containing three structural proteins, premembrane (prM), envelope (E), and capsid (C), as well as seven nonstructural proteins (6). Dengue virus is categorized into four distinct serotypes, dengue serotypes 1 to 4 (DENV1 to DENV4), with amino acid sequence variations of 30 to 35% across serotypes.

Most countries where dengue is endemic are affected by all four serotypes (1). Infection with a single serotype of DENV does not protect against a secondary infection of a heterologous serotype. Instead, primary infection increases an individual's probability of developing severe clinical symptoms, including shock and death, upon a secondary heterotypic challenge. In this scenario, humoral immune responses after a primary infection produce cross-reactive, nonneutralizing antibodies. These antibodies can bind to infectious virus particles from a secondary, heterotypic challenge and lead to increased infection of cells possessing Fcγ receptors via antibody-dependent enhancement (ADE). This poses a challenge for vaccination, as a successful vaccine must elicit a neutralizing, long-lasting immune response balanced equally against all four serotypes of DENV.

DENV vaccines that have progressed the furthest in clinical evaluation include CYD-TDV (Dengvaxia; Sanofi-Pasteur), TAK-003 (DENVax; Takeda), and TV003 (NIAID/NIH) (7–11). All three of these vaccines are tetravalent, live attenuated vaccines that encode the membrane-embedded DENV viral proteins prM and E, in different viral backbones. Other vaccine strategies are in various preclinical stages, including recombinant E and subunit vaccines (12–15), purified inactive viruses (16), DNA encoding prM and E (17, 18), and purified virus-like particles (VLPs) (19–21). VLPs, like an infectious viral particle, are comprised of ENV dimers on the surface, resulting in production of particles that have many of the same three-dimensional epitopes as an infectious virus particle (21, 22).

Previously, we developed an mRNA vaccine against the related Zika virus encoding the viral prM and E proteins (23, 24). This vaccine elicited a robust neutralizing antibody response that protected mice from a lethal Zika viral challenge and prevented vertical transmission of the virus to the fetus. mRNA vaccines have also been shown to provide protective immunity against viral pathogens in nonhuman primates (25, 26). In this study, we have developed an mRNA vaccine against DENV serotype 1. A construct coding for prM and E proteins was *in vitro* transcribed using the modified nucleotide pseudouridine, and the resulting mRNA was packaged into lipid nanoparticles (LNPs). Following intramuscular injection, mRNA-LNPs are taken up into the muscle cells at the site of injection, as well as antigen-presenting cells in the draining lymph node (27, 28). Once the cells endocytose the mRNA-LNP, the LNP degrades in the acidified endosome, releasing the mRNA into the cytoplasm. The mRNA is then translated into the viral prM/E proteins. The prM/E polyprotein is embedded in the membrane of the endoplasmic reticulum (ER) and cleaved by host protease into the individual viral proteins. The prM and E self-assemble into VLPs on the surface of the ER membrane, and then the VLPs are trafficked through the trans-Golgi network and secreted from the cell. Administration of the DENV1 prM/E mRNA-LNP vaccine elicited neutralizing antibody titers and antivirus-specific T cells in wild-type (WT) C57BL/6J mice and conferred protection in DENV permissive immunocompromised AG129 mice. Importantly the mRNA-LNP vaccine induced serotype-specific immunity with low levels of ADE.

RESULTS

Design of DENV1 prM/E construct and viral protein expression. We designed a construct comprising the wild-type nucleotide sequence encoding prM and E proteins from dengue serotype 1 (DENV1) strain 16007 downstream of a Japanese encephalitis

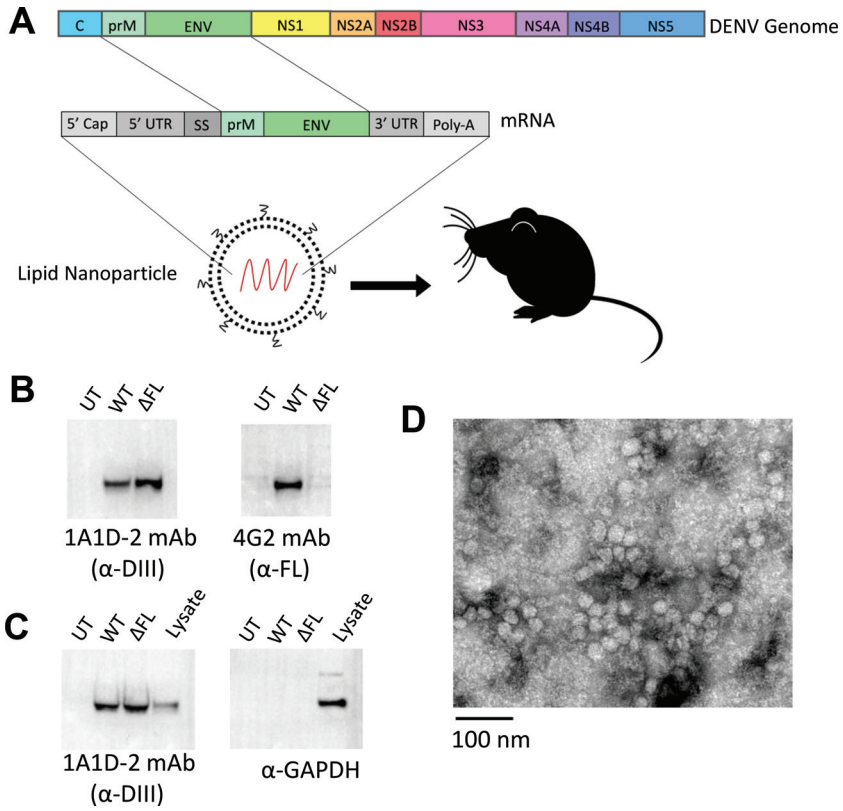

FIG 1 DENV prM/E vaccine design and viral protein expression. (A) Schematic of the DENV genome and engineered mRNA construct. An mRNA encoding the prM and ENV viral proteins was engineered with N-terminal signal peptide sequence, 5′ and 3′ untranslated regions (UTR) flanking the coding sequence, a 3′ poly(A) tail, and a 5′ cap-1 structure. *In vitro*-synthesized mRNA is encapsulated in a lipid nanoparticle for use in *in vitro* and *in vivo* experiments. (B) 293T cells were transfected with the *in vitro*-transcribed mRNA encoding the wild-type sequence (WT) or a mutant version with amino acid substitutions in the fusion loop epitope (ΔFL). Lysate was analyzed by Western blotting with the domain III-specific 1A1D-2 monoclonal antibody and the fusion loop-specific 4G2 monoclonal antibody. (C) Supernatant from transfected cells was purified and concentrated through ultracentrifugation and analyzed for VLPs by Western blotting with the 1A1D-2 monoclonal antibody or anti-GAPDH. Unpurified cell lysate from WT mRNA-transfected cells is included as a control. Shown are representative blots. (D) Electron microscopy image of VLPs from purified supernatant of transfected 293T cells showing homogenous shape and size of approximately 30 nm.

virus (JEV) signal peptide. The coding sequence was flanked by a 5′ untranslated region (UTR) previously utilized in other mRNA vaccines (23) and the 3′ UTR from the human hemoglobin subunit alpha 1 mRNA (HBA1) (Fig. 1A). The 5′ and 3′ UTRs contribute to translation regulation and mRNA stability essential for optimum protein expression. We *in vitro* transcribed mRNA from a T7 RNA polymerase promoter site upstream of the 5′ UTR. A 5′ cap-1 structure and a 3′ poly(A) tail were enzymatically added to produce fully mature mRNA that resembles host mRNA. We also generated a separate construct (ΔFL) containing the amino acid substitutions G106R, L107D, and F108A to remove the fusion loop epitope of the envelope protein. These mutations have been previously characterized and shown to ablate both fusion loop activity and production of fusion loop-specific antibodies responsible for ADE (29–31).

In vitro-synthesized mRNA was transfected into 293T cells, followed by collection of cell lysate and supernatant. We performed immunoblot analysis with the monoclonal antibodies (MAb) 1A1D-2 and 4G2. 1A1D-2 is specific for domain III of the E protein (32–34), and 4G2 binds to the fusion loop epitope. Western blotting with the monoclonal antibody 1A1D-2 identified a band representing DENV1 E after transfection with both WT and ΔFL constructs (Fig. 1B), demonstrating successful viral protein expression. Western blotting with 4G2 resulted in a band only in the lysate from wild-type-

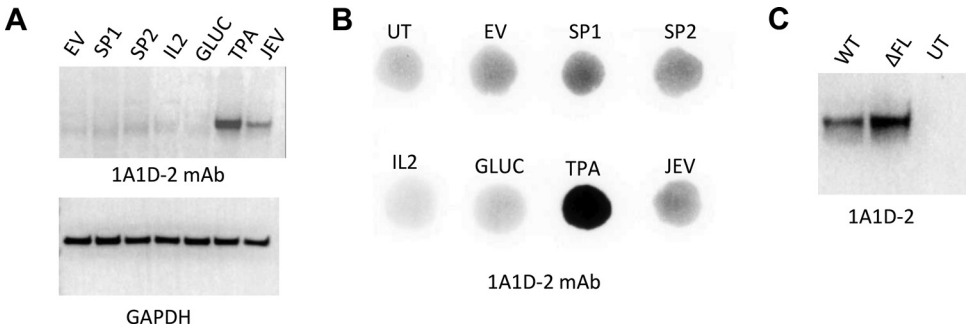

FIG 2 Optimization of signal peptide and LNP delivery. (A) Constructs were engineered with alternative signal peptides, and *in vitro*-transcribed mRNA was transfected into differentiated murine muscle myoblast C2C12 cells. Cell lysate was analyzed by Western blotting with 1A1D-2 monoclonal antibody or anti-GAPDH antibodies. (B) Supernatant of transfected C2C12 cells was analyzed by dot blotting with 1A1D-2. (C) *In vitro*-synthesized WT or ΔFL mRNA was encapsulated in a lipid nanoparticle and administered to C2C12 cells. Lysate was analyzed by Western blotting with 1A1D-2 antibody. Shown are representative blots.

transfected cells, thus revealing successful ablation of the fusion loop epitope in the ΔFL construct (Fig. 1B). Expression of prM and E alone is sufficient to induce the formation and secretion of VLPs (23, 35, 36). To detect secreted VLPs, we purified the supernatant from the transfected cells via ultracentrifugation and analyzed it on immunoblots. We detected E protein bands with the 1A1D-2 antibody in the purified supernatant of WT and ΔFL construct-transfected supernatants (Fig. 1C), demonstrating that fusion loop ablation did not affect secretion of VLPs from transfected cells. We did not detect any GAPDH (glyceraldehyde-3-phosphate dehydrogenase) in the purified supernatants, verifying that ultracentrifugation removed any cytoplasmic contamination. Particles secreted from transfected cells had properties similar to those of VLPs, with relatively uniform semismooth surfaces and diameters of approximately 30 nm, as confirmed by electron microscopy (Fig. 1D). Together, these results show that *in vitro*-synthesized mRNAs can induce viral structural protein expression and secretion of VLPs. Further, mutation of key amino acids within the fusion loop successfully ablates the antigenic epitope while maintaining protein expression and VLP excretion.

Optimization of protein expression and LNP delivery. Signal peptides are short N-terminal peptides that traffic proteins through the appropriate processing and secretory pathways within the trans-Golgi network. We compared different signal peptides on the DENV1 ΔFL construct to optimize protein expression. We generated five new ΔFL mRNA constructs, with the original JEV signal peptide exchanged for signal peptides from either interleukin-2 (IL-2), tissue plasminogen activator (tPA), or *Gaussia* luciferase (GLUC). Additionally, we synthesized two constructs with theoretical signal peptides computationally predicted to elicit robust protein secretion in skeletal muscle cells (SP1 and SP2) (37). Mice are administered the mRNA-LNP vaccine intramuscularly, so characterization and optimization of protein expression in muscle cells is key. We transfected differentiated skeletal muscle myoblast C2C12 cells with the different constructs and blotted for E protein expression with the 1A1D-2 antibody. The tPA signal peptide resulted in the most robust E protein expression (Fig. 2A). To ensure that signal peptide modification did not alter VLP secretion and directly compare VLP secretion across the different mRNA constructs, we also analyzed the supernatant of transfected cells via dot blotting with the 1A1D-2 MAb. The tPA signal peptide also resulted in the highest levels of VLP secretion (Fig. 2B).

For *in vivo* administration, mRNA is synthesized with the modified nucleotide, pseudouridine, in place of uridine. This replacement dampens innate immune stimulation and interferon activation which inhibits protein translation (38). *In vitro*-synthesized mRNA is further purified and encapsulated in a lipid nanoparticle (LNP). Encapsulation within an LNP shields the mRNA from extracellular RNases and ensures efficient delivery into cells (39). LNPs are composed of pH-sensitive lipids that bind to endogenous

apolipoprotein E, which facilitates entry. When the mRNA-LNP is endocytosed, the acidic environment of the late endosome initiates degradation of the LNP, leading to release of the mRNA to the cytoplasm. We encapsulated mRNA containing the original JEV signal peptide that has been utilized in previous flavivirus mRNA vaccines. We achieved >90% encapsulation efficiency, as determined by a Ribogreen RNA quantification assay, and stored encapsulated mRNA at 4°C for extended periods of time to accommodate a two- or three-shot vaccination schedule. Delivery of nucleotide-modified WT and ΔFL prM/E mRNA-LNPs to C2C12 cells resulted in E protein expression in cell lysate (Fig. 2C).

DENV1 prM/E mRNA vaccines elicit adaptive immune responses. Initially, wild-type C57BL/6 mice were vaccinated according to a three-shot vaccination schedule with 10 μg of mRNA per dose and serum collections at day 0 (prevaccination), day 28 (post primary), day 42 (post secondary), and day 56 (post tertiary), as shown in Fig. 3A. We quantified neutralizing antiviral antibody titers in serial dilutions of serum with a focus reduction neutralization test (FRNT) against the homologous DENV1 strain 16007. All mice within each cohort of WT and ΔFL vaccine groups seroconverted, with EC_{50} neutralizing titers (serum concentration at which 50% of the virus is neutralized) reaching a maximum of ~1/200. WT and ΔFL prM/E mRNA-LNP vaccines elicited neutralizing antibody responses after a single dose, with secondary and tertiary doses boosting titers (Fig. 3B). A third vaccine dose did not significantly enhance the neutralizing antibody titers from that of a second dose (*P* value = 0.20; WT). As such, a two-dose, prime-boost vaccination schedule was used in future studies. These data reveal that *in vivo* delivery of an mRNA-LNP vaccine induces a humoral immune response against the exogenous viral protein.

A separate cohort of mice were administered high or low doses (10 μg or 3 μg per injection) of WT or ΔFL prM/E mRNA-LNP vaccine in a prime-boost schedule (Fig. 3C). We also included mice infected with live DENV1 virus (10^5 focus-forming units [FFU] DENV1) as a positive control and an mRNA vaccine encoding green fluorescent protein (GFP) (10 μg) as a negative control. We quantified the levels of antiviral IgG in the sera isolated from the different vaccine groups via an ELISA against purified DENV1 strain 16007. All mice receiving the infectious DENV1, WT mRNA vaccine, or ΔFL mRNA vaccine had significantly higher titers than mice receiving the GFP mRNA control vaccine (Fig. 3D). No statistical differences were observed between results for the WT and ΔFL vaccines. Virus-infected mice and mice receiving the high dose of the WT or ΔFL vaccines all had antibody endpoint dilution titers of approximately 1×10^5. The 3-μg low dose of the vaccine induced antibody titers slightly lower than the titers induced by the higher dose of 10 μg. Serum neutralization titers were determined via FRNTs (Fig. 3E and F) against infectious DENV1 strain 16007. High and low doses of the WT prM/E mRNA vaccine elicited EC_{50} values of 1/420 and 1/263, respectively, revealing little to no dose-dependent response (Fig. 3F) (*P* value = 0.36). Additionally, high and low doses of the ΔFL vaccine resulted in similar EC_{50} values of 1/329 and 1/175, respectively. These differences were not statistically significant (Fig. 3F) (*P* value = 0.29). The mice vaccinated with the WT and ΔFL vaccines had lower neutralizing titers than the DENV1 virus-infected mice (EC_{50} = 1/729), although these differences were not statistically significant. All vaccines or infections resulted in higher neutralizing values than those of the GFP-vaccinated mice (Fig. 3E) (*P* value < 0.001). Neutralizing titers of WT and ΔFL construct-vaccinated mice were very similar, indicating that the fusion loop mutation did not alter humoral immune responses.

To quantify antiviral T cells, splenocytes were harvested from vaccinated mice at day 56 after a tertiary vaccination schedule and stimulated with a pooled 15mer overlapping peptide array for the ENV protein from DENV1 or DENV2 as well as the NS1 protein from DENV1. Stimulated cells were analyzed for intracellular gamma interferon (IFN-γ) by flow cytometry, and antiviral IFN-γ^+ T cells were quantified. prM/E mRNA vaccines elicited modest yet significant antiviral $CD4^+$ and $CD8^+$ T cell responses specific for the DENV1 ENV protein, with equivalent levels between the WT and ΔFL vaccines

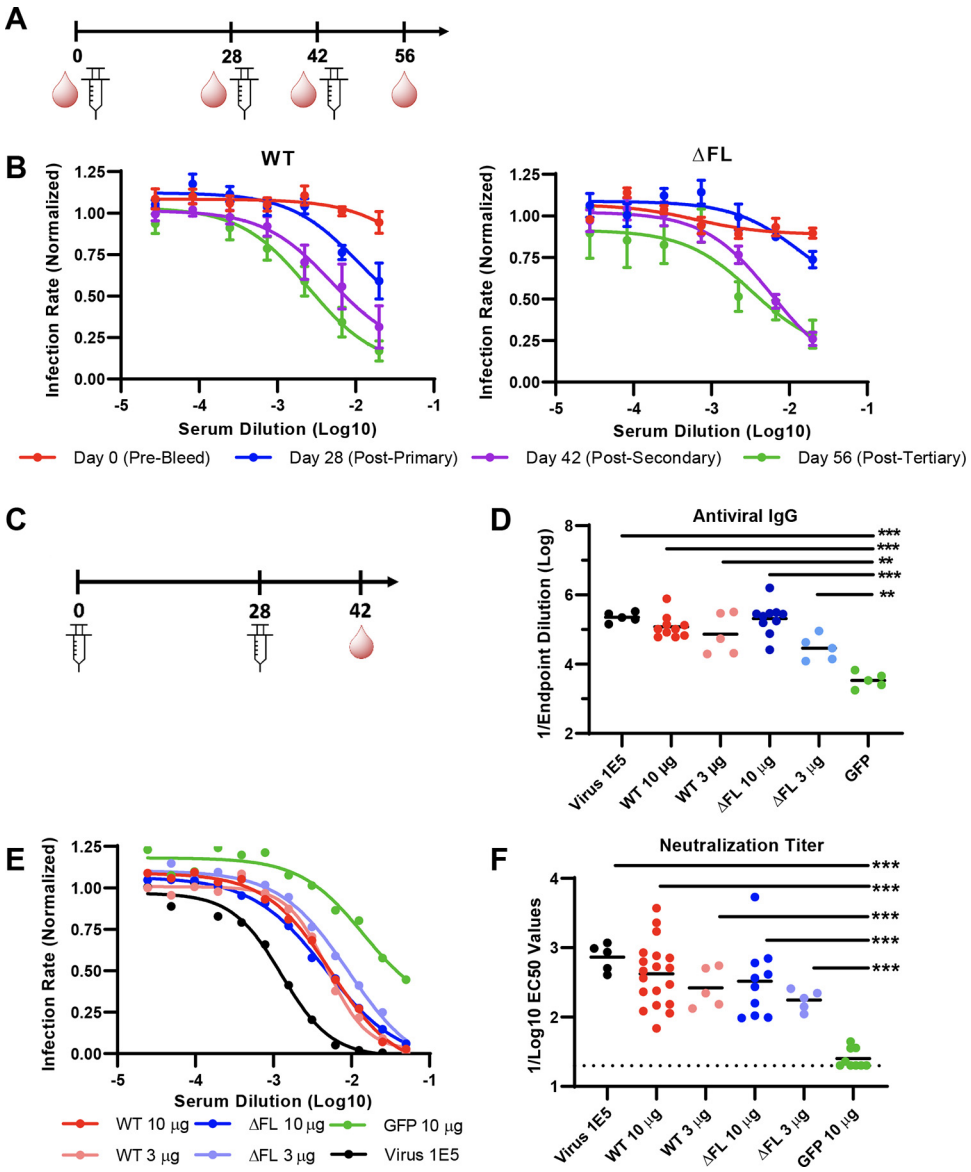

FIG 3 DENV1 prM/E mRNA vaccines induce neutralizing antibody responses. DENV1 prM/E mRNA-LNP vaccines were administered to 10-week-old C57BL/6 mice. (A) Mice were administered 10 μg of mRNA vaccine in a three-shot schedule, and serum was collected at the indicated time points. (B) Serial dilutions of serum from vaccinated mice were analyzed for neutralization activity by an FRNT against DENV1 strain 16007. Neutralization curves at each time point are shown for WT vaccine recipients (left) and ΔFL vaccine recipients (right). The average values ± standard errors of the mean (SEM) of results for five vaccinated mice are shown. (C) Mice were administered a high (10 μg) or low (3 μg) dose of the mRNA vaccines or vaccine encoding GFP. A separate group of mice were infected with wild-type DENV1 by following the same schedule. (D) Antiviral IgG titers were determined by ELISAs, and the endpoint dilution titer was calculated. (E) Serum was analyzed by FRNTs, and the normalized percentage of infection of each group is plotted as the mean ± SEM for each serum dilution. $n = 5$ mice per group of mice infected with virus or receiving 3-μg vaccine doses. $n = 10$ mice per group in mice receiving 10-μg doses of the ΔFL and GFP vaccines. $n = 15$ for mice receiving 10-μg doses of the WT vaccine. (F) EC_{50} values of the neutralization curves for individual mice are shown. The statistical significance of results for each group in comparison to that for the GFP control was determined via unpaired *t* test. **, $P < 0.01$; ***, $P < 0.001$. Statistical comparisons with *P* values of >0.05 are not shown in this figure.

(Fig. 4). No T cell responses were detected against the homologous DENV2 E protein or the irrelevant DENV1 NS1 protein. Thus, prM/E mRNA-LNP vaccines elicit both humoral and cellular immune responses against DENV1 E protein.

DENV1 prM/E mRNA vaccines protect against a lethal challenge. AG129 mice lack the type I interferon α/β receptor and the type II interferon γ receptor, and they are permissive to a lethal DENV challenge (40–42). All serotypes of DENV are capable of

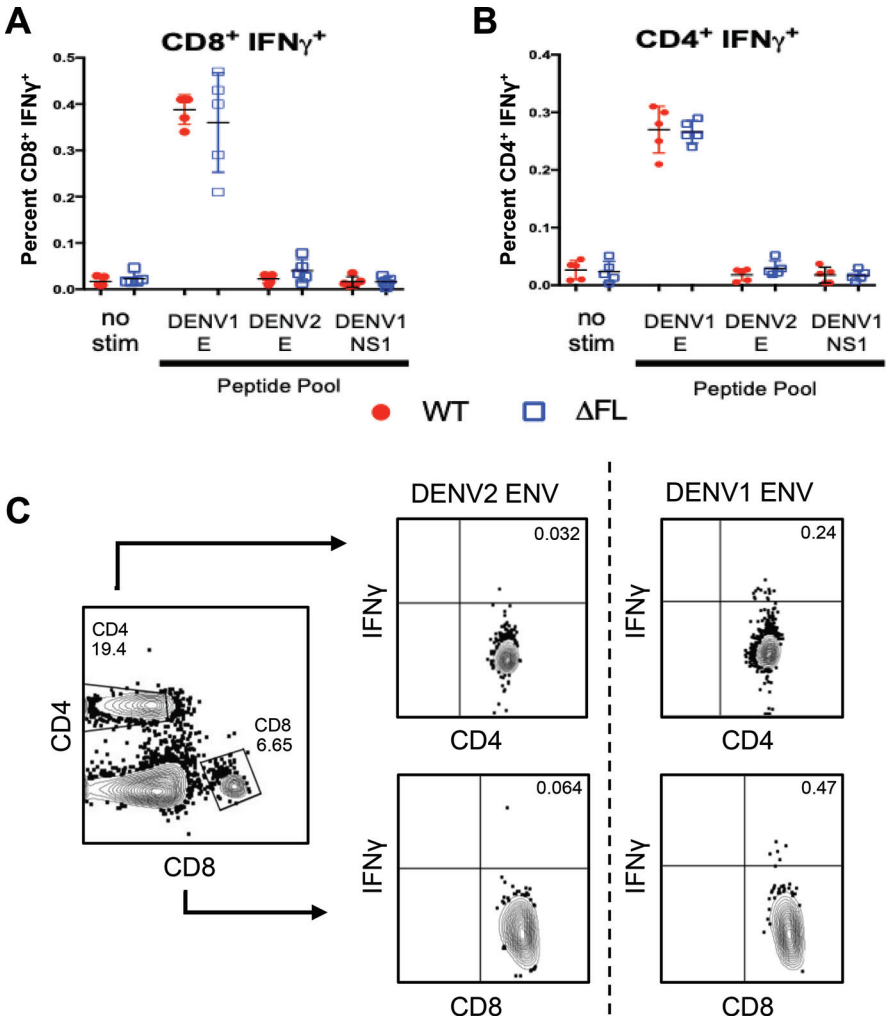

FIG 4 DENV1 prM/E mRNA vaccines induce antiviral CD8$^+$ and CD4$^+$ T cells. DENV1 prM/E mRNA-LNP vaccines were administered to 10-week-old C57BL/6 mice in a three-shot vaccination schedule. Spleens were harvested after the final vaccination dose (day 56) and stimulated with an overlapping peptide array of DENV1 E protein, DENV2 E protein, or DENV1 NS1 protein. Stimulated cells were stained for the intracellular cytokine IFN-γ and analyzed by flow cytometry. Plotted are the IFN-γ^+ T cells as a percentage of total CD8$^+$ T cells (A) or CD4$^+$ T cells (B). $n = 5$ mice in the WT and ΔFL construct-vaccinated groups. (C) Representative flow cytometry plots and gates from a single mouse.

replication in AG129 mice with quantifiable viremia, vascular leakage, and increased cytokine levels. Some strains can induce more severe disease states, indicative of severe disease, in humans, such as DENV2 D2S20 or DENV1 Western Pacific (40, 42). AG129 mice were vaccinated according to the previously described schedule (Fig. 3C) with GFP mRNA-LNP or DENV1 wild-type prM/E mRNA-LNP. Serum was collected from vaccinated mice and analyzed for neutralization titers as previously described. DENV1 prM/E mRNA-LNP vaccination induced EC_{50} values of greater than 1/3,000 (Fig. 5A and B). Vaccinated AG129 mice were challenged with 10^6 FFU DENV1 Western Pacific strain and monitored for 40 days postinfection. Mice receiving the GFP mRNA-LNP vaccine lost weight beginning at day 6, and all mice succumbed to viral infection by day 32 postinfection. DENV1 prM/E mRNA-LNP-vaccinated mice did not show any signs of morbidity or mortality, with weight remaining stable postinfection and 100% of the mice surviving (Fig. 5C and D). These data demonstrate that a DENV1 prM/E mRNA-LNP vaccine protects against a lethal DENV1 challenge in an immunocompromised mouse model.

The DENV1 prM/E mRNA vaccine elicited both antiviral antibodies and an antiviral T cell response. We hypothesized that the antiviral antibodies are sufficient to protect

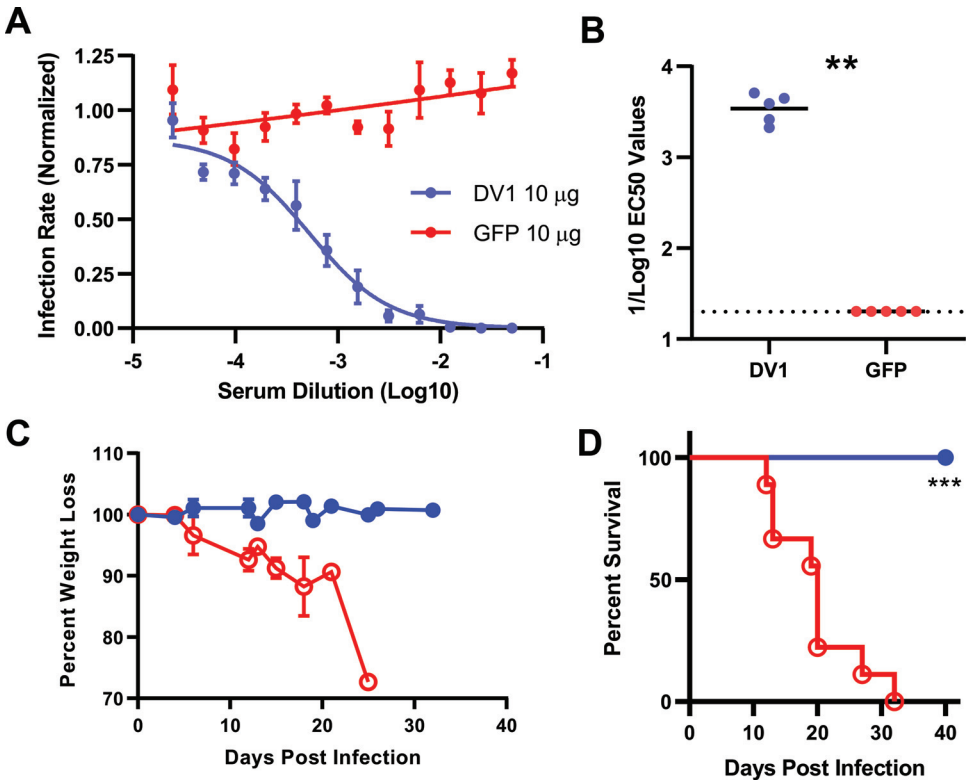

FIG 5 DENV1 prM/E mRNA vaccines protect against a lethal challenge. Ten micrograms of DENV1 prM/E or GFP mRNA-LNP vaccines was administered to AG129 mice in a prime-boost schedule 4 weeks apart. $n = 5$ mice per group. (A) Serum from vaccinated mice was isolated 2 weeks after the boost and analyzed for neutralization by FRNT of serially diluted serum samples. Plotted are the means ± SEM of results from five mice for each dilution. (B) EC_{50} values for each mouse are plotted. The vaccinated mice were then challenged with a lethal dose of DENV1 strain Western Pacific. Mice were monitored for weight (C) and survival (D) postchallenge. **, $P < 0.01$; ***, $P < 0.00$.

against a lethal challenge. To address this hypothesis, we adoptively transferred pooled serum from WT construct-vaccinated mice into AG129 mice. As controls, a second group of mice received pooled serum from naive mice and a third group of mice received phosphate-buffered saline (PBS). One day after adoptive transfer, mice were challenged with 10^6 FFU DENV1 Western Pacific strain and monitored for 40 days postinfection (Fig. 6). Seven of 8 mice that received serum from the vaccinated mice were protected against lethality. Six of seven mice that received naive serum lost weight and succumbed to viral lethality postchallenge. Thus, antibodies elicited by the DENV1 prM/E mRNA-LNP vaccine are sufficient for protection.

DENV1 prM/E mRNA vaccination induces serotype-specific humoral immunity. Infection with DENV will lead to antibodies that cross-react with heterotypic DENV serotypes with the potential to cause ADE. We characterized the cross-reactive immune response in serum of the prM/E mRNA-vaccinated mice. We quantified ADE by incubating DENV2 with serial dilutions of serum from vaccinated mice before infecting Fcγ receptor-positive K562 cells. Infection was determined via flow cytometry with the monoclonal antibody 1A1D-2 against the viral E protein. The percentage of infected cells was compared to that of a DENV2 infection in the absence of immune sera (Fig. 7A). Serum from DENV1 virus-infected mice significantly enhanced DENV2 infections, even with dilutions as high as 1/6,000. At a serum dilution of 1/100, an 8-fold enhancement was observed. Conversely, serum from mRNA-vaccinated mice induced very low levels of DENV2 enhancement (Fig. 7A), with only a 1.2-fold enhancement at a 1/100 serum dilution (Fig. 7B). The amino acid sequence of the WT prM/E mRNA-LNP vaccine was identical to the sequence of the infecting virus. Surprisingly, WT and ΔFL mRNA

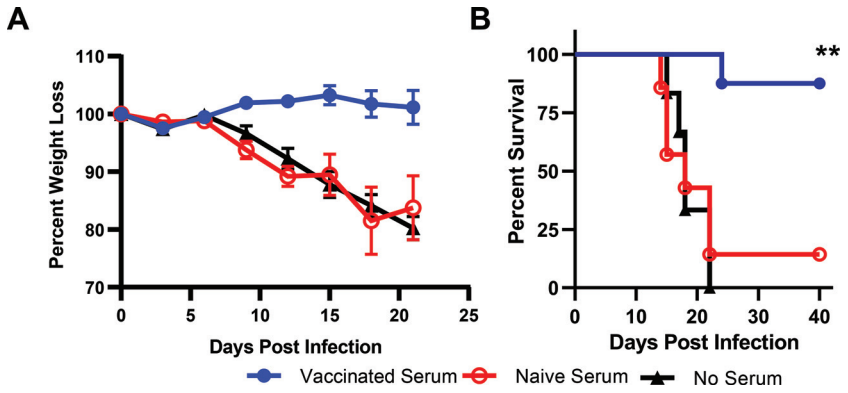

FIG 6 Passive transfer of immune sera protects against a lethal challenge. Serum from naive or WT prM/E mRNA-vaccinated mice was passively transferred into AG129 mice. One day after transfer, mice were challenged with a lethal dose of DENV1 strain Western Pacific. Mice were monitored for weight (A) and survival (B) postchallenge. Survival curves comparing vaccinated and naive serum recipients were analyzed by log rank test. **, $P < 0.01$.

vaccines enhanced heterotypic DENV2 to nearly identical values. Similar results were seen with DENV4 (data not shown). As a negative control, serum from naive mice showed no enhancement at any dilution. To assess the role of ADE on viral replication and egress, we quantified the levels of infectious virus in the supernatant of K562 cells infected with immunocomplexed virus. Serum from WT or ΔFL mRNA-vaccinated mice enhanced viral replication relative to serum from GFP-vaccinated mice; however, enhancement was significantly lower than that of serum from virus-infected mice, in agreement with the flow cytometry data (Fig. 7C). Importantly, DENV1 vaccines did not elicit neutralizing antibodies against DENV2 (strain New Guinea C) in an FRNT (Fig. 7D). These data demonstrate that DENV1 prM/E mRNA vaccines do not induce cross-reactive antibodies which elicit heterotypic enhancement, in contrast to a viral infection.

DISCUSSION

Despite a longstanding effort in the field, there still remains an unmet need for a DENV vaccine that elicits robust, balanced immune response against all four serotypes. Here, we developed a vaccine against DENV1 with a modified mRNA encoding the prM and ENV viral proteins encapsulated in a lipid nanoparticle (LNP). The mRNA-LNP vaccine platform has now been developed for several viruses, including rabies virus (26), influenza virus (26), and HIV (43). More recently, mRNA vaccines have been rapidly developed against severe acute respiratory syndrome coronavirus 2 (SARS-CoV-2). Moderna's mRNA-1273 and BioNTech's mRNA BNT162b1 were the first vaccine candidates to show safety and efficacy in human trials, demonstrating the speed of the mRNA platform and its role in emerging infectious diseases (44–46). In the flavivirus field, mRNA vaccines have been developed against Zika virus (23, 24) and Powassan virus (47). These flavivirus vaccines encode the viral structural proteins which are expressed and lead to the development of neutralizing antibodies against the viral structural proteins. Recently, another group published the results of a mRNA vaccine against DENV2 (48). Zhang et al. developed mRNA vaccines encoding full-length prM-ENV, the soluble portion of ENV, and NS1. Vaccination with the mRNA encoding the soluble portion of DENV2 ENV (E80) elicited humoral and cell-mediated immune responses that protected against a lethal challenge with a homologous serotype of DENV2, similar to our findings with a DENV1 serotype mRNA vaccine. However, the DENV2 E80 mRNA vaccine induced serotype cross-reactive immune responses and high levels of heterologous ADE (48). The significant reduction of DENV2 ADE seen with the DENV1 mRNA vaccine we outline here shows promise for future efforts that aim to produce a safer dengue vaccine that offers broad protection while successfully avoiding ADE, a major hurdle in the development of protective flavivirus vaccines.

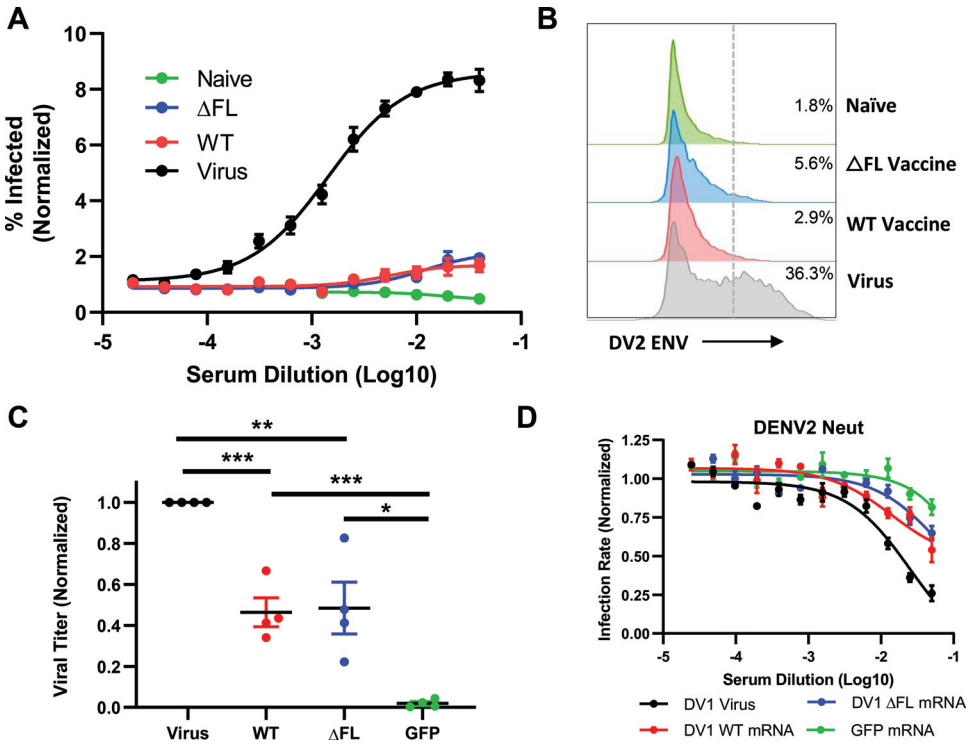

FIG 7 DENV1 prM/E mRNA vaccination results in reduced ADE levels. Serum from naive mice, WT prM/E mRNA-vaccinated mice, ΔFL prM/E mRNA-vaccinated mice, or mice infected with DENV1 2 weeks after boost were analyzed for enhancement of DENV2 infection. Serial dilutions of serum were incubated with DENV2 and added to Fcγ receptor-positive K562 cells. Fifteen hours later, infected cells were stained for intracellular ENV and quantified by flow cytometry. The percentage of infected cells was normalized to that of infection in the absence of serum. (A) The fold change in percentage of cells infected is shown compared to that of infections in the absence of serum. The average fold enhancement ± SEM for five mice per group is graphed. (B) A representative flow cytometry histogram of the ENV signal for each different treatment at a 1/100 serum dilution is shown. (C) A 1/100 dilution of serum was incubated with DENV2 for 1 h and added to K562 cells at an MOI of 1. At 48 h later, viral titers in the supernatant were quantified via a focus-forming assay. Viral titers were normalized to virus-infected serum within each independent experiment, and the results of four independent experiments are shown. *, $P < 0.05$; **, $P < 0.01$. (D) Serial dilutions of serum from vaccinated mice were analyzed for neutralization activity against DENV2 (strain New Guinea C) with an FRNT. The average values ± SEM of results for five vaccinated mice are shown.

A high level of antigen expression is key for the success of mRNA vaccines. The signal peptide plays a critical role in directing the translated protein into the appropriate locations for processing and secretion. Previous flaviviral mRNA vaccines have included an N-terminal JEV or IgE signal peptide (23, 24, 48). In our study, the tPA signal peptide led to far greater ENV expression and VLP secretion in C2C12 cells than other signal peptides, including the JEV signal peptide. All *in vivo* studies here were performed with the original vaccine construct encoding the JEV signal peptide, but we predict that future vaccine formulations with the tPA signal peptide will lead to greater antigen expression and higher antiviral antibody titers.

The DENV1 mRNA-LNP vaccine elicited humoral and cell-mediated immunity following a two-dose vaccination regimen, with antibody titers of 1/120,000 and neutralizing titers of 1/420 (WT, 10 μg). The antiviral antibodies were sufficient for protection. The neutralizing antibody titers reported here are similar to those of other DENV1 vaccination strategies. Neutralization EC_{50} titers of approximately 1/100 were achieved by administration of a DNA vaccine encoding the modified viral structural proteins (29). DENV1 purified-VLP vaccine generated with fusion loop mutants resulted in neutralization EC_{50} titers of approximately 1/1,000 (31). In phase III human clinical trials, the CYD-TDV (Dengvaxia) vaccine elicited EC_{50} neutralization titers of approximately 1/60 in seronegative individuals (49), and TAK-003 neutralization titers reached 1/184 (50). In

phase I human studies, TV003 elicited EC_{50} neutralization titers of 1/63 against DENV1 (51).

The neutralizing antibody titers in the vaccinated AG129 mice (EC_{50} of 1/3,125) were significantly higher than those in the C57BL/6 mice (EC_{50} of 1/420) following equivalent vaccination schedules (P value < 0.001). Likely, the lower neutralization titers in C57BL/6 mice are due to decreased antigen expression in the presence of an intact type I interferon response. Indeed, previous studies have demonstrated that mRNA vaccines engage RNA-sensing pattern recognition receptors and activate the type I IFN pathway, leading to eIF2α phosphorylation and blunted translation of the exogenous transcript (39, 52). Increasing vaccine efficacy could be achieved through lowering the RNA-sensing and IFN response. We have included the pseudouridine modification in our DENV1 prM/E mRNA-LNP vaccine, but further modifications such as 5-methylcytosine could further lower innate immune stimulation and increase antigen expression and associated antibody titers (39).

In humans, $CD4^+$ and $CD8^+$ T cells predominantly target capsid and NS3, respectively, following a DENV infection (53). Although our vaccine does not encode these immunodominant T cell epitopes, we detected antiviral $CD4^+$ and $CD8^+$ T cell responses against the E protein in the vaccinated mice. Intriguingly, the $CD4^+$ and $CD8^+$ T cell responses were not cross-reactive with other DENV serotypes, likely due to the high variability across the different DENV serotypes in the E protein. The overall magnitude of the T cell response from our vaccine was lower than that of a recently described mRNA vaccine against DENV1 which encoded the immunodominant HLA epitopes from the nonstructural proteins of DENV (54). Our vaccine was designed to elicit antibodies against the structural proteins to neutralize infectious virus particles as opposed to robust T cell responses. Although we cannot rule out a role for antiviral T cells in a vaccinated host, neutralizing antibodies in serum were sufficient to protect against a lethal homotypic challenge in a passive transfer model. Together, these studies demonstrate that mRNA vaccines can be developed to induce both protective T and antibody-dependent immunity against DENV.

Interestingly, the prM/E mRNA vaccines elicited serotype-specific antibody responses. Here, we demonstrate vaccine protection against two DENV1 strains, but further studies will be required to demonstrate broad serotype specificity. Serum from DENV1 virus-infected mice enhanced a DENV2 *in vitro* infection, whereas heterotypic ADE was largely absent with serum from the mRNA-vaccinated mice. These observations are surprising, given that neutralization titers were similar between the virus-infected and vaccinated mice and the identical amino acid sequences shared between the WT mRNA vaccine and the infecting DENV1 16007 strain. Further, this suggests that the polyclonal antibody repertoire induced by the mRNA vaccine is inherently different than the polyclonal repertoire induced during a viral infection. In our previous study, mutation of the fusion loop epitope in the Zika virus mRNA vaccine led to ablation of cross-reactive DENV enhancement through ADE (23). Similarly, in previous studies with VLP- and DNA-based vaccines, mutation of the fusion loop epitope lowered the prevalence of ADE (29, 55). Unexpectedly, mutation of the fusion loop epitope in the mRNA vaccine did not alter ADE. These findings suggest that antibodies against the fusion loop epitope are not dominant in the polyclonal response to our mRNA vaccine. Future efforts will focus on identification of the structural epitopes within the VLP secreted from a viral infection and an mRNA-LNP vaccine.

In this study, we have demonstrated that an mRNA vaccine encoding the prM and E proteins from DENV1 can elicit robust adaptive immune responses and protect against a lethal viral challenge. This study paves the way for future development of mRNA vaccines against the remaining DENV serotypes, with the ultimate goal of developing a tetravalent vaccine that will elicit a balanced, protective immune response against all four DENV serotypes. Current leading vaccination efforts rely on live attenuated virus, yet these vaccines fall short in either their ability to induce a broadly neutralizing antibody response or their ability to avoid ADE. In contrast to live attenuated vaccines in

which differential replication of the attenuated viruses dictates antigen dosing *in vivo*, the antigen dose can be carefully modulated with mRNA vaccines to elicit a balanced immune response. Additionally, mRNA vaccines will allow the modification of epitopes which elicit ADE yet are impossible to incorporate into a live attenuated vaccine due to their critical role in viral replication.

MATERIALS AND METHODS

Viruses and cells. DENV serotype 1 strain 16007 and DENV serotype 2 strain New Guinea C were provided by Michael Diamond at Washington University in St. Louis. DENV serotype 4 strain UIS 497 was obtained through BEI Resources (NR-49724), NIAID, NIH, as part of the WRCEVA program. Viral stocks were propagated in C6/36 cells, and titers were determined by a focus-forming assay (FFA). All propagated viral stocks were deep sequenced to confirm the viral strain. FFAs were performed to titer viral stocks with monoclonal antibody clone 9.F.10 obtained through Santa Cruz Biotechnology (catalog no. SC-70959). Experiments with DENV were conducted under biosafety level 2 (BSL2) containment at the University of Illinois College of Medicine or St. Louis University College of Medicine with institutional Biosafety Committee approval. Vero-E6 cells (catalog no. CRL 1586) and K562 cells (catalog no. CCL-243) were obtained from American Type Culture Collection (ATCC) and maintained for low passage number in accordance with ATCC guidelines. C6/36 cells were provided by the Diamond lab at Washington University in St. Louis, C2C12 cells were obtained from Ahke Heydemann, University of Illinois at Chicago (UIC), and 293T cells were obtained from Donna MacDuff at the University of Illinois at Chicago.

Generation of mRNA and mRNA-LNP. Wild-type constructs encoding dengue serotype 1 strain 16007 prM and Env viral proteins were synthesized by Integrated DNA Technologies (IDT). Constructs contained a T7 promoter site for *in vitro* transcription of mRNA, 5′ and 3′ UTRs, and a Japanese encephalitis virus signal peptide. The sequences of the 5′ and 3′ UTRs were identical to those of previous publications with a Zika virus (ZIKV) mRNA vaccine (23, 24). mRNA was synthesized from linearized DNA with T7 *in vitro* transcription kits from CellScript and in accordance with the manufacturer's protocol. Standard mRNA was produced with unmodified nucleotides (catalog no. C-MSC11610). RNA to be encapsulated in lipid nanoparticles was generated with pseudouridine in place of uridine with the Incognito mRNA synthesis kit (catalog no. C-ICTY110510). The 5′ cap-1 structure and 3′ poly(A) tail were enzymatically added. mRNA was encapsulated in lipid nanoparticles using the PNI Nanosystems NanoAssemblr benchtop system. mRNA was dissolved in PNI formulation buffer (catalog no. NWW0043) and run through a laminar flow cartridge with GenVoy ILM (catalog no. NWW0041) encapsulation lipids at a flow ratio of 3:1 (RNA in PNI buffer; Genvoy ILM) at a total flow rate of 12 ml/min to produce mRNA-LNPs. These mRNA-LNPs were characterized for encapsulation efficiency and mRNA concentration via RiboGreen assay using Invitrogen's Quant-iT Ribogreen RNA assay kit (catalog no. R11490).

Mouse experiments. C57BL/6J mice were purchased from Jackson Laboratory and housed in the pathogen-free Biomedical Resources Laboratory at the University of Illinois College of Medicine. AG129 mice were bred in the animal facilities at St. Louis University. For vaccinations, mice were injected intramuscularly in the thigh with 50 μl of the indicated amount and type of mRNA-LNP suspended in PBS. Vaccinated C57BL/6J mice were challenged with 1×10^5 FFU of DENV1 strain 16007, retro-orbitally. Vaccinated AG129 mice were challenged with 10^6 FFU of DENV1 strain West Pac, intravenously (i.v.). For serum adoptive transfer studies, sera from vaccinated or naive mice were pooled and then 200 μl was administered i.v. into naive AG129 mice 1 day prior to challenge with DENV1. The vaccination and viral challenge protocols were approved by the Institutional Animal Care and Use Committee (IACUC) at the University of Illinois College of Medicine (protocol no. 18-114) and St. Louis University (assurance no. D16-00141).

***In vitro* transfections.** 293T and C2C12 cells were transfected with mRNA using the Mirus TransIT RNA transfection kit (catalog no. MIR 2225) according to the manufacturer's protocol. 293T cells were 60 to 70% confluent at the time of transfection, with C2C12 cells being 100% confluent at the time of transfection to achieve differentiation into muscle tissue. Supernatant was collected 24 h posttransfection. To collect lysate, cells were washed with PBS and lysed with radioimmunoprecipitation (RIPA) buffer (Millipore-Sigma; catalog no. R0278). Lysate and supernatant were centrifuged at 16,000 $\times$ *g* for 10 min at 4°C to remove cell debris. Supernatant from transfected cells was purified using a 20% sucrose cushion and ultracentrifugation at 141,000 $\times$ *g* overnight (16 h) at 4°C. Purified protein complexes were resuspended in 50 μl of 1% bovine serum albumin (BSA) in PBS for subsequent storage and analysis.

Viral protein detection. For Western blot analysis, 10 μl of lysate or purified supernatant samples was run on a 4-to-12% Bis-Tris SDS-PAGE gel (Invitrogen; catalog no. NW04120BOX) with subsequent transfer to a 0.45-μm-pore-size polyvinylidene difluoride (PVDF) membrane. Membranes were blocked in TBST (10 nM Tris-HCl, pH 7.5, 150 nM NaCl, and 1% Tween 20) buffer with 5% skim milk. Membranes were blotted with envelope domain III-specific 1A1D-2 (1:600) monoclonal antibody (CDC Arbovirus Reference Collection) or envelope fusion loop-specific 4G2 (3.33 mg/ml) (BEI catalog no. NR-50327, Novus Biologicals catalog no. NBP2-52709FR). Secondary antibody goat anti-mouse–horseradish peroxidase (HRP) (200 ng/ml) (Invitrogen catalog no. A16072) in blocking buffer allowed for detection of dengue viral envelope proteins. Western blots were imaged on a ChemiDoc Image Lab system (Bio-Rad).

For dot blot analysis, clarified transfection supernatant was diluted 1/4 in a 20-μl volume of transfer buffer (Life Technologies catalog no. NP0006-1) and applied dropwise to a presoaked 0.45-μm-pore-size PVDF membrane. Sample was allowed to infiltrate the membrane through capillary action for no more

than 1 h (before the blot starts to dry). Blots were stained and imaged in the same manner as described for Western blots above.

Electron microscopy. One T-75 cell culture flask was seeded with 293T cells at 70 to 80% confluence the day of transfection. The flask was transfected with 20 μg of mRNA encoding WT DENV1 prM and envelope protein using the Mirus TransIT RNA transfection kit (catalog no. MIR 2225) according to the manufacturer's protocol. Supernatant was collected 48 h posttransfection. Supernatant was centrifuged at 16,000 $\times$ *g* for 10 min at 4°C to remove cell debris. Six milliliters of supernatant was then dialyzed overnight at 4°C in 20,000-molecular-weight-cutoff (MWCO) Slide-A-Lyzer dialysis cassettes (catalog no. 66003) submerged and spinning in PBS. Dialyzed sample was provided to the University of Illinois at Chicago electron microscopy core for imaging by using the following parameters. Ten to 15 μl of sample was loaded dropwise onto a 300-mesh, Formvar/carbon-coated copper electron microscopy (EM) grid with the excess removed by filter paper via capillary action. One drop of 2% uranyl acetate solution was deposited onto the EM grid with the excess removed by filter paper via capillary action. Once the grid was allowed to dry further, the sample was examined via transmission electron microscopy using a JEOL JEM-1400F transmission electron microscope, operating at 80 kV. Digital micrographs were acquired using an AMT BioSprint 12M-B charge-coupled device (CCD) camera and AMT software (version 701).

ELISA. Four T-150 cell culture flasks of C6/36 cells were infected with WT DENV1 at a multiplicity of infection (MOI) of 0.1. Seven days after infection, 60 ml of supernatant was collected and clarified via centrifugation at 3,200 $\times$ *g* for 10 min at 4°C. Supernatant was further purified via 20% sucrose cushion ultracentrifugation at 141,000 $\times$ *g* for 2 h at 4°C to pellet virus. Virus pellets were resuspended in PBS for a total volume of 5 ml. ELISA plates were coated overnight at 4°C with 50 μl/well of a 1:25 dilution of concentrated viral stock (1E3 FFU/well) in coating buffer (0.1 M sodium carbonate, 0.1 sodium bicarbonate, 0.02% sodium azide, at pH 9.6). After the plates were coated overnight, they were incubated with blocking buffer (PBS with Tween 20 [PBST], 2% BSA, 0.025% sodium azide) for 1 h at 37°C. The plates were then incubated with 50 μl of serial dilutions of vaccine and virus-enhanced mouse serum at 4°C overnight. The plates were subsequently incubated with goat anti-mouse–HRP secondary antibody (200 ng/ml) (Invitrogen catalog no. A16072) in blocking buffer for 1 h at room temperature. ELISA plates were developed using 100 μl of TMB (3,3′,5,5′-tetramethylbenzidine) substrate (Thermo Fisher catalog no. 34029). The optical density at 450 nm (OD_{450}) reading was measured with a BioTek ELISA microplate reader.

Serum neutralization assay. Focus reduction neutralization tests (FRNT) were performed as described previously (23). Briefly, serial dilutions of heat-inactivated serum from vaccinated mice were incubated with 50 to 70 FFU of DENV for 1 h at 37°C before infection of a monolayer of Vero cells in a 96-well plate. One hour after infection, cells were overlaid with 1% (wt/vol) methylcellulose in 2% fetal bovine serum (FBS), 1$\times$ minimal essential medium (MEM). Plates were fixed for 30 min with 4% paraformaldehyde (PFA) 48 h after infection. Staining involved primary antibody 9.F.10 (500 ng/ml) and secondary antibody goat anti-mouse–HRP (200 ng/ml) in PermWash buffer (0.1% saponin, 0.1% BSA, in PBS). Treatment with TrueBlue peroxidase substrate (KPL) produced focus-forming units that were quantified on an ImmunoSpot ELISpot plate scanner (Cellular Technology Limited).

Antiviral T cell quantification. Spleens were collected from vaccinated mice, and splenocytes were collected. An overlapping 15mer peptide library from DENV2 ENV, DENV1 ENV, and DENV NS1 was obtained from BEI Resources, NIAID, NIH (catalog no. NR-507, NR-9241, and NR-2751). Individual peptides were pooled for *ex vivo* T cell stimulation. Spleens were ground over a 40-μm-pore-size cell strainer and brought up in RPMI 1640 medium with 10% FBS, HEPES, and 0.05 mM β-mercaptoethanol. Then, 2×10^6 cells were plated per well in a round-bottom 96-well plate and stimulated for 6 h at 37°C, 5% CO_2, in the presence of 10 μg/ml brefeldin A and 10 μg of pooled peptide in 90% dimethyl sulfoxide (DMSO). Following peptide stimulation, cells were washed once with PBS and stained for the following surface markers: anti-CD8-PerCP-Cy 5.5 (clone 53-6.7), anti-CD3-AF700 (clone 500A2), and anti-CD19-BV605 (clone 1D3). Cells were then fixed, permeabilized, and stained for the following intracellular marker: anti-IFN-γ-APC (clone B27). The cells were analyzed by flow cytometry using an Attune-NXT.

ADE flow assay. Serial dilutions of heat-inactivated serum from naive, vaccinated, or virus-infected mice were mixed with DENV2 and incubated for 1 h at 37°C. Fcγ receptor (CD32A)-positive K562 cells were infected with immunocomplexed virus at an MOI of 1 in a 96-well plate. After a 15-h incubation, cells were fixed with 4% PFA for 30 min and stained for intracellular ENV with 1A1D-2 (1/500) monoclonal antibody and anti-mouse 647-conjugated antibody (2 μg/ml; Invitrogen catalog no. A21235).

ADE viral replication assay. Serum samples from virus-infected mice and mice receiving the WT, ΔFL, or GFP mRNA vaccine were separately pooled and heat inactivated. Serum was mixed with DENV2 and incubated for 1 h at 37°C at a 1/100 dilution. A total of 10,000 Fcγ receptor (CD32A)-positive K562 cells were infected with immunocomplexed virus at an MOI of 1 in a 200-μl volume in a 96-well plate. After a 48-h incubation to allow viral replication and egress, cells were centrifuged to separate cells from supernatant. Viral titers in supernatant were determined via FFA as described above.

Data analysis. All data were analyzed with GraphPad Prism software. Statistical significance was determined by unpaired *t* tests for comparison of antibody titers and by log rank tests for comparisons of survival curves. Flow cytometry data were analyzed using FlowJo software (BD Biosciences).

ACKNOWLEDGMENTS

This work was funded by DoD grant PR192269 to A.K.P. and institutional startup funds to J.M.R.

This work made use of instruments at the Electron Microscopy Core of UIC's Research Resource Center. Sequencing was performed at the University of Illinois at the Chicago Sequencing Core (UICSQC).

REFERENCES

1. Messina JP, Brady OJ, Scott TW, Zou C, Pigott DM, Duda KA, Bhatt S, Katzelnick L, Howes RE, Battle KE, Simmons CP, Hay SI. 2014. Global spread of dengue virus types: mapping the 70 year history. Trends Microbiol 22:138–146. https://doi.org/10.1016/j.tim.2013.12.011.
2. Bhatt S, Gething PW, Brady OJ, Messina JP, Farlow AW, Moyes CL, Drake JM, Brownstein JS, Hoen AG, Sankoh O, Myers MF, George DB, Jaenisch T, Wint GRW, Simmons CP, Scott TW, Farrar JJ, Hay SI. 2013. The global distribution and burden of dengue. Nature 496:504–507. https://doi.org/10.1038/nature12060.
3. World Health Organization. 2020 Dengue and severe dengue. World Health Organization, Geneva, Switzerland. https://www.who.int/news-room/fact-sheets/detail/dengue-and-severe-dengue. Accessed 5 August 2020.
4. Srikiatkhachorn A, Mathew A, Rothman AL. 2017. Immune-mediated cytokine storm and its role in severe dengue. Semin Immunopathol 39:563–574. https://doi.org/10.1007/s00281-017-0625-1.
5. World Health Organization. 2009. Dengue: guidelines for diagnosis, treatment, prevention, and control, new ed. World Health Organization, Geneva.
6. Pierson TC, Diamond MS. 2013. Flaviviruses. *In* Knipe DM, Howley P (ed), Fields virology. Wolters Kluwer Health/Lippincott Williams & Wilkins, Philadelphia, PA.
7. Vannice KS, Wilder-Smith A, Barrett ADT, Carrijo K, Cavaleri M, de Silva A, Durbin AP, Endy T, Harris E, Innis BL, Katzelnick LC, Smith PG, Sun W, Thomas SJ, Hombach J. 2018. Clinical development and regulatory points for consideration for second-generation live attenuated dengue vaccines. Vaccine 36:3411–3417. https://doi.org/10.1016/j.vaccine.2018.02.062.
8. Juraska M, Magaret CA, Shao J, Carpp LN, Fiore-Gartland AJ, Benkeser D, Girerd-Chambaz Y, Langevin E, Frago C, Guy B, Jackson N, Duong Thi Hue K, Simmons CP, Edlefsen PT, Gilbert PB. 2018. Viral genetic diversity and protective efficacy of a tetravalent dengue vaccine in two phase 3 trials. Proc Natl Acad Sci U S A 115:E8378–E8387. https://doi.org/10.1073/pnas.1714250115.
9. de Silva AM, Harris E. 2018. Which dengue vaccine approach Is the most promising, and should we be concerned about enhanced disease after vaccination? The path to a dengue vaccine: learning from human natural dengue infection studies and vaccine trials. Cold Spring Harb Perspect Biol 10:a029371. https://doi.org/10.1101/cshperspect.a029371.
10. Whitehead SS, Durbin AP, Pierce KK, Elwood D, McElvany BD, Fraser EA, Carmolli MP, Tibery CM, Hynes NA, Jo M, Lovchik JM, Larsson CJ, Doty EA, Dickson DM, Luke CJ, Subbarao K, Diehl SA, Kirkpatrick BD. 2017. In a randomized trial, the live attenuated tetravalent dengue vaccine TV003 is well-tolerated and highly immunogenic in subjects with flavivirus exposure prior to vaccination. PLoS Negl Trop Dis 11:e0005584. https://doi.org/10.1371/journal.pntd.0005584.
11. Sharma M, Glasner DR, Watkins H, Puerta-Guardo H, Kassa Y, Egan MA, Dean H, Harris E. 2020. Magnitude and functionality of the NS1-specific antibody response elicited by a live-attenuated tetravalent dengue vaccine candidate. J Infect Dis 221:867–877. https://doi.org/10.1093/infdis/jiz081.
12. Khetarpal N, Poddar A, Nemani SK, Dhar N, Patil A, Negi P, Perween A, Viswanathan R, Lünsdorf H, Tyagi P, Raut R, Arora U, Jain SK, Rinas U, Swaminathan S, Khanna N. 2013. Dengue-specific subviral nanoparticles: design, creation and characterization. J Nanobiotechnol 11:15. https://doi.org/10.1186/1477-3155-11-15.
13. Poggianella M, Campos JLS, Chan KR, Tan HC, Bestagno M, Ooi EE, Burrone OR. 2015. Dengue E protein domain III-based DNA immunisation induces strong antibody responses to all four viral serotypes. PLoS Negl Trop Dis 9:e0003947. https://doi.org/10.1371/journal.pntd.0003947.
14. Ramasamy V, Arora U, Shukla R, Poddar A, Shanmugam RK, White LJ, Mattocks MM, Raut R, Perween A, Tyagi P, de Silva AM, Bhaumik SK, Kaja MK, Villinger F, Ahmed R, Johnston RE, Swaminathan S, Khanna N. 2018. A tetravalent virus-like particle vaccine designed to display domain III of dengue envelope proteins induces multi-serotype neutralizing antibodies in mice and macaques which confer protection against antibody dependent enhancement in AG129 mice. PLoS Negl Trop Dis 12:e0006191. https://doi.org/10.1371/journal.pntd.0006191.
15. Arora U, Tyagi P, Swaminathan S, Khanna N. 2013. Virus-like particles displaying envelope domain III of dengue virus type 2 induce virus-specific antibody response in mice. Vaccine 31:873–878. https://doi.org/10.1016/j.vaccine.2012.12.016.
16. Schmidt AC, Lin L, Martinez LJ, Ruck RC, Eckels KH, Collard A, De La Barrera R, Paolino KM, Toussaint J-F, Lepine E, Innis BL, Jarman RG, Thomas SJ. 2017. Phase 1 randomized study of a tetravalent dengue purified inactivated vaccine in healthy adults in the United States. Am J Trop Med Hyg 96:1325–1337. https://doi.org/10.4269/ajtmh.16-0634.
17. Danko JR, Kochel T, Teneza-Mora N, Luke TC, Raviprakash K, Sun P, Simmons M, Moon JE, De La Barrera R, Martinez LJ, Thomas SJ, Kenney RT, Smith L, Porter KR. 2018. Safety and immunogenicity of a tetravalent dengue DNA vaccine administered with a cationic lipid-based adjuvant in a phase 1 clinical trial. Am J Trop Med Hyg 98:849–856. https://doi.org/10.4269/ajtmh.17-0416.
18. Danko JR, Beckett CG, Porter KR. 2011. Development of dengue DNA vaccines. Vaccine 29:7261–7266. https://doi.org/10.1016/j.vaccine.2011.07.019.
19. Rajpoot RK, Shukla R, Arora U, Swaminathan S, Khanna N. 2018. Dengue envelope-based 'four-in-one' virus-like particles produced using Pichia pastoris induce enhancement-lacking, domain III-directed tetravalent neutralising antibodies in mice. Sci Rep 8:8643. https://doi.org/10.1038/s41598-018-26904-5.
20. Boigard H, Cimica V, Galarza JM. 2018. Dengue-2 virus-like particle (VLP) based vaccine elicits the highest titers of neutralizing antibodies when produced at reduced temperature. Vaccine 36:7728–7736. https://doi.org/10.1016/j.vaccine.2018.10.072.
21. Shen W-F, Galula JU, Liu J-H, Liao M-Y, Huang C-H, Wang Y-C, Wu H-C, Liang J-J, Lin Y-L, Whitney MT, Chang G-JJ, Chen S-R, Wu S-R, Chao D-Y. 2018. Epitope resurfacing on dengue virus-like particle vaccine preparation to induce broad neutralizing antibody. Elife 7:e38970. https://doi.org/10.7554/eLife.38970.
22. Metz SW, Thomas A, White L, Stoops M, Corten M, Hannemann H, de Silva AM. 2018. Dengue virus-like particles mimic the antigenic properties of the infectious dengue virus envelope. Virol J 15:60–60. https://doi.org/10.1186/s12985-018-0970-2.
23. Richner JM, Himansu S, Dowd KA, Butler SL, Salazar V, Fox JM, Julander JG, Tang WW, Shresta S, Pierson TC, Ciaramella G, Diamond MS. 2017. Modified mRNA vaccines protect against Zika virus infection. Cell 169:176. https://doi.org/10.1016/j.cell.2017.03.016.
24. Richner JM, Jagger BW, Shan C, Fontes CR, Dowd KA, Cao B, Himansu S, Caine EA, Nunes BTD, Medeiros DBA, Muruato AE, Foreman BM, Luo H, Wang T, Barrett AD, Weaver SC, Vasconcelos PFC, Rossi SL, Ciaramella G, Mysorekar IU, Pierson TC, Shi P-Y, Diamond MS. 2017. Vaccine mediated protection against Zika virus-induced congenital disease. Cell 170:273–283.e12. https://doi.org/10.1016/j.cell.2017.06.040.
25. Pardi N, Hogan MJ, Naradikian MS, Parkhouse K, Cain DW, Jones L, Moody MA, Verkerke HP, Myles A, Willis E, LaBranche CC, Montefiori DC, Lobby JL, Saunders KO, Liao H-X, Korber BT, Sutherland LL, Scearce RM, Hraber PT, Tombácz I, Muramatsu H, Ni H, Balikov DA, Li C, Mui BL, Tam YK, Krammer F, Karikó K, Polacino P, Eisenlohr LC, Madden TD, Hope MJ, Lewis MG, Lee KK, Hu S-L, Hensley SE, Cancro MP, Haynes BF, Weissman D. 2018. Nucleoside-modified mRNA vaccines induce potent T follicular helper and germinal center B cell responses. J Exp Med 215:1571–1588. https://doi.org/10.1084/jem.20171450.
26. Lutz J, Lazzaro S, Habbeddine M, Schmidt KE, Baumhof P, Mui BL, Tam YK, Madden TD, Hope MJ, Heidenreich R, Fotin-Mleczek M. 2017. Unmodified mRNA in LNPs constitutes a competitive technology for prophylactic vaccines. NPJ Vaccines 2:29. https://doi.org/10.1038/s41541-017-0032-6.
27. Firdessa-Fite R, Creusot RJ. 2020. Nanoparticles versus dendritic cells as vehicles to deliver mRNA encoding multiple epitopes for immunotherapy. Mol Ther Methods Clin Dev 16:50–62. https://doi.org/10.1016/j.omtm.2019.10.015.
28. Liang F, Lindgren G, Lin A, Thompson EA, Ols S, Röhss J, John S, Hassett K, Yuzhakov O, Bahl K, Brito LA, Salter H, Ciaramella G, Loré K. 2017. Efficient targeting and activation of antigen-presenting cells in vivo after modified

mRNA vaccine administration in rhesus macaques. Mol Ther 25:2635–2647. https://doi.org/10.1016/j.ymthe.2017.08.006.
29. Crill WD, Hughes HR, Trainor NB, Davis BS, Whitney MT, Chang G-JJ. 2012. Sculpting humoral immunity through dengue vaccination to enhance protective immunity. Front Immunol 3:334–334. https://doi.org/10.3389/fimmu.2012.00334.
30. Allison SL, Schalich J, Stiasny K, Mandl CW, Heinz FX. 2001. Mutational evidence for an internal fusion peptide in flavivirus envelope protein E. J Virol 75:4268–4275. https://doi.org/10.1128/JVI.75.9.4268-4275.2001.
31. Urakami A, Ngwe Tun MM, Moi ML, Sakurai A, Ishikawa M, Kuno S, Ueno R, Morita K, Akahata W. 2017. An envelope-modified tetravalent dengue virus-like-particle vaccine has implications for flavivirus vaccine design. J Virol 91:e01181-17. https://doi.org/10.1128/JVI.01181-17.
32. Lok S-M, Kostyuchenko V, Nybakken GE, Holdaway HA, Battisti AJ, Sukupolvi-Petty S, Sedlak D, Fremont DH, Chipman PR, Roehrig JT, Diamond MS, Kuhn RJ, Rossmann MG. 2008. Binding of a neutralizing antibody to dengue virus alters the arrangement of surface glycoproteins. Nat Struct Mol Biol 15:312–317. https://doi.org/10.1038/nsmb.1382.
33. Sukupolvi-Petty S, Austin SK, Purtha WE, Oliphant T, Nybakken GE, Schlesinger JJ, Roehrig JT, Gromowski GD, Barrett AD, Fremont DH, Diamond MS. 2007. Type- and subcomplex-specific neutralizing antibodies against domain III of dengue virus type 2 envelope protein recognize adjacent epitopes. J Virol 81:12816–12826. https://doi.org/10.1128/JVI.00432-07.
34. Roehrig JT, Bolin RA, Kelly RG. 1998. Monoclonal antibody mapping of the envelope glycoprotein of the dengue 2 virus, Jamaica. Virology 246:317–328. https://doi.org/10.1006/viro.1998.9200.
35. Allison SL, Stadler K, Mandl CW, Kunz C, Heinz FX. 1995. Synthesis and secretion of recombinant tick-borne encephalitis virus protein E in soluble and particulate form. J Virol 69:5816–5820. https://doi.org/10.1128/JVI.69.9.5816-5820.1995.
36. Shang W, Liu J, Yang J, Hu Z, Rao X. 2012. Dengue virus-like particles: construction and application. Appl Microbiol Biotechnol 94:39–46. https://doi.org/10.1007/s00253-012-3958-7.
37. Figueiredo Neto M, Figueiredo ML. 2016. Skeletal muscle signal peptide optimization for enhancing propeptide or cytokine secretion. J Theor Biol 409:11–17. https://doi.org/10.1016/j.jtbi.2016.08.036.
38. Karikó K, Muramatsu H, Welsh FA, Ludwig J, Kato H, Akira S, Weissman D. 2008. Incorporation of pseudouridine into mRNA yields superior nonimmunogenic vector with increased translational capacity and biological stability. Mol Ther 16:1833–1840. https://doi.org/10.1038/mt.2008.200.
39. Karikó K, Muramatsu H, Ludwig J, Weissman D. 2011. Generating the optimal mRNA for therapy: HPLC purification eliminates immune activation and improves translation of nucleoside-modified, protein-encoding mRNA. Nucleic Acids Res 39:e142. https://doi.org/10.1093/nar/gkr695.
40. Balsitis SJ, Williams KL, Lachica R, Flores D, Kyle JL, Mehlhop E, Johnson S, Diamond MS, Beatty PR, Harris E. 2010. Lethal antibody enhancement of dengue disease in mice is prevented by Fc modification. PLoS Pathog 6:e1000790. https://doi.org/10.1371/journal.ppat.1000790.
41. Zellweger RM, Shresta S. 2014. Mouse models to study dengue virus immunology and pathogenesis. Front Immunol 5:151. https://doi.org/10.3389/fimmu.2014.00151.
42. Sarathy VV, Milligan GN, Bourne N, Barrett ADT. 2015. Mouse models of dengue virus infection for vaccine testing. Vaccine 33:7051–7060. https://doi.org/10.1016/j.vaccine.2015.09.112.
43. Pardi N, LaBranche CC, Ferrari G, Cain DW, Tombácz I, Parks RJ, Muramatsu H, Mui BL, Tam YK, Karikó K, Polacino P, Barbosa CJ, Madden TD, Hope MJ, Haynes BF, Montefiori DC, Hu S-L, Weissman D. 2019. Characterization of HIV-1 nucleoside-modified mRNA vaccines in rabbits and rhesus macaques. Mol Ther Nucleic Acids 15:36–47. https://doi.org/10.1016/j.omtn.2019.03.003.
44. Jackson LA, Anderson EJ, Rouphael NG, Roberts PC, Makhene M, Coler RN, McCullough MP, Chappell JD, Denison MR, Stevens LJ, Pruijssers AJ, McDermott A, Flach B, Doria-Rose NA, Corbett KS, Morabito KM, O'Dell S, Schmidt SD, Swanson PA, Padilla M, Mascola JR, Neuzil KM, Bennett H, Sun W, Peters E, Makowski M, Albert J, Cross K, Buchanan W, Pikaart-Tautges R, Ledgerwood JE, Graham BS, Beigel JH. 2020. An mRNA vaccine against SARS-CoV-2—preliminary report. N Engl J Med 383:1920–1931. https://doi.org/10.1056/NEJMoa2022483.
45. Mulligan MJ, Lyke KE, Kitchin N, Absalon J, Gurtman A, Lockhart S, Neuzil K, Raabe V, Bailey R, Swanson KA, Li P, Koury K, Kalina W, Cooper D, Fontes-Garfias C, Shi P-Y, Türeci Ö, Tompkins KR, Walsh EE, Frenck R, Falsey AR, Dormitzer PR, Gruber WC, Şahin U, Jansen KU. 2020. Phase I/II study of COVID-19 RNA vaccine BNT162b1 in adults. Nature 586:589–593. https://doi.org/10.1038/s41586-020-2639-4.
46. Anderson EJ, Rouphael NG, Widge AT, Jackson LA, Roberts PC, Makhene M, Chappell JD, Denison MR, Stevens LJ, Pruijssers AJ, McDermott AB, Flach B, Lin BC, Doria-Rose NA, O'Dell S, Schmidt SD, Corbett KS, Swanson PA, Padilla M, Neuzil KM, Bennett H, Leav B, Makowski M, Albert J, Cross K, Edara VV, Floyd K, Suthar MS, Martinez DR, Baric R, Buchanan W, Luke CJ, Phadke VK, Rostad CA, Ledgerwood JE, Graham BS, Beigel JH, mRNA-1273 Study Group. 2020. Safety and immunogenicity of SARS-CoV-2 mRNA-1273 vaccine in older adults. N Engl J Med 383:2427–2438. https://doi.org/10.1056/NEJMoa2028436.
47. VanBlargan LA, Himansu S, Foreman BM, Ebel GD, Pierson TC, Diamond MS. 2018. An mRNA vaccine protects mice against multiple tick-transmitted flavivirus infections. Cell Rep 25:3382–3392.e3. https://doi.org/10.1016/j.celrep.2018.11.082.
48. Zhang M, Sun J, Li M, Jin X. 2020. Modified mRNA-LNP vaccines confer protection against experimental DENV-2 infection in mice. Mol Ther Methods Clin Dev 18:702–712. https://doi.org/10.1016/j.omtm.2020.07.013.
49. Henein S, Swanstrom J, Byers AM, Moser JM, Shaik SF, Bonaparte M, Jackson N, Guy B, Baric R, de Silva AM. 2017. Dissecting antibodies induced by a chimeric yellow fever-dengue, live-attenuated, tetravalent dengue vaccine (CYD-TDV) in naive and dengue-exposed individuals. J Infect Dis 215:351–358. https://doi.org/10.1093/infdis/jiw576.
50. Biswal S, Reynales H, Saez-Llorens X, Lopez P, Borja-Tabora C, Kosalaraksa P, Sirivichayakul C, Watanaveeradej V, Rivera L, Espinoza F, Fernando L, Dietze R, Luz K, Venâncio da Cunha R, Jimeno J, López-Medina E, Borkowski A, Brose M, Rauscher M, LeFevre I, Bizjajeva S, Bravo L, Wallace D, TIDES Study Group. 2019. Efficacy of a tetravalent dengue vaccine in healthy children and adolescents. N Engl J Med 381:2009–2019. https://doi.org/10.1056/NEJMoa1903869.
51. Kirkpatrick BD, Durbin AP, Pierce KK, Carmolli MP, Tibery CM, Grier PL, Hynes N, Diehl SA, Elwood D, Jarvis AP, Sabundayo BP, Lyon CE, Larsson CJ, Jo M, Lovchik JM, Luke CJ, Walsh MC, Fraser EA, Subbarao K, Whitehead SS. 2015. Robust and balanced immune responses to all 4 dengue virus serotypes following administration of a single dose of a live attenuated tetravalent dengue vaccine to healthy, flavivirus-naive adults. J Infect Dis 212:702–710. https://doi.org/10.1093/infdis/jiv082.
52. Anderson BR, Karikó K, Weissman D. 2013. Nucleofection induces transient eIF2α phosphorylation by GCN2 and PERK. Gene Ther 20:136–142. https://doi.org/10.1038/gt.2012.5.
53. Tian Y, Grifoni A, Sette A, Weiskopf D. 2019. Human T cell response to dengue virus infection. Front Immunol 10:2125. https://doi.org/10.3389/fimmu.2019.02125.
54. Roth C, Cantaert T, Colas C, Prot M, Casadémont I, Levillayer L, Thalmensi J, Langlade-Demoyen P, Gerke C, Bahl K, Ciaramella G, Simon-Loriere E, Sakuntabhai A. 2019. A modified mRNA vaccine targeting immunodominant NS epitopes protects against dengue virus infection in HLA class I transgenic mice. Front Immunol 10:1424. https://doi.org/10.3389/fimmu.2019.01424.
55. Hughes HR, Crill WD, Chang G-JJ. 2012. Manipulation of immunodominant dengue virus E protein epitopes reduces potential antibody-dependent enhancement. Virol J 9:115–115. https://doi.org/10.1186/1743-422X-9-115.

frontiers | Frontiers in Endocrinology

REVIEW
published: 20 June 2022
doi: 10.3389/fendo.2022.898810

Impact of Obesity on Vaccination to SARS-CoV-2

Michaella-Jana C. Nasr, Elizabeth Geerling and Amelia K. Pinto *

Department of Molecular Microbiology and Immunology, Saint Louis University School of Medicine, St. Louis, MO, United States

To combat the immense toll on global public health induced by severe acute respiratory syndrome coronavirus 2 (SARS-CoV-2), new vaccines were developed. While these vaccines have protected the populations who received them from severe SARS-CoV-2 infection, the effectiveness and durability of these vaccines in individuals with obesity are not fully understood. Our uncertainty of the ability of these novel vaccines to induce protective immunity in humans with obesity stems from historical data that revealed obesity-associated immune defects to influenza vaccines. This review analyzes the efficacy of SARS-CoV-2 vaccines in humans with obesity. According to the vaccine safety and efficacy information for the Pfizer, Moderna, and Johnson & Johnson formulations, these vaccines showed a similar efficacy in both individuals with and without obesity. However, clinical trials that assess BMI and central obesity showed that induced antibody titers are lower in individuals with obesity when compared to healthy weight subjects, highlighting a potential early waning of vaccine-induced antibodies linked to obesity rates. Thus, the desired protective effects of SARS-CoV-2 vaccination were potentially diminished in humans with obesity when compared to the healthy weight population, but further studies outlining functional implications of the link between obesity and lower antibody titers need to be conducted to understand the full impact of this immune phenomenon. Further, additional research must be completed to truly understand the immune responses mounted against SARS-CoV-2 in patients with obesity, and whether these responses differ from those elicited by previously studied influenza viruses.

Keywords: COVID- 19, Moderna vaccine, Pfizer, Johnson & Johnson, SARS – CoV – 2, obesity, BMI - body mass index

OPEN ACCESS

Edited by:
Marwan El Ghoch,
Beirut Arab University, Lebanon

Reviewed by:
Lucio Gnessi,
Sapienza University of Rome, Italy
Rashika Bansal,
Cleveland Clinic, United States

***Correspondence:**
Amelia K. Pinto
amelia.pinto@health.slu.edu

Specialty section:
This article was submitted to Obesity, a section of the journal Frontiers in Endocrinology

Received: *17 March 2022*
Accepted: *17 May 2022*
Published: *20 June 2022*

Citation:
Nasr M-JC, Geerling E and Pinto AK (2022) Impact of Obesity on Vaccination to SARS-CoV-2. Front. Endocrinol. 13:898810. doi: 10.3389/fendo.2022.898810

INTRODUCTION

In November 2019, a new, highly infectious RNA virus in the *Coronaviridae* family, termed severe acute respiratory syndrome coronavirus 2 (SARS-CoV-2), emerged. SARS-CoV-2 infections became uncontrolled worldwide and caused a widespread illness coined coronavirus-2019 disease (COVID-19) (1). SARS-CoV-2 has infected and killed millions of individuals worldwide with numbers still rising, leaving the world suspended in a pandemic state (1, 2). The severity of this viral disease and its associated negative outcomes correlate with multiple risk factors, including age (1) and presence of other diseases (3), with obesity being a major risk factor for COVID-19 and subsequent death (1–5).

As COVID-19 continues to pose a public health threat and new, more infectious variants arise, the importance of vaccinations and booster vaccines have become more apparent (6). However, based upon previous research studying the vaccine responses to Influenza A (H1N1) in populations with high obesity rates, we predict that SARS-CoV-2 vaccine responses will wane more rapidly in individuals with obesity. Thus, patients of obesity, who are at a higher risk of severe viral infection and death by COVID-19, might not have the same duration of vaccine-conferred protection as individuals without obesity (7, 8). Further compounding the importance of studying the impact of obesity on vaccine-induced immune responses, studies done over the course of 2021 after SARS-CoV-2 vaccinations became widely available to the public indicated that obesity may be linked to breakthrough infections (9–16).

THE ETIOLOGIES AND CONSEQUENCES OF THE OBESITY PANDEMIC

The SARS-CoV-2 pandemic is not the only current pandemic; the prevalence of obesity has tripled from 1975 to 2016 worldwide (2). Almost 2 billion people worldwide are either overweight or obese, and the global prevalence of obesity in the younger population has increased by 47% between 1980 and 2013 (17). Currently in the United States, about one third of adults and 17% of children are obese or overweight (18).

Obesity is characterized by abnormal or excessive fat accumulation that causes pathophysiology, threatening overall health (19). One standard to measure obesity is body mass index (BMI), where individuals with a BMI of > 30kg/m^2 are classified as obese, while another is by using central obesity in which waist circumference is ≥ 80 cm for women and ≥94 cm for men (16, 19). Obesity is a multifactorial disease that is commonly caused by excess dietary intake relative to energy expenditure (2, 20). The complex etiology of obesity is not limited to overeating and sedentary lifestyles (21). This disease can develop from a mixture of genetic, physiologic, psychologic, environmental, political, and social factors. Commonly used medications including corticosteroids and some anti-depressants, endocrine disruptors, lack of sleep and microbiome diversity have all been implicated in obesity (20, 22, 23). The combination of inexpensive, high caloric, fat-laden foods and decreased physical activity over the last few decades are often listed as significant contributors to the prevalence of obesity (20). In addition, the cessation of smoking may be a contributor to the obesity pandemic, as weight gain is a common consequence of smoking cessation (20, 24). As the etiological factors that lead to obesity are multifactorial and often difficult to counteract, efforts on improving treatments and vaccines for individuals with obesity are essential.

Obesity is associated with increased all-cause mortality and the risk of developing other complications, such as cardiovascular disease, hypertension, several types of cancer, diabetes mellitus, gallbladder disease, kidney disease, osteoarthritis, and stroke (2, 17). Additionally, obesity is shown to increase the risk of acquiring respiratory tract infections, like SARS-CoV-2 and influenza A virus and can impede pulmonary function through decreased expiratory reserve volume, functional capacity, and lung compliance (4, 25). In the obese state, pulmonary function is compromised due to higher abdominal fat which can also decrease diaphragm excursion (4). Treatment of obesity and its related sequelae requires approximately 21% of the United States health care expenditure, which poses an economic burden on top of a public health concern (26). Thus, the pandemic state of obesity, coupled with its related illnesses and risks, makes having appropriate medical tools to counteract rising obesity rates — the treatment, prevention, and surveillance — a public health necessity (18, 27). As such, it is imperative that scientific efforts and funding are geared toward obesity research.

THE EFFECTS OF OBESITY ON THE IMMUNE SYSTEM

Underlying the association between poor vaccine responses and obesity is the effect of obesity on the immune system. Obesity is associated with immune cell-mediated inflammation (7, 28), and the influence of this inflammation on immune responses is only now beginning to be understood. Expansion of adipose tissue is linked to increased inflammation (29). While adipose tissue in individuals with a healthy weight predominately contains regulatory and suppressive cytokines including IL-4, IL-10, IL-13, and IL-33, adipose tissue in individuals who are obesity is associated inflammatory cytokines including IL-1β, IL-6, IL-12, IL-18, TNF-α, and IFN-γ (30–32). Adipokines and cytokines direct the immune responses to pathogens and the presence or absence of adipokines and cytokines during vaccination can alter adaptive immune response development leading to differences in the protective efficacy following vaccination.

Previous studies have also reported an association between leptin and altered influenza vaccine responses (33, 34). Leptin, an adipokine (cell-signaling hormone) that regulates appetite and controls energy metabolism (35), is found throughout the immune system on innate immune cells (macrophages, dendritic cells, and mast cells) and on adaptive immune cells (B and T cells). Leptin plays a major role in the chronic inflammation found in patients with obesity (35). Leptin's effect on neutrophils is especially important in COVID-19 progression in the obese state: increased leptin levels, characterized by increased neutrophilic lung inflammation, causes more severe lung injury (1). Higher leptin in obesity also correlates with a decreased levels of T_{reg} cells, resulting in more pro-inflammatory than anti-inflammatory cytokine expression, and an increased activation of neutrophils (1). Leptin has also been shown to direct T cell proliferation and reactivity by activating the JAK/STAT pathway, thereby enhancing immune inflammation (36, 37). However, based on some studies in humans and animals, it is thought that the hyperleptinemia state in patients with obesity may eventually induce leptin resistance (35, 38, 39). Leptin sensitivity and

resistance remain active areas of research and the clinical criteria for defining leptin resistance and its diagnostic use have not yet been established.

As previously described, the expansion of adipose tissue in the obese state is known to contribute to chronic, low-grade inflammation due to adipocyte hypoxia and resulting immune cell infiltration (21, 40). Chronic inflammation not only directly increases the risk for cardiovascular disease (CVD) and diabetes, but also causes upregulation of proteins and cytokines (like p38 MAPK and TNF-α), which can cause tissue damage (1, 21, 40) and result in a positive feedback loop that further promotes inflammation. This chronic immune stimulation can weaken the humoral responses and cell-mediated immunity, specifically lowering T cell response magnitude and increasing the time it takes for such responses to be mounted (7, 8). For example, individuals with obesity show suppressed T cell activation and differentiation in response to influenza infection when compared to individuals of healthy weights. Also, decreases in T cell production of effector molecules like IFN-γ and granzyme B is associated with obesity (7, 28). Further, obesity can induce B cell defects, including a lower frequency of regulatory B cells (with phenotypes $CD19^{+}$ $CD27^{+}$ $CD38^{High}$, $CD19^{+}$ $CD24^{High}$ $CD38^{High}$, and $CD19^{+}$ $CD24^{High}$ $CD38^{High}$ $IL\text{-}10^{+}$), in response to infection (41, 42). This obesity-induced immune suppression, particularly regarding B cell impairment, makes it unsurprising that individuals with obesity have inadequate seroconversion rates following vaccination. This is shown with decreased antibody titers in response to vaccination to hepatitis B, tetanus, and rabies (43). In addition to decreased antibody titers following vaccination, antibody responses also wane rapidly in individuals with obesity compared to people of healthy weights (44). Furthermore, the influenza vaccine is not as effective in individuals with obesity compared to individuals of healthy weights, potentially in part due to decreased antibody titers, decreased CD8+ T-cell activation, and decreased production of functional proteins IFN-ɣ and granzyme B (44, 45).

Data gathered from previous vaccine trials have shown that development of personalized vaccines might be necessary to surmount the immune suppression induced by obesity (7). Identifying the effects of obesity on immune responses mounted post-influenza infection or vaccination have provided key insights on how to improve vaccine design so vaccination can better protect populations with high obesity rates from severe viral disease and confer lifelong protection that does not rapidly wane.

EFFECTS OF OBESITY ON SARS-COV-2 INFECTION AND SEVERITY

First identified during the 2009 influenza A (H1N1) pandemic, obesity is a major risk factor for severe respiratory viral infection and increased mortality of infected individuals (19, 46). Obesity is associated with increased hospitalizations, intensive care unit (ICU) admissions, intubations, invasive mechanical ventilations (IMV), and viral exposures when compared to patients of healthy weight (19, 47–49). The exacerbation of COVID-19 disease progression in the population with obesity is thought to be linked to higher viral load and slower antiviral responses seen in COVID-19 patients with obesity (19).

Similar to the H1N1 pandemic, enhanced viral disease severity among COVID-19 patients with obesity have been noted amidst the SARS-CoV-2 pandemic. First, hospital admissions, stays, and recovery time of COVID-19 patients with obesity are longer than those of individuals of healthy weights (19, 50). Specifically, patients with obesity took 19 ± 8 days to achieve a negative nasopharyngeal swab for SARS-CoV-2 resolution compared to individuals of healthy weights who took 13 ± 7 days (50). Furthermore, among ICU COVID-19 patients, a higher BMI was reported in comparison with non-ICU patients (19). Interestingly, in a study conducted in Italy among 1591 ICU patients, 68% had at least one comorbidity, including hypertension, CVD, and diabetes, which are all obesity-related illnesses (51). Similarly, IMV indications were positively correlated with elevated BMI, and were greatest in COVID patients with a BMI ≥ 35 kg/m^2 (19). Obesity also increased the risk of pneumonia in COVID-19 patients compared to individuals without obesity (52). In addition, acute respiratory distress syndrome (ARDS), embodied by respiratory failure and hypoxemia, is a severe consequence of COVID-19, and reports highlight that obesity increases the ARDS risk and incidence in COVID-19 patients compared to COVID-19 patients of healthy weights (19). Due to the severe effects of COVID-19 infections in individuals with obesity and their diminished immune responses contributing to viral disease progression, targeted treatments are necessary to avoid long-term health effects and death in this patient population. Similar to data from influenza infections, SARS-CoV-2 patient outcome statistics again highlight the importance of formulating personalized vaccines or modifying vaccine schedules on a per patient basis.

SARS-COV-2 VACCINE TRIALS AND OBESITY

To combat the SARS-CoV-2 pandemic, multiple vaccine platforms were adapted for rapid Phase I, II and III clinical trials with limited or emergency use. Four vaccines are currently approved for use and being used worldwide from the following manufacturers: Moderna, Johnson & Johnson (J&J, Jansen Ad26), AstraZeneca and Pfizer-BioNTech (Pfizer, BNT162b2 mRNA). Along with the Pfizer-BioNTech vaccine, the Moderna vaccine was granted full FDA approval. During the clinical trial phases, Pfizer, Moderna, and J&J collected data on vaccine efficacy (VE) in individuals with obesity against the ancestral SARS-CoV-2 strain and alpha variant of concern; however, AstraZeneca has not provided data about VE in subjects with obesity. Thus, the remainder of our review will focus on the three vaccine platforms currently used in the United States that assessed VE in the context of obesity: Moderna, J&J and Pfizer.

Pfizer BioNTech BNT162b2

The Pfizer BNT162b2 formulation is an mRNA vaccine encoding the full-length spike (S) protein (53, 54). The phase III trial for this vaccine included a sample size of about 43,000 people and was a randomized, placebo-controlled trial (53). In this trial, participants received 2 doses (21 days apart) of either the vaccine or a placebo (53). Independent of weight, the VE was 95% in people without a previous COVID-19 infection who received the vaccine compared to the ones who received the placebo (53).

In this phase III trial, 13,218 subjects were classified as having obesity based on a BMI ≥ 30 kg/m^2 (53). The vaccinated group had 6,556 participants with obesity, and the placebo group had 6,662 participants with obesity (53). Based on results from this trial, obesity did not impact VE (53). Specifically, this study looked seven days after the second dose where VE was 95.4% in individuals with obesity versus 94.8% VE in subjects without obesity (53). When these data were stratified for age, no significant differences in VE were noted; VE in younger adults with obesity (ages:16-64) was ~95%, whereas in older adults with obesity (age >65), VE was 100% (53). While these data are promising, VE tests were completed only seven days after the second dose; VE studies were not conducted at later time points post-vaccination. Similarities in the vaccine responses early after vaccination between either individuals with obesity or of healthy weights have previously been seen in studies of the seasonal influenza vaccine (44). However, in such studies, virus specific antibody responses wane significantly in individuals with obesity after one year as compared to antibody titers of individuals of healthy weights (44).

The impact of obesity on the durability of vaccine-conferred protection is critical to understand as multiple studies have shown that a booster or third dose of a SARS-CoV-2 vaccine helps provide protection as immunity against this virus wanes (55–58). In at least one limited study consisting of 1,060 subjects, antibody levels to SARS-CoV-2 following the Pfizer BNT162b2 mRNA vaccination were measured at baseline, 21 days post first dose, 30-40 days post second dose and 90-100 days post second dose and compared between subjects with obesity versus those without. Consistent with studies conducted following seasonal influenza virus vaccination, early antibody titers were essentially equivalent between individuals with obesity versus those without, but by one month post second dose, antibody titers reported for subjects with obesity were significantly lower than those noted for subjects of healthy weight. Similarly, antibody titers of individuals with obesity were further significantly reduced at three months post-second dose when compared to levels reported for individuals of healthy weights (59). However, these studies only report a waning of the antibody response and did not address the implications of decreased antibody titers in individuals with obesity. Further studies using functional assays need to be conducted to determine if lower antibody titers correlate with functional defects in the ability for individuals with obesity.

In concordance with the previously described study, a study done by Watanabe et al. enrolled 22 adult subjects experiencing central obesity and at least one obesity-associated comorbidity, such as hypertension. This study was conducted to examine the impact of obesity on immune responses elicited by the Pfizer BNT162b2 mRNA vaccine (60). Prior to entering the study, these subjects were not vaccinated against SARS-CoV-2 and upon enrollment into the study, patients were placed on dietary intervention, with energy requirements calculated by adjusting for the physical activity level of each individual (60). Patients were vaccinated against SARS-CoV-2, and data generated following both doses in the vaccine schedule highlighted that BMI was inversely correlated with both cell-mediated and humoral immune responses (60). Interestingly, while following the dietary restrictions established upon enrollment into this study, patients lost ~10% of their body weight (accompanied by metabolic improvements), and this weight loss positively correlated with improved cell-mediated responses following vaccination (60). This study provides a unique perspective on vaccination in individuals plagued by obesity as it highlights that losing weight, or improving metabolic health, may counteract the immune defects that occur during priming in the obese state, showing that these cellular changes can be reversed.

Moderna mRNA-1273

The Moderna SARS-CoV-2 vaccine also utilizes an mRNA platform, coined mRNA-1273. This vaccine encodes a stabilized pre-fusion form of the S protein, a desirable vaccine design due to stabilized pre-fusion viral glycoproteins being highly immunogenic (54, 61). A randomized, placebo-controlled trial was conducted with a sample size of 30,351 participants (61). These participants were adults (age >18). Similar to the Pfizer trial, two doses were given to participants, but they were administered 28 days apart instead of 21 (61). The overall efficacy of this vaccine was 94.1%, but when VE was measured separately only among the vaccinated individuals with obesity (901 subjects), VE only dropped slightly from 94.1% to 91.2%. However, 11 cases of COVID-19 were reported in the vaccinated group, one of which was severe and did occur in a subject with obesity (61). On the other hand, 185 COVID-19 cases were reported in the placebo group. Of the 185 cases, 30 cases were severe, and one case led to death (61). Similarly, these data were further broken down to examine infection rates about placebo subjects with obesity. Of the 30 severe COVID-19 cases reported among the placebo group, 11 of them were diagnosed in subjects with obesity. Thus, overall, mRNA-1273 VE appeared to be similar between subjects with obesity or those of healthy weights, although reported viral disease severity did trend higher in the subjects with obesity.

However, similar to the Pfizer BioNTech BNT162b2 phase three trial, the primary endpoint for this study was 15 days after the second vaccine dose was given. While the VE reported in this clinical trial appears promising for individuals with obesity, as noted above, prior research suggests that it is essential to look at the long-term durability of VE to conclude if obesity impacts SARS-CoV-2 vaccine-conferred protection. Further studies should be conducted to examine the durability of vaccine specific responses in humans with obesity to determine if administering booster vaccinations earlier might could sustain long-term immunity to viral pathogens.

Janssen/Johnson & Johnson Ad26.CoV2.S

J&J developed a replication-incompetent adenovirus serotype 26 vectored vaccine (Ad26.CoV2.S) and similarly conducted a randomized, double blind, placebo-controlled trial. The sample size of this trial was 39,321 individuals (62). In this vaccine schedule, only one dose is administered to each subject. Fourteen days post-vaccination, VE was reported as 67.4%. By 28 days post-vaccination, VE was noted to be 66.2%.

In this trial, 28.5% of the cohort were classified as having obesity based on BMI > 30kg/m^2. VE in this group was 66.8% 2 weeks post-vaccination and 65.9% 28 days post-vaccination. No deaths were reported among subjects with obesity in the vaccinated group, but 6 out of 7 fatalities in the placebo group were subjects with obesity (62). Based on this phase three trial, the reported VE was consistent in individuals with obesity compared to subjects of healthy weights as reported for the Pfizer BioNTech and Moderna formulations, but viral disease severity did trend higher in the unvaccinated subjects with obesity. Again, although VE reported in this trial appears equivalent among subjects with obesity versus those without, tracking vaccine-specific immune responses as time progresses post-vaccination could illuminate implications for obesity on durability of VE.

CURRENT RESEARCH MAY ILLUSTRATE EFFECTS OF OBESITY ON VACCINATION AGAINST SARS-COV-2

Although information provided from the SARS-CoV-2 vaccine trials did not appear to show differences in terms of VE between individuals with obesity versus those of healthy weights, several longitudinal studies have highlighted some immune defects in populations with high obesity rates. One longitudinal study measured the effects of central obesity on Pfizer/BioNTech vaccination in 86 healthcare workers in Italy (16). This study showed that central obesity was associated with lower antibody titers following vaccination, but this phenomenon occurred independently from BMI (16). In a study looking at the antibody titers of individuals who were overweight, obese or of healthy weight between the first and second dose of the Pfizer/BioNTech vaccine, Pellini et al. noted that a single vaccination activated the humoral immune response in individuals of healthy weights, but some subjects with obesity or who were reported as being overweight (age >47 and BMI >25 kg/m^2) did not have a change in their IgG antibody levels (41). The authors concluded that IgG antibody titers in populations classified as having healthy weights or being young in age were higher than antibody responses in populations classified as being overweight or older in age, but more research has to be done regarding its direct correlation to protection against severe viral disease (41). While both studies noted a difference in antibody responses following vaccination, the results differ as to the association with BMI and central obesity. The current randomized, controlled trials assessed different measures of obesity, but both showed that obesity can be associated with a lower antibody titer following vaccination to COVID-19. These studies suggest that variabilities in how vaccine efficacy is measured, the time elapsed post vaccination, and the specific vaccine formulation administered can lead to confounding results. However, these studies, as well as the phase three trial discussed above, reveal that vaccination of the individuals with obesity against SARS-CoV-2 is effective, at least for conferring short-term protection. While the duration of the effectiveness may be shortened, there is a window of time where protection is observed. As the SARS-CoV-2 pandemic is ongoing, follow up studies comparing vaccine-induced immune responses among individuals with obesity versus those of healthy weights are essential studies to conduct.

DISCUSSION

Data from the phase III SARS-CoV-2 vaccine trials and subsequent clinical trials conducted to measure immune responses primed in the obese state after inoculation produced results that contradict each other, likely due to the physiological complexity of obesity. Overall, the vaccine trials of the three SARS-CoV-2 vaccines administered in the US show that they are efficacious in individuals with obesity; however, statistical analyses were not completed on these data to validate the outcomes. Moreover, other clinical trial cohorts report decreased antibody titers and weakened immune responses following SARS-CoV-2 vaccination in individuals who are overweight or obese. The current research is limited, and the contradiction sparks a need for further studies to be conducted. The clinical trials that measured central obesity did not find an association to BMI and a decreased immune response. This finding does not match with Pellini et al. (41) and their study on BMI, in which a high BMI was associated with lower antibody titers. Watanabe et al. explain that BMI is not an appropriate way of measuring obesity, highlighting that central obesity presents a more accurate measure of the severity of obesity and its sequalae in those with high waist circumferences, a phenomenon that has shifted the field of obesity to now focus on classifying individuals as having metabolic syndrome. Thus, different measures of obesity might indicate a varying response than what is seen in the vaccine trials, as the vaccine trials used BMI to assess efficacy of the vaccine in individuals with obesity, and it is possible that a different measure of obesity might yield a different result. Hence, more research is necessary to resolve these scientific questions.

Additionally, the study methods differed in a way that might lead to significant differences in vaccine efficacy results, such as measuring antibody titers at varying time points or using different antibody measuring kits. Moreover, the sample sizes in the clinical trials measuring the effects of obesity on vaccine responses in individuals with obesity were small compared to samples sizes utilized in vaccine trials and not entirely representative of the general population of individuals with obesity. For example, Watanabe et al. and Pellini et al. (41, 60) recruited study participants who were healthcare workers, a group that generally has more access to health care to help with any current or future obesity-related illnesses, in contrast to

the general population which may not have immediate or affordable health care access. Further, although some pre-existing medical conditions were noted for the subjects analyzed in these studies, information regarding their medication use to treat such conditions was not disclosed, potentially skewing the data generated.

Even with the present research presented, many questions remain unanswered, such as how immune responses change depending on the age demographic. The clinical trials discussed throughout this review focused on adults, but with an increasing population of children becoming overweight and obese, studies must be expanded to include subjects of varying ages to determine whether vaccines are efficacious in conferring protection against severe viral diseases in children with obesity. It is also difficult to assess how people with obesity-related comorbidities benefit from the current vaccines, especially regarding lifelong, durable protection. Furthermore, if vaccine efficacy is similar in individuals with obesity to those individuals of healthy weights during a close time frame to when the vaccine is administered, how durable vaccine efficacy is in individuals with obesity is unknown and could pose threats to public health as time post vaccination increases. It is possible that additional vaccine boosters will be necessary for individuals with obesity to achieve protective and durable vaccine-induced immunity.

CONCLUSION

We believe that more research needs to be done to assess the impact of obesity on vaccination to SARS-CoV-2. The currently reported research is contradictory, and numerous questions remain unanswered. We believe more work needs to be done to assess long-term efficacy of the available vaccines to SARS-CoV-2, what the best scheduling for boosters is, and how different patterns of fat distribution could be affecting immune responses to vaccination. However, it is clear that obesity hinders immune responses to vaccines and infections. As obesity rates are projected to continually rise globally, it is important to gear medical treatments towards populations with high obesity incidences and to increase awareness about non-dietary causes of obesity. Furthermore, more data needs to be gathered concerning the growing number of young individuals with obesity and if they will be protected from severe viral disease by SARS-CoV-2 vaccines. With these future research efforts in mind, we are confident that vaccine development can improve to induce long-lasting, protective immune responses in patients with obesity.

AUTHOR CONTRIBUTIONS

All authors listed have made a substantial, direct, and intellectual contribution to the work, and approved it for publication.

FUNDING

This work was supported in part by the National Institutes of Health, National Institute of Allergy and Infectious Diseases (NIAID): 5R01AI137424-03, and in part by the Department of Defense (award no. PR192269). The funders had no role in decision to publish, or preparation of the manuscript.

ACKNOWLEDGMENTS

We would like to acknowledge the efforts of Dr. James Brien and graduate students Valerie Murphy and E. Taylor Stone whose thoughtful comments and suggestions have improved this manuscript.

REFERENCES

1. Alberca RW, Oliveira LM, Branco A, Pereira NZ, Sato MN. Obesity as a Risk Factor for COVID-19: An Overview. *Crit Rev Food Sci Nutr* (2021) 61:2262–76. doi: 10.1080/10408398.2020.1775546
2. Rychter AM, Zawada A, Ratajczak AE, Dobrowolska A, Krela-Kazmierczak I. Should Patients With Obesity be More Afraid of COVID-19? *Obes Rev* (2020) 21:e13083. doi: 10.1111/obr.13083
3. Jordan RE, Adab P, Cheng KK. Covid-19: Risk Factors for Severe Disease and Death. *BMJ* (2020) 368:m1198. doi: 10.1136/bmj.m1198
4. Dietz W, Santos-Burgoa C. Obesity and its Implications for COVID-19 Mortality. *Obes (Silver Spring)* (2020) 28:1005. doi: 10.1002/oby.22818
5. Neidich SD, Green WD, Rebeles J, Karlsson EA, Schultz-Cherry S, Noah TL, et al. Increased Risk of Influenza Among Vaccinated Adults Who are Obese. *Int J Obes (Lond)* (2017) 41:1324–30. doi: 10.1038/ijo.2017.131
6. Dinleyici EC, Borrow R, Safadi MAP, van Damme P, Munoz FM. Vaccines and Routine Immunization Strategies During the COVID-19 Pandemic. *Hum Vaccin Immunother* (2021) 17:400–7. doi: 10.1080/21645515.2020.1804776
7. Poland GA, Ovsyannikova IG, Kennedy RB. Personalized Vaccinology: A Review. *Vaccine* (2018) 36:5350–7. doi: 10.1016/j.vaccine.2017.07.062
8. Ledford H. How Obesity Could Create Problems for a COVID Vaccine. *Nature* (2020) 586:488–9. doi: 10.1038/d41586-020-02946-6
9. Gao M, Piernas C, Astbury NM, Hippisley-Cox J, O'Rahilly S, Aveyard P, et al. Associations Between Body-Mass Index and COVID-19 Severity in 6.9 Million People in England: A Prospective, Community-Based, Cohort Study. *Lancet Diabetes Endocrinol* (2021) 9:350–9. doi: 10.1016/S2213-8587(21)00089-9
10. Niemi MEK, Karjalainen J, Liao RG, Neale BM, Daly M, Ganna A, et al. Mapping the Human Genetic Architecture of COVID-19. *Nature* (2021) 600 (7889):472–7. doi: 10.1038/s41586-021-03767-x
11. Stefan N, Birkenfeld AL, Schulze MB. Global Pandemics Interconnected - Obesity, Impaired Metabolic Health and COVID-19. *Nat Rev Endocrinol* (2021) 17:135–49. doi: 10.1038/s41574-020-00462-1
12. Frasca D, Reidy L, Cray C, Diaz A, Romero M, Kahl K, et al. Influence of Obesity on Serum Levels of SARS-CoV-2-Specific Antibodies in COVID-19 Patients. *PloS One* (2021) 16:e0245424. doi: 10.1371/journal.pone.0245424
13. Ward H, Whitaker M, Flower B, Tang SN, Atchison C, Darzi A, et al. Population Antibody Responses Following COVID-19 Vaccination in 212,102 Individuals. *Nat Commun* (2022) 13:907. doi: 10.1038/s41467-022-28527-x
14. Murillo-Zamora E, Sanchez-Pina RA, Trujillo X, Huerta M, Rios-Silva M, Mendoza-Cano O. Independent Risk Factors of COVID-19 Pneumonia in Vaccinated Mexican Adults. *Int J Infect Dis* (2022) 118:244–6. doi: 10.1016/j.ijid.2022.02.003
15. Saciuk Y, Kertes J, Mandel M, Hemo B, Shamir Stein N, Ekka Zohar A. Pfizer-BioNTech Vaccine Effectiveness Against Sars-Cov-2 Infection: Findings From a Large Observational Study in Israel. *Prev Med* (2022) 155:106947. doi: 10.1016/j.ypmed.2021.106947

16. Watanabe M, Balena A, Tuccinardi D, Tozzi R, Risi R, Masi D, et al. Central Obesity, Smoking Habit, and Hypertension are Associated With Lower Antibody Titres in Response to COVID-19 mRNA Vaccine. *Diabetes Metab Res Rev* (2022) 38:e3465. doi: 10.1002/dmrr.3465
17. Smith KB, Smith MS. Obesity Statistics. *Prim Care* (2016) 43:121–35. doi: 10.1016/j.pop.2015.10.001
18. Ogden CL, Carroll MD, Kit BK, Flegal KM. Prevalence of Childhood and Adult Obesity in the United States, 2011-2012. *JAMA* (2014) 311:806–14. doi: 10.1001/jama.2014.732
19. Yu W, Rohli KE, Yang S, Jia P. Impact of Obesity on COVID-19 Patients. *J Diabetes Complications* (2021) 35:107817. doi: 10.1016/j.jdiacomp.2020.107817
20. Wright SM, Aronne LJ. Causes of Obesity. *Abdom Imaging* (2012) 37:730–2. doi: 10.1007/s00261-012-9862-x
21. Schmidt FM, Weschenfelder J, Sander C, Minkwitz J, Thormann J, Chittka T, et al. Inflammatory Cytokines in General and Central Obesity and Modulating Effects of Physical Activity. *PloS One* (2015) 10:e0121971. doi: 10.1371/journal.pone.0121971
22. Pelletier C, Imbeault P, Tremblay A. Energy Balance and Pollution by Organochlorines and Polychlorinated Biphenyls. *Obes Rev* (2003) 4:17–24. doi: 10.1046/j.1467-789X.2003.00085.x
23. Keith SW, Redden DT, Katzmarzyk PT, Boggiano MM, Hanlon EC, Benca RM, et al. Putative Contributors to the Secular Increase in Obesity: Exploring the Roads Less Traveled. *Int J Obes (Lond)* (2006) 30:1585–94. doi: 10.1038/sj.ijo.0803326
24. Filozof C, Fernandez Pinilla MC, Fernandez-Cruz A. Smoking Cessation and Weight Gain. *Obes Rev* (2004) 5:95–103. doi: 10.1111/j.1467-789X.2004.00131.x
25. Stefan N, Birkenfeld AL, Schulze MB, Ludwig DS. Obesity and Impaired Metabolic Health in Patients With COVID-19. *Nat Rev Endocrinol* (2020) 16:341–2. doi: 10.1038/s41574-020-0364-6
26. Cawley J, Meyerhoefer C. The Medical Care Costs of Obesity: An Instrumental Variables Approach. *J Health Econ* (2012) 31:219–30. doi: 10.1016/j.jhealeco.2011.10.003
27. Kelly T, Yang W, Chen CS, Reynolds K, He J. Global Burden of Obesity in 2005 and Projections to 2030. *Int J Obes (Lond)* (2008) 32:1431–7. doi: 10.1038/ijo.2008.102
28. Geerling E, Stone ET, Steffen TL, Hassert M, Brien JD, Pinto AK. Obesity Enhances Disease Severity in Female Mice Following West Nile Virus Infection. *Front Immunol* (2021) 12:739025. doi: 10.3389/fimmu.2021.739025
29. Karczewski J, Śledzińska E, Baturo A, Jończyk I, Maleszko A, Samborski P, et al. Obesity and Inflammation. *Eur Cytokine Netw* (2018) 29:83–94. doi: 10.1684/ecn.2018.0415
30. Reilly SM, Saltiel AR. Adapting to Obesity With Adipose Tissue Inflammation. *Nat Rev Endocrinol* (2017) 13:633–43. doi: 10.1038/nrendo.2017.90
31. Mraz M, Haluzik M. The Role of Adipose Tissue Immune Cells in Obesity and Low-Grade Inflammation. *J Endocrinol* (2014) 222:R113–27. doi: 10.1530/JOE-14-0283
32. Han JM, Levings MK. Immune Regulation in Obesity-Associated Adipose Inflammation. *J Immunol* (2013) 191:527–32. doi: 10.4049/jimmunol.1301035
33. Ovsyannikova IG, White SJ, Larrabee BR, Grill DE, Jacobson RM, Poland GA. Leptin and Leptin-Related Gene Polymorphisms, Obesity, and Influenza A/H1N1 Vaccine-Induced Immune Responses in Older Individuals. *Vaccine* (2014) 32:881–7. doi: 10.1016/j.vaccine.2013.12.009
34. Li M, Wei H, Zhong S, Cheng Y, Wen S, Wang D, et al. Association of Single Nucleotide Polymorphisms in LEP, LEPR, and PPARG With Humoral Immune Response to Influenza Vaccine. *Front Genet* (2021) 12. doi: 10.3389/fgene.2021.725538
35. Perez-Perez A, Vilarino-Garcia T, Fernandez-Riejos P, Martin-Gonzalez J, Segura-Egea JJ, Sanchez-Margalet V. Role of Leptin as a Link Between Metabolism and the Immune System. *Cytokine Growth Factor Rev* (2017) 35:71–84. doi: 10.1016/j.cytogfr.2017.03.001
36. Kim SY, Lim JH, Choi SW, Kim M, Kim ST, Kim MS, et al. Preferential Effects of Leptin on CD4 T Cells in Central and Peripheral Immune System are Critically Linked to the Expression of Leptin Receptor. *Biochem Biophys Res Commun* (2010) 394:562–8. doi: 10.1016/j.bbrc.2010.03.019
37. Agrawal S, Gollapudi S, Su H, Gupta S. Leptin Activates Human B Cells to Secrete TNF-Alpha, IL-6, and IL-10 *via* JAK2/STAT3 and P38mapk/ERK1/2 Signaling Pathway. *J Clin Immunol* (2011) 31:472–8. doi: 10.1007/s10875-010-9507-1
38. Maffei á, Halaas J, Ravussin E, Pratley R, Lee G, Zhang Y, et al. Leptin Levels in Human and Rodent: Measurement of Plasma Leptin and Ob RNA in Obese and Weight-Reduced Subjects. *Nat Med* (1995) 1:1155–61. doi: 10.1038/nm1195-1155
39. Frederich RC, Hamann A, Anderson S, Löllmann B, Lowell BB, Flier JS. Leptin Levels Reflect Body Lipid Content in Mice: Evidence for Diet-Induced Resistance to Leptin Action. *Nat Med* (1995) 1:1311–4. doi: 10.1038/nm1295-1311
40. Vandanmagsar B, Youm YH, Ravussin A, Galgani JE, Stadler K, Mynatt RL, et al. The NLRP3 Inflammasome Instigates Obesity-Induced Inflammation and Insulin Resistance. *Nat Med* (2011) 17:179–88. doi: 10.1038/nm.2279
41. Pellini R, Venuti A, Pimpinelli F, Abril E, Blandino G, Campo F, et al. Early Onset of SARS-COV-2 Antibodies After First Dose of BNT162b2: Correlation With Age, Gender and BMI. *Vaccines (Basel)* (2021) 9(7):685.
42. Garcia-Hernandez MH, Rodriguez-Varela E, Garcia-Jacobo RE, Hernandez-De la Torre M, Uresti-Rivera EE, Gonzalez-Amaro R, et al. Frequency of Regulatory B Cells in Adipose Tissue and Peripheral Blood From Individuals With Overweight, Obesity and Normal-Weight. *Obes Res Clin Pract* (2018) 12:513–9. doi: 10.1016/j.orcp.2018.07.001
43. Painter SD, Ovsyannikova IG, Poland GA. The Weight of Obesity on the Human Immune Response to Vaccination. *Vaccine* (2015) 33:4422–9. doi: 10.1016/j.vaccine.2015.06.101
44. Sheridan PA, Paich HA, Handy J, Karlsson EA, Hudgens MG, Sammon AB, et al. Obesity is Associated With Impaired Immune Response to Influenza Vaccination in Humans. *Int J Obes (Lond)* (2012) 36:1072–7. doi: 10.1038/ijo.2011.208
45. Park HL, Shim SH, Lee EY, Cho W, Park S, Jeon HJ, et al. Obesity-Induced Chronic Inflammation is Associated With the Reduced Efficacy of Influenza Vaccine. *Hum Vaccin Immunother* (2014) 10:1181–6. doi: 10.4161/hv.28332
46. Louie JK, Acosta M, Samuel MC, Schechter R, Vugia DJ, Harriman K, et al. A Novel Risk Factor for a Novel Virus: Obesity and 2009 Pandemic Influenza A (H1n1). *Clin Infect Dis* (2011) 52(3):301–12.
47. Watanabe M, Caruso D, Tuccinardi D, Risi R, Zerunian M, Polici M, et al. Visceral Fat Shows the Strongest Association With the Need of Intensive Care in Patients With COVID-19. *Metabolism* (2020) 111:154319. doi: 10.1016/j.metabol.2020.154319
48. Martin V, Castilla J, Godoy P, Delgado-Rodriguez M, Soldevila N, Fernandez-Villa T, et al. High Body Mass Index as a Risk Factor for Hospitalization Due to Influenza: A Case-Control Study. *Arch Bronconeumol* (2016) 52:299–307. doi: 10.1016/j.arbr.2015.11.011
49. Viasus D, Pano-Pardo JR, Pachon J, Campins A, Lopez-Medrano F, Villoslada A, et al. Novel Influenza ASGotSNfRiID. 2011. Factors Associated With Severe Disease in Hospitalized Adults With Pandemic (H1N1) 2009 in Spain. *Clin Microbiol Infect* (2011) 17:738–46.
50. Moriconi D, Masi S, Rebelos E, Virdis A, Manca ML, De Marco S, et al. Obesity Prolongs the Hospital Stay in Patients Affected by COVID-19, and may Impact on SARS-COV-2 Shedding. *Obes Res Clin Pract* (2020) 14:205–9. doi: 10.1016/j.orcp.2020.05.009
51. Grasselli G, Zangrillo A, Zanella A, Antonelli M, Cabrini L, Castelli A, et al. Baseline Characteristics and Outcomes of 1591 Patients Infected With SARS-CoV-2 Admitted to ICUs of the Lombardy Region, Italy. *JAMA* (2020) 323:1574–81. doi: 10.1001/jama.2020.5394
52. Yu T, Cai S, Zheng Z, Cai X, Liu Y, Yin S, et al. Association Between Clinical Manifestations and Prognosis in Patients With COVID-19. *Clin Ther* (2020) 42:964–72. doi: 10.1016/j.clinthera.2020.04.009
53. Polack FP, Thomas SJ, Kitchin N, Absalon J, Gurtman A, Lockhart S, et al. Safety and Efficacy of the BNT162b2 mRNA Covid-19 Vaccine. *N Engl J Med* (2020) 383:2603–15. doi: 10.1056/NEJMoa2034577
54. Kyriakidis NC, Lopez-Cortes A, Gonzalez EV, Grimaldos AB, Prado EO. SARS-CoV-2 Vaccines Strategies: A Comprehensive Review of Phase 3 Candidates. *NPJ Vaccines* (2021) 6:28. doi: 10.1038/s41541-021-00292-w
55. Accorsi EK, Britton A, Fleming-Dutra KE, Smith ZR, Shang N, Derado G, et al. Association Between 3 Doses of mRNA COVID-19 Vaccine and Symptomatic Infection Caused by the SARS-CoV-2 Omicron and Delta Variants. *JAMA* (2022) 327:639–51. doi: 10.1001/jama.2022.0470

56. Barda N, Dagan N, Cohen C, Hernan MA, Lipsitch M, Kohane IS, et al. Effectiveness of a Third Dose of the BNT162b2 mRNA COVID-19 Vaccine for Preventing Severe Outcomes in Israel: An Observational Study. *Lancet* (2021) 398:2093–100. doi: 10.1016/S0140-6736(21)02249-2
57. Tenforde MW, Patel MM, Gaglani M, Ginde AA, Douin DJ, Talbot HK, et al. Effectiveness of a Third Dose of Pfizer-BioNTech and Moderna Vaccines in Preventing COVID-19 Hospitalization Among Immunocompetent and Immunocompromised Adults - United States, August-December 2021. *MMWR Morb Mortal Wkly Rep* (2022) 71:118–24. doi: 10.15585/mmwr.mm7104a2
58. Thompson MG, Natarajan K, Irving SA, Rowley EA, Griggs EP, Gaglani M, et al. Effectiveness of a Third Dose of mRNA Vaccines Against COVID-19-Associated Emergency Department and Urgent Care Encounters and Hospitalizations Among Adults During Periods of Delta and Omicron Variant Predominance - VISION Network, 10 States, August 2021-January 2022. *MMWR Morb Mortal Wkly Rep* (2022) 71:139–45. doi: 10.15585/mmwr.mm7104e3
59. Malavazos AE, Basilico S, Iacobellis G, Milani V, Cardani R, Boniardi F, et al. Antibody Responses to BNT162b2 mRNA Vaccine: Infection-Naive Individuals With Abdominal Obesity Warrant Attention. *Obes (Silver Spring)* (2022) 30:606–13. doi: 10.1002/oby.23353
60. Watanabe M, Balena A, Masi D, Tozzi R, Risi R, Caputi A, et al. Rapid Weight Loss, Central Obesity Improvement and Blood Glucose Reduction Are Associated With a Stronger Adaptive Immune Response Following COVID-19 mRNA Vaccine. *Vaccines (Basel)* (2022) 10(1):49. doi: 10.3390/vaccines10010079
61. Baden LR, El Sahly HM, Essink B, Kotloff K, Frey S, Novak R, et al. Efficacy and Safety of the mRNA-1273 SARS-CoV-2 Vaccine. *N Engl J Med* (2021) 384:403–16. doi: 10.1056/NEJMoa2035389
62. Butsch WS, Hajduk A, Cardel MI, Donahoo WT, Kyle TK, Stanford FC, et al. COVID-19 Vaccines are Effective in People With Obesity: A Position Statement From The Obesity Society. *Obes (Silver Spring)* (2021) 29:1575–9. doi: 10.1002/oby.23251

Conflict of Interest: The authors declare that the research was conducted in the absence of any commercial or financial relationships that could be construed as a potential conflict of interest.

Publisher's Note: All claims expressed in this article are solely those of the authors and do not necessarily represent those of their affiliated organizations, or those of the publisher, the editors and the reviewers. Any product that may be evaluated in this article, or claim that may be made by its manufacturer, is not guaranteed or endorsed by the publisher.

Cell Reports

Article

Balanced T and B cell responses are required for immune protection against Powassan virus in virus-like particle vaccination

Graphical abstract

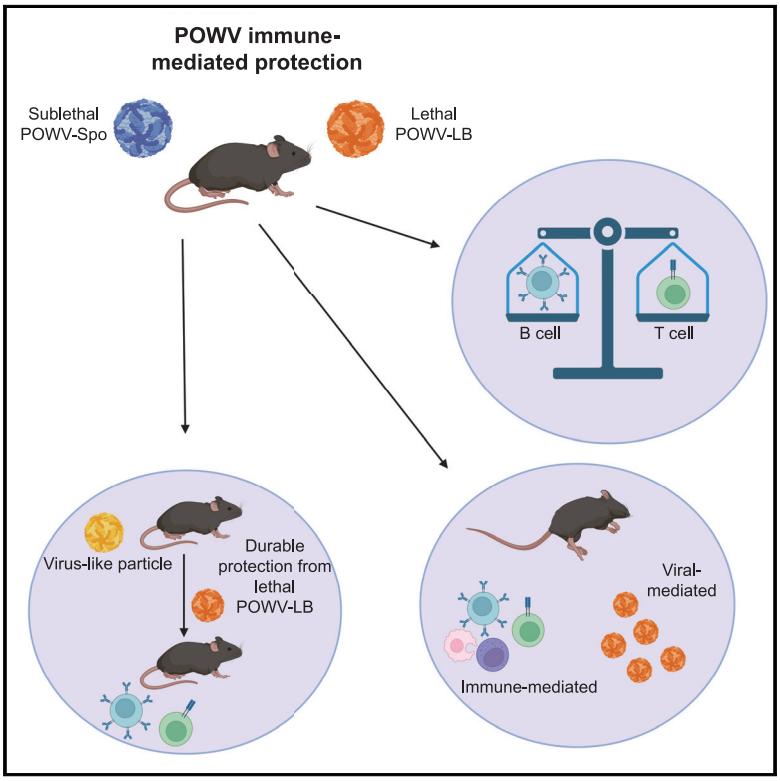

Authors

E. Taylor Stone, Mariah Hassert, Elizabeth Geerling, ..., Cody German, Jessica L. Smith, Amelia K. Pinto

Correspondence

amelia.pinto@health.slu.edu

In brief

Stone et al. describe Powassan virus (POWV) adaptive immune protection in a murine model of infection. This understanding culminates in a vaccination approach that elicits protective adaptive immune responses against POWV morbidity and mortality. These findings will aid in fulfilling the unmet need for rational design of POWV vaccinations.

Highlights

- Robust B and T cell responses are necessary for protection against POWV
- POWV lethality is comprised of both viral- and host-mediated mechanisms
- A VLP-based vaccine protects against lethal POWV challenge

Stone et al., 2022, Cell Reports *38*, 110388
February 15, 2022
https://doi.org/10.1016/j.celrep.2022.110388

CellPress

Cell Reports

CellPress
OPEN ACCESS

Article

Balanced T and B cell responses are required for immune protection against Powassan virus in virus-like particle vaccination

E. Taylor Stone,[1] Mariah Hassert,[1] Elizabeth Geerling,[1] Colleen Wagner,[1] James D. Brien,[1] Gregory D. Ebel,[2] Alec J. Hirsch,[3,4] Cody German,[3,4] Jessica L. Smith,[3,4] and Amelia K. Pinto[1,5,*]

[1]Department of Molecular Microbiology and Immunology, Saint Louis University, St. Louis, MO 63104, USA
[2]Center for Vector-borne Infectious Diseases, Department of Microbiology, Immunology, and Pathology, Colorado State University, Fort Collins, CO 80523, USA
[3]The Vaccine & Gene Therapy Institute, Oregon Health & Science University, Beaverton, OR 97006, USA
[4]Division of Pathobiology & Immunology, Oregon National Primate Research Center, Oregon Health & Science University, Beaverton, OR 97006, USA
[5]Lead contact
*Correspondence: amelia.pinto@health.slu.edu
https://doi.org/10.1016/j.celrep.2022.110388

SUMMARY

Powassan virus (POWV) is a tick-borne pathogen for which humans are an incidental host. POWV infection can be fatal or result in long-term neurological sequelae; however, there are no approved vaccinations for POWV. Integral to efficacious vaccine development is the identification of correlates of protection, which we accomplished in this study by utilizing a murine model of POWV infection. Using POWV lethal and sub-lethal challenge models, we show that (1) robust B and T cell responses are necessary for immune protection, (2) POWV lethality can be attributed to both viral- and host-mediated drivers of disease, and (3) knowledge of the immune correlates of protection against POWV can be applied in a virus-like particle (VLP)-based vaccination approach that provides protection from lethal POWV challenge. Identification of these immune protection factors is significant as it will aid in the rational design of POWV vaccines.

INTRODUCTION

Powassan virus (POWV) is a flavivirus and emerging arthropod-borne virus of public health concern. Predictions that the range of ticks transmitting POWV to humans will expand as the climate warms situate POWV as a pathogen of national importance (Clow et al., 2017; Sonenshine, 2018; Gasmi et al., 2018; Ogden et al., 2008; Pierson and Diamond, 2020). Although rare, incidence of POWV infection in humans has increased substantially in the past two decades, a phenomenon that cannot wholly be explained by increased reporting and surveillance (Centers for Disease Control and Prevention, 2020; Nofchissey et al., 2013; Kemenesi and Bányai, 2019; Hinten et al., 2008). A high proportion (>50%) of reported POWV infections are accompanied by long-term neurological sequelae, which range in severity from mild to debilitating (Hermance and Thangamani, 2017; Kemenesi and Bányai, 2019; Goldfield et al., 1973; Tavakoli et al., 2009) and in 10%–15% of cases is fatal (Kemenesi and Bányai, 2019; Tavakoli et al., 2009). Although nucleic acid-based vaccination approaches can prevent severe disease and neurological sequelae in murine models of POWV infection (Choi et al., 2020, Vanblargan et al., 2018), there are no approved vaccines or therapeutics for individuals infected with POWV. Currently, there are six approved vaccinations for the flavivirus tick-borne encephalitis virus (TBEV) that can prevent the development of severe disease and neurological sequelae (Chernokhaeva et al., 2016; Chumakov et al., 1963; Kubinski et al., 2020), but these vaccines are not effective in preventing POWV infection (Chernokhaeva et al., 2016; Shamanin et al., 1991, Mcauley et al., 2017). Taken together, the success of TBEV vaccination strategies in humans, and the advent of successful POWV vaccinations in murine models, suggests that a protective vaccine against POWV is achievable.

Despite its increasing incidence, the immune correlates of protection for POWV are unknown. This is largely because POWV is a rare and relatively recently described virus (Mclean and Donohue, 1959). The enzootic cycle of POWV is thought to be dependent upon transmission from the bite of an infected tick on an uninfected host during a bloodmeal, although other modes of transmission have been described as important (Costero and Grayson, 1996; Nonaka et al., 2010). There are two lineages of POWV, known as lineage I (POWV-LB) and lineage II (POWV-Sponer [POWV-Spo], or deer tick virus). Of these two lineages, POWV-LB is predominantly transmitted by *Ixodes cookei* ticks, which primarily feed on small woodland mammals such as groundhogs (*Marmota monax*) (Ebel et al., 2001). As *Ixodes cookei* ticks have less promiscuous feeding patterns relative to other *Ixodid* ticks, human infection with POWV-LB is less frequent. POWV-Spo, on the other hand, is transmitted by black-legged deer ticks (*Ixodes scapularis*). As these ticks have

a broader range of host species, most incidence of POWV infection in humans is attributable to POWV-Spo infection. POWV-LB infection in humans is more common in far eastern portions of Russia, while in North America, POWV-Spo is the predominant human-infecting lineage. Despite these distinct geographic ranges and host species, the two lineages are serologically indistinguishable, and there is a large degree of nucleic acid (~86%) and amino acid (aa) (~96%) similarity between the two viruses (Ebel et al., 2001). How these differences inform the viral life cycle, tissue tropism, and interactions with host immune systems are all active areas of research (Robertson et al., 2009; Best Sonja et al., 2005; Mlera et al., 2017; Hermance et al., 2016).

POWV is a member of the family Flaviviridae and a single-stranded positive sense RNA virus with a genome ~11 kbp in length. The genome encodes a single polyprotein cleaved by viral and host proteases into three structural proteins (pre-membrane or prM, capsid or C, and envelope or E) and seven non-structural (NS) proteins: NS1, NS2A, NS2B, NS3, NS4A, NS4B, and NS5. The E protein is the main antigenic determinant for flaviviruses, such as TBEV (Kuivanen et al., 2014), and is 500 aa in length with three functional domains: DI, DII, and DIII. It has been well documented that antibodies directed against the E protein can be either neutralizing or non-neutralizing (Ershova et al., 2016; Matveev et al., 2019; Kuivanen et al., 2014). Epitopes recognized by T cells have also been documented in the NS (Lampen et al., 2018; Aberle et al., 2015) and structural proteins of TBEV (Varnaitė et al., 2020; Schwaiger et al., 2014), including the E protein, although the contribution of E-specific T cells in flavivirus infection is an active area of research (Hassert et al., 2018, 2019, 2021).

Among flaviviruses, POWV is a member of the tick-borne encephalitis (TBE) serocomplex of viruses, examples of which include TBEV and Langat virus (LGTV) (Pesko et al., 2010; Ebel et al., 2001). In this serocomplex of viruses, TBEV is the most common infection in humans and therefore the most well studied. It is the only TBE serocomplex member for which there are licensed vaccines available for human use. The six available vaccinations cover three different TBEV subtypes and are immunogenic inactivated, whole virus-based vaccines (Kubinski et al., 2020). While it is widely appreciated that cellular and humoral components of adaptive immunity are important for protective responses following TBEV vaccination (Aberle et al., 2015; Schwaiger et al., 2014; Blom et al., 2015, 2018; Best Sonja et al., 2005; Robertson et al., 2009), the correlates of protection for POWV remain unknown. While others have characterized the contribution of monoclonal antibodies to POWV immunity, the polyclonal response is less well characterized (Errico et al., 2020, Vanblargan et al., 2021). Furthermore, multiple studies have demonstrated that approved TBEV vaccines do not provide protection against POWV in humans (Shamanin et al., 1991; Chernokhaeva et al., 2016), although it is unclear why. Identifying the correlates of immune protection is critical to aid development of therapeutics and vaccines, a yet unmet need for POWV infection.

Integral to the development of future vaccinations is establishing the immune correlates of protection for POWV. In these studies, we describe a murine model of POWV infection, which we used to determine the correlates of protection and demonstrate that both the B and T cell compartments of adaptive immunity contribute to durable protection against POWV. In addition, we identify $CD8^+$ and $CD4^+$ T cell epitopes in the structural proteins of POWV and show that $CD8^+$ T cell responses against POWV can drive immune-mediated pathology. We also demonstrate that a virus-like particle (VLP)-based vaccination strategy can be effective against POWV-LB, eliciting robust and durable neutralizing antibodies and detectable $CD8^+$ T cell responses. The adaptive immune response elicited by POWV-LB VLPs resulted in uniform protection from lethal POWV-LB challenge. Because these studies will allow for a more targeted design of POWV vaccines—which has previously been limited to empirical approaches—the findings presented here will have important implications for future POWV vaccine development.

RESULTS

POWV-LB and POWV-Spo cause morbidity and mortality in C57BL/6 mice

With the goal of studying POWV-specific adaptive immune responses and identifying factors associated with protection, we established a susceptible mouse model of POWV infection using the POWV lineage 1 strain LB (POWV-LB). We infected C57BL/6 (B6) mice subcutaneously (s.c.) with 10^3 or 10^2 infectious units (focus-forming units [FFU]) of POWV-LB and monitored mice for 15 days post infection (dpi). As observed by others following challenge of B6 mice, POWV-LB infection with 10^3 FFU resulted in high mortality in B6 mice (Santos et al., 2016; Mlera et al., 2017; Hermance et al., 2015). In our studies, challenge with POWV-LB s.c. resulted in all mice succumbing to infection 7–13 days dpi with a median survival time (MST) of 7 days when challenged with 10^3 FFU (Figure 1A). At a lower infectious dose, 10^2 FFU, POWV-LB challenge resulted in uniform mortality, but with a slightly longer MST of 8.5 days.

In this POWV mouse model, we observed substantial morbidity among infected mice, with weight loss beginning at 5 dpi and continuing until mice succumb to infection (Figure 1B). Time to exhibit signs of disease for mice infected with OWV-LB did not appear to be dose dependent, and typically occurred at 6 dpi (Figure 1C). POWV-LB-infected mice displayed a limp tail and ruffled appearance, progressing rapidly to moribund posture and shallow breathing with few disease indicators in the days preceding death (Figure 1C). In the case of a lower infectious dose, more mice adopted a ruffled posture, limp tail, and hindlimb weakness, but displayed few other signs of disease before succumbing (Figure 1C). As others have noted, we observed hindlimb paralysis usually corresponding to the site of injection, albeit in a smaller number (<1%) of POWV-LB infections (Mlera et al., 2017). We did, however, note substantial weakness and reduced usage of the hindlimbs as disease progressed and, in the case of the higher infectious doses, we noted that disease progression may have been too rapid for hindlimb paralysis to be observed.

Because of the constraints posed by uniform mortality in this model of POWV-LB infection, we wanted to establish a model of infection with POWV lineage 2 strain, Spooner (POWV-Spo). Interestingly, at the same infectious doses used for POWV-LB (10^3 or 10^2 FFU), we observed a lineage-specific survival rate

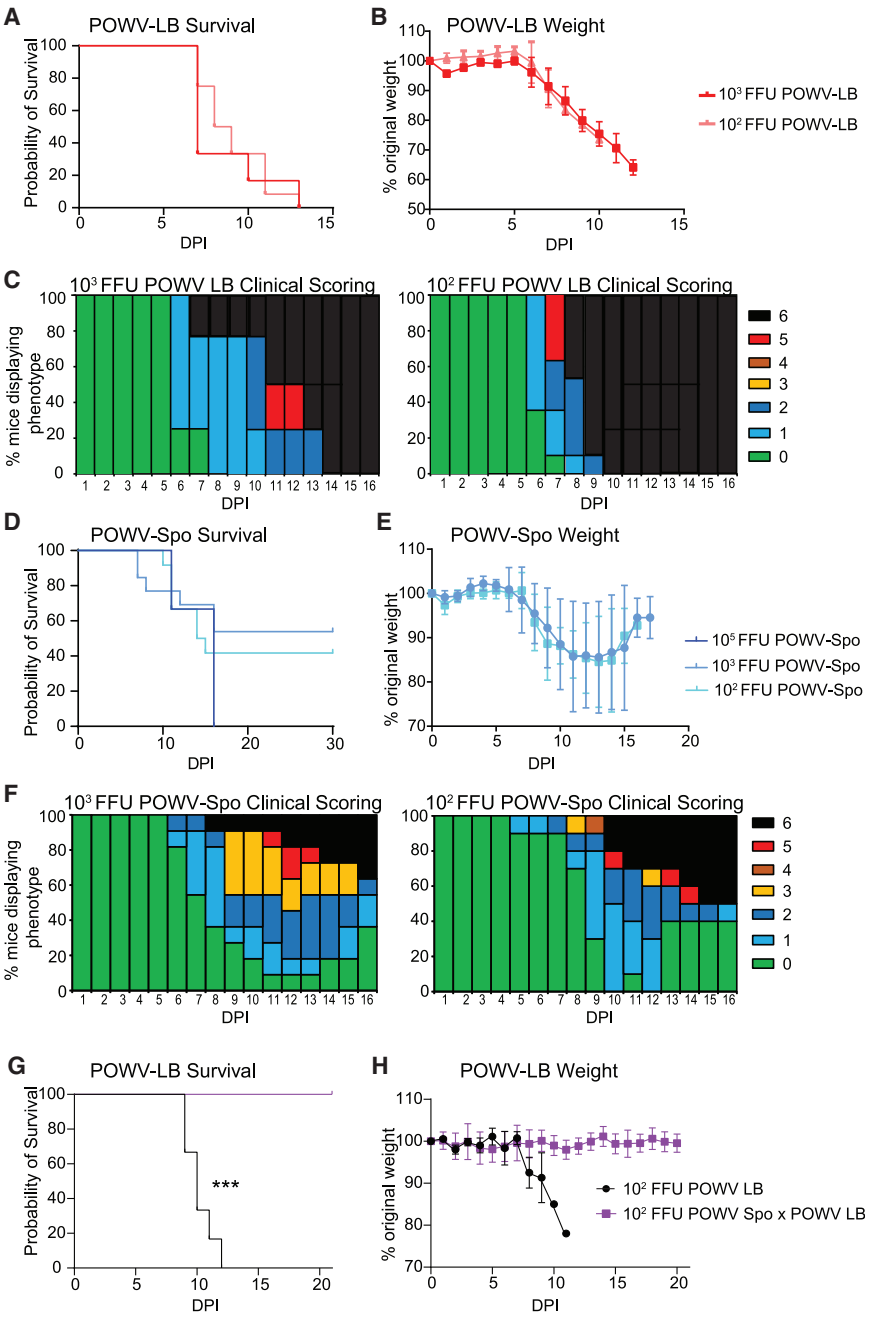

Figure 1. POWV-LB and POWV-Spooner cause morbidity and mortality in C57BL/6 mice

(A) Mortality of C57BL/6 (B6) mice challenged subcutaneously (s.c.) with 10^3 (n = 6) or 10^2 (n = 12) focus-forming units (FFU) of POWV-LB and monitored for 14 days post infection (dpi).

(B) Weight loss for B6 mice challenged s.c. with POWV-LB and monitored for 14 dpi.

(C) Clinical scoring results for B6 mice challenged s.c. with 10^3 FFU (middle, n = 5), and 10^2 FFU (right, n = 8) of POWV-LB and monitored for 16 dpi.

(D) Mortality of B6 mice challenged s.c. with 10^3 (n = 12) or 10^2 (n = 12) FFU of POWV-Spo and monitored for 30 dpi.

(E) Weight loss for B6 mice challenged s.c. with POWV-Spo and monitored for weight loss for 16 dpi.

(F) Clinical scoring results for mice B6 mice challenged s.c. with 10^3 FFU (left, n = 9) or 10^2 FFU (right, n = 10) of POWV-Spo and monitored for 16 dpi.

(G and H) (G) Mortality and (H) weight loss curves for naive (black, n = 6) or POWV-Spooner immune (purple, n = 7) B6 mice challenged s.c. with 10^2 FFU of POWV-LB. Mice were monitored daily for 21 dpi. Prior exposure to 10^2 FFU of POWV-Spooner significantly (p = 0.0002, Mantel-Cox test) improved POWV-LB survival. All data are reported as mean ± SEM.

phenomenon, as infection by the same s.c. route resulted in 58% and 42% survival, respectively, but uniform mortality at 10^5 FFU (Figure 1D). This contrasts sharply with the uniform mortality seen in POWV-LB challenge. Like POWV-LB, weight loss following infection with POWV-Spo began at 5 dpi. But, unlike POWV-LB, surviving POWV-Spo-infected mice recovered lost weight at 12–16 dpi (Figure 1E). In general, mice challenged with POWV-LB exhibited no or few signs of disease before succumbing. In contrast, POWV-Spo-challenged mice displayed signs of disease around the same 6 dpi window, but worsened disease progression between days 9 and 14 was apparent (Figure 1F). Hindlimb weakness tended to be exacerbated in these mice. Of note, we did not observe significant differences in morbidity or mortality on the basis of sex in either POWV-LB or POWV-Spo mice (Figure S1). The similar but delayed onset of morbidity associated with POWV-Spo compared with POWV-LB supported the use of these two highly similar viruses to study the correlates of protection for POWV.

Observing distinct disease phenotypes between these two similar POWV lineages, we next evaluated the kinetics of viral replication of POWV-LB and POWV-Spo in our murine model, and found that POWV-LB tended to replicate more quickly and to higher titers than POWV-Spo, consistent with previous reports (Figure S2) (Grabowski et al., 2019). We also wanted to examine the structural envelope protein of the two POWVs in conjunction with other neuroinvasive arthropod-borne flaviviruses for which the correlates of protection are established or licensed vaccines available. To this end, we performed an aa alignment of the envelope (E) proteins of both lineages of POWV, as well as TBFVs LGTV, and TBEV, and the mosquito-borne virus West Nile virus (WNV). There is a high degree of homology in the envelope (E) protein between POWV-LB and POWV-Spo lineages, but

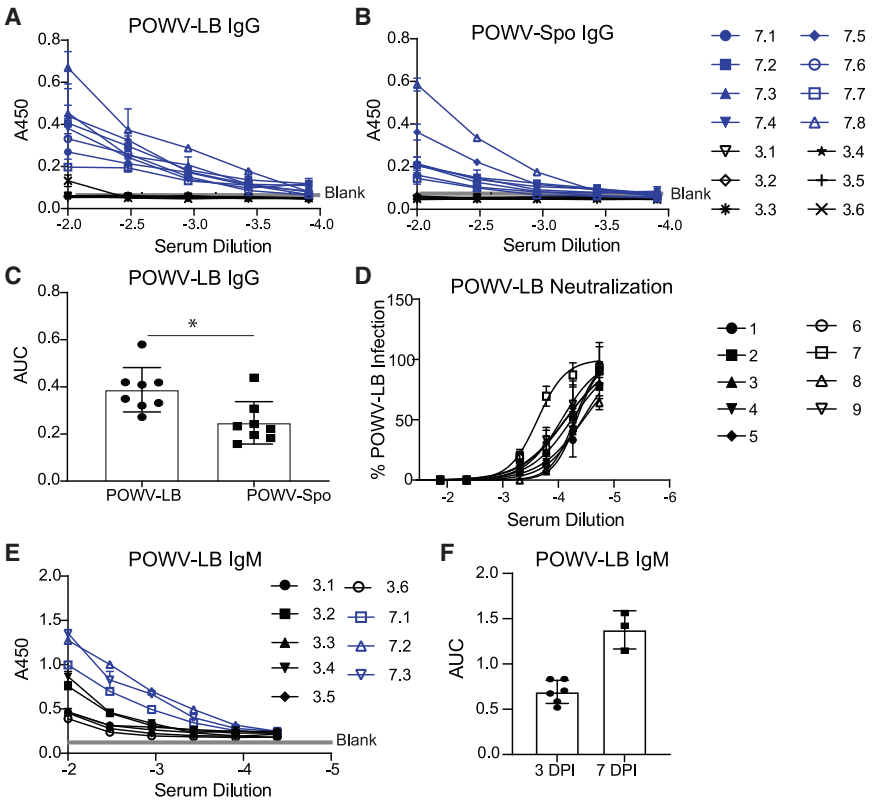

Figure 2. POWV-specific antibodies are present at 7 dpi

(A) Whole virion POWV-LB IgG ELISA using sera of B6 mice challenged s.c. with 10^2 FFU POWV-LB and harvested at 3 dpi (black, n = 6) and 7 dpi (blue, n = 8).

(B) Whole virion POWV-Spooner (POWV-Spo) IgG ELISA using sera of B6 mice (n = 8) challenged s.c. with 10^2 FFU POWV-LB and harvested at 3 dpi (black, n = 6) or 7 dpi (blue, n = 8).

(C) Area under the curve for IgG ELISAs as shown in (A and B) (p = 0.0272, Student's unpaired t test).

(D) FRNTs performed on baby hamster kidney cells (BHK-21 clone 13 ATCC) examining the neutralization capacity against 10^2 FFU POWV-LB of sera from mice challenged s.c. with 10^2 FFU POWV-LB and harvested 7 dpi (n = 9).

(E) Whole virion POWV-LB IgM ELISA using sera of B6 mice challenged s.c. with 10^2 FFU POWV-LB and harvested 3 dpi (n = 6) or 7 dpi (n = 3).

(F) Area under the curve for IgM ELISAs as shown in (E). Data are reported as mean ± SEM.

POWV is notably distinct from LGTV, TBEV, and WNV in terms of envelope aa identity (Figures S3A and S3B). Importantly for our study, the sequence similarity between the two lineages, combined with the survival differences between POWV-LB and POWV-Spo, enabled our group to use the two viruses to interrogate different elements of POWV immune-mediated protection. In this work, we examined antigen-specific adaptive immune responses to POWV using the sub-lethal POWV-Spo challenge model and determined factors critical for immune protection using the lethal POWV-LB challenge model.

Having demonstrated that POWV-Spo infection resulted in distinct disease outcomes despite striking aa identity with the more lethal POWV-LB lineage, we considered whether mice recovered from the serologically indistinguishable POWV-Spo lineage would generate a memory response providing protection from lethal, but biologically relevant POWV-LB challenge (Ebel and Kramer, 2004). To this end, we challenged mice recovered from POWV-Spo with a lethal dose of POWV-LB. We observed that POWV-Spo convalescent mice were protected from lethal POWV-LB infection (p = 0.002, Figure 1G). These mice demonstrated no appreciable indicators of disease nor signs of weight loss following challenge (Figure 1H). These results indicated that POWV-Spo immune memory was protective against POWV-LB and thereby suitable for evaluating immune protection for POWV.

POWV-specific antibodies are present at 7 dpi

Prior POWV-Spo infection provided protection against lethal POWV-LB infection, suggesting that adaptive immune responses can mitigate POWV disease. With the goal of determining whether POWV-specific antibodies are present when mice succumb to infection, we examined the kinetics of the antibody response to POWV-LB, as we had previously done with Zika virus (ZIKV) (Hassert et al., 2018, 2019). However, unlike in the case of ZIKV, POWV-LB-infected B6 mice all succumb to infection within 2 weeks, therefore determination of the functionality and kinetics of the adaptive immune response was severely limited. We began to characterize the humoral response by terminally bleeding mice infected with 10^2 FFU POWV-LB at 7 dpi to examine serum binding and neutralization capacity. We were able to detect POWV-specific IgG responses by 7 dpi using whole virion antigen in an indirect enzyme-linked immunosorbent assay (ELISA), and confirmed that the two POWV lineages are serologically indistinguishable (Figures 2A and 2B). We did not detect binding to either lineage by IgG at 3 dpi. IgG raised against POWV-LB bound to virions of both lineages, with a slight but significant preference for POWV-LB (p = 0.0272, Figure 2C). We were able to detect neutralization of POWV-LB in a focus reduction neutralization test (FRNT), with an average reciprocal serum dilution of 1.7×10^5 for 50% neutralization (Figure 2D). Analysis of IgM levels at 3 and 7 dpi with POWV-LB showed detectable binding at 3 dpi, which was increased at 7 dpi (Figures 2E and 2F). Our analysis of the kinetics of the POWV-Spo antibody binding yielded similar results, with detectable IgG levels by 8 dpi and increasing at 15 and 30+ dpi (Figures S4A–S4C). Levels of IgM for POWV-Spo-infected mice were increased from 4 to 8 dpi and decreased at 15 and 30+ dpi as IgG binding increased (Figures S4D and S4E). The results of this kinetics study suggest that, while POWV-specific B cells are present and producing IgG and IgM antibodies during the acute infection, they are incapable of protecting mice from a lethal POWV-LB infection as these mice uniformly succumb to infection by 13 dpi (Figure 1A).

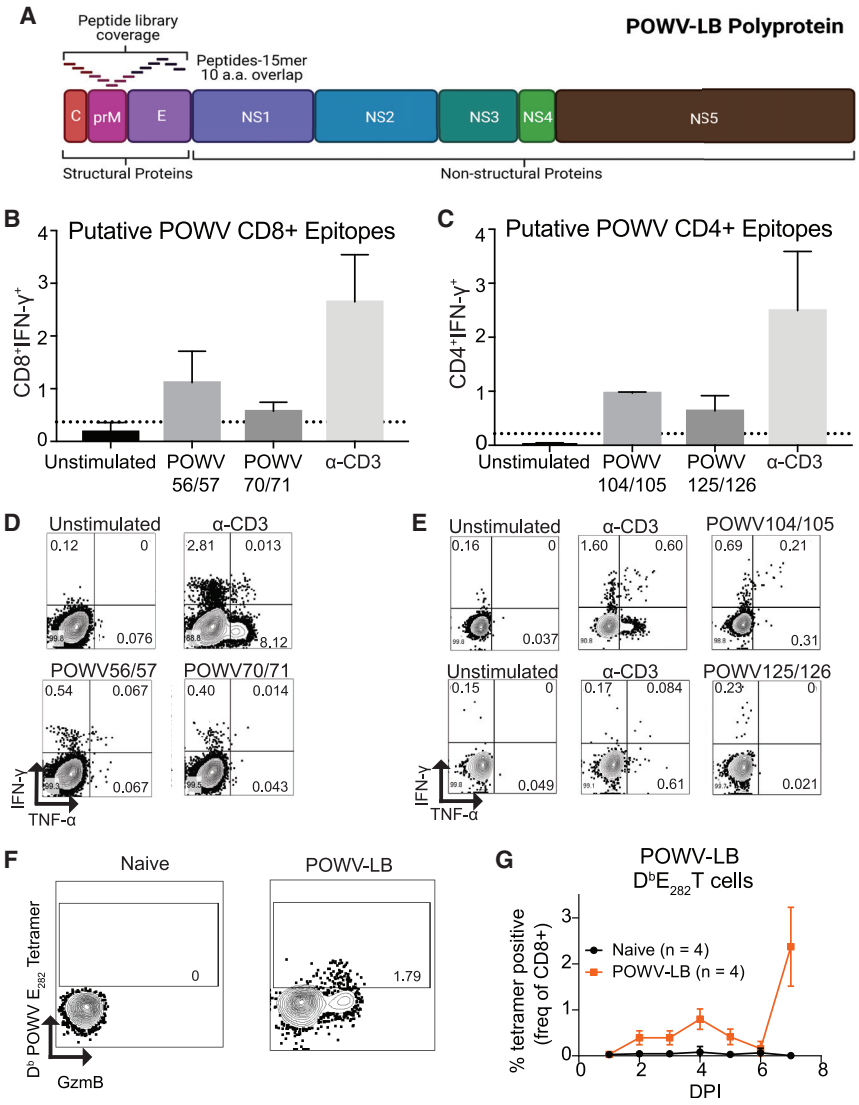

Figure 3. POWV-specific T cells are present during infection

(A) Schematic representation of the POWV-LB polyprotein (not to scale). Structural proteins capsid (red) (C) pre-membrane (pink, prM), and envelope (purple) (E) are located near the N terminus. Also depicted is the coverage of the POWV peptide library, comprised of a 15-mer peptide library designed with a 10-amino-acid (aa) overlap.

(B) Potential $CD8^+$ T cell epitope hits as determined by interferon-gamma (IFN-γ) production by $CD8^+$ T cells ($CD19^-$ $CD8^+$) in response to the peptide library illustrated in (A). Candidate epitopes were determined in two independent experiments by stimulating splenocytes *ex vivo* from POWV-LB infected B6 mice s.c. infected with 10^3 FFU (n = 2) 7 dpi in the presence of brefeldin A for 6 h. Positive hits were considered those that elicited a T cell response 2-fold above background (dashed line).

(C) Potential $CD4^+$ T cell epitope hits determined in the same manner as (B), at 11 dpi (n = 2).

(D) Representative flow plots depicting $CD8^+$ T cell responses to POWV-LB infection described in (B). The cytokines tumor necrosis factor alpha (TNF-α) and IFN-γ are shown on the x and y axes, respectively. Reponses to no stimulation (top left), α-CD3 (top right), POWV56/57 peptide (bottom left) and POWV70/71 peptide (bottom right) are shown.

(E) Representative flow plots depicting $CD4^+$ T cell responses to POWV-LB infection described in (B). Reponses to no stimulation (left), α-CD3 (middle), POWV104/105 peptide (top right), and POWV125/126 peptide (bottom right) are shown.

(F) Representative image of tetramer staining for POWV-E_{282}-specific $CD8^+$ T cells using H2-b restricted D^b tetramer from naive B6 mice (left) or mice challenged s.c. with 10^3 FFU POWV-LB and harvested 7 dpi. Cells are gated on $CD19^-CD8^+$.

(G) Frequency of POWV-E_{282}-specific $CD8^+$ T cells by tetramer staining relative to total $CD8^+$ T cells from B6 mice challenged s.c. with 10^3 FFU POWV-LB and bled longitudinally over a period of 7 days. All data are reported as mean ± SEM.

POWV-specific T cells are present during infection

We next sought to describe the kinetics of the T cell response to POWV. Previous studies with TBEV have described both protective and pathogenic roles for T cells during infection (Hassert et al., 2018, 2019; Grifoni et al., 2019, 2020; Brien et al., 2008; Růžek et al., 2009). To describe the contribution of the T cell compartment to POWV immunity, we used our $H2^b$ restricted B6 model of infection to map the $CD4^+$ and $CD8^+$ T cell epitopes within the structural proteins of POWV-LB. Using approaches previously adapted for ZIKV epitope mapping in our lab, we designed a peptide library of 157 peptides, each 15 aa in length and 10 with aa of overlap (Hassert et al., 2018, 2019). This library spanned the structural proteins capsid (C), pre-membrane (prM), and envelope (E) (Figure 3A).

Total splenocytes from POWV-LB infected B6 mice were harvested 8 or 10 dpi, corresponding to the peak of the $CD8^+$ and $CD4^+$ T cell responses, respectively. T cells were stimulated *ex vivo* in the presence of brefeldin A and individual peptides in the library for 6 h. As a positive control, anti-CD3 was used to stimulate antigen-experienced $CD4^+$ and $CD8^+$ T cells and a well of unstimulated cells served as a negative control. Following stimulation, cells were fixed, permeabilized, and stained for flow cytometric analysis to identify the production of cytokines IFN-γ and TNF-α. Putative epitope candidates were identified as peptides that elicited a response greater than 2-fold over background determined from the unstimulated wells. We were unable to detect cytokine production following peptide stimulation in uninfected animals (Figure S5A). Using this approach, we identified two $CD8^+$ and two $CD4^+$ candidate epitopes (Figures 3B–3E). The POWV peptide $CD8^+$ and $CD4^+$ T cell epitopes are named with the same nomenclature used previously for both WNV and ZIKV, with the flavivirus followed by the abbreviated name of the viral protein and number of the aa, based on the POWV open reading frame (ORF) (Hassert et al., 2018, 2019; Brien et al., 2008) (e.g., POWV-E_{282} epitope is located in the E protein at the 282nd aa in the ORF). $H2^b$ restricted $CD4^+$T cell

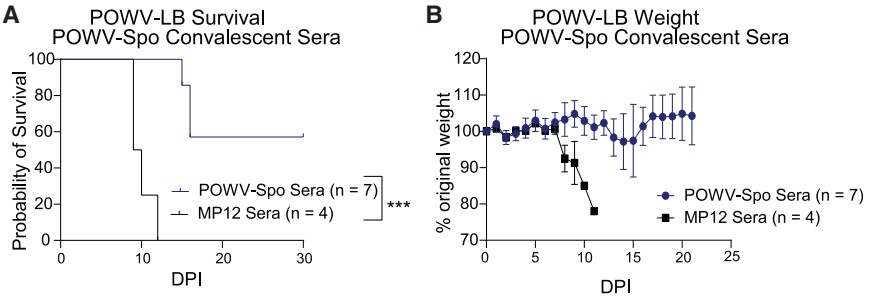

Figure 4. POWV-Spooner infection elicits partially protective antibody responses against lethal POWV-LB

Mortality (A) and weight loss (B) of alphavirus-negative control (Rift Valley fever virus [RVFV] vaccine strain MP-12) (n = 4) or POWV-Spooner (n = 7) sera-recipient B6 mice following lethal challenge with 10^2 FFU POWV-LB s.c.. One day prior to challenge, mice were treated with sera from convalescent MP-12 or POWV-Spo mice diluted 1:10 in saline and administered via intraperitoneal (i.p.) injection. Mice receiving POWV-Spo sera were significantly protected relative to MP-12 sera recipients (p = 0.0005, Mantel-Cox test). For generation of convalescent sera, B6 mice were challenged s.c. with 10^2 FFU POWV-Spo or MP-12 and sera collected via cardiac puncture in memory phase 30 dpi. All data are reported as mean ± SEM.

epitopes are listed as 15-mer peptides (Table S1). Because our study examined structural POWV proteins, there are likely CD4 T cell epitopes within the NS proteins that were not screened in this study. The possibility that there are multiple unidentified POWV-specific $CD4^+$ T cell epitopes within NS proteins is supported by studies with other flaviviruses in both humans and mice (Blom et al., 2015; Hassert et al., 2018, 2019; Elong Ngono et al., 2019; Brien et al., 2007, 2008; Graham et al., 2020; Grifoni et al., 2019, 2020).

For putative $CD8^+$ T cell candidates, we sought to determine the optimal 8-mer or 9-mer $H2^b$ restricted POWV $CD8^+$ T cell peptides. To do this, we generated a panel of possible POWV $CD8^+$T epitopes based on previously identified K^b and D^b conserved peptide anchor residues (Hoof et al., 2009) and repeated the experiments in the presence of predicted 8- or 9-mer peptides (Figures 3D; Table S1). Notably, the $E_{351\text{-}361}$ $CD8^+$T cell epitope—although it consistently yielded strong responses as a 15-mer peptide (POWV70/71) —could not be optimized to determine the ideal 8- or 9-mer peptide, nor could the K^b and D^b restriction be determined. The difficulty determining the optimal epitope was attributable to the stronger response to the $E_{282\text{-}291}$ $CD8^+$ T cell epitope. This epitope—designated POWV-E_{282}—elicited the strongest $CD8^+$ T cell response and appears to be a prominent target for CD8+ T cells during POWV-LB and POWV-Spo challenge. We determined via RMA-S stabilization assay that this epitope is $H2^b$-D^b restricted (Figures S5B and S5C) and can be quantified by tetramer staining (Figure 3F).

To describe the kinetics of the POWV-specific $CD4^+$ and $CD8^+$ T cell response, we challenged mice with 10^3 FFU of POWV-LB and isolated blood over the course of infection for tetramer staining (Figure 3G). We found that the POWV-E_{282} $CD8^+$T cell response is detectable 5 dpi with 1% of $CD8^+$ T cells responding to POWV-E_{282} and increases until 7 dpi with 3% of $CD8^+$ T cells responding to POWV-E_{282}. Of these, a low but detectable number of POWV-E_{282}-specific T cells produce granzyme B. We were limited to blood collected at or before 7 dpi, as B6 mice succumb to POWV-LB infection within this time frame. The $CD4^+$ T cell response was not strong enough to be detected with the identified peptides at the 1–7 dpi time points, and cytokines produced in response to anti-CD3 were difficult to detect before 10 dpi. However, a detectable $CD4^+$ T cell response was present from 10 dpi until mice succumb to infection, suggesting that the $CD4^+$ T cell compartment was not sufficient for control of POWV replication, as was observed with $CD8^+$ T cells. Examinations of POWV-E_{282} in POWV-LB- or POWV-Spo-infected mice showed no significant differences in the number of antigen-specific $CD8^+$ T cells in splenocytes, nor did we see differences in granzyme B production (Figures S5D–S5F). We did see a significantly (p = 0.0025) higher number of antigen-specific T cells in the brains of POWV-LB-infected mice at 8 dpi relative to POWV-Spo-infected mice (Figure S5G). The results of the kinetics study suggest that, while POWV-specific $CD4^+$ and $CD8^+$ T cells are primed, producing cytokines, and infiltrating infected tissues during the acute infection, they are not sufficient for protecting mice from lethal POWV-LB infection.

POWV-Spo infection elicits partially protective antibody responses against lethal POWV-LB

Our studies of POWV-LB infection of B6 mice revealed detectable antibody binding and neutralization responses as early as 7 dpi, as well as polyfunctional $CD8^+$ T cell responses peaking at 7 dpi and $CD4^+$ T cell responses at 10 dpi. These responses were not sufficient to protect mice from POWV-LB challenge, and infection resulted in uniform mortality.

We wanted to examine the protective capacity of convalescent POWV-Spo sera in immune competent mice. To do this, we passively transferred sera from recovered POWV-Spo or an irrelevant alphavirus-negative control (Rift Valley fever virus vaccine strain, MP-12) mice into naive B6 mice. B6 mice were challenged s.c. with 10^3 FFU POWV-Spo or 10^2 FFU MP-12. We saw no mortality from the mice infected with the control MP12 and a survival rate of 60% of mice challenged with POWV-Spo as observed previously (Figure 4A). POWV-Spo- and MP12-infected mice that survived >30 dpi, recovered weight loss, and had no apparent indicators of disease, were considered recovered from infection and terminally bled for collection of sera. Sera was diluted 1:10 in saline and passively transferred into naive B6 mice. These mice were challenged s.c. with 10^2 FFU POWV-LB within 24 h of serum transfer and monitored daily (Figure 4B).

We found that B6 mice which received sera from POWV-Spo immune mice were somewhat protected from lethal POWV-LB challenge, with a significantly improved survival rate of 60% relative to no protection for MP-12 recipient mice (p = 0.0005, Figure 4A). POWV-Spo recipient mice experienced mild weight loss beginning at around 13 dpi, later than MP-12 recipient mice, which began losing weight at around 6 dpi (Figure 4B).

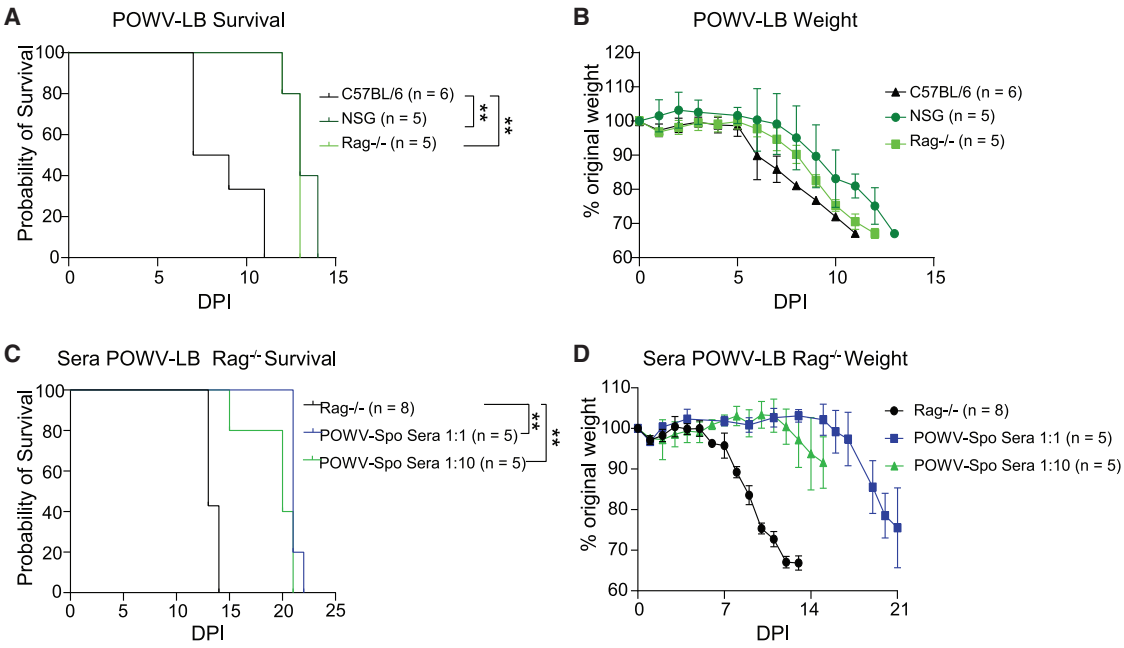

Figure 5. POWV-LB neuroinvasive disease and death occurs independent of host immune response

(A and B) Mortality (A) and weight loss (B) of NOD SCID gamma (NSG) (n = 5), recombination-activating gene 1-deficient (Rag1$^{-/-}$, n = 5), and C57BL/6 (B6, n = 6) mice challenged s.c. with 10^2 FFU POWV-LB and monitored for 14 dpi. Immunocompromised mice survived significantly longer than B6 counterparts (p_{NSG} = 0.0443, $p_{Rag1-/-}$ = 0.0493, Mantel-Cox test). There was no difference between NSG and Rag1$^{-/-}$ mice (p = 0.65, Mantel-Cox test).

(C and D) Mortality (C) and weight loss (D) for saline Rag1$^{-/-}$ (n = 8) mice, as well as recipient Rag1$^{-/-}$ mice that received POWV-Spo convalescent sera diluted 1:10 (green, n = 5) or 1:1 (blue, n = 5) prior to s.c. challenge with 10^2 FFU POWV-LB. Rag1$^{-/-}$ mice that received POWV-Spo sera diluted 1:10 (**p = 0.031) or 1:1 (**p = 0.013) had significantly prolonged survival times relative to Rag1$^{-/-}$ mice receiving saline (Mantel-Cox test). All data are reported as mean ± SEM.

These mice displayed few indicators of disease compared with control mice that received sera from MP-12 immune mice (not shown). For POWV-Spo recipient mice that recovered from POWV-LB challenge, weight loss was recovered by 18 dpi. We did not observe long-term neurological sequelae in surviving mice following the resolution of disease indicators and weight loss. Our results using passive transfer of convalescent POWV-Spo sera into B6 mice suggest that—while humoral responses raised against POWV-Spo can delay disease onset in isolation—only the combination of cellular and humoral adaptive immune responses is sufficient to provide protection from lethal POWV-LB challenge in this model.

POWV-LB neuroinvasive disease and death occurs independent of host immune response

As we had previously observed that 7–8 dpi corresponded to the peak of the CD8$^+$ T cell response in our mouse model of both ZIKV and POWV, we wanted to further investigate the role of the T cell compartment in POWV-LB challenge. To determine whether mortality following POWV-LB infection was attributable to the T cell compartment, we infected recombination-activating gene 1-deficient (Rag1$^{-/-}$) mice and NOD SCID gamma (NSG) mice with 10^2 FFU of POWV-LB. Rag1$^{-/-}$ mice are T and B cell deficient and NSG mice are also deficient in T and B cells, as well as NK cells and hemolytic complement, and have defects in macrophage and dendritic cell functions (Mombaerts et al., 1992; Shultz et al., 2005; Coughlan et al., 2016). By challenging with a low dose of POWV-LB, we anticipated that we would gain insight into whether POWV-LB could cause morbidity and mortality independent of the T and B cell compartments.

Following infection of B6, Rag1$^{-/-}$, and NSG mice with 10^2 FFU POWV-LB, mice were monitored for 21 days (Figure 5). We observed that Rag1$^{-/-}$ and NSG mice had significantly longer survival times relative to B6 mice (p = 0.0493, p = 0.0443) (Figure 5A). However, both groups uniformly succumb to infection, with Rag1$^{-/-}$ mice succumbing to disease with an MST of 12.8 dpi and NSG mice succumbing to disease with an MST of 13.2 dpi, compared with an MST of 8.5 dpi for B6 mice. Weight loss for Rag1$^{-/-}$ mice began at 6 dpi and persisted until mice succumbed (Figure 5B). Similarly, for NSG mice, weight loss began at 6 dpi and persisted until mice succumbed to infection, with no significant differences between immunocompromised mice (p = 0.65) (Figure 5B). Interestingly, we observed distinct disease pathology in Rag1$^{-/-}$ and NSG mice relative to infected B6 mice. Whereas B6 mice began to show signs of infection as early as 5 dpi, and by 8 dpi all showed evidence of infection, Rag1$^{-/-}$ and NSG mice had delayed onset of disease. In immunocompromised mice, the first indicators of disease did not appear until 8 dpi, with all mice showing evidence of disease by 10 dpi. We also noted distinct signs of disease among Rag1$^{-/-}$ and NSG mice. POWV-LB infection in B6 mice typically results in ruffled fur and hunched posture, limp tail, hindlimb and forelimb weakness, and eventually moribund posture, before succumbing to infection (Figure 1C). In Rag1$^{-/-}$ and NSG

mice, however, we observed that, after 10 dpi, mice developed a shaking or twitching phenotype, and often displayed a reduction in or loss of coordination. Occasionally, mice had muscle spasms, and one Rag1$^{-/-}$ mouse developed right hindlimb paralysis. Because these mice exhibited different disease progression, disease scoring by the same system established for B6 mice was not possible and is therefore not represented in this dataset. In summary, infection of mice lacking functional B and T cell compartments (Rag1$^{-/-}$ and NSG) with POWV-LB resulted in prolonged survival and distinct disease progression. These findings suggest that the adaptive immune response could drive morbidity and mortality. Importantly, this finding also suggests that, in this murine model, POWV-LB lethality involves two components: one independent of the adaptive immune response and one that is immune mediated.

As we had previously seen that POWV-Spo infection could generate an antibody response with binding and neutralization capabilities that provided partial protection in B6 mice, we next sought to understand the protective capacity of POWV-specific antibodies against lethal POWV-LB challenge independent of the T cell compartment. To this end, we harvested sera from recovered POWV-Spo mice, which was diluted in saline and passively transferred via intraperitoneal (i.p.) injection into Rag1$^{-/-}$ mice 24 h before lethal POWV-LB challenge. Mice were then monitored daily for weight loss and signs of disease.

We found that POWV-Spo sera diluted 10-fold and passively transferred into Rag1$^{-/-}$ mice significantly prolonged survival time ($p = 0.0031$) but was insufficient to provide protection against lethal POWV-LB challenge (Figure 5C). Instead, Rag1$^{-/-}$ mice that received POWV-Spo sera displayed delayed onset of weight loss and indicators of disease. Mice that received more concentrated POWV-Spo sera (diluted only 2-fold) showed significantly prolonged survival ($p = 0.0013$) relative to Rag1$^{-/-}$ mice receiving no sera (Figure 5C). Notably, these mice still succumb to disease by 22 dpi. Whereas Rag1$^{-/-}$ mice that received saline alone displayed signs of weight loss at 6 dpi, weight loss for Rag1$^{-/-}$ mice receiving POWV-Spo sera diluted 10-fold showed signs of weight loss around 11 dpi, which persisted until mice succumbed between 15 and 21 dpi (Figure 5D). Rag1$^{-/-}$ mice that received more concentrated POWV-Spo sera (diluted only 2-fold) displayed signs of weight loss at around 15 dpi but succumbed at around 21 dpi (Figure 5D). Signs of disease exhibited by passive transfer recipients were effectually identical to the saline-treated mice, but occurred later, at around 13–16 dpi. Altogether, the inability of convalescent POWV-Spo sera to provide protection from lethal POWV-LB challenge in Rag1$^{-/-}$ mice suggests that humoral responses alone are insufficient for long-term control of POWV-LB infection as polyclonal antibodies in sera, and that the T cell compartment is an important factor in sustained protection from POWV-LB.

T cell-mediated immunity alone is insufficient for protection against POWV-LB

We have observed a detectable T cell response specific to POWV-LB that arises in wild-type B6 mice and observed that Rag1$^{-/-}$ and NSG mice lacking adaptive immune cell compartments have a longer MST compared with immune competent mice. However, passive transfer of sera alone is insufficient for durable protection in Rag1$^{-/-}$ mice. Furthermore, CD4$^+$ and CD8$^+$ T cells have been shown to be important for immune protection from tick-borne flaviviruses (Blom et al., 2015, 2018). Taken together with our data, this suggested to us that the T cell compartment does contribute to durable protection against POWV. We therefore undertook T cell adoptive transfer studies. As before, donor B6 mice for adoptive T cell transfers were challenged s.c. with 10^3 FFU POWV-Spo or 10^2 FFU MP-12. Upon recovery, total CD4$^+$ and CD8$^+$ T cells were harvested from splenocytes and purified by negative selection before 1×10^6 total T cells were administered intravenously (i.v.) to B6 mice. Within 24 h, mice were s.c. challenged with 10^2 FFU POWV-LB. Unlike most previous studies with flaviviruses (Brien et al., 2008; Hassert et al., 2018, 2019; Elong Ngono et al., 2019; Watson et al., 2016; Bassi et al., 2015; Regla-Nava et al., 2018; Wen et al., 2017; Yauch et al., 2009), we saw no significant differences between survival time of naive recipient mice and mice that received T cells from POWV-Spo immune donors ($p = 0.97$, Figure 6A). We also saw no differences in weight loss between the naive and POWV-Spo T cell recipient groups (Figure 6B).

To further assess the contribution of the T cell compartment in POWV-LB infection, we performed CD4$^+$ and CD8$^+$ T cell depletions by administering CD4$^+$ or CD8$^+$ T cell-depleting antibody before challenge with 10^2 FFU POWV-LB. Confirmation of T cell depletion was performed by flow cytometric analysis of peripheral blood collected 3 dpi (Figure S6). We saw no significant differences in survival or weight loss between control and CD4$^+$ T cell-depleted mice (Figures 6C and 6D). We also saw no significant differences in signs of disease between control and CD4$^+$ T cell-deplete groups (not shown). Depletion of CD8$^+$ T cells, however, was able to significantly prolong survival relative to control mice ($p = 0.0003$, Figure 6E). Despite prolonged survival times of CD8$^+$ T cell-deplete mice, we saw no significant weight loss differences between depleted and non-depleted groups (Figure 6F). However, in CD8$^+$ T cell-deplete animals we observed slightly worsened signs of disease (not shown). Taken together, our T cell adoptive transfer and depletion studies show that memory T cells primed in POWV-Spo infection are not capable of providing protection against lethal POWV-LB challenge alone. In addition, the prolonged survival observed following CD8$^+$ T cell depletion in the lethal POWV-LB challenge model suggests that CD8$^+$ T cells may be partly responsible for immunopathogenesis in B6 mice.

VLP-based vaccination confers protection against lethal POWV-LB challenge

Applying what we learned about the requirement for humoral and cell-mediated immunity for control of POWV-LB infection, we sought to utilize a VLP-based vaccination approach to protect against lethal POWV-LB challenge. Expression of flavivirus prM and E proteins in cultured cells has previously been shown to result in secretion of VLPs into culture media (Garg et al., 2017; Espinosa et al., 2018; Salvo et al., 2018). We constructed a cell line that inducibly expresses POWV-prME upon addition of doxycycline resulting in VLP secretion (Figures S7A–S7C). VLPs were purified from culture supernatant and used as the antigen in vaccination experiments. We adopted a prime-boost strategy for POWV-VLP vaccination in B6 mice. In our approach,

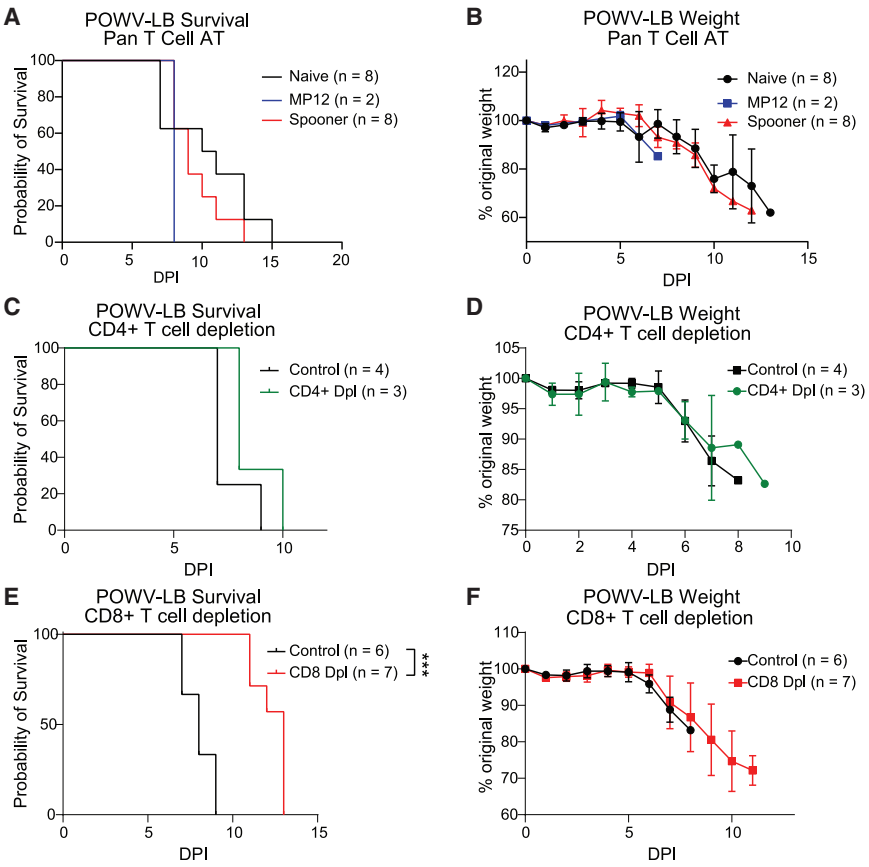

Figure 6. T cell-mediated immunity alone is insufficient for protection against POWV-LB

(A and B) Mortality (A) and weight loss (B) for mice receiving adoptively transferred T cells (both $CD4^+$ and $CD8^+$) from POWV-Spooner (red, POWV-Spo, n = 8) experienced, alphavirus-negative control (RVFV vaccine strain MP-12) experienced T cells (blue, MP12, n = 2) or naive T cells (black, n = 8) into naive B6 mice. B6 mice were challenged s.c. with 10^2 FFU POWV-Spo or saline and harvested in memory phase 30 dpi. $CD4^+$ and $CD8^+$ T cells were enriched via negative selection and 1×10^6 cells were administered i.v. to B6 mice. Within 24 h, recipient mice were challenged s.c. with 10^2 FFU POWV-LB and monitored for 21 dpi. No significant differences in mortality were observed between naive and POWV-Spo recipient mice (p = 0.3592, Mantel-Cox test).

(C and D) Mortality (C) and weight loss (D) for B6 mice s.c. challenged with 10^2 FFU POWV-LB in control (black, n = 3) or $CD4^+$ T cell-deplete (green, n = 3) conditions and monitored for 14 dpi. No significant difference in mortality (p = 0.6877) as determined by Mantel-Cox test.

(E and F) Mortality (E) and weight loss (F) for B6 mice s.c. challenged with 10^2 FFU POWV-LB in control (black, n = 6) or $CD8^+$ T cell deplete (red, n = 7) conditions and monitored for 14 dpi (p = 0.0003, Mantel-Cox test). All data are reported as mean ± SEM.

mice were administered 2×10^7 plaque-forming units equivalents of POWV-LB VLP intramuscularly (i.m.) in aluminum hydroxide gel (Alum) adjuvant for a primary vaccination. At 21 days post vaccination, mice were boosted in a manner identical to the primary vaccination and bled for B and T cell analysis (Figure 7A).

We performed an indirect ELISA to examine the capacity of POWV-VLP sera to bind whole POWV-LB, POWV-Spo, and WNV virions. We found that POWV-VLP vaccination induces antibodies that bind both POWV lineages (Figures 7B and 7C). We also see a lower degree of cross-binding to WNV, suggesting the presence of antibodies recognizing conserved portions of structural proteins (Figure 7D).

In addition to binding capacity, we wanted to examine the neutralization capacity of antibodies raised during VLP vaccination. To this end, we performed FRNTs as described previously (Brien et al., 2013; Smith and Hirsch, 2020). We found that POWV-LB neutralization was low but detectable following primary VLP vaccination (Figure 7E). We observed with a limited subset of samples that neutralization increased following boosting (not shown). We also wanted to assess the durability of antibody responses using this approach. To this end, we vaccinated mice with a single dose of adjuvanted VLP or adjuvant only control in the same manner as Figure 7A. Blood from vaccinated (n = 3) or Alum control mice (n = 2) was collected via submandibular cheek bleed 15 weeks following vaccination and neutralization determined by FRNT against POWV-LB. We were able to detect neutralizing antibody titers for the duration of the experiment, up to 15 weeks post vaccination (Figure S7D). This suggested that POWV-VLP-based vaccination could induce durable neutralizing antibody responses.

To determine whether VLP-based vaccination-induced T cell responses, we stimulated T cells *ex vivo* using the epitopes identified in Figure 4 and Table S1, followed by flow cytometric analysis, to examine cytokine production. Responses were not detectable in peripheral blood following the boost (Figure S7E), but we did observe polyfunctional POWV-E_{282}-specific $CD8^+$ T cells in the blood 3 days after POWV-LB challenge (Figure 7F). This response was similar in magnitude to anamnestic responses observed in POWV-Spo convalescent mice 4 days after challenge with POWV-LB (Figure S7F). This response was absent in Alum-only-vaccinated mice, indicating that POWV-VLP-vaccinated mice mounted a POWV-specific T cell response. However, we were unable to detect $CD8^+$ T cell responses to the $POWV_{351\text{-}361}$ epitope and the POWV-specific $CD4^+$ T cell epitopes at the indicated time points.

With the understanding that B and T cell responses are critical for POWV-LB immune-mediated protection, we challenged mice vaccinated with POWV-VLP + Alum or Alum only with 10^2 FFU POWV-LB. The POWV-VLP-vaccinated mice uniformly survived lethal POWV-LB challenge (Figure 7G). POWV-VLP-vaccinated mice experienced no weight loss or apparent indicators of disease (Figure 7H). Together, these results suggest that the combination of humoral and cellular responses were necessary

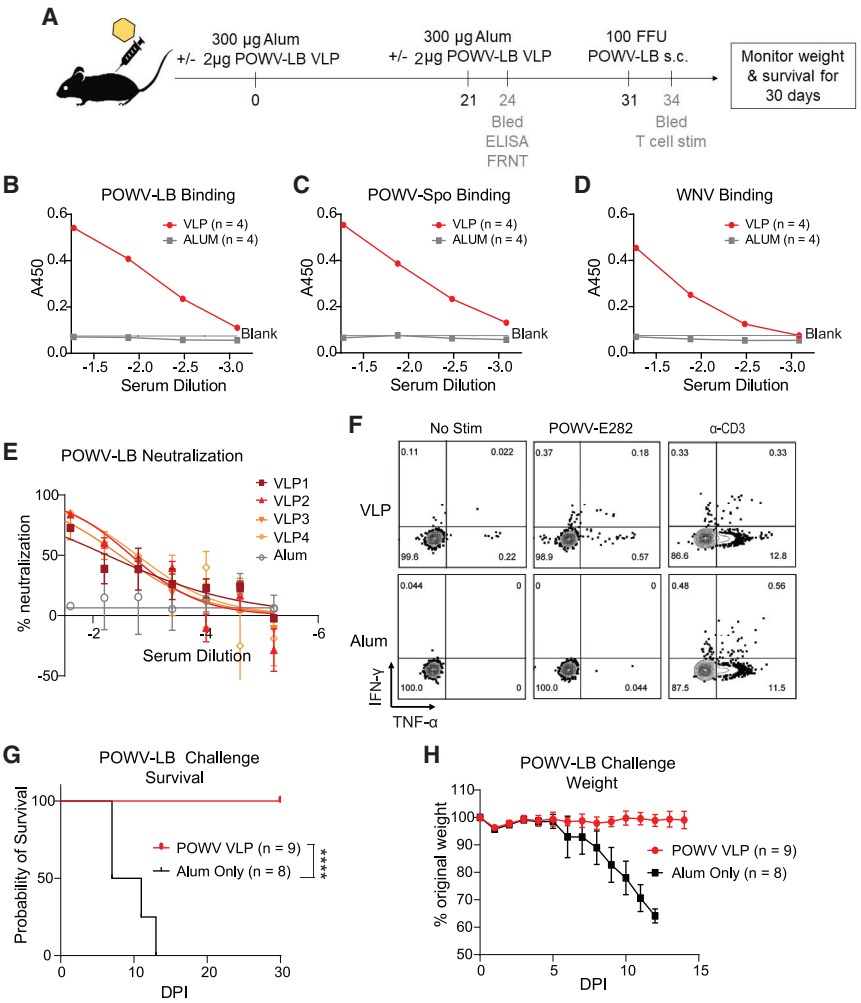

Figure 7. VLP-based vaccination confers protection against lethal POWV-LB challenge

(A) Vaccination strategy and relevant time points for 10- to 14-week-old B6 mice. Mice were vaccinated with 300 µg per mouse of 2% Alhydrogel (Alum only) ± 2 µg POWV-LB VLP i.m. and allowed to develop a memory response for 21 days post vaccination (dpv). At 21 dpv, mice were boosted with identical formulations of Alum ± 2 µg POWV-LB VLP i.m. Three days after boosting, submandibular bleeds were performed to examine the binding and neutralization activity via ELISA and FRNT. Thirty-one days following initial vaccination, mice were challenged s.c. with 10^2 FFU POWV-LB and monitored for morbidity and mortality. At 3 dpi, submandibular bleeds were performed to examine $CD4^+$ and $CD8^+$ T cell responses.

(B) Representative graph from two independent experiments with ELISAs examining binding to whole virions using sera collected from mice 24 dpv with Alum ± 2 µg POWV-LB VLP (n = 8 and n = 9, respectively). Binding indicated by absorbance (A450) to POWV-LB.

(C and D) POWV-Spooner (C) and West Nile virus (WNV) (D) is shown.

(E) Representative graph from two independent experiments with FRNTs performed on BHK-21 cells examining neutralization activity against 10^2 FFU POWV-LB for sera collected 24 dpv (n = 2 and n = 4, respectively).

(F) Representative flow plots showing T cell responses in blood of mice VLP vaccinated (n = 4) or Alum adjuvant only (n = 3)-treated mice 3 days after 10^2 FFU POWV-LB challenge. T cells were treated *ex vivo* with either no stimulus (left), 10 µM peptide (middle), or α-CD3 (right) in the presence of BFA for 6 h and stained and analyzed as in Figure 3.

(G and H) Mortality (G) and weight loss (H) of B6 mice vaccinated and boosted with Alum ± 2 µg POWV-LB VLP (n = 8 and n = 9, respectively) and challenged s.c. with 10^2 FFU POWV-LB and monitored for 30 dpi. Mice vaccinated with POWV-VLP were protected from lethal POWV-LB challenge ($p < 0.0001$, Mantel-Cox test). All data are reported as mean ± SEM.

for protection against lethal POWV-LB challenge, and that a prime-boost strategy for POWV-LB-based VLPs can provide durable protection in a lethal POWV-LB challenge model.

DISCUSSION

Using B6 mice, we have gained insights into immune protection against POWV disease. We have demonstrated that POWV-Spo infection in our model can drive a protective immune response against POWV-LB. We also described detectable binding and neutralizing antibody profiles in POWV-LB-infected mice. However, we showed via passive transfer studies in B6 and $Rag1^{-/-}$ mice that POWV-Spo sera alone appears to delay, but not entirely mitigate, POWV-LB morbidity and mortality. Furthermore, we identified two $CD8^+$ and 2 $CD4^+$ T cell epitopes within the structural proteins of POWV-LB, including one H2-D^b-restricted $CD8^+$ T cell epitope, POWV-E_{282}. Finally, we demonstrate, via T cell adoptive transfer of POWV-Spooner primed cells and depletion studies, that POWV-specific T cells are insufficient for complete protection from lethal POWV-LB challenge. Ultimately, our findings reveal that B and T cell-mediated protection is critical for protection, as exemplified by the successful implementation of a POWV-LB VLP-based vaccination strategy. In these studies, we utilized a mouse model of POWV-LB infection to establish factors associated with immune protection against lethal POWV-LB challenge. Our main findings include: (1) the requirement of B and T cell responses for protection against lethal POWV-LB challenge, (2) viral- and host-mediated components of POWV-LB mortality, and (3) application of this knowledge to design a successful VLP vaccination approach.

In addition to establishing a mouse model of POWV-LB infection, our work using immunocompromised mouse models indicate that the POWV-LB neurotropism can drive mortality independent of the host adaptive immune system. This was best illustrated by uniform mortality in B and T cell-deficient NSG and $Rag1^{-/-}$ mice challenged with POWV-LB. These mice displayed a distinct disease progression, implying that POWV neurological involvement in mice is possibly independent of

adaptive immunity. Future studies should consider whether cellular targets of infection or replication kinetics are altered in NSG and Rag1$^{-/-}$ mice, which may impact POWV disease.

The implication that adaptive immunity may contribute to immune-mediated pathogenesis is noteworthy. The disease phenotype observed in B and T cell-deficient (NSG, Rag1$^{-/-}$) mice was similar to depletion of CD8$^+$ T cells in B6 mice prior to POWV-LB challenge, indicating that CD8$^+$ T cells are important drivers of immune-mediated pathogenesis in our model. This finding may be relevant to POWV morbidity and mortality, and the development of neurological symptoms during POWV disease. CD8$^+$ T cells contributing to immune-mediated pathogenesis in POWV infection is consistent with reports for other flaviviruses (Hassert et al., 2020, 2021) and flaviviruses causing TBE (Růžek et al., 2009; Blom et al., 2018). Strikingly, immunocompromised SCID mice challenged with TBEV have longer survival times than BALB/c or B6 mice. Furthermore, studies of mice lacking CD8$^+$ T cells during TBEV challenge found survival time was extended (Růžek et al., 2009) and adoptive transfer of TBEV-specific CD8$^+$ T cells into SCID reduced survival times (Růžek et al., 2009). This suggests that the presence of CD8$^+$ T cells is sufficient for immune-mediated pathogenesis of these neurotropic tick-borne flaviviruses. This phenomenon has relevance for efforts to develop vaccinations against tick-borne flaviviruses and should be the subject of further study.

Interestingly, the POWV$_{351\text{-}359}$ region containing a CD8$^+$ T cell epitope also contains an POWV-specific B cell epitope identified by Choi et al. (2020) in their synthetic enhanced DNA-based POWV vaccination approach (Choi et al., 2020). These concomitant findings, as well as other studies (Cimica et al., 2021), underscore the benefit of a VLP-based vaccination strategy that elicits responses to B and T cell epitopes. This finding also highlights the need to better understand immune responses elicited by different vaccine formulations (i.e., different adjuvants driving T-helper profiles, T_H1 versus T_H2) to provide optimal immunity against POWV-LB. Future studies should explore the role of CD8$_+$ T cell responses in VLP-based vaccination strategies against POWV-LB to elucidate the role of CD8$^+$ T cells in protection versus pathogenesis during POWV infection. Notably, in our studies of CD8$^+$ T cell responses within the POWV model, mice mount a response lower in magnitude relative to other flaviviruses (ZIKV, WNV) utilized in our lab. This is true for both lineages, although the mechanisms underlying this reduced response remain unclear to us. It is also notable that antibody responses detected against POWV-LB were similar in magnitude to responses against POWV-Spo, suggesting that the ability to generate an antibody response to POWV does not solely dictate survival outcome among B6 mice infected with the two lineages.

The contribution of CD4$^+$ T cells in the context of POWV immunity is unclear. Although our studies did not examine the impact of adoptively transferring POWV-experienced CD4$^+$ T cells alone, we observed no significant differences in morbidity or mortality of POWV-LB challenged mice when pan T cells were transferred to B6 mice. We also saw no significant differences in mice depleted of CD4$^+$ T cells prior to POWV-LB challenge. It has been shown for other flaviviruses that CD4$^+$ T cell responses are important for protection from disease (Brien et al., 2008; Elong Ngono et al., 2019; Hassert et al., 2018; Watson et al., 2016). In particular, the role of CD4$^+$ T cells in POWV infection and CNS disease (Ciurkiewicz et al., 2020) should be a subject of further inquiry.

From our studies, it appears that no single component of POWV immunity in isolation is sufficient for durable protection against POWV, as only sera transferred to B6 mice with a functional T cell compartment resulted in limited protection from death and severe disease.

Limitations of the study

One limitation of our studies of the POWV-LB-adaptive immune response is the necessity of using POWV-Spo for the generation of donor sera and T cells. The discrepancies in disease progression between the two lineages underscore the need to better each POWV lineage, but also to dissect the molecular mechanisms that drive the distinct disease outcomes observed among two lineages that differ very little in terms of aa identity. Overall, our studies suggest that the balance of T and B cell-mediated immunity is critical for prevention of severe POWV disease, and that POWV neurological sequelae are the result of viral- and host-mediated pathologies. Our findings support the careful consideration of a balanced B and T cell response elicited by future POWV vaccines to provide protection from disease. The finding that balanced T and B cell responses are critical for immune-mediated protection from POWV disease will aid the rational design of future POWV vaccines.

STAR★METHODS

Detailed methods are provided in the online version of this paper and include the following:

- KEY RESOURCES TABLE
- RESOURCE AVAILABILITY
  - Lead contact
  - Materials availability
  - Data and code availability
- EXPERIMENTAL MODEL AND SUBJECT DETAILS
  - Viruses and cells
  - Ethics statement
  - Mice and infections
- METHOD DETAILS
  - CD8$^+$ and CD4$^+$ T cell depletions
  - Peptide library
  - Peptide stimulation
  - Flow cytometry
  - Passive transfer of sera
  - Adoptive transfer of T cells
  - Virus-like particle (VLP) preparation and vaccination
  - Enzyme-linked immunosorbent assays (ELISAs)
  - Focus forming assay (FFA)
  - Focus reduction neutralization tests (FRNTs)
  - RMA-S stabilization assay
- QUANTIFICATION AND STATISTICAL ANALYSIS

SUPPLEMENTAL INFORMATION

Supplemental information can be found online at https://doi.org/10.1016/j.celrep.2022.110388.

ACKNOWLEDGMENTS

This research was supported in part by the National Institutes of Health, National Institute of Allergy and Infectious Diseases (NIAID): 5R01AI152192-02, 5R01AI137424-03, and F31AI152460-01, and in part by the Department of Defense (award no. PR192269). The funders had no role in study design, data collection and analysis, decision to publish, or preparation of the manuscript.

AUTHOR CONTRIBUTIONS

Experimental conceptualization, A.K.P., E.T.S., and J.D.B.; data curation, E.T.S., J.L.S., and M.H.; formal analysis, E.T.S., J.D.B., M.H., E.G., C.G., and A.K.P.; funding acquisition, G.D.E., A.K.P., M.H., and A.J.H.; investigation, E.T.S., C.G., J.L.S., E.G., and M.H.; methodology, A.K.P. and E.T.S.; project administration, A.K.P.; resources, all authors; software, A.K.P. and J.D.B.; supervision, A.K.P.; validation, A.K.P., J.L.S., G.D.E., and A.J.H.; visualization, A.K.P., E.T.S., and J.D.B.; writing – original draft, A.K.P. and E.T.S.; writing – review & editing, all authors, who reviewed and approved the content and submission of the final manuscript.

DECLARATION OF INTERESTS

The authors declare no competing interests.

INCLUSION AND DIVERSITY

We worked to ensure sex balance in the selection of non-human subjects. One or more of the authors of this paper self-identifies as an underrepresented ethnic minority in science. One or more of the authors of this paper self-identifies as a member of the LGBTQ+ community. While citing references scientifically relevant for this work, we also actively worked to promote gender balance in our reference list.

Received: July 30, 2021
Revised: November 7, 2021
Accepted: January 24, 2022
Published: February 15, 2022

REFERENCES

Aberle, J.H., Schwaiger, J., Aberle, S.W., Stiasny, K., Scheinost, O., Kundi, M., Chmelik, V., and Heinz, F.X. (2015). Human CD4+ T helper cell responses after tick-borne encephalitis vaccination and infection. PLoS One *10*, e0140545.

Centers for disease control and prevention (2020). Powassan Virus Statistics & Maps.https://www.cdc.gov/powassan/statistics.html.

Bassi, M.R., Kongsgaard, M., Steffensen, M.A., Fenger, C., Rasmussen, M., Skjødt, K., Finsen, B., Stryhn, A., Buus, S., Christensen, J.P., and Thomsen, A.R. (2015). CD8$^+$ T cells complement antibodies in protecting against yellow fever virus. J. Immunol. *194*, 1141.

Best Sonja, M., Morris Keely, L., Shannon Jeffrey, G., Robertson Shelly, J., Mitzel Dana, N., Park Gregory, S., Boer, E., Wolfinbarger James, B., and Bloom Marshall, E. (2005). Inhibition of interferon-stimulated JAK-STAT signaling by a tick-borne Flavivirus and identification of NS5 as an interferon antagonist. J. Virol. *79*, 12828–12839.

Blom, K., Braun, M., Pakalniene, J., Dailidyte, L., Béziat, V., Lampen, M.H., Klingström, J., Lagerqvist, N., Kjerstadius, T., Michaëlsson, J., et al. (2015). Specificity and dynamics of effector and memory CD8 T cell responses in human tick-borne encephalitis virus infection. PLOS Pathog. *11*, e1004622.

Blom, K., Cuapio, A., Sandberg, J.T., Varnaite, R., Michaëlsson, J., Björkström, N.K., Sandberg, J.K., Klingström, J., Lindquist, L., Gredmark Russ, S., and Ljunggren, H.-G. (2018). Cell-mediated immune responses and immunopathogenesis of human tick-borne encephalitis virus-infection. Front. Immunol. *9*, 2174.

Brien, J.D., Lazear, H.M., and Diamond, M.S. (2013). Propagation, quantification, detection, and storage of West Nile virus. Curr. Protoc. Microbiol. *31*, 15D.3.1-15D.3.18.

Brien, J.D., Uhrlaub, J.L., and Nikolich-Zugich, J. (2007). Protective capacity and epitope specificity of CD8(+) T cells responding to lethal West Nile virus infection. Eur. J. Immunol. *37*, 1855–1863.

Brien, J.D., Uhrlaub, J.L., and Nikolich-Zugich, J. (2008). West Nile virus-specific CD4 T cells exhibit direct antiviral cytokine secretion and cytotoxicity and are sufficient for antiviral protection. J. Immunol. *181*, 8568–8575.

Chernokhaeva, L.L., Rogova, Y.V., Vorovitch, M.F., Romanova, L., Kozlovskaya, L.I., Maikova, G.B., Kholodilov, I.S., and Karganova, G.G. (2016). Protective immunity spectrum induced by immunization with a vaccine from the TBEV strain Sofjin. Vaccine *34*, 2354–2361.

Choi, H., Kudchodkar, S.B., Ho, M., Reuschel, E.L., Reynolds, E., Xu, Z., Bordoloi, D., Ugen, K.E., Tebas, P., Kim, J., Abdel-Mohsen, M., Thangamani, S., Weiner, D.B., and Muthumani, K. (2020). A novel synthetic DNA vaccine elicits protective immune responses against Powassan virus. PLOS Negl. Trop. Dis. *14*, e0008788.

Chumakov, M.P., Gagarina, A.V., Vilner, L.M., Khanina, M.K., Rodin, I.M., Vasenovich, M.I., Lakina, V.I., and Finogenova, E.V. (1963). [Experience in the experimental production and control of tissue culture vaccine against tick encephalitis]. Vopr Virusol *29*, 415–420.

Cimica, V., Saleem, S., Matuczinski, E., Adams-Fish, D., Mcmahon, C., Rashid, S., and Stedman, T.T. (2021). A virus-like particle-based vaccine candidate against the tick-borne powassan virus induces neutralizing antibodies in a mouse model. Pathogens *10*.

Ciurkiewicz, M., Herder, V., and Beineke, A. (2020). Beneficial and detrimental effects of regulatory T cells in neurotropic virus infections. Int. J. Mol. Sci. *21*, 1705.

Clow, K.M., Leighton, P.A., Ogden, N.H., Lindsay, L.R., Michel, P., Pearl, D.L., and Jardine, C.M. (2017). Northward range expansion of Ixodes scapularis evident over a short timescale in Ontario, Canada. PLoS One *12*, e0189393.

Costero, A., and Grayson, M.A. (1996). Experimental transmission of powassan virus (Flaviviridae) by Ixodes scapularis ticks (Acari:ixodidae). Am. J. Trop. Med. Hyg. *55*, 536–546.

Coughlan, A.M., Harmon, C., Whelan, S., O'brien, E.C., O'reilly, V.P., Crotty, P., Kelly, P., Ryan, M., Hickey, F.B., O'farrelly, C., and Little, M.A. (2016). Myeloid engraftment in humanized mice: impact of granulocyte-colony stimulating factor treatment and transgenic mouse strain. Stem Cells Dev. *25*, 530–541.

Ebel, G.D., Foppa, I., Spielman, A., and Telford, S.R., 2nd. (1999). A focus of deer tick virus transmission in the northcentral United States. Emerg. Infect. Dis. *5*, 570–574.

Ebel, G.D., and Kramer, L.D. (2004). Short report: duration of tick attachment required for transmission of powassan virus by deer ticks. Am. J. Trop. Med. Hyg. *71*, 268–271.

Ebel, G.D., Spielman, A., and Telford, S.R. (2001). Phylogeny of North American powassan virus. J. Gen. Virol. *82*, 1657–1665.

Elong Ngono, A., Young, M.P., Bunz, M., Xu, Z., Hattakam, S., Vizcarra, E., Regla-Nava, J.A., Tang, W.W., Yamabhai, M., Wen, J., and Shresta, S. (2019). CD4+ T cells promote humoral immunity and viral control during Zika virus infection. PLOS Pathog. *15*, e1007474.

Ermler, M.E., Yerukhim, E., Schriewer, J., Schattgen, S., Traylor, Z., Wespiser, A.R., Caffrey, D.R., Chen, Z.J., King, C.H., Gale, M., Jr., et al. (2013). RNA helicase signaling is critical for type i interferon production and protection against Rift Valley fever virus during mucosal challenge. J. Virol. *87*, 4846–4860.

Errico, J.M., Vanblargan, L.A., Nelson, C.A., Diamond, M.S., and Fremont, D.H. (2020). Structural basis of neutralization of Powassan virus by monoclonal antibodies. J. Immunol. *204*, 247.9.

Ershova, A.S., Gra, O.A., Lyaschuk, A.M., Grunina, T.M., Tkachuk, A.P., Bartov, M.S., Savina, D.M., Sergienko, O.V., Galushkina, Z.M., Gudov, V.P., et al. (2016). Recombinant domains III of Tick-Borne Encephalitis Virus envelope protein in combination with dextran and CpGs induce immune response

and partial protectiveness against TBE virus infection in mice. BMC Infect. Dis. *16*, 544.

Espinosa, D., Mendy, J., Manayani, D., Vang, L., Wang, C., Richard, T., Guenther, B., Aruri, J., Avanzini, J., Garduno, F., Farness, P., Gurwith, M., Smith, J., Harris, E., and Alexander, J. (2018). Passive transfer of immune sera induced by a Zika virus-like particle vaccine protects AG129 mice against lethal Zika virus challenge. EBioMedicine *27*, 61–70.

Garg, H., Sedano, M., Plata, G., Punke, E.B., and Joshi, A. (2017). Development of virus-like-particle vaccine and reporter assay for Zika virus. J. Virol. *91*, e00834–17.

Gasmi, S., Bouchard, C., Ogden, N.H., Adam-Poupart, A., Pelcat, Y., Rees, E.E., Milord, F., Leighton, P.A., Lindsay, R.L., Koffi, J.K., and Thivierge, K. (2018). Evidence for increasing densities and geographic ranges of tick species of public health significance other than Ixodes scapularis in Québec, Canada. PLoS One *13*, e0201924.

Goldfield, M., Austin, S.M., Black, H.C., Taylor, B.F., and Altman, R. (1973). A non-fatal human case of powassan virus encephalitis. The American Journal of Tropical Medicine and Hygiene. Am. J. Trop. Med. Hyg. *22*, 78–81.

Grabowski, J.M., Nilsson, O.R., Fischer, E.R., Long, D., Offerdahl, D.K., Park, Y., Scott, D.P., and Bloom, M.E. (2019). Dissecting flavivirus biology in salivary gland cultures from fed and unfed Ixodes scapularis (Black-Legged tick). mBio *10*, e02628–18.

Graham, N., Eisenhauer, P., Diehl, S.A., Pierce, K.K., Whitehead, S.S., Durbin, A.P., Kirkpatrick, B.D., Sette, A., Weiskopf, D., Boyson, J.E., and Botten, J.W. (2020). Rapid induction and maintenance of virus-specific CD8(+) T(EMRA) and CD4(+) T(EM) cells following protective vaccination against dengue virus challenge in humans. Front. Immunol. *11*, 479.

Grifoni, A., Voic, H., Dhanda, S.K., Kidd, C.K., Brien, J.D., Buus, S., Stryhn, A., Durbin, A.P., Whitehead, S., Diehl, S.A., De Silva, A.D., Balmaseda, A., Harris, E., Weiskopf, D., and Sette, A. (2020). T cell responses induced by attenuated flavivirus vaccination are specific and show limited cross-reactivity with other flavivirus species. J. Virol. *94*, e00089–20.

Grifoni, A., Voic, H., Sidney, J., De Silva, A.D., Durbin, A., Diehl, S.A., Harris, E., Sette, A., and Weiskopf, D. (2019). Crosseactivity of flaviviruses specific CD8+T cell responses across different viral species. J. Immunol. *202*, 76.12..

Hassert, M., Brien, J.D., and Pinto, A.K. (2020). $CD8^+$ T cell cross-reactivity during heterologous flavivirus infection results in cross-reactive immunodomination and enhanced cytolytic capacity at the expense of virus-specific responses. J. Immunol. *204*, 95.9.

Hassert, M., Harris, M.G., Brien, J.D., and Pinto, A.K. (2019). Identification of protective CD8 T cell responses in a mouse model of Zika virus infection. Front. Immunol. *10*, 1678.

Hassert, M., Steffen, T.L., Scroggins, S., Coleman, A.K., Shacham, E., Brien, J.D., and Pinto, A.K. (2021). Prior heterologous flavivirus exposure results in reduced pathogenesis in a mouse model of Zika virus infection. J. Virol. *95*, Jvi0057321.

Hassert, M., Wolf, K.J., Schwetye, K.E., Dipaolo, R.J., Brien, J.D., and Pinto, A.K. (2018). CD4+T cells mediate protection against Zika associated severe disease in a mouse model of infection. PLoS Pathog. *14*, e1007237.

Hermance, M.E., Santos, R.I., Kelly, B.C., Valbuena, G., and Thangamani, S. (2016). Immune cell targets of infection at the tick-skin interface during powassan virus transmission. PLoS ONE *11*, e0155889.

Hermance, M.E., and Thangamani, S. (2017). Powassan virus: an emerging arbovirus of public health concern in North America. Vector Borne Zoonotic Dis. *17*, 453–462.

Hermance, M.E., Thangamani, S., and Diamond, M.S. (2015). Tick saliva enhances powassan virus transmission to the host, influencing its dissemination and the course of disease. J. Virol. *89*, 7852–7860.

Hinten, S.R., Beckett, G.A., Gensheimer, K.F., Pritchard, E., Courtney, T.M., Sears, S.D., Woytowicz, J.M., Preston, D.G., Smith, R.P., Jr., and Rand, P.W. (2008). Increased recognition of Powassan encephalitis in the United States, 1999-2005. Vector Borne Zoonotic Dis. *8*, 733–740.

Hoof, I., Peters, B., Sidney, J., Pedersen, L.E., Sette, A., Lund, O., Buus, S., and Nielsen, M. (2009). NetMHCpan, a method for MHC class I binding prediction beyond humans. Immunogenetics *61*, 1–13.

Kemenesi, G., and Bányai, K. (2019). Tick-borne flaviviruses, with a focus on Powassan virus. Clin. Microbiol. Rev. *32*, e00106–17.

Kubinski, M., Beicht, J., Gerlach, T., Volz, A., Sutter, G., and Rimmelzwaan, G.F. (2020). Tick-borne encephalitis virus: a quest for better vaccines against a virus on the rise. Vaccines *8*, 451.

Kuivanen, S., Hepojoki, J., Vene, S., Vaheri, A., and Vapalahti, O. (2014). Identification of linear human B-cell epitopes of tick-borne encephalitis virus. Virol. J. *11*, 115.

Lampen, M.H., Uchtenhagen, H., Blom, K., Varnaite, R., Pakalniene, J., Dailidyte, L., Walchli, S., Lindquist, L., Mickiene, A., Michaelsson, J., and et al.. (2018). Breadth and dynamics of HLA-A2- and HLA-B7-restricted CD8(+) T cell responses against nonstructural viral proteins in acute human tick-borne encephalitis virus infection. Immunohorizons *2*, 172–184.

Mandl, C.W., Holzmann, H., Kunz, C., and Heinz, F.X. (1993). Complete genomic sequence of Powassan virus: evaluation of genetic elements in tick-borne versus mosquito-borne flaviviruses. Virology *194*, 173–184.

Matveev, A.L., Kozlova, I.V., Stronin, O.V., Khlusevich, Y.A., Doroshchenko, E.K., Baykov, I.K., Lisak, O.V., Emelyanova, L.A., Suntsova, O.V., Matveeva, V.A., et al. (2019). Post-exposure administration of chimeric antibody protects mice against European, Siberian, and Far-Eastern subtypes of tick-borne encephalitis virus. PLoS One *14*, e0215075.

Mcauley, A.J., Sawatsky, B., Ksiazek, T., Torres, M., Korva, M., Lotrič-Furlan, S., Avšič-Županc, T., Von Messling, V., Holbrook, M.R., Freiberg, A.N., et al. (2017). Cross-neutralisation of viruses of the tick-borne encephalitis complex following tick-borne encephalitis vaccination and/or infection. npj Vaccin. *2*, 5.

Mclean, D.M., and Donohue, W.L. (1959). Powassan virus: isolation of virus from a fatal case of encephalitis. Can. Med. Assoc. J. *80*, 708–711.

Mlera, L., Meade-White, K., Saturday, G., Scott, D., and Bloom, M.E. (2017). Modeling Powassan virus infection in Peromyscus leucopus, a natural host. PLOS Negl. Trop. Dis. *11*, e0005346.

Mombaerts, P., Iacomini, J., Johnson, R.S., Herrup, K., Tonegawa, S., and Papaioannou, V.E. (1992). RAG-1-deficient mice have no mature B and T lymphocytes. Cell *68*, 869–877.

Nofchissey, R.A., Deardorff, E.R., Blevins, T.M., Anishchenko, M., Bosco-Lauth, A., Berl, E., Lubelczyk, C., Mutebi, J.-P., Brault, A.C., Ebel, G.D., and Magnarelli, L.A. (2013). Seroprevalence of powassan virus in New England deer, 1979?2010. Am. Soc. Trop. Med. Hyg. *88*, 1159–1162.

Nonaka, E., Ebel, G.D., and Wearing, H.J. (2010). Persistence of pathogens with short infectious periods in seasonal tick populations: the relative importance of three transmission routes. PLoS One *5*, e11745.

Ogden, N.H., St-Onge, L., Barker, I.K., Brazeau, S., Bigras-Poulin, M., Charron, D.F., Francis, C.M., Heagy, A., Lindsay, L., Maarouf, A., et al. (2008). Risk maps for range expansion of the Lyme disease vector, Ixodes scapularis, in Canada now and with climate change. Int. J. Health Geographics *7*, 24.

Pesko, K.N., Torres-Perez, F., Hjelle, B.L., and Ebel, G.D. (2010). Molecular epidemiology of powassan virus in North America. J. Gen. Virol. *91*, 2698–2705.

Pierson, T.C., and Diamond, M.S. (2020). The continued threat of emerging flaviviruses. Nat. Microbiol. *5*, 796–812.

Regla-Nava, J.A., Elong Ngono, A., Viramontes, K.M., Huynh, A.-T., Wang, Y.-T., Nguyen, A.-V.T., Salgado, R., Mamidi, A., Kim, K., Diamond, M.S., and Shresta, S. (2018). Cross-reactive Dengue virus-specific CD8(+) T cells protect against Zika virus during pregnancy. Nat. Commun. *9*, 3042.

Robertson, S.J., Mitzel, D.N., Taylor, R.T., Best, S.M., and Bloom, M.E. (2009). Tick-borne flaviviruses: dissecting host immune responses and virus countermeasures. Immunologic Res. *43*, 172–186.

Růžek, D., Salát, J., Palus, M., Gritsun, T.S., Gould, E.A., Dyková, I., Skallová, A., Jelínek, J., Kopecký, J., and Grubhoffer, L. (2009). CD8+ T-cells mediate immunopathology in tick-borne encephalitis. Virology *384*, 1–6.

Salvo, M.A., Kingstad-Bakke, B., Salas-Quinchucua, C., Camacho, E., and Osorio, J.E. (2018). Zika virus like particles elicit protective antibodies in mice. PLoS Negl. Trop. Dis. *12*, e0006210.

Santos, R.I., Hermance, M.E., Gelman, B.B., and Thangamani, S. (2016). Spinal cord ventral horns and lymphoid organ involvement in powassan virus infection in a mouse model. Viruses *8*, 220.

Schwaiger, J., Aberle, J.H., Stiasny, K., Knapp, B., Schreiner, W., Fae, I., Fischer, G., Scheinost, O., Chmelik, V., and Heinz, F.X. (2014). Specificities of human CD4+ T cell responses to an inactivated flavivirus vaccine and infection: correlation with structure and epitope prediction. J. Virol. *88*, 7828–7842.

Shamanin, V.A., Pletnev, A.G., Rubin, S.G., and Zlobin, V.I. (1991). [The differentiation of viruses of the tick-borne encephalitis complex by means of RNA-DNA hybridization]. Vopr Virusol *36*, 27–31.

Shultz, L.D., Lyons, B.L., Burzenski, L.M., Gott, B., Chen, X., Chaleff, S., Kotb, M., Gillies, S.D., King, M., Mangada, J., et al. (2005). Human lymphoid and myeloid cell development in NOD/LtSz-scid IL2R gamma null mice engrafted with mobilized human hemopoietic stem cells. J. Immunol. *174*, 6477–6489.

Smith, J.L., and Hirsch, A.J. (2020). Analysis of serum anti-Zika virus antibodies by focus reduction neutralization test. Methods Mol. Biol. *2142*, 73–80.

Sonenshine, D.E. (2018). Range expansion of tick disease vectors in North America: implications for spread of tick-borne disease. Int. J. Environ. Res. Public Health *15*, 478.

Tavakoli, N.P., Wang, H., Dupuis, M., Hull, R., Ebel, G.D., Gilmore, E.J., and Faust, P.L. (2009). Fatal case of deer tick virus encephalitis. New Engl. J. Med. *360*, 2099–2107.

Vanblargan, L.A., Errico, J.M., Kafai, N.M., Burgomaster, K.E., Jethva, P.N., Broeckel, R.M., Meade-White, K., Nelson, C.A., Himansu, S., Wang, D., et al. (2021). Broadly neutralizing monoclonal antibodies protect against multiple tick-borne flaviviruses. J. Exp. Med. *218*, e20210174.

Vanblargan, L.A., Himansu, S., Foreman, B.M., Ebel, G.D., Pierson, T.C., and Diamond, M.S. (2018). An mRNA vaccine protects mice against multiple tick-transmitted flavivirus infections. Cell Rep. *25*, 3382–3392.e3.

Varnaitė, R., Blom, K., Lampen, M.H., Vene, S., Thunberg, S., Lindquist, L., Ljunggren, H.G., Rombo, L., Askling, H.H., and Gredmark-Russ, S. (2020). Magnitude and functional profile of the human CD4(+) T cell response throughout primary immunization with tick-borne encephalitis virus vaccine. J. Immunol. *204*, 914–922.

Watson, A.M., Lam, L.K.M., Klimstra, W.B., and Ryman, K.D. (2016). The 17d-204 vaccine strain-induced protection against virulent yellow fever virus is mediated by humoral immunity and CD4+ but not CD8+ T cells. PLOS Pathog. *12*, e1005786.

Wen, J., Elong Ngono, A., Regla-Nava, J.A., Kim, K., Gorman, M.J., Diamond, M.S., and Shresta, S. (2017). Dengue virus-reactive CD8(+) T cells mediate cross-protection against subsequent Zika virus challenge. Nat. Commun. *8*, 1459.

Yauch, L.E., Zellweger, R.M., Kotturi, M.F., Qutubuddin, A., Sidney, J., Peters, B., Prestwood, T.R., Sette, A., and Shresta, S. (2009). A protective role for dengue virus-specific $CD8^+$ T cells. J. Immunol. *182*, 4865.

STAR★METHODS

KEY RESOURCES TABLE

REAGENT or RESOURCE	SOURCE	IDENTIFIER
Antibodies		
Anti-Mouse IgG (whole molecule)–Peroxidase antibody produced in goat	Sigma-Aldrich	Cat# A8924, RRID:AB_258426
Alexa Fluor® 488 anti-mouse CD19 Antibody, Isotype Rat IgG2a, κ, clone 6D5	BioLegend	Cat# MCA1439A488T, RRID:AB_1101006
PerCP/cyanine5.5 anti-mouse CD8α Antibody, Isotype Rat IgG2a, κ, clone 53–6.7	BioLegend	Cat# 100734, RRID:AB_2075238
Brilliant Violet 605™ anti-mouse CD4 antibody, Rat IgG2a, κ, clone RM4-5	BioLegend	Cat# 100548, RRID:AB_2563054
APC anti-mouse IFN-gamma antibody, Rat IgG1, κ, clone XMG1.2	BioLegend	Cat# 505810, RRID:AB_315404
PE anti-mouse TNF-alpha antibody, Rat IgG1, κ, clone MP6-XT22	BioLegend	Cat# 506306, RRID:AB_315427
PE mouse anti-human Granzyme B antibody, clone GB11	BD Biosciences	Cat# 561142, RRID:AB_10561690
Bacterial and virus strains		
POWV strain LB	Ebel laboratory	Mandl et al., 1993
POWV-DTV strain Spooner	Ebel laboratory	Ebel et al., 1999
Rift Valley Fever Virus vaccine strain (MP-12)	A. Hise & M. Buller	Ermler et al., 2013
Chemicals, peptides, and recombinant proteins		
POWV peptide library, accession #: NP_620099.1	21st Century Biochemicals	N/A
Experimental models: Cell lines		
BHK-21 clone 13	ATCC	ATCC Cat# CCL-10, RRID:CVCL_1915
Vero CCL-81™	ATCC	Cat# CCL-81, RRID:CVCL_0059
RMA-S Cells	ATCC	RRID:CVCL_2180
Experimental models: Organisms/strains		
C57BL/6J mice	The Jackson Laboratory	000664
B6.129S7-*Rag1*^{tm1Mom}/J mice	The Jackson Laboratory	002216
NOD.Cg-*Prkdc*^{scid}*Il2rg*^{tm1Wjl}/SzJ mice	The Jackson Laboratory	005557
Oligonucleotides		
POWV LB qPCR primer 5' - GGCTGCA AATGAGACCAATTC -3′	IDT	N/A
POWV LB qPCR primer 5′'-CAGCGACA CATCTCCATAGTC -3′	IDT	N/A
POWV LB qPCR probe 5'-/56-FAM/TGGCATCCG/ Zen/AGAAAGTGATCCTGC/3IABkFQ/-3'	IDT	N/A
POWV Spooner qPCR primer 5′- GCAGCAC CATAGGTAGAATGT-3′	IDT	N/A
POWV Spooner qPCR primer 5′-CCACCC ACTGAACCAAAGT-3′	IDT	N/A
POWV Spooner qPCR probe 5' -/56-FAM/ TCTCAGTGG/Zen/TTGGAGAACACGCAT/ 3IABkFQ-3′	IDT	N/A
Other		
POWV-E_{282} H2-D^{b} Tetramer, Alexa Fluor® 647	NIH Tetramer Core	N/A

RESOURCE AVAILABILITY

Lead contact

Further information and requests for resources and reagents should be directed to and will be fulfilled by the lead contact, Amelia K. Pinto (amelia.pinto@health.slu.edu).

Materials availability

All unique/stable reagents generated in this study are available from the lead contact upon request.

Data and code availability

- All data reported in this paper will be shared by the lead contact upon request.
- This paper does not report original code.
- Any additional information required to reanalyze the data reported in this paper is available from the lead contact upon request.

EXPERIMENTAL MODEL AND SUBJECT DETAILS

Viruses and cells

POWV-LB (lineage I) (Mandl et al., 1993) and POWV-Spooner (lineage II) (Ebel et al., 1999) were obtained courtesy of G. Ebel and passaged once on BHK-21 clone 13 cells (Mesocricetus auratus, Syrian golden hamster kidney fibroblasts) purchased from American Type Culture Collection (ATCC CCL-10). Rift Valley Fever Virus vaccine (strain MP-12, GenBank accession numbers: DQ375404 (L), DQ380208 (M), and DQ380154 (S)) (Ermler et al., 2013) was gifted from A. Hise and M. Buller and passaged twice in African green monkey kidney epithelial cells (Vero-WHO) purchased from American Type Culture Collection (ATCC CCL-81). All supernatants of these cultures were clarified of cellular debris by centrifugation at 3,500 RPM prior to being aliquoted and frozen at −80°C. Infectious virus titer was measured using a standard focus forming assay (FFA) on Vero cells for MP-12 or BHK-21 (clone-13) cells for POWV as described previously (Brien et al., 2013; Smith and Hirsch, 2020).

Ethics statement

All animal studies were conducted in accordance with the Guide for Care and Use of Laboratory Animals of the National Institutes of Health and approved by the Saint Louis University Animal Care and Use Committee (IACUC protocol # 2777).

Mice and infections

Wild type C57BL/6J (B6, 000664), Nod SCID gamma (NSG, 005557) and recombination activating genes 1 (Rag−/-, 002216) mice were purchased commercially from Jackson Laboratories and housed in a pathogen-free mouse facility at the Saint Louis University School of Medicine. Female Swiss Webster mice (SW-F) were purchased from Taconic Biosciences and housed in the same manner. Unless otherwise noted, approximately equal ratios of male and female mice were utilized for these studies. For CD8+ and CD4+ T cell depletion studies, 10- to 12-week-old B6 mice were infected subcutaneously (s.c.) via footpad injection with 102 focus forming units (FFU) of POWV-LB. For epitope identification, wild type B6 mice were injected with heat-inactivated serum from POWV-immune mice at -1 days post infection (DPI). Within 24 hours, serum-treated mice were infected s.c. with 102 FFU of POWV-LB virus. For Pan T-cell adoptive transfer studies, 10-12-week-old B6 mice were infected with 103 FFU of POWV-LB one day after adoptive transfer of cells. During the course of infection mice were assessed for weight loss, signs of neurological disease, and mortality daily. Signs of disease range and in the most severe cases accelerate in the following manner from no apparent disease, limp tail, hind limb weakness, hind limb paralysis, complete paralysis and death. Clinical scoring system was as follows: 0=clinically normal, 1 = limp tail, slight ruffled appearance, 2 = highly ruffled appearance, hunched posture, 3 = hindlimb weakness, conjunctivitis, 4 = hindlimb paralysis, severe conjunctivitis, urinary incontinence, 5 = moribund, animal is not moving, 6 = deceased. Mice displaying multiple signs of disease at once, such as limp tail accompanied by hindlimb weakness, are scored as the more severe sign of disease (e.g. hindlimb weakness).

METHOD DETAILS

$CD8^+$ and $CD4^+$ T cell depletions

B6 mice were treated with 100 μg of either CD8-depleting antibody (Anti-mouse CD8b.2, 53–5.8, Leinco, C2832) or CD4-depleting antibody (GK1.5, InVivoMab, BE0003-1) two times via intraperitoneal (i.p.) injection; once on day −3 and again on day 0. To confirm T cell depletions, blood was collected by submandibular bleed on day 3 post-infection and analyzed by flow cytometry using antibodies denoted in the Key Resources Table.

Peptide library

A POWV peptide library was constructed based on amino acid (a.a.) sequences from POWV-LB polyprotein (Accession #: NP_620099.1). The library consists of 157 15-mer peptides, overlapping by 10 a.a. Together, it spans the nucleocapsid (Anc),

pre-membrane (prM), and envelope (E) portion of the polyprotein. Lyophilized peptides were reconstituted to 10 mg/mL in 90% DMSO and stored at −80°C. until use. Within this library, all peptides appeared soluble. For epitope identification, the peptides in the library were diluted such that the final concentration of each peptide was 2μM.

Peptide stimulation

Splenocytes were harvested from mice 7 DPI in the case of CD8+ epitope identification or 10 DPI in the case of CD4+ epitope identification for acute experiments or >30 days post infection for assessment of memory and vaccination responses. Spleens were processed to a single-cell suspension over a 40 μm cell strainer and suspended in RPMI supplemented with 5% FBS and 1% HEPES. 1×10^6 cells were plated per well in a round-bottom 96-well plate and stimulated for 6 hours at 37°C, 5% CO2 in the presence of 10 μg/mL brefeldin A and either α-CD3 (clone 2C11) as a positive control or 10 μg of peptide.

Flow cytometry

Following peptide stimulation, cells were washed with PBS and stained for surface markers using antibodies denoted in the key resources table. The cells were analyzed by flow cytometry using an Attune NxT.

Passive transfer of sera

Ten to 12-week-old B6 mice were infected via s.c. footpad injection with 102 FFU of POWV-Spooner or Rift Valley Fever virus vaccine strain MP-12 and allowed to develop a memory response. Mice were considered convalescent when they displayed: 1) survived >30 days post infection, 2) completely recovered weight loss, and 3) showed no apparent indicators of disease. >30 DPI, mice were terminally bled via cardiac puncture and whole blood was collected and subjected to centrifugation for 15 min at 12,000 × g. Sera was stored at −80°C until further use. Sera was diluted in sterile tissue-culture grade PBS and injected i.p. 24 hours before infection with POWV.

Adoptive transfer of T cells

Ten to 12-week-old B6 mice were infected via s.c. footpad injection with 102 FFU of POWV-Spooner, Rift Valley Fever Virus vaccine strain MP-12, or PBS as a negative control. >30 DPI, splenocytes were harvested and prepared for use in a Milteyni enrichment kit. T cells were purified to >90% purity using a Miltenyi negative selection kit (130-095-130) according to manufacturer's specifications. $\sim 1 \times 10^6$ cells were administered to B6 mice i.v. 24 hours prior to infection. Successful adoptive transfer of T cells into recipient mice was confirmed by submandibular bleed at 3 DPI and flow cytometric analysis using antibodies denoted in the key resources table. When CD45.1 congenic donors were used, α-CD45.1-FITC (clone A20) was also included in the panel.

Virus-like particle (VLP) preparation and vaccination

POWV genomic RNA was isolated from a purified virus stock using Trizol reagent (Invitrogen) according to manufacturer's protocol. POWV-LB nucleotides 361–2415 (Accession: NC_003687), encoding the transmembrane anchor and signal sequence of the C protein, prM, and E were reverse transcribed and PCR amplified using primers 5′-GATCGCGGCCGCACCATGCAGAGCCTTCACATGA GAGG-3′ and 5′-GATCGGAATTCCTATGCCCCAACTCCCATTGTCATC-3′ (restriction sites, NotI and EcoRI respectively in bold, POWV genomic sequence underlined). The amplified product was restriction digested and cloned into vector pLVX tight-puro (Takara) to create plasmid pLVX-POWVprME. To create a cell line for inducible expression of POWV VLPs, HEK293 cells (Microbix) were transfected with pLVX-Tet-On Advanced (Takara), which expresses the tetracycline-controlled transactivator. Stable transformants were selected with G418 and cloned by limiting dilution. POWV prME-expressing pseudotyped lentiviruses were then produced by co-transfection of pLVX-POWVprME with the lentiviral packaging vector pSPAX2 (psPAX2 was a gift from Didier Trono (Addgene plasmid # 12,260; RRID: Addgene_12260) and vesicular stomatitis virus G protein expression vector pMD2.G (also from Didier Trono (Addgene plasmid # 12259; RRID: Addgene_12259). The resulting pseudotyped lentiviruses were used to transduce the tet-transactivator expressing HEK293 cells. Transductants were selected with1 μg/mL puromycin. For VLP production, cells were cultured in DMEM (Corning) supplemented with 2% fetal bovine serum, penicillin and streptomycin and 1 μg/mL doxycycline. VLPs were purified and concentrated by collecting supernatants at 7 d post doxycycline addition, filtration through a 0.45 μm filter, and centrifugation at 150,000 × g for 2 hours through a 20% sorbitol cushion. Pellets containing VLP were resuspended in PBS at 1/100th original volume and analyzed by SDS-PAGE, followed by immunoblot and detection with a POWV E-specific antibody (Anti-Langat virus E, clone 10F6, BEI Resources). Preparations of VLP were quantified by comparing dilutions of VLP to known quantities of POWV expressed at FFU equivalents/μL, and total protein quantified by BCA assay.

Ten to 12-week-old B6 mice were vaccinated i.m. in the right quadricep with 2 μg of POWV-VLP adjuvanted with 300 μg of 2% aluminum hydroxide gel, Alhydrogel (InvivoGen, 21645-51-2) or 300 μg per mouse Alhydrogel alone, (denoted 'Alum' or 'Alum only'). Twenty-one days later, mice were boosted with an identical formulation of POWV-VLP or Alum.

Enzyme-linked immunosorbent assays (ELISAs)

For POWV-LB or POWV-Spooner ELISAs measuring binding to whole virions, Nuc MaxiSorp Plates (ThermoFisher, 460984) were coated with 75μL/well of virus stock diluted 1:30 in carbonate coating buffer (0.1 M Na2CO3, 0.1 M NaHCO3, pH 9.3) and stored at−20°C until further use. Following coating, plates were washed with four times with 200 μL/well of ELISA wash buffer (1XPBS,

0.5% Tween) and blocked with 250 μL/well of blocking buffer (PBS + 5%BSA + 0.5% Tween) at room temperature for 1 hour. Sera from POWV-challenged mice was diluted in blocking buffer starting at 1:50 with 4-fold serial dilutions. Plates were washed with ELISA wash buffer and 50 μL/well of sera was allowed to incubate for 1 hour at 37°C. Following incubation, plates were washed with ELISA wash buffer and 50μL/well of a 1:5000 dilution of secondary antibody was allowed to incubate for 2 hours at room temperature. Plates were washed with ELISA wash buffer and 100 μL/well of enhanced TBD substrate (Neogen 308176) was allowed to incubate for 10–15 minutes during development of color change. Finally, 50μL/well of 1 N HCl was used to quench the reaction and absorbance at 450 nm was read immediately using a BioTek Instruments Epoch plate reader.

Focus forming assay (FFA)

One day prior to the assay, tissue-culture treated 96-well plates (MidSci, TP92696) were seeded with 2 × 104 cells/well and allowed to grow at 37°C, 5% CO2 to a target confluency of ∼90%. Samples were serially diluted and added to BHK monolayers in 96-well plates for 1 h at 37°C to allow virus adsorption. Cells were overlaid with 2% methylcellulose mixed with DMEM containing 5% FBS, 1% HEPES and incubated for 24 hours at 37ºC. Media was removed and cell monolayers were fixed with 5% paraformaldehyde in 1X PBS for 15 min at room temperature, rinsed, and permeabilized in Perm Wash (PBS, 0.05% Triton-X). Infected cell foci were stained by incubating cells with sera from Swiss-Webster mice challenged with 103 FFU-equivalents of β-propiolactone (BPL, Sigma-Aldrich, P5648-5ML)-inactivated POWV-LB. Sera was diluted 1:5,000 in Perm Wash and 50 μL/well was allowed to incubate for overnight at 4°C and then washed three times with Perm Wash. Foci were detected with 50 μL/well of 1:5,000 dilution of horseradish peroxidase-conjugated goat anti-mouse IgG for 2 hours. After three washes with Perm Wash, staining was visualized by addition of 50 μL/well TrueBlue detection reagent (KPL). Infected foci were enumerated by CTL Elispot.

Focus reduction neutralization tests (FRNTs)

One day prior to the assay, tissue-culture treated 96-well plates (MidSci, TP92696) were seeded with 2 × 104 cells/well and allowed to grow at 37°C, 5% CO2 to a target confluency of ∼90%. Four-fold serial dilutions of sera of POWV-infected mice were mixed with 102 FFU of infectious virus, incubated at 37°C for 1 h, and added to BHK monolayers in 96-well plates for 1 h at 37°C to allow virus adsorption. Cells were overlaid with 2% methylcellulose mixed with DMEM containing 5% FBS, 1% HEPES and incubated for 24 hours at 37ºC. Media was removed and cell monolayers were fixed with 5% paraformaldehyde in 1X PBS for 15 min at room temperature, rinsed, and permeabilized in Perm Wash (PBS, 0.05% Triton-X). Infected cell foci were stained by incubating cells with sera from Swiss-Webster mice challenged with 103 FFU-equivalents of β-propiolactone (BPL, Sigma-Aldrich, P5648-5ML)-inactivated POWV-LB. Sera was diluted 1:5,000 in Perm Wash and 50 μL/well was allowed to incubate for overnight at 4°C and then washed three times with Perm Wash. Foci were detected with 50 μL/well of 1:5,000 dilution of horseradish peroxidase-conjugated goat anti-mouse IgG for 2 hours. After three washes with Perm Wash, staining was visualized by addition of 50 μL/well TrueBlue detection reagent (KPL). Infected foci were enumerated by CTL Elispot. FRNT curves were generated by log-transformation of the x axis followed by non-linear curve fit regression analysis using GraphPad Prism 9.

RMA-S stabilization assay

RMA-S cells were cultured in complete RPMI medium at 37 degrees Celsius, 5% CO2 until the night before the assay, when the cells were shifted to 29 degrees Celsius, 5% CO2. The cells were then incubated for 4 hours with decreasing concentrations of each peptide at 29 degrees Celsius, and then shifted back to 37 degrees Celsius, 5% CO2 for 1 hour. The cells were then washed with cold PBS and stained for Db (clone 28-14-8) MHC molecule at 4°C. Cells were washed with ice cold PBS and run on an Attune focusing flow cytometer. Fluorescence index was calculated by dividing the geometric mean fluorescence intensity (gMFI) of the peptide pulsed cells by non-peptide pulsed cells. Data is reported a percentage of the maximum fluorescence index of each peptide serial dilution.

QUANTIFICATION AND STATISTICAL ANALYSIS

All statistical analyses for were performed using GraphPad Prism 9 (version 9.1.2). Statistical differences in survival were determined using a Mantel-Cox test. Statistical significance in area under the curve for ELISAs was determined by Student's unpaired t-test. Data for epitope candidates is represented as mean ± SEM for two individual experiments. Statistical significance has been indicated within the figures with asterisks (*p = 0.05, **p = 0.01, ***p = 0.001, ****p < 0.0001).

AMERICAN SOCIETY FOR MICROBIOLOGY | Journal of Virology®

PATHOGENESIS AND IMMUNITY

Prior Heterologous Flavivirus Exposure Results in Reduced Pathogenesis in a Mouse Model of Zika Virus Infection

Mariah Hassert,[a] Tara L. Steffen,[a] Stephen Scroggins,[b,c] Abigail K. Coleman,[a] Enbal Shacham,[b] James D. Brien,[a] Amelia K. Pinto[a]

[a]Department of Molecular Microbiology and Immunology, School of Medicine, Saint Louis University, Saint Louis, Missouri, USA
[b]College for Public Health and Social Justice, Saint Louis University, Saint Louis, Missouri, USA
[c]Sinquefield Center for Applied Economic Research, Saint Louis, Missouri, USA

James D. Brien and Amelia K. Pinto are co-last authors.

ABSTRACT The 2015/2016 Zika virus epidemic in South and Central America left the scientific community urgently trying to understand the factors that contribute to Zika virus pathogenesis. Because multiple other flaviviruses are endemic in areas where Zika virus emerged, it is hypothesized that a key to understanding Zika virus disease severity is to study Zika virus infection in the context of prior flavivirus exposure. Human and animal studies have highlighted the idea that having been previously exposed to a different flavivirus may modulate the immune response to Zika virus. However, it is still unclear how prior flavivirus exposure impacts Zika viral burden and disease. In this murine study, we longitudinally examine multiple factors involved in Zika disease, linking viral burden with increased neurological disease severity, weight loss, and inflammation. We show that prior heterologous flavivirus exposure with dengue virus type 2 or 3 or the vaccine strain of yellow fever provides protection from mortality in a lethal Zika virus challenge. However, reduction in viral burden and Zika disease varies depending on the infecting primary flavivirus; with primary Zika virus infection being most protective from Zika virus challenge, followed by dengue virus 2, with yellow fever and dengue virus 3 protecting against mortality but showing more severe disease. This study demonstrates the variation in protective effects of prior flavivirus exposure on Zika virus pathogenesis and identifies distinct relationships between primary flavivirus infection and the potential for Zika virus disease.

IMPORTANCE The emergence and reemergence of various vector-borne diseases in recent years highlights the need to understand the mechanisms of protection for each pathogen. In this study, we investigated the impact of prior exposure to Zika virus, dengue virus serotypes 2 or 3, or the vaccine strain of yellow fever on pathogenesis and disease outcomes in a mouse model of Zika virus infection. We found that prior exposure to a heterologous flavivirus was protective from mortality, and to varying degrees, prior flavivirus exposure was protective against neurological disease, weight loss, and severe viral burden during a lethal Zika challenge. Using a longitudinal and cross-sectional study design, we were able to link multiple disease parameters, including viral burden, with neurological disease severity, weight loss, and inflammatory response in the context of flavivirus infection. This study demonstrates a measurable but varied impact of prior flavivirus exposure in modulating flavivirus pathophysiology. Given the cyclic nature of most flavivirus outbreaks, this work will contribute to the forecasting of disease severity for future outbreaks.

KEYWORDS flavivirus, Zika virus, dengue virus, yellow fever, cross-protection, vaccination, heterologous virus

Zika virus (ZIKV) made a devastating impact when it was introduced in the Americas in 2015 and was declared a public health emergency by the World Health Organization (WHO) (1). During this ZIKV epidemic, it was reported that nearly 800,000

Citation Hassert M, Steffen TL, Scroggins S, Coleman AK, Shacham E, Brien JD, Pinto AK. 2021. Prior heterologous flavivirus exposure results in reduced pathogenesis in a mouse model of Zika virus infection. J Virol 95:e00573-21. https://doi.org/10.1128/JVI.00573-21.

Editor Mark T. Heise, University of North Carolina at Chapel Hill

Address correspondence to James D. Brien, james.brien@health.slu.edu, or Amelia K. Pinto, amelia.pinto@health.slu.edu.

Received 1 April 2021
Accepted 27 April 2021
Accepted manuscript posted online 2 June 2021
Published 26 July 2021

people in the Americas had either suspected or confirmed cases of ZIKV infection (2). While the population in the Americas was naive to ZIKV, multiple flaviviruses including yellow fever virus (YFV) and the four serotypes of dengue virus (DENV1 to 4) are endemic to the area (3, 4). With the introduction of ZIKV into the flavivirus endemic areas of the Americas, the question of how and if prior flavivirus exposure could impact the course of disease with a subsequent flavivirus has become one of the most outstanding questions in flavivirus biology.

The *Flavivirus* genus consists of a number of related arthropod-borne viruses (arboviruses), which represent a substantial burden to global health and economic stability. Flaviviruses are small enveloped positive-stranded RNA viruses in the family *Flaviviridae*. Following entry into susceptible cells, viral replication occurs in the cytosol (5). The flavivirus genome is contained within a single open reading frame, which encodes a single polyprotein. The polyprotein is cleaved into 10 proteins: three structural proteins, the capsid (C), premembrane/membrane (prM/M), and envelope (E), as well as seven nonstructural proteins (6). As the structure and replication of flaviviruses are thought to be highly similar, our understanding of intra and extracellular pathways of flavivirus replication cycles comes from studies of multiple different flaviviruses (reviewed in references 5–8). Similarly, studies have long used existing knowledge of flavivirus structure to build and support the structural studies of emerging flaviviruses, including ZIKV (9–11). The high degree of relatedness between flaviviruses has provided a foundation for understanding emerging flaviviruses but has also confounded epidemiological studies and diagnostics, as the high degree of relatedness makes flaviviruses more difficult to serologically distinguish *in vivo*.

The high degree of genetic and structural similarities between flaviviruses (12) has led to the hypothesis that prior flavivirus exposure could afford some cross-protection against a novel circulating flaviviruses like ZIKV. The dengue literature provides some evidence for cross-protection, with a single DENV serotype showing short-term protection against infection with heterologous serotypes (13). Additionally, multiple studies have recently been published looking at the impact of prior dengue infection on the generation of adaptive immune responses to ZIKV, noting that cross-reactivity exists for both the T cells and antibody responses (reviewed in references 14–17). Based on longstanding literature with DENV (18), there is also substantial concern surrounding potential impact of a prior flavivirus exposure on enhancing disease severity of a subsequent ZIKV infection. There is a well-established link between prior DENV exposure and enhanced disease during infection with a heterologous DENV serotype (18). With the introduction of ZIKV into areas of South and Central America where DENV and YFV are endemic, there is a question regarding whether prior exposure to a heterologous flavivirus could enhance disease severity. However, what is missing from these studies, and field studies of ZIKV infection in the Americas, is the ability to systematically monitor infection and ZIKV disease course in the context of prior flavivirus infection. So, while epidemiological studies have provided excellent insight into potential correlations between prior heterologous flavivirus exposure and ZIKV pathogenesis, murine models of heterologous infection, where more invasive systematic studies can be completed, are important for testing potential correlations provided by field studies.

What we have learned from animal studies and clinical observations of flavivirus infection is that the high degree of similarity in flavivirus replication cycles, genetics, and structures does not necessarily translate into similarities in cell tropism, pathogenesis, disease course, and outcomes following infection. An example of this would be the comparison between YFV and ZIKV. ZIKV infection is primarily asymptomatic in adults and children and has shown significant tropism for the central nervous system (CNS); where YFV is primarily thought of as a hemorrhagic fever virus causing mild to severe disease in 45% of those infected and can have a mortality rate as high as 8% (WHO). So, while we have been able to use the strong structural studies of flaviviruses including DENV and YFV to make rapid advancements in our understanding of ZIKV

biology, we have had to rely more heavily on animal models to understand the implications for disease. This is especially true in addressing the question of how a prior flavivirus infection impacts the disease course of a subsequent flavivirus infection, where prior studies have relied heavily on the structural and immunological similarities between flaviviruses to predict disease outcomes.

Small animal models of infection have been critical for defining the correlates of protection and modeling disease for several flaviviruses, including DENV (19), YFV (20, 21), and ZIKV (22–24). In the case of ZIKV, the type 1 interferon receptor knockout mouse model (Ifnar1$^{-/-}$) has been used extensively for these purposes. A few studies in murine systems have demonstrated that prior infection with a mouse-adapted strain of DENV2 (strain D2S20) protects from a lethal ZIKV challenge (25) and to some degree is protective from fetal loss in maternal infection models (26). However, whether ZIKV cross-protection is similar, independent of prior flavivirus infection, is unclear. In addition, while murine models have shown that prior DENV2 infection prevents mortality, the impact of prior flavivirus exposure on pathogenesis and disease course still remains unclear, namely, the consequences for viral neuroinvasion and physical indicators of neurological disease.

To address the gaps in knowledge of heterologous flavivirus exposure, we have completed a comprehensive longitudinal cross-protection study, collecting multiparametric data to evaluate the impact of prior exposure to ZIKV, DENV2, DENV3, and the vaccine strain of YFV (YF-17D) on ZIKV neurological disease. With this study, we demonstrated that a sublethal heterologous flavivirus exposure confers varying degrees of protection from ZIKV mortality, weight loss, neurological disease, and excessive cytokine production in the CNS. Prior exposure to either ZIKV, DENV2, DENV3, or YF-17D significantly reduced viral burden in the spleen, liver, kidney, brain, and spinal cord of mice infected with ZIKV in comparison to a primary ZIKV infection. Importantly, there were significant differences in the degrees of protection afforded by heterologous flaviviruses, with prior exposure to either ZIKV or DENV2 being the most protective from ZIKV challenge. Exposure to YF-17D or DENV3 lessened mortality, disease severity, as well as duration of disease, though some animals still succumbed to infection. These data demonstrate that prior heterologous flavivirus exposure has a significant but varied effect on ZIKV replication and disease burden. The results of this study suggest that, along with cross-reactive immune responses, infection history can influence flavivirus disease course.

RESULTS

DENV, ZIKV, and YFV share a significant degree of geographic and genetic overlap. Many areas in South and Central America are considered endemic for circulation of flaviviruses including YFV and the four serotypes of DENV (WHO/Pan American Health Organization [PAHO]). ZIKV, DENV, YFV, and YF-17D vaccine coverage collected from case incidence data from the WHO/PAHO database for South and Central American countries from 2015 to 2019 (Fig. 1A) demonstrate the relative infection and vaccination rates for the flaviviruses during and following the ZIKV epidemic. Most people living in these regions had likely never been exposed to ZIKV prior to the 2015/2016 ZIKV outbreak (27), yet by 2019, ZIKV was endemic in most South and Central American countries. In 2017, as ZIKV infections continued to be documented, the northern region of Brazil was experiencing a surge of YFV cases, prompting a large vaccination campaign. Additionally, the reemergence and dramatic increase in DENV cases in South America over the last 50 years has resulted in many regions in South America being termed "dengue hyperendemic" (3). These most recent outbreaks are reflected in the WHO/PAHO data and demonstrate that the vast majority of South and Central American countries have reported the circulation of more than one of these flaviviruses over the past 5 years (Fig. 1B). The cyclic nature of the endemic flavivirus infections within this region suggests that even in years where disease incidence is relatively low, the prior flavivirus exposure rate within the population is relatively high (28, 29). Given the recent ZIKV outbreak and the high likelihood that ZIKV, or another flavivirus, will

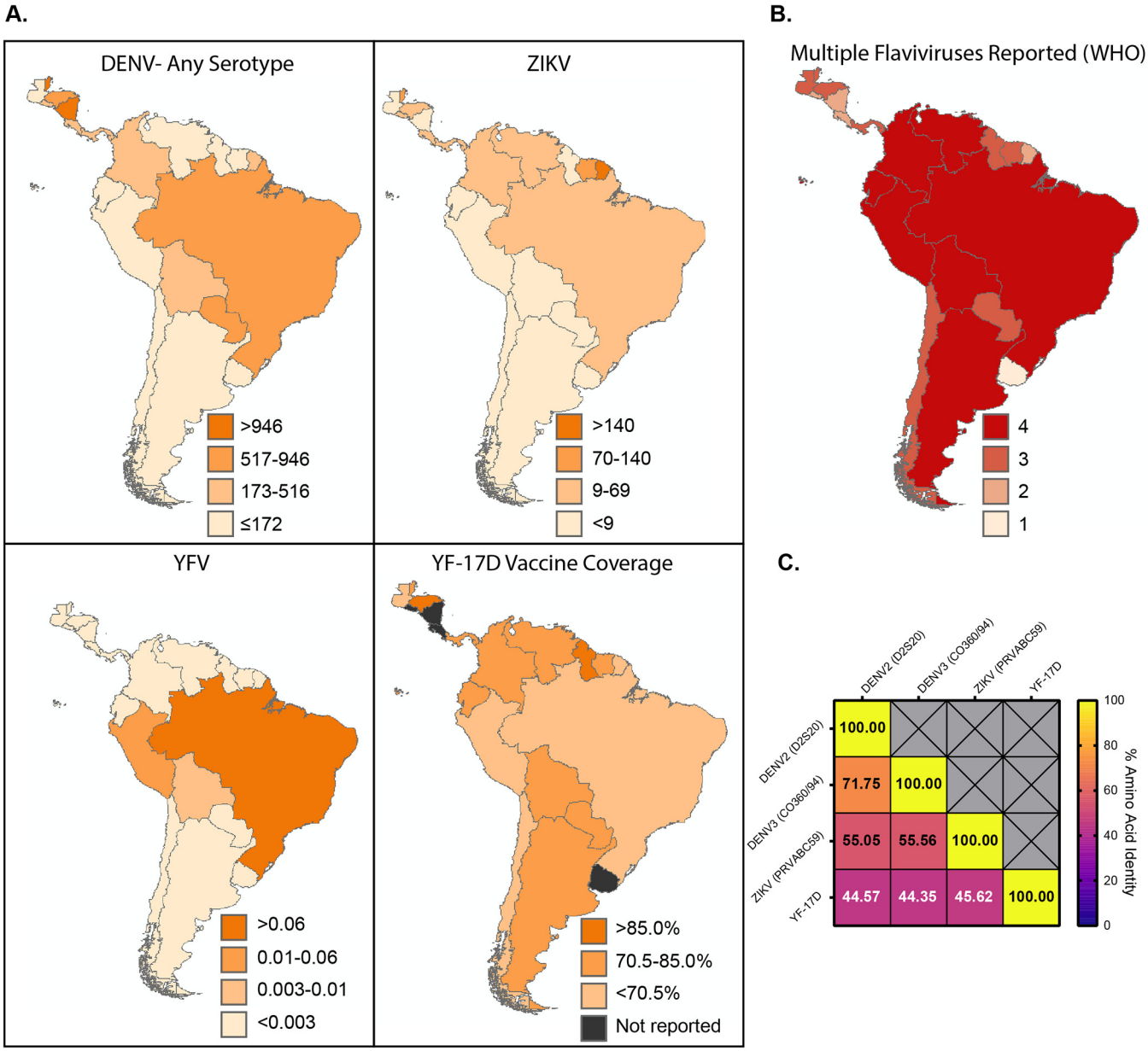

FIG 1 The flaviviruses contained within this study share a substantial degree of geographic and genetic overlap. (A) Average annual incidence rates per 100,000 people in South and Central American countries from 2015 to 2019. DENV, ZIKV, and YFV infections and YF-17D vaccine coverage were reported by the WHO/PAHO. Data is displayed as annual average incidence per 100,000 people in a given country for infections or percent reported vaccine coverage for YF-17D. (B) The number of each of the flaviviruses of interest reported in each country from 2015 to 2019 ranging from 1 to 4. (C) Amino acid identity of the full-length polyprotein of each virus used in the current study.

reemerge and cause disease, the question of how prior flavivirus exposure influences infection and disease of a subsequent flavivirus is crucial.

There are a significant number of genetic and antigenic similarities between ZIKV, the four serotypes of DENV, and YFV (12, 30). Comparison of the amino acid identity of the full-length polyproteins between ZIKV (strain PRVABC59), DENV2 (strain D2S20), DENV3 (strain CO360/94), and YFV (strain YF-17D) demonstrates between 44% to 71% identity between the viruses in various combinations (Fig. 1C). Based on epidemiological studies demonstrating the potential for immune mediated cross-protection (29, 31) as well as extensive genetic overlap (Fig. 1C) (32), we hypothesized in this study that exposure to DENV or YFV would confer some protection from ZIKV pathogenesis in a murine model.

Prior flavivirus exposure impacts ZIKV disease progression and mortality. To examine the cumulative effects of prior flavivirus exposure on protection from ZIKV through longitudinal study, sequential challenge experiments were performed in a mouse model of infection and pathogenesis (24, 33). Four- to five-week-old Ifnar1$^{-/-}$ female and male mice were vaccinated intravenously (i.v.) with 10^5 focus-forming units (FFU) of either DENV2 (mouse-adapted strain D2S20) or DENV3 (strain CO360/94). Eight-week-old Ifnar1$^{-/-}$ mice were vaccinated subcutaneously (s.c.) with 10^5 FFU of the vaccine strain of YFV (YF-17D). As positive and negative controls for this experiment, 8-week-old female and male Ifnar1$^{-/-}$ mice were vaccinated with 10^5 FFU of ZIKV (s.c.) or phosphate-buffered saline (PBS), respectively. Primary viral infection was confirmed by reverse transcriptase PCR (RT-PCR) from bleeds 3 days post primary infection (data not shown). All primary viral infections were given to mice at specific ages and at specific doses and routes of infection that were sufficient to result in infection but not mortality (19, 21–23). Approximately 30 days following primary infection, flavivirus-immune and -naive Ifnar1$^{-/-}$ mice were challenged with 10^5 FFU of ZIKV i.v. route. We have previously established that this, in a naive animal, is a lethal route of infection, resulting in 80 to 90% of mice succumbing to infection by day 14 (22, 23). During the i.v. ZIKV challenge, the mice were then monitored daily for 14 days for mortality and indicators of disease, such as weight loss and limb weakness or paralysis. At multiple time points following ZIKV infection (days 4, 7, 14, 30), blood was collected in a subset of mice via cheek bleed and analyzed for viral burden via reverse transcription-quantitative PCR (qRT-PCR) (Fig. 2A).

Consistent with previous literature (34), mice with prior ZIKV exposure (ZIKV $\times$ ZIKV) were completely protected from overt ZIKV-induced morbidity and mortality (Fig. 2B to D) compared to mice with no prior flavivirus exposure (flavi-naive $\times$ ZIKV) that lost a significant amount of weight (Fig. 2C) and all suffered from ZIKV-induced neurological indicators of disease, including flaccid tail, limb weakness, hind limb paralysis, or complete limb weakness or paralysis (Fig. 2D). Approximately 75% of mice challenged with ZIKV in the absence of prior flavivirus exposure eventually succumbed to infection, consistent with our previous reports (22, 23) (Fig. 2B).

Upon infection with ZIKV, mice with prior heterologous flavivirus exposure had significantly reduced mortality relative to flavivirus-naive mice infected with ZIKV. One hundred percent of mice with prior DENV2 exposure (DENV2 $\times$ ZIKV), 80% of mice with prior DENV3 exposure (DENV3 $\times$ ZIKV), and 80% of mice with YF-17D exposure (YF-17D $\times$ ZIKV) survived ZIKV challenge (Fig. 2B). As we had hypothesized, these data show that prior heterologous flavivirus exposure is protective from ZIKV-induced morbidity and mortality in the Ifnar1$^{-/-}$ mouse model. However, what was surprising was the varying degrees of cross-protection observed depending upon the primary infecting virus.

Comparison of the protection from morbidity afforded by prior sublethal ZIKV infection to that of prior heterologous flavivirus exposure revealed unexpected differences in protection between the flaviviruses (Fig. 2C and D). In the case of DENV2 exposure, these mice lost significantly less weight than the flavivirus-naive mice during ZIKV challenge (flavi-naive $\times$ ZIKV), and only on days 2 to 4 post ZIKV challenge did prior DENV2 exposure result in significant differences in weight loss between the mice that had received a prior DENV2 (DENV2 $\times$ ZIKV) infection and the mice that had previously seen ZIKV (ZIKV $\times$ ZIKV) (Fig. 2C). This mild evidence of disease in the DENV2-immune mice is also seen in the clinical scoring, where only 20% of the mice showed any signs of neurological impairment (Fig. 2D). However, in the case of prior DENV3 exposure (DENV3 $\times$ ZIKV), partial protection from ZIKV was conferred as indicated by only a mild reduction in weight loss relative to the flavi-naive $\times$ ZIKV group during ZIKV challenge (Fig. 2C). Conversely, comparison of the weight loss between ZIKV-immune and DENV3-immune mice showed a significant weight loss in the DENV3-immune mice starting day 4 post ZIKV infection and continuing until day 13, and all mice within this group displayed some signs of neurological involvement (Fig. 2D), suggesting that

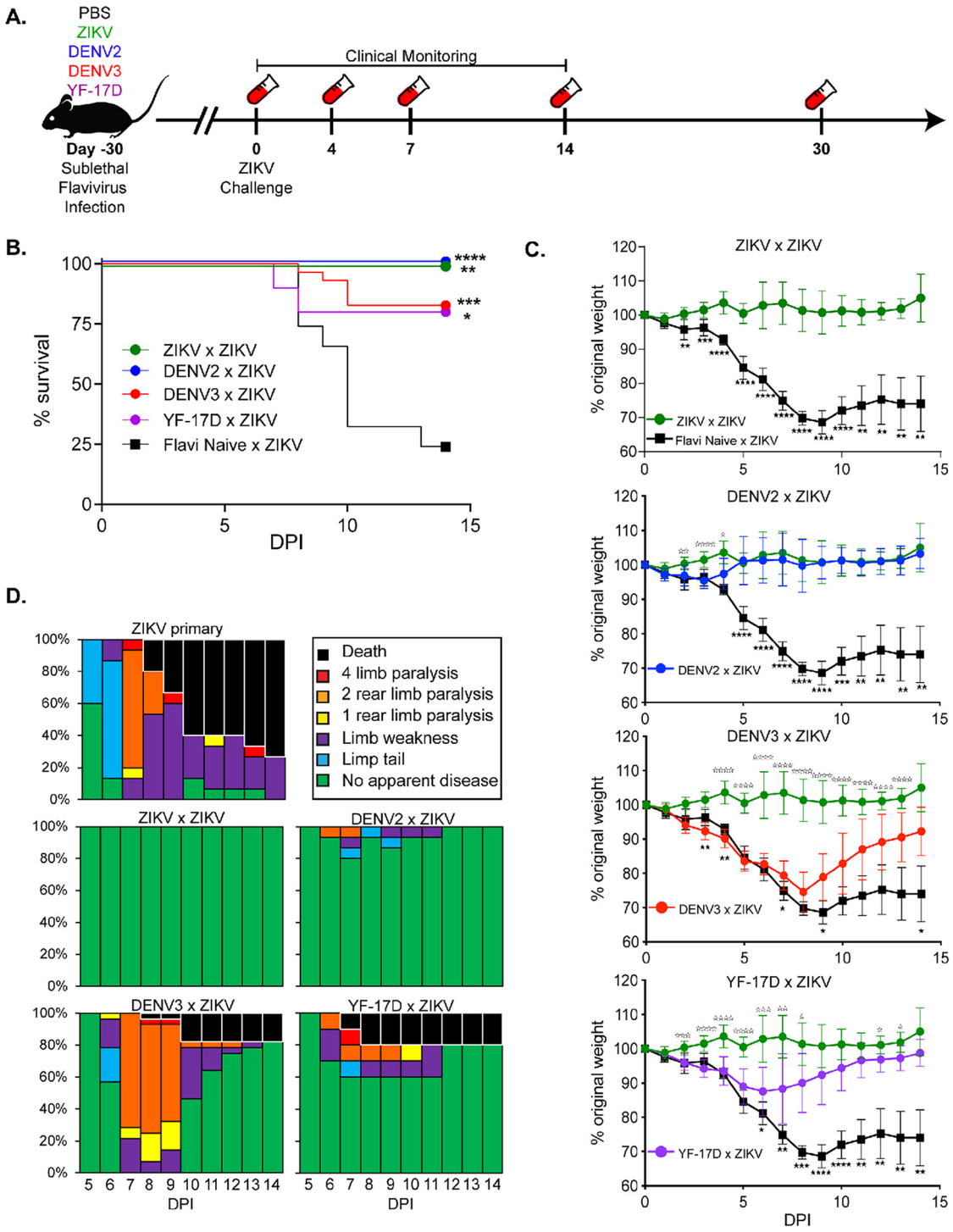

FIG 2 Prior flavivirus exposure leads to reduced disease severity and mortality during ZIKV challenge. (A) Experimental design. Ifnar1$^{-/-}$ mice were sublethally infected with either ZIKV ($n = 8$), DENV2 ($n = 15$), DENV3 ($n = 30$), YF-17D ($n = 10$), or PBS as a flavivirus-naive control ($n = 11$). Thirty days following primary infection, mice were challenged with ZIKV by i.v. administration. For 14 days following ZIKV challenge, mice were monitored for indicators of neurological disease as previously described (22, 23), weight loss, and mortality. At days 4, 7, 14, and 30 post ZIKV challenge, blood was collected to measure viremia by qRT-PCR. Data is a compilation of 4 independent experiments with at least 8 animals per group. (B) Survival of Ifnar1$^{-/-}$ mice with or without prior flavivirus exposure during i.v. ZIKV challenge. Statistically significant differences in survival rates were determined by Mantel-Cox test (*, $P = 0.03$; **, $P = 0.002$; ***, $P = 0.0002$; ****, $P < 0.0001$). (C) Weight loss during ZIKV challenge. As a measure of disease burden, mice were weighed daily for 14 days post ZIKV challenge. Weight change is displayed by normalizing relative to the starting weight of each animal on the day of ZIKV challenge. Statistical significance in weight loss over time was determined by two-way ANOVA with Dunnett's *post hoc* analysis (*, $P = 0.03$; **, $P = 0.002$; ***, $P = 0.0002$; ****, $P < 0.0001$). Closed stars represent statistical significance from flavi-naive × ZIKV, and open stars demonstrate statistical difference from ZIKV × ZIKV. (D) Neurological indicators of ZIKV disease. Mice were evaluated daily for sequela associated with ZIKV infection and graphed as a percentage of the total number of mice per group.

these mice were not as resistant to ZIKV-induced weight loss and disease. In examining the protection provided by prior exposure to YF-17D, we saw an intermediate phenotype between DENV2 and DENV3. All of the YF-17D mice lost some weight following ZIKV challenge, with the YF-17D-immune mice showing a significant difference in weight loss compared to the flavi-naive × ZIKV group beginning on day 6 and with a peak weight loss occurring between days 6 and 7 before the mice began to recover (Fig. 2C). Most YF-17D-immune mice did not completely recover to their original body weight by day 14 post ZIKV infection. The neurological disease score showed a similar trend, with 40% of the mice showing evidence of neurological disease (Fig. 2D). These results suggest that prior heterologous flavivirus infection can protect against mortality, and individual heterologous flaviviruses have distinct influences on the severity of morbidity associated with ZIKV.

ZIKV viremia over time but not ZIKV neutralization is differentially influenced by prior heterologous flavivirus exposure. Throughout the course of this longitudinal study (Fig. 2A), whole blood was collected at multiple time points post ZIKV exposure and analyzed by qRT-PCR to assess the impact of heterologous flavivirus exposure on ZIKV viremia over time. Consistent with our previous studies using this model (22, 23), during a primary ZIKV infection (flavi-naive × ZIKV), viral RNA is detectable in the blood by day 4 postinfection and trends in a downward trajectory over time; however, the virus is not cleared even by day 30 in these animals (Fig. 3). Sublethal vaccination with ZIKV prior to ZIKV challenge results in a substantial reduction in viremia (relative to mice with no prior flavivirus exposure) starting as early as 4 days postchallenge and continuing throughout the course of the experiment (Fig. 3A). This is consistent with previous reports demonstrating the protective capacity of ZIKV immunity upon challenge with ZIKV (34–36).

Similar to the influence of prior heterologous flavivirus infection on ZIKV neurological disease and weight loss, viremia was variable and dependent upon the virus that was given upon primary infection. In mice with prior DENV2 exposure, ZIKV viremia was statistically lower throughout the course of infection, with the exception of day 7, relative to mice with no prior flavivirus exposure and was not dramatically different from mice that had received a prior ZIKV infection (Fig. 3B). However, in mice with prior DENV3, only on days 4 and 30 was there a statistically significant reduction in ZIKV viremia relative to a primary infection (Fig. 3C). Comparison of ZIKV viremia from DENV3-immune mice to that of mice that had previously received ZIKV demonstrated significant differences at all time points tested. An intermediate phenotype was observed in the YF-17D-immune mice, where at early time points post ZIKV infection, viremia was significantly higher in the YF-17D-immune mice than in the ZIKV-immune mice, and by day 14 postinfection, viremia was lower in the YF-17D-immune mice than in the ZIKV-naive group. These results demonstrate that prior heterologous flavivirus exposure results in a significant reduction in detectable viral genome copies by day 30 post ZIKV infection.

In the context of a primary ZIKV infection, multiple murine studies have linked protection from disease and reduction in viral burden to a robust neutralizing antibody response (37, 38). Moreover, there have been numerous reports of flavivirus antibody cross-reactivity as measured by enzyme-linked immunosorbent assay (ELISA) in humans, nonhuman primates, and murine models of infection (37–42). One hypothesis would suggest that the observed cross-protection, in the form of reduction in viral burden, may be mediated by cross-neutralizing antibodies generated during the primary heterologous flavivirus exposure. To test this hypothesis, serum was collected from mice during heterologous ZIKV challenge at days 0, 4, 7, and 14 post-ZIKV challenge. The serum was used to evaluate the impact of prior heterologous flavivirus exposure on ZIKV neutralization potential of polyclonal serum samples during a secondary infection via focus reduction neutralization test (FRNT) (39). Using this technique, we determined the concentration of serum at which 50% of ZIKV particles were neutralized (NT_{50}) (Fig. 3E to H and Table 1). The inverse of this value was used to indicate serum neutralization potential, with greater values indicating greater neutralization.

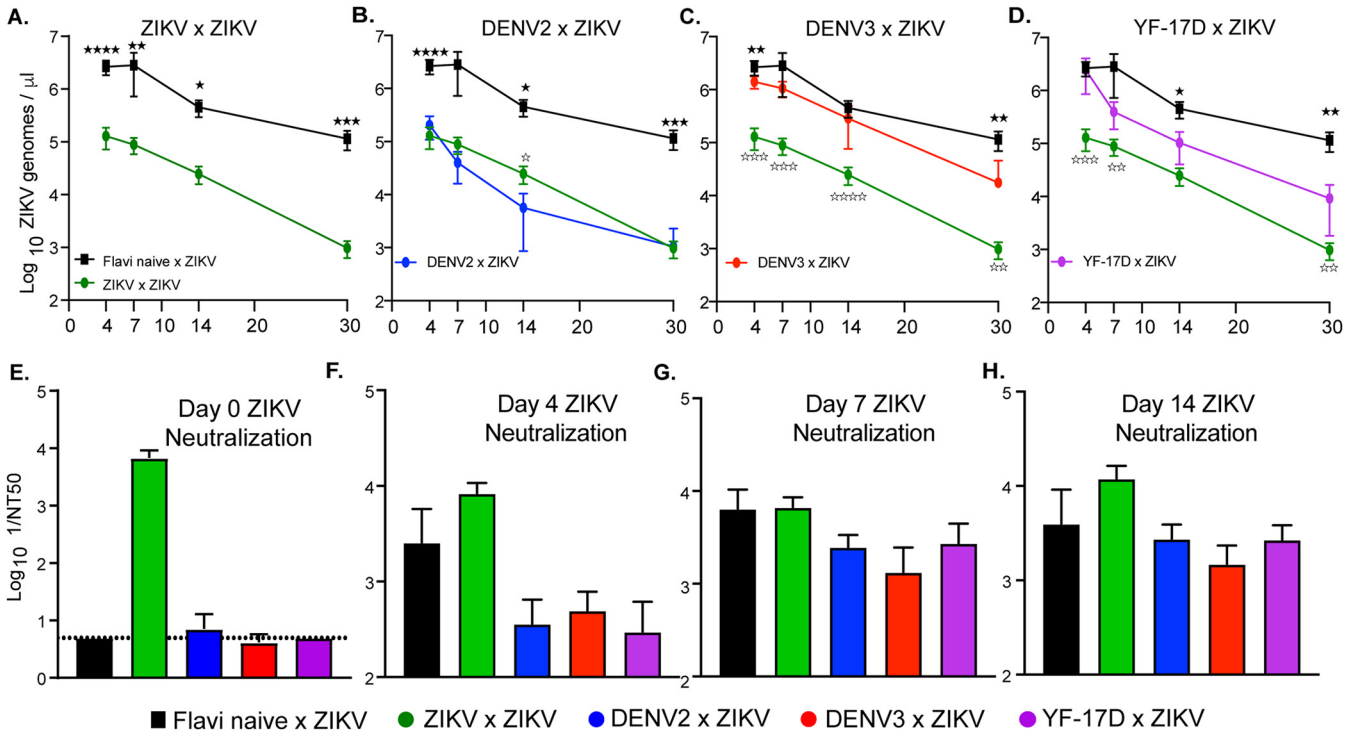

FIG 3 ZIKV viremia over time and ZIKV neutralization potential following heterologous challenge. Following ZIKV challenge, blood was collected via submandibular bleed on days 4, 7, 14, and 30 to evaluate viremia over time by qRT-PCR. (A) ZIKV viremia of homologously primed and boosted (ZIKV × ZIKV) mice compared to that of mice with no prior flavivirus exposure during ZIKV challenge. (B) ZIKV viremia of DENV2-immune mice during ZIKV challenge (DENV2 × ZIKV) compared to that of mice with no prior flavivirus exposure during ZIKV challenge. (C) ZIKV viremia of DENV3-immune mice during ZIKV challenge (DENV3 × ZIKV) compared to that of mice with no prior flavivirus exposure during ZIKV challenge. (D) ZIKV viremia of YF-17D-vaccinated mice during ZIKV challenge (YF-17D × ZIKV) compared to that of mice with no prior flavivirus exposure during ZIKV challenge. (E) At days 0 and 14 post ZIKV challenge, serum was collected and used in a ZIKV focus reduction neutralization test (FRNT) to measure the capacity of serum from each mouse to neutralize ZIKV. Neutralization was determined by enumerating a reduction in infectious particles with increased serum concentration and determining the NT_{50} or serum dilution at which 50% of infectious virus is neutralized. Neutralization potential over time is displayed as $1/NT_{50}$ in which higher values indicate more effective neutralization. Statistically significant differences in viremia over time were determined by two-way ANOVA with Dunnett's *post hoc* analysis (*, $P = 0.03$; **, $P = 0.002$; ***, $P = 0.0002$; ****, $P < 0.0001$) with closed stars representing a statistical significance from flavi-naive × ZIKV and open stars demonstrating a statistical difference from ZIKV × ZIKV. Differences in neutralizing antibody were determined by a Mann-Whitney test.

As expected, mice with no prior flavivirus exposure exhibited no neutralizing antibodies against ZIKV prior to challenge, mice with prior ZIKV exposure had high ZIKV-neutralizing antibody titers at the start of lethal ZIKV challenge, and over the course of ZIKV infection the mice that had received a prior ZIKV challenge maintained a significantly higher level of neutralization than the mice that had received a prior heterologous flavivirus infection (Fig. 3E to H and Table 1). Mice with prior exposure to DENV2, DENV3, or YF-17D began with little to no detectable neutralizing antibodies against ZIKV (Fig. 3E and Table 1). Interestingly, on days 4 and 7 postinfection, ZIKV-neutralizing antibody responses were not significantly higher and appeared to be slightly lower in the heterologous immune animals compared to those of naive animals challenged with ZIKV (Fig. 3F and G and Table 1). By day 14 following ZIKV infection, the ZIKV-neutralizing antibody response in these animals did not differ from animals in the flavi-naive × ZIKV group (Fig. 3H and Table 1). These data lead to the conclusion that within this model of heterologous infection, ZIKV cross-protection is not primarily mediated by cross-neutralizing antibodies. These findings, however, do not rule out any potential nonneutralizing antibody functions that could be mediating cross-protection, such as complement activation or antibody dependent cellular cytotoxicity (ADCC).

Global ZIKV viral burden is reduced with prior flavivirus exposure. While we observed a reduction in ZIKV viremia over time in mice that had been previously exposed to another flavivirus, it was unclear if heterologous flavivirus exposure could influence viral burden in tissues both within the peripheral organs and central nervous

TABLE 1 Statistical comparison between ZIKV serum neutralization capacity at days 0, 4, 7, and 14 post ZIKV challenge for each group[a]

ZIKV Serum Neutralization Day 0					
	Flavi Naïve x ZIKV	**ZIKV x ZIKV**	**DENV2 x ZIKV**	**DENV3 x ZIKV**	**YF17D x ZIKV**
Flavi Naïve x ZIKV		0.0016	ns	ns	ns
ZIKV x ZIKV	0.0121		0.004	0.002	0.002
DENV2 x ZIKV	ns	0.0025		ns	ns
DENV3 x ZIKV	ns	0.0001	ns		ns
YF17D x ZIKV	ns	0.0002	ns	0.0278	
ZIKV Serum Neutralization Day 4					
ZIKV Serum Neutralization Day 7					
	Flavi Naïve x ZIKV	**ZIKV x ZIKV**	**DENV2 x ZIKV**	**DENV3 x ZIKV**	**YF17D x ZIKV**
Flavi Naïve x ZIKV		ns	ns	ns	ns
ZIKV x ZIKV	ns		0.0242	0.0167	0.0041
DENV2 x ZIKV	ns	0.0238		ns	ns
DENV3 x ZIKV	ns	0.0121	0.0127		ns
YF17D x ZIKV	ns	0.167	ns	0.0401	
ZIKV Serum Neutralization Day 14					

[a]On each day, serum was collected and used in ZIKV FRNT. $1/NT_{50}$ values were compared between each group by Mann-Whitney test. Significant *P* values are indicated for comparison between the groups; ns is used to denote the comparison were the *P* value was above 0.05.

system (CNS). ZIKV invasion of the CNS appears to be a crucial factor in disease pathology within murine models of infection, as well as in human disease (23, 24, 34, 43), although the mechanism that drives this is not fully understood. To determine the impact of prior heterologous flavivirus exposure on the viral burden in various organs during ZIKV infection, we sublethally infected mice with either ZIKV, DENV2, DENV3, YF-17D, or a PBS control. Thirty days postinfection, the mice were challenged i.v. with ZIKV as described in Fig. 2A. At days 4 and 8 post ZIKV challenge, the spleen, liver, kidney, brain, and spinal cord were harvested and homogenized in complete Dulbecco modified Eagle medium (DMEM). A ZIKV focus forming assay (FFA) was completed on organ homogenates, and RNA was extracted from these homogenates to determine ZIKV viral burden by qRT-PCR (Fig. 4).

Similar to previous reports of primary ZIKV infection in the Ifnar1$^{-/-}$ model (23, 24, 33), day 4 is the peak in viral burden in most peripheral organs (Fig. 4A to C) while day 8 is the peak for viral burden in CNS tissues (Fig. 4D and E). By the time of peak neurological pathology in mice with no prior flavivirus exposure (days 8 and 9), the virus has invaded both the brain and spinal cord and replicated to high titers. As expected, mice with prior ZIKV exposure display significantly reduced viral burden in the spleen (Fig. 4A), liver (Fig. 4B), kidney (Fig. 4C), brain (Fig. 4D), and spinal cord (Fig. 4E) relative to flavi-naive $\times$ ZIKV mice on both days 4 and 8. However, we find it important to note that this significant reduction does not appear to be completely sterilizing, as viral genomes are still being detected on both days in all tissues. We have previously reported that ZIKV is a persistent infection in the Ifnar1$^{-/-}$ model (23), which could potentially be the reason for this observation.

In the case of mice with prior heterologous flavivirus exposure (DENV2, DENV3, or YF-17D), we saw a significant reduction in ZIKV viral burden in peripheral tissues on both days 4 and 8 relative to that of the flavi-naive $\times$ ZIKV group (Fig. 4A to C). The most drastic of these reductions came from mice with prior DENV2 exposure, which trends with the observation of reduced pathogenesis (Fig. 2 and Table 2). On day 4 postinfection, we observed a significant reduction in ZIKV viral load in the brains of all groups of mice with prior flavivirus exposure (Fig. 4D and Table 2). However, in the spinal cord, only heterologously challenged mice with prior DENV2 exposure had

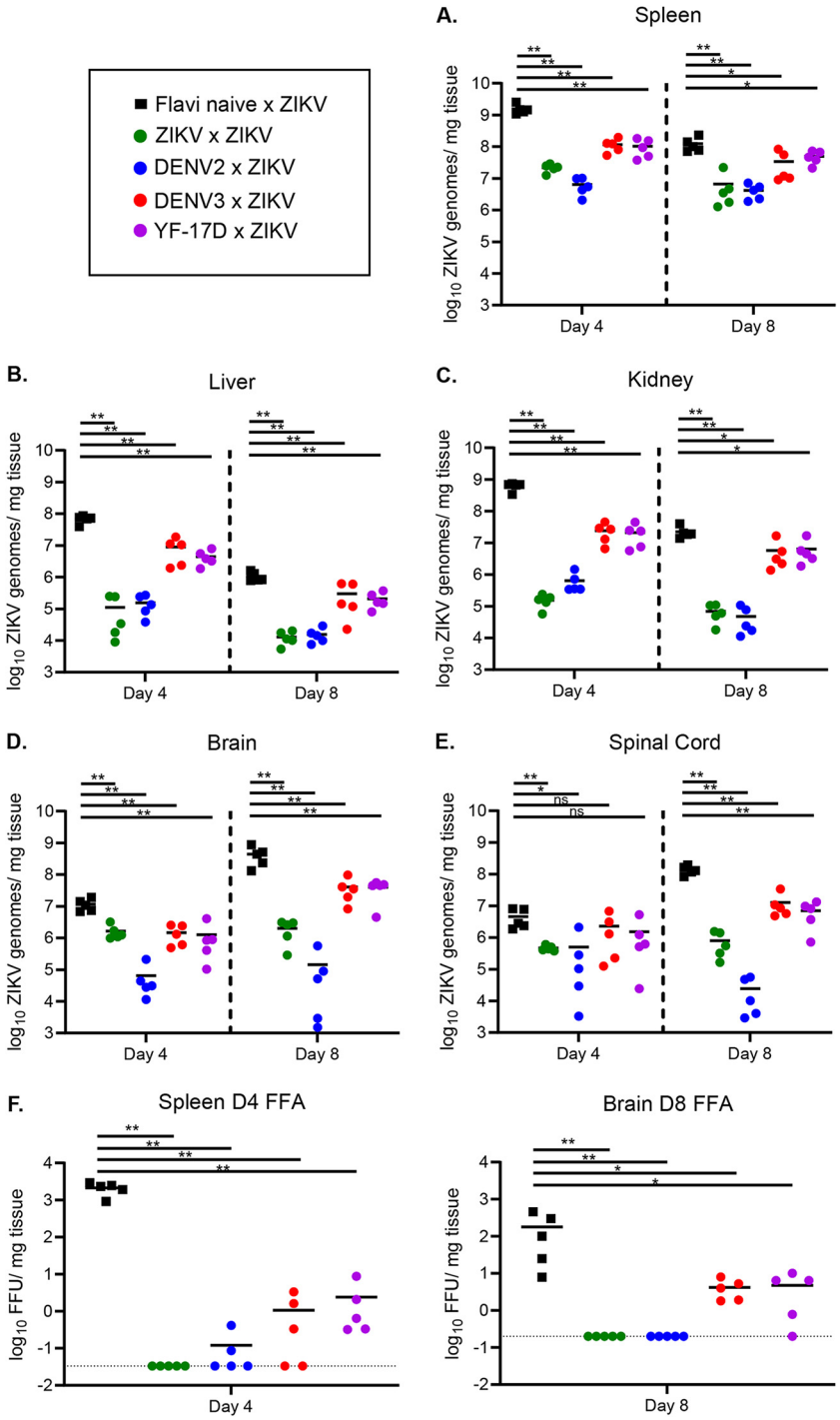

FIG 4 ZIKV viral burden in the peripheral organs and CNS is reduced with prior flavivirus exposure. Ifnar1$^{-/-}$ mice were sublethally infected with either ZIKV ($n = 10$), DENV2 ($n = 10$), DENV3 ($n = 10$), YF-17D ($n = 10$), or PBS as a flavivirus-naive control ($n = 10$). Thirty days following primary infection, mice were challenged with ZIKV by i.v. administration. At days 4 and 8 post ZIKV challenge ($n = 5$ mice per group per day), mice were euthanized, perfused with PBS, and organs were weighed and snap-frozen. RNA was extracted, and qRT-PCR was performed to measure viral burden in the spleen (A), liver (B), kidney (C), brain (D), and spinal cord (E). (F) Infectious virus was quantified in the spleen and brain homogenates of infected mice on days 4 and 8 post ZIKV challenge, respectively, via a standard FFA. Data are displayed as Log_{10} ZIKV genome copies per milligram of tissue. Statistical significance was determined by Mann-Whitney test (*, $P = 0.03$; **, $P = 0.002$; ***, $P = 0.0002$; ****, $P < 0.0001$).

TABLE 2 Statistical comparison between ZIKV titers measured by qRT-PCR in the spleens and brains at days 4 and 8 post ZIKV challenge[a]

Spleen Day 4					
	Flavi Naïve x ZIKV	**ZIKV x ZIKV**	**DENV2 x ZIKV**	**DENV3 x ZIKV**	**YF-17D x ZIKV**
Flavi Naïve x ZIKV		0.008	0.008	0.008	0.008
ZIKV x ZIKV	0.008		0.008	0.008	0.008
DENV2 x ZIKV	0.008	0.008		0.008	0.008
DENV3 x ZIKV	0.008	ns	0.008		ns
YF-17D x ZIKV	0.008	ns	0.016	ns	
Brain Day 4					
Spleen Day 8					
	Flavi Naïve x ZIKV	**ZIKV x ZIKV**	**DENV2 x ZIKV**	**DENV3 x ZIKV**	**YF-17D x ZIKV**
Flavi Naïve x ZIKV		0.008	0.008	0.032	0.016
ZIKV x ZIKV	0.008		0.024	ns	0.016
DENV2 x ZIKV	0.008	0.016		0.008	0.008
DENV3 x ZIKV	0.008	0.008	0.008		ns
YF-17D x ZIKV	0.008	0.008	0.008	ns	
Brain Day 8					

[a]Viral load was compared between each group by Mann-Whitney test. Significant *P* values are indicated for comparison between the groups; ns is used to denote the comparison were the *P* value was above 0.05.

statistically significantly reduced viral loads on day 4 (Fig. 4E). By day 8, the peak in disease burden and viral burden in the CNS, all groups of heterologously challenged mice displayed reduced viral load in both the brain and spinal cord (Fig. 4D and E and Table 2). As was seen in Fig. 2, the heterologously challenged mice displayed considerable variation in the control of ZIKV in the periphery and CNS, with the DENV2-immune mice controlling virus as well if not better than the ZIKV-immune mice, and the DENV3- and YF-17D-immune mice controlling virus slightly better than the flavi-naive $\times$ ZIKV challenge but significantly worse than the DENV2- or ZIKV-immune mice.

To confirm that the differences that we observed in viral burden via qRT-PCR translated to analogous differences in infectious virus, we performed focus forming assays (FFA) to measure infectious virus in the spleen and brain homogenates at the peak of viral replication in each tissue (day 4 and day 8, respectively) (Fig. 4F). Consistent with the qRT-PCR data, we found high levels of infectious virus in the flavivirus-naive $\times$ ZIKV group in both the spleen and brain on these days. Infectious virus was not detected above the limit of detection in the brain or spleen of mice from the ZIKV $\times$ ZIKV group. The level of viral replication was significantly reduced, though still detectable in most animals in the DENV3 $\times$ ZIKV and YF-17D $\times$ ZIKV groups in the spleen and brain. Infectious virus was not present above the limit of detection in the brains of the animals in the DENV2 $\times$ ZIKV group and only above the limit of detection in the spleens of 2 animals in this group. Collectively, this data demonstrates that prior heterologous flavivirus exposure impacts the outcome of ZIKV challenge by a global reduction in viral burden on days 4 and 8 postinfection.

During heterologous infection, mice display reduced expression of proinflammatory cytokines in the CNS relative to mice experiencing a primary infection. In murine and nonhuman primate models of ZIKV infection, immune cell infiltration in the CNS has been linked to neuronal damage and pathogenesis (44–46). In addition, studies evaluating differences in pathogenicity between different ZIKV lineages have linked expression of multiple cytokines and chemokines in the brain to more severe disease (47). To determine if this could be an underlying contributor to the altered pathogenesis that we observed during heterologous infection, we measured mRNA expression levels of various inflammatory cytokines in the brains of these mice at day 8 post ZIKV challenge (Fig. 5). This cytokine mRNA expression analysis was

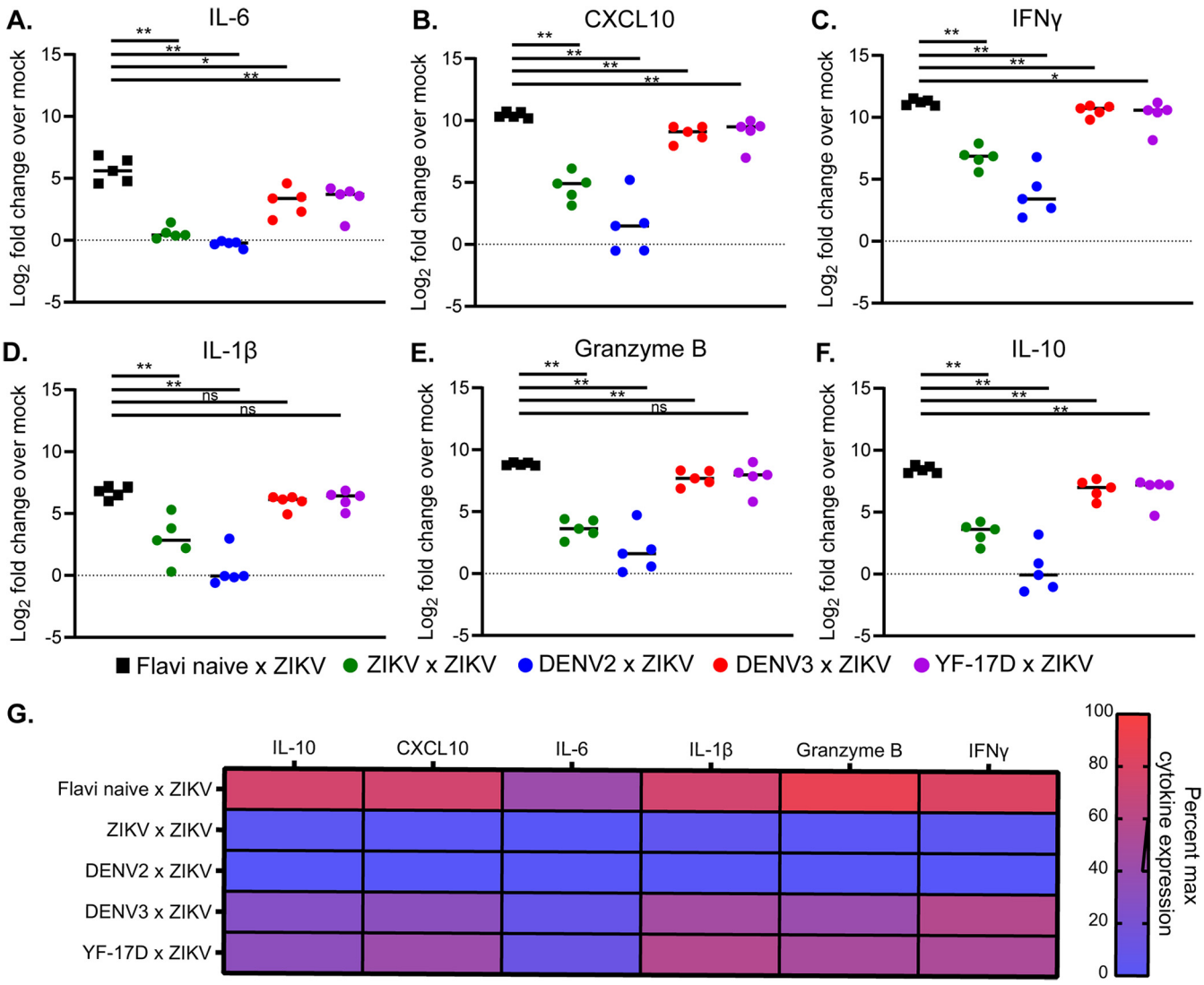

FIG 5 Cytokine expression profiles in the brain during heterologous infection. At day 8 post ZIKV challenge, RNA was isolated from the brains of infected mice or a naive control group ($n = 5$ per group) (the same mice that were used to determine viral burden in the CNS by qRT-PCR were used). qRT-PCR was performed to measure the mRNA expression levels of IL-6 (A), CXCL10 (B), IFN-γ (C), IL-1β (D), granzyme B (E), and IL-10 (F). Differences in mRNA expression levels were determined by $2^{-\Delta\Delta CT}$ analysis. Expression levels are displayed as Log_2 fold increases over expression of the cytokine in the brains of naive Ifnar1$^{-/-}$ mice. Statistical significance was determined by Mann-Whitney test (*, $P = 0.03$; **, $P = 0.002$; ***, $P = 0.0002$; ****, $P < 0.0001$). (G) Heat map displaying mean cytokine expression data for each group represented as a percent of the maximum expression level for a given cytokine.

done using the same RNA extracts that were used to quantify viral burden in the brain (Fig. 4D). Relative to expression levels in the brains of naive Ifnar1$^{-/-}$ mice, we observed an induction in mRNA expression of inflammatory cytokines, such as interleukin-6 (IL-6) (Fig. 5A), CXCL10 (Fig. 5B), and gamma interferon (IFN-γ) (Fig. 5C) in addition to the antiviral molecule IL-1β (48) (Fig. 5D), granzyme B (Fig. 5E), and IL-10 (Fig. 5F). Consistent with our observed pattern of pathogenesis in this heterologous infection system, each cytokine was induced to the greatest extent during primary ZIKV infection (flavi-naive $\times$ ZIKV) (Fig. 5G and Table 3), followed by mice with prior DENV3 or YF-17D exposure challenged with ZIKV (DENV3 $\times$ ZIKV or YF-17D $\times$ ZIKV), and only minimal cytokine induction was observed in mice with prior ZIKV exposure or DENV2 exposure (ZIKV $\times$ ZIKV or DENV2 $\times$ ZIKV). Overall, this finding is consistent with the literature linking inflammation in the CNS with pathogenesis during primary ZIKV infection and demonstrates that enhanced pathogenesis in murine models of heterologous ZIKV infection is linked with levels of inflammatory cytokines in the CNS.

TABLE 3 Statistical comparison of IL-1β and IL-6 cytokine production between infected groups of mice as measured by qRT-PCR and $\Delta\Delta CT$ analysis in the brains at day 8 post ZIKV challenge[a]

IL-1β					
	Flavi Naïve x ZIKV	ZIKV x ZIKV	DENV2 x ZIKV	DENV3 x ZIKV	YF-17D x ZIKV
Flavi Naïve x ZIKV		0.008	0.008	ns	ns
ZIKV x ZIKV	0.008		ns	0.016	0.016
DENV2 x ZIKV	0.008	0.008		0.008	0.008
DENV3 x ZIKV	0.016	0.008	0.008		ns
YF-17D x ZIKV	0.008	0.016	0.008	ns	
IL-6					

[a]Cytokine load was compared between each group by Mann-Whitney test. Significant *P* values are indicated for comparison between the groups; ns is used to denote the comparison were the *P* value was above 0.05.

Defining the relationships of multiple disease metrics during heterologous ZIKV challenge. Disease metrics assessed during ZIKV infection in mouse models are diverse. Studies using these models (including our own) have quantified disease using noninvasive techniques, such as weight loss, neurological disease assessment, mortality, viremia, and viral shedding in the urine, as well as more invasive techniques, such as viral burden in multiple target organs, fetal resorption and loss, and neuroinvasion, inflammation, and apoptosis histologically (22–24, 26, 33, 43, 49–52). However, it is unclear how each disease parameter in this complex system is related to the others and whether this is influenced by prior heterologous flavivirus exposure. Therefore, we generated a data bank using longitudinal data points from variables measured in Fig. 2 and 3 from each individual mouse. We used these data to determine correlative relationships between various metrics of disease, including peak percent weight loss, day of peak weight loss, peak disease score, day of peak disease, number of days of disease, and viremia on days 4, 7, 14, and 30 post ZIKV infection by linear regression and Pearson correlation (Fig. 6A to F and Table 4). The peak weight loss percentage was determined by normalizing the starting weights of each animal at day 0 to 100% and assessing weight daily and noting the peak percentage of weight lost through the course of infection. The peak disease score was determined by tracking neurological indicators as previously described daily following ZIKV infection (22, 23). Each indicator of disease was assigned a number from 0 to 6, indicative of severity (0 = no disease, 1 = limp tail, 2 = hind limb weakness, 3 = single hind limb paralysis, 4 = bilateral hind limb paralysis, 5 = full body weakness/paralysis, and 6 = death). The peak day of disease corresponded to the day of peak neurological disease based on this scoring system. The number of disease days was determined by counting each day for each mouse that the disease score was above 0 and ending at the time of death if applicable.

Of the 36 bivariate permutations, we identified 25 statistically significant correlative interactions. The strength and directionality of each correlation are indicated by the Pearson coefficient (*r*), and the statistical significance of each correlation is indicated by the *P* value (Table 4). From these data, we identified several interactions of particular interest (Fig. 6A to F). The strongest correlation resulted when comparing the peak neurological disease score from each mouse to the peak percent weight lost ($r = 0.8973$; $P < 0.0001$) (Fig. 6A). As one might expect, as the peak neurological disease score identified in each animal increased, so did the amount of weight lost. Importantly, each infection group (flavi-naive × ZIKV, DENV2 × ZIKV, DENV3 × ZIKV, YF-17D × ZIKV, and ZIKV × ZIKV) generally clustered together and along the pattern determined by linear regression. This would suggest similarities in the biological characteristics of these groups. We were also interested in the relationship between the number of days each infected animal displayed a neurological disease phenotype and the severity of the disease phenotype (Fig. 6B). We found that the peak disease score and the number of measured disease days strongly positively correlated with one

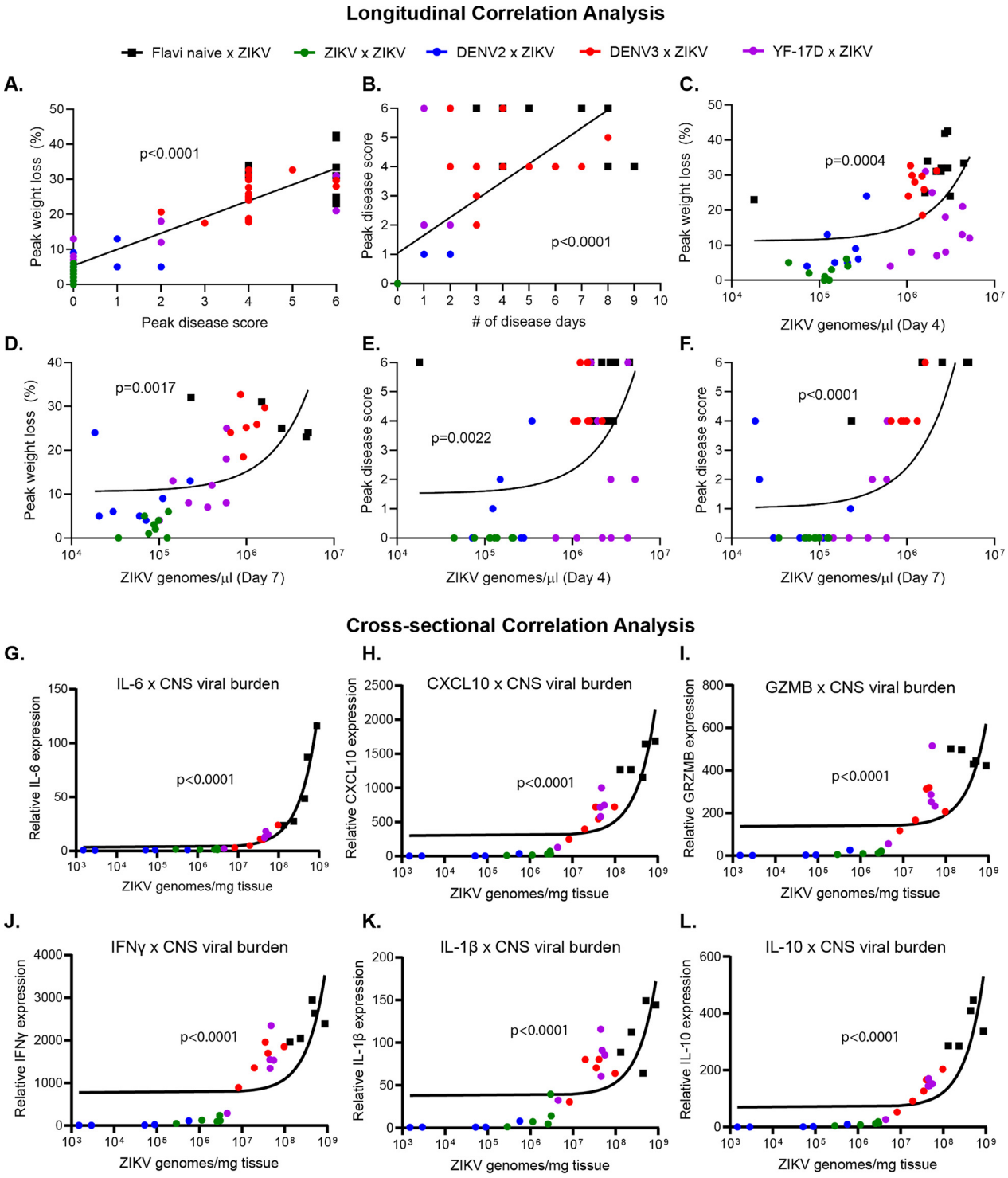

FIG 6 Multiple metrics of ZIKV infection and disease burden are correlated. The data collected from Fig. 2 and 3 were used to generate a data bank and analyzed using linear regression and Pearson correlation analysis to define the relationships of multiple disease metrics during heterologous ZIKV challenge. (A) Linear regression and correlation between the peak weight loss of each animal and peak in disease score. Mice were weighed daily and observed for clinical signs of disease. Each phenotype was assigned a number from 0 to 6 (0 = no disease, 1 = limp tail, 2 = hind limb weakness, 3 = single hind limb paralysis, 4 = bilateral hind limb paralysis, 5= full body weakness/paralysis, and 6 = death). (B) Linear regression and correlation between peak disease score and the number of days a given animal experienced clinical signs of neurological disease. (C) Linear regression and correlation between ZIKV genomes detected in the blood by qRT-PCR on day 4 post ZIKV infection and peak weight loss. (D) Linear regression and correlation between ZIKV genomes detected in the blood by qRT-PCR on day 7 post ZIKV infection and peak weight loss. (E) Linear regression and correlation between ZIKV genomes detected in the blood by qRT-PCR on day 4 post ZIKV infection and peak disease score. (F) Linear regression and correlation between ZIKV genomes detected in the blood by qRT-PCR on day 7 post ZIKV infection and peak disease score. (G–L) The correlative relationship between viral burden in the brain (as measured by qRT-PCR on day 8 postinfection) and inflammatory cytokine expression (as measured by qRT-PCR on day 8 postinfection) in the brain by linear regression and Pearson analysis. IL-6 expression (G), CXCL10 expression (H), granzyme b expression (I), IFN-γ expression (J), IL-1β expression (K), and IL-10 expression (L).

TABLE 4 Correlation matrix defining the relationship between multiple disease metrics in a longitudinal heterologous infection study[a]

p value									
	Peak weight loss %	**Peak weight loss day**	**Peak disease score**	**Peak disease day**	**# of disease days**	**Viremia D4**	**Viremia D7**	**Viremia D14**	**Viremia D30**
Peak weight loss %		<0.0001	<0.0001	0.02	<0.0001	0.00	0.00	0.00	0.00
Peak weight loss day	0.51		0.00	0.00	<0.0001	ns	ns	0.00	ns
Peak disease score	0.90	0.38		ns	<0.0001	0.00	<0.0001	0.00	0.01
Peak disease day	0.39	0.46	0.31		ns	0.05	ns	ns	ns
# of disease days	0.86	0.52	0.72	0.23		0.04	0.04	0.00	0.00
Viremia D4	0.51	0.20	0.45	0.39	0.31		ns	0.02	ns
Viremia D7	0.52	0.15	0.72	0.21	0.35	0.20		<0.0001	ns
Viremia D14	0.53	0.46	0.43	0.02	0.43	0.40	0.65		0.01
Viremia D30	0.61	0.20	0.52	-0.12	0.66	0.40	0.19	0.55	
Pearson Coefficient (r)									

[a]The data collected from Fig. 2 and 3 were used to generate a data bank and analyzed using linear regression and Pearson correlation analysis to define the relationships of the coefficient (*r*) (lower left) demonstrating the strength and directionality of the correlation between each variable and the *P* value (upper right) demonstrating the statistical significance of each correlation.

another ($r = 0.7234$; $P < 0.0001$); that is, in general, the more severe the disease phenotype, the longer it would take to resolve.

We were particularly interested in the relationship between viremia and less invasive metrics of disease burden, such as weight loss and disease score. When comparing viral burden on day 4 or day 7 to peak percentage of weight loss (Fig. 6C and D, respectively), we found a statistically significant positive correlation ($r = 0.5078$ and 0.5184 and $P = 0.0004$ and 0.0017, respectively). This was also true when comparing viral burden on day 4 or day 7 to peak disease score (Fig. 6E and F) ($r = 0.45$ and 0.7213 and $P = 0.022$ and <0.0001, respectively). That is, with increased viremia on these days came increased weight loss and neurological disease throughout the course of infection. The correlative analyses associating disease severity and viral load at day 4 are of particular interest due to the timing. As demonstrated in Fig. 2, neurological indicators of disease are not overtly detectable until day 5 postinfection and typically do not peak until days 7 to 9 (Fig. 2D), and the most significant drop in weight also occurs from days 7 to 9 (Fig. 2C). However, using the disease metric of early viremia on day 4, it is clear that information could be used in linear regression analysis to predict the severity and outcome of infection days earlier than the occurrence of overt disease (Fig. 6C and 6E).

Finally, in order to understand the relationship between viral burden and inflammation as a metric of disease in the context of heterologous infection, we compared the viral burden in the brain at day 8 post ZIKV challenge (Fig. 4D) and cytokine expression levels in the brain at day 8 post ZIKV challenge in the same animals (Fig. 5). We used these data to determine correlative relationships between CNS viral load and cytokine expression during ZIKV challenge by linear regression and Pearson correlation analysis (Fig. 6G to L and Table 5). For each cytokine that was analyzed (IL-6, CXCL10, granzyme B, IFN-γ, IL-1β, and IL-10), we observed a pronounced and statistically significant positive correlation between its expression level and viral burden in the CNS ($r = 0.9808$, 0.9815, 0.9231, 0.9585, 0.9123, and 0.9862, respectively) (Fig. 6G to L). The strength of the correlation of viral burden and cytokine expression in the CNS during ZIKV infection is consistent with previous studies that have linked ZIKV-induced disease to enhanced expression of proinflammatory cytokines in the CNS (Table 5) (47). Overall, these data demonstrate the bivariate interactions between

TABLE 5 The correlative relationship between viral burden in the brain and inflammatory cytokine expression[a]

p value							
	Brain Virus D8	**IL-6**	**CXCL10**	**Granzyme B**	**IFNγ**	**IL1-β**	**IL-10**
Brain Virus D8		>0.0001	>0.0001	>0.0001	>0.0001	>0.0001	>0.0001
IL-6	0.98		>0.0001	>0.0001	>0.0001	>0.0001	>0.0001
CXCL10	0.98	0.97		>0.0001	>0.0001	>0.0001	>0.0001
Granzyme B	0.92	0.90	0.95		>0.0001	>0.0001	>0.0001
IFNγ	0.96	0.95	0.97	0.96		>0.0001	>0.0001
IL1-β	0.91	0.90	0.94	0.92	0.92		>0.0001
IL-10	0.99	0.97	0.97	0.92	0.95	0.89	
Pearson Coefficient (r)							

[a]Both cytokine expression and viral burden were measured by qRT-PCR on day 8 postinfection in the brains of the infected animals. Linear regression and Pearson correlation analysis were used to define the relationships of the coefficient (*r*) (lower left) demonstrating the strength and directionality of the correlation between each variable and the *P* value (upper right) demonstrating the statistical significance of each correlation.

various metrics that are commonly used to assess ZIKV disease burden in mouse models of infection and importantly show that, in the context of heterologous infection, these correlations are still appropriate and comparable.

DISCUSSION

Increased globalization, deforestation, climate change, and the lack of effective vaccines has resulted in most of the world's population being at risk for infection with multiple flaviviruses (53). There is no vaccine available for ZIKV, and current vaccines for flaviviruses including the yellow fever vaccine, while highly effective, have not prevented outbreaks from these highly prevalent arboviruses. While the current number of ZIKV cases in the Americas has dropped significantly compared to that in 2016, based on the infection cycles of similar flaviviruses, it is believed that ZIKV will follow a similar cyclical pattern of emergence and reemergence (54, 55). Therefore, it is highly likely that ZIKV is in an interepidemic period and will reemerge and continue to spread throughout the Americas as has been seen with both DENV1 to 4 and YFV.

The influence of prior flavivirus exposure on ZIKV protection and pathogenesis remains an important question. Epidemiological studies do provide some insight into these competing concerns. A study in Brazil comparing YFV vaccination coverage with incidence rates of ZIKV-associated microcephaly found that Northeast Brazil, which had the highest incidence of ZIKV-associated microcephaly, also had relatively low YFV vaccination rates, suggesting that a lack of YFV vaccination left that population without a cross-protective response and, therefore, they were more susceptible to ZIKV morbidity (31). Moreover, the Harris group has examined the relationship between prior DENV exposure and the incidence of asymptomatic ZIKV infection in a pediatric cohort in Nicaragua, finding that children with prior DENV infection had lower rates of symptomatic ZIKV infection, again suggesting ZIKV cross-protection was mediated by previous DENV exposure (29). However, drawing clear causal links between previous exposure and infection outcomes are a challenge in human populations for several reasons in this case. These cocirculating flaviviruses share antigenic similarities, which can confound many serologically based diagnostic tests, which makes confirming records of the natural history of infection particularly challenging. Additionally, the length of time between exposures of heterologous serotypes of DENV plays a major role in whether increased incidence of enhanced pathogenesis or cross-protection occurs (18, 56, 57).

In this study, we challenged the hypothesis that prior heterologous flavivirus exposure to DENV serotypes 2 or 3 or YF-17D would confer equal cross-protection from ZIKV in a mouse model. We ultimately showed that a sublethal heterologous flavivirus exposure confers varying degrees of protection from ZIKV mortality, weight loss, and neurological disease. Prior exposure to ZIKV or DENV2 was the most protective from ZIKV challenge, with no mice succumbing to infection and few, if any, displaying any signs of neurological disease and weight loss (Fig. 2). Exposure to YF-17D or DENV3 lessened mortality, disease severity, and viral burden, though some animals still

succumbed to infection. Importantly, prior exposure to either ZIKV, DENV2, DENV3, or YF-17D significantly reduced viral burden in the spleen, liver, kidney, brain, and spinal cord of mice infected with ZIKV (Fig. 4). These data demonstrate a cross-protective effect of prior flavivirus exposure on ZIKV replication and disease burden.

When analyzing ZIKV neutralization potential of polyclonal serum samples from mice with prior flavivirus exposure during ZIKV infection, we found that prior exposure to ZIKV resulted in high levels of circulating neutralizing antibodies that persisted during ZIKV challenge (Fig. 3E and F). However, mice with prior heterologous flavivirus exposure did not have detectable neutralizing antibodies to ZIKV prior to ZIKV challenge. This demonstrates that the mechanism of this observed cross-protection is not likely mediated by ZIKV cross-neutralizing antibodies. However, these studies are limited in that they did not address the potential for other mechanisms of cross-protection, including nonneutralizing antibody functions (58) or the presence of cross-reactive T cells (25, 59).

Murine studies have linked inflammation in the brain to increased ZIKV pathogenesis (47). We found that prior heterologous flavivirus exposure conferred varying degrees of cross-protection from ZIKV pathogenesis that was dependent upon the identity of the primary infecting virus. Based on the established link between inflammation and ZIKV pathogenesis in a primary ZIKV infection, we hypothesized that the different levels of pathogenesis that we observed in this system would associate with the induction of cytokine expression in the brains of these mice. We found that in groups that displayed elevated pathogenesis (DENV3 $\times$ ZIKV or YF-17D $\times$ ZIKV), there were higher levels of inflammatory transcripts in the brain relative to those of groups that displayed minimal pathogenesis (ZIKV $\times$ ZIKV or DENV2 $\times$ ZIKV) (Fig. 5). Importantly, we found that the level of inflammatory cytokine induction strongly correlated with viral burden in the CNS of these animals (Fig. 6G to L), which demonstrates that, even in the added context of heterologous infection, the established correlation between ZIKV-induced disease and inflammatory cytokine expression is appropriate and comparable to a primary ZIKV infection. These findings provide insight into the cause of the variable degrees of ZIKV cross-protection observed.

Murine models of ZIKV infection and heterologous flavivirus challenge have used diverse metrics for quantifying disease burden (22–24, 26, 33, 43, 49–52). Until now, the relationship of many of these variables has not been evaluated. In this longitudinal heterologous challenge experiment, we performed linear regression and correlation analysis to determine the relationship between multiple variables in individual mice, including peak weight loss, day of peak weight loss, peak disease score, day of peak disease score, number of disease days, and viremia on days 4, 7, 14, and 30. Within this longitudinal analysis, we identified 25 statistically significant correlative interactions (Table 4). Importantly, we found that viral burden on day 4 strongly correlated with the peak weight loss and peak disease score that an animal would eventually experience (typically on days 7 to 9 postinfection) (Fig. 6C and E). This allows for the possibility of using early viremia data as a predictor of severe disease outcomes using linear regression analysis that can also be applied in the context of heterologous infection scenarios.

Ultimately, these data provide additional evidence of the cross-protective effect of prior heterologous flavivirus exposure on ZIKV disease. These findings are important given that the majority of the world is at risk of flavivirus exposure and multiple flaviviruses are endemic in many regions. Addressing this is not only important for being able to predict the outcome of ZIKV exposure in areas of flavivirus endemicity but will support efforts to generate a pan-flavivirus vaccine. While this study provides significant insight into cross-protection from ZIKV, additional studies are desperately needed to understand the mechanism behind this. Studies such as these will be essential to control these significant public health threats.

MATERIALS AND METHODS

Ethics statement. All animal studies were done in accordance with the Guide for Care and Use of Laboratory Animals of the National Institutes of Health and approved by the Saint Louis University Animal Care and Use Committee (IACUC protocol number 2667).

Viruses and cells. P_0 stocks of ZIKV strain PRVABC59 (GenBank accession number KU501215.1) and YFV strain 17D (GenBank accession number X03700) were acquired from Biodefense and Emerging Infection (BEI) Resources. Each virus was passaged in African green monkey kidney epithelial cells (Vero-WHO) that were purchased from the American Type Culture Collection (ATCC CCL-81). The supernatants of these cultures were clarified of cellular debris by centrifugation at 3,500 rpm prior to being aliquoted and frozen at −80°C. DENV2 strain D2S20 (GenBank accession number HQ891024) was a kind gift from Michael Diamond (60). DENV3 strain C0360/94 (GenBank accession number AY923865) was obtained from ATCC. Both DENV2 and DENV3 were grown in C6/36 *Aedes albopictus* cells (ATCC CRL-1660). At the time of harvest, the medium supernatant was clarified of cellular debris by centrifugation at 3,500 rpm. Each virus was then concentrated by ultracentrifugation at 30,000 rpm over a 25% glycerol cushion before being aliquoted and frozen at −80°C (19). The infectious titer of each viral stock was quantified by focus forming assay (FFA) as previously described (49). Briefly, a 90% confluent monolayer or Vero-WHO cells was plated in a 96-well flat-bottom plate. Serial dilutions of each viral stock were added to each well for 1 h, prior to the addition of a methyl cellulose layer, to restrict lateral spread of the virus. After 48 h (ZIKV and YF-17D) or 72 h (DENV2 and DENV3), the cells were fixed and permeabilized. The cells were incubated with a flavivirus cross-reactive monoclonal primary antibody (4G2) for 1 h at room temperature, washed, incubated with a horseradish peroxidase conjugated anti-mouse secondary antibody for 1 h at room temperature, and washed. Foci of infected cells were visualized and quantified following the addition of True-Blue peroxidase substrate.

Mice and infections. IFN-α/β receptor 1 knockout (Ifnar1$^{-/-}$) mice were purchased from Jackson Laboratories. They were bred and maintained at Saint Louis University in a specific pathogen-free mouse facility. To achieve a primary infection, at 4 to 5 weeks of age, equal ratios of male and female mice were administered a sublethal intravenous (i.v.) challenge of either DENV2 (10^5 FFU) or DENV3 (10^5 FFU). To generate mice with prior ZIKV or YF-17D exposure, 8-week-old mice at equal ratios of male and female animals, were administered a sublethal subcutaneous (s.c.) challenge of either ZIKV (10^5 FFU) or YF-17D (10^5 FFU). The viral doses, routes of administration, and ages of mice were deliberately chosen based on optimized dosing experiments in our lab known to induce detectable viral replication and immune responses but not cause mortality (19, 21–23). As a flavivirus-naive group, 8-week-old littermate controls were administered PBS. At least 30 days following primary challenge, mice were administered an i.v. ZIKV challenge (10^5 FFU), previously demonstrated by our lab to result in severe neurological sequela and weight loss in 100% of adult Ifnar1$^{-/-}$ mice with no prior flavivirus exposure, with 80 to 100% ultimately succumbing to infection (22, 23). Following ZIKV challenge, mice were monitored daily for 14 days for weight loss, indicators of neurological disease, and mortality. Whole blood was collected longitudinally from each mouse at day 0, 4, 7, 14, and 30 to monitor peripheral viral burden or at day 0 and 14 to assess neutralizing antibody responses from serum.

Measurement of viral burden. For longitudinal studies, whole blood was collected by cheek bleed into EDTA coated tubes. Fifty microliters of blood was transferred to RNAsol BD reagent, and RNA was extracted according to the manufacturer's instructions. For studies evaluating global viral burden, on day 4 and 8 post ZIKV infection, mice were administered a lethal cocktail of ketamine/xylazine before intracardiac perfusion with 20 ml of PBS. The spleen, liver, kidney, brain, and spinal cord were collected from each mouse and snap-frozen in a dry ice bath. Organs were weighed and homogenized in DMEM using a Bead Mill 24 from Fisher Scientific. RNA was extracted from 100 μl of homogenate using Tri Reagent RT according to the manufacturer's instructions. ZIKV RNA was quantified by qRT-PCR using a PrimeTime primer-probe set (forward, CCGCTGCCCAACACAAG; reverse, CCACTAACGTTCTTTTGCAGACAT; probe, AGCCTACCTTGACAAGCAGTCAGACACTCAA) and an in-house ZIKV RNA copy control. To measure infectious virus, spleen, and brain homogenate on day 4 or 8 post ZIKV, challenge was serially diluted and utilized in a standard focus forming assay (FFA) as previously described (49).

ZIKV FRNT. The ability of murine polyclonal serum samples to neutralize ZIKV was measured by a focus reduction neutralization test (FRNT). Briefly, murine serum was serially diluted and incubated with a consistent quantity of infectious ZIKV at 37°C for 1 h to allow for complex formation. Following incubation, the virus-serum complex was added to each well of a 96-well plate containing a confluent monolayer of Vero-WHO cells. Following a 1-h incubation to allow for attachment, a methyl cellulose overlay was added to restrict lateral viral spread. Following 2 days of infection, the cell monolayer was fixed and infectious virus was quantified by a standard FFA, as previously described (49). Neutralization potential is displayed as $1/NT_{50}$ with higher values indicating higher neutralization potential.

Measurement of cytokine expression. mRNA expression of IL-6, CXCL10, granzyme B, IFN-γ, IL-1β, and IL-10 was determined in RNA extracts from brains 8 days postinfection by qRT-PCR using TaqMan primer probe sets from Integrated DNA Technologies (IDT) (assay identifiers—Mm.PT.58.41769240 [IFNG], Mm.PT.58.10005566 [IL-6], Mm.PT.58.42155916 [GZMB], Mm.PT.58.41616450 [IL-1β], Mm.PT.58.43575827 [CXCL10], and Mm.PT.58.13531087 [IL-10]). Relative expression for each cytokine was determined by $2^{-\Delta\Delta CT}$ analysis with fold induction being relative to cytokine levels in brain RNA extracts of naive Ifnar1$^{-/-}$ mice.

Statistical analysis. For DENV, ZIKV, YFV, and YF-17D incidence maps, incidence data and vaccine coverage data were collected for South and Central American countries from the WHO/PAHO for the years 2015 to 2019 and displayed as the annual average number of cases per 100,000 individuals using the spatial data program GeoDa (61). Amino acid identity for each flavivirus of interest was determined by performing a global alignment allowing for free ends using a Blosum62 cost matrix in the software Geneious. Statistical analyses for *in vivo* studies were performed using GraphPad Prism. Statistical differences in survival were determined using a Mantel-Cox test. Differences in weight loss and viral burden over time were determined using a two-way analysis of variance (ANOVA) with *post hoc* analysis.

Statistical significance in viral burden and cytokine expression in various organs was determined by Mann-Whitney test. Correlative analysis was performed using linear regression analysis and a two-tailed Pearson analysis. Statistical significance has been indicated within the figures with asterisks (*, $P = 0.03$; **, $P = 0.002$; ***, $P = 0.0002$; ****, $P < 0.0001$).

Data availability. Data are available online (62–65).

ACKNOWLEDGMENTS

This work was supported by National institutes of Health grant F31 AI152460-01 from the National Institute of Allergy and Infectious Diseases (NIAID) awarded to M.H., NIH grant R0112781495 from the NIAID awarded to A.K.P. and J.D.B., Saint Louis University Presidential Research Fund 9083, Discovery award USAMRDCPR192269 from Department of Defense awarded to A.K.P., and an NIH K22 AI104794 early investigator award from the NIAID awarded to J.D.B.

The funders had no role in study design, data collection and interpretation, or the decision to submit this work for publication.

We declare that no competing interests exist.

Conceptualization, M.H., J.D.B., and A.K.P.; Data Curation, M.H. and S.S.; Formal Analysis, M.H.; Investigation, M.H. and T.L.S.; Methodology, M.H., J.D.B., A.K.P., and S.S.; Funding Acquisition, M.H., J.D.B., and A.K.P.; Resources, A.K.C., S.S., E.S., and T.L.S.; Visualization, M.H. and S.S.; Writing (Original Draft), M.H., J.D.B., and A.K.P.; Writing (Review and Editing), M.H., S.S., T.L.S., A.K.C., E.S., J.D.B., and A.K.P.; Project Administration, J.D.B. and A.K.P.

REFERENCES

1. World Health Organization. 2016. WHO declares Zika virus a public health emergency. World Health Organization, Geneva, Switzerland. https://www.who.int/health-topics/zika-virus-disease#tab=tab_1.
2. World Health Organization, Pan American Health Organization. 2017. Case of Zika virus disease by country or territory. World Health Organization, Geneva, Switzerland. https://www.paho.org/en/topics/zika.
3. Rodriguez-Barraquer I, Cordeiro MT, Braga C, de Souza WV, Marques ET, Cummings DAT. 2011. From re-emergence to hyperendemicity: the natural history of the dengue epidemic in Brazil. PLoS Negl Trop Dis 5:e935. https://doi.org/10.1371/journal.pntd.0000935.
4. Jácome R, Carrasco-Hernández R, Campillo-Balderas JA, López-Vidal Y, Lazcano A, Wenzel RP, Ponce de León S. 2019. A yellow flag on the horizon: the looming threat of yellow fever to North America. Int J Infect Dis 87:143–150. https://doi.org/10.1016/j.ijid.2019.07.033.
5. Chambers TJ, Hahn CS, Galler R, Rice CM. 1990. Flavivirus genome organization, expression, and replication. Annu Rev Microbiol 44:649–688. https://doi.org/10.1146/annurev.mi.44.100190.003245.
6. Roby JA, Setoh YX, Hall RA, Khromykh AA. 2015. Post-translational regulation and modifications of flavivirus structural proteins. J Gen Virol 96:1551–1569. https://doi.org/10.1099/vir.0.000097.
7. Carbaugh DL, Lazear HM. 2020. Flavivirus envelope protein glycosylation: impacts on viral infection and pathogenesis. J Virol 94:e00104-20. https://doi.org/10.1128/JVI.00104-20.
8. Barrows NJ, Campos RK, Liao KC, Prasanth KR, Soto-Acosta R, Yeh SC, Schott-Lerner G, Pompon J, Sessions OM, Bradrick SS, Garcia-Blanco MA. 2018. Biochemistry and molecular biology of flaviviruses. Chem Rev 118:4448–4482. https://doi.org/10.1021/acs.chemrev.7b00719.
9. Kuhn RJ, Zhang W, Rossmann MG, Pletnev SV, Corver J, Lenches E, Jones CT, Mukhopadhyay S, Chipman PR, Strauss EG, Baker TS, Strauss JH. 2002. Structure of dengue virus: implications for flavivirus organization, maturation, and fusion. Cell 108:717–725. https://doi.org/10.1016/s0092-8674(02)00660-8.
10. Sirohi D, Kuhn RJ. 2017. Zika virus structure, maturation, and receptors. J Infect Dis 216:S935–s944. https://doi.org/10.1093/infdis/jix515.
11. Volk DE, May FJ, Gandham SH, Anderson A, Von Lindern JJ, Beasley DW, Barrett AD, Gorenstein DG. 2009. Structure of yellow fever virus envelope protein domain III. Virology 394:12–18. https://doi.org/10.1016/j.virol.2009.09.001.
12. Heinz FX, Stiasny K. 2017. The antigenic structure of Zika virus and its relation to other flaviviruses: implications for infection and immunoprophylaxis. Microbiol Mol Biol Rev 81:e00055-16. https://doi.org/10.1128/MMBR.00055-16.
13. Reich NG, Shrestha S, King AA, Rohani P, Lessler J, Kalayanarooj S, Yoon I-K, Gibbons RV, Burke DS, Cummings DAT. 2013. Interactions between serotypes of dengue highlight epidemiological impact of cross-immunity. J R Soc Interface 10:20130414. https://doi.org/10.1098/rsif.2013.0414.
14. Zimmerman MG, Wrammert J, Suthar MS. 2020. Cross-reactive antibodies during Zika virus infection: protection, pathogenesis, and placental seeding. Cell Host Microbe 27:14–24. https://doi.org/10.1016/j.chom.2019.12.003.
15. Culshaw A, Mongkolsapaya J, Screaton GR. 2017. The immunopathology of dengue and Zika virus infections. Curr Opin Immunol 48:1–6. https://doi.org/10.1016/j.coi.2017.07.001.
16. Andrade DV, Harris E. 2018. Recent advances in understanding the adaptive immune response to Zika virus and the effect of previous flavivirus exposure. Virus Res 254:27–33. https://doi.org/10.1016/j.virusres.2017.06.019.
17. Priyamvada L, Hudson W, Ahmed R, Wrammert J. 2017. Humoral cross-reactivity between Zika and dengue viruses: implications for protection and pathology. Emerg Microbes Infect 6:e33. https://doi.org/10.1038/emi.2017.42.
18. Halstead SB, Nimmannitya S, Cohen SN. 1970. Observations related to pathogenesis of dengue hemorrhagic fever. IV. Relation of disease severity to antibody response and virus recovered. Yale J Biol Med 42:311–328.
19. Pinto AK, Brien JD, Lam CY, Johnson S, Chiang C, Hiscott J, Sarathy VV, Barrett AD, Shresta S, Diamond MS. 2015. Defining new therapeutics using a more immunocompetent mouse model of antibody-enhanced dengue virus infection. mBio 6:e01316-15. https://doi.org/10.1128/mBio.01316-15.
20. Meier KC, Gardner CL, Khoretonenko MV, Klimstra WB, Ryman KD. 2009. A mouse model for studying viscerotropic disease caused by yellow fever virus infection. PLoS Pathog 5:e1000614. https://doi.org/10.1371/journal.ppat.1000614.
21. Watson AM, Lam LKM, Klimstra WB, Ryman KD. 2016. The 17D-204 vaccine strain-induced protection against virulent yellow fever virus is mediated by humoral immunity and CD4+ but not CD8+ T cells. PLoS Pathog 12:e1005786. https://doi.org/10.1371/journal.ppat.1005786.
22. Hassert M, Harris MG, Brien JD, Pinto AK. 2019. Identification of protective CD8 T cell responses in a mouse model of Zika virus infection. Front Immunol 10:1678. https://doi.org/10.3389/fimmu.2019.01678.
23. Hassert M, Wolf KJ, Schwetye KE, DiPaolo RJ, Brien JD, Pinto AK. 2018. CD4+T cells mediate protection against Zika associated severe disease in a mouse model of infection. PLoS Pathog 14:e1007237. https://doi.org/10.1371/journal.ppat.1007237.

24. Lazear HM, Govero J, Smith AM, Platt DJ, Fernandez E, Miner JJ, Diamond MS. 2016. A mouse model of Zika virus pathogenesis. Cell Host Microbe 19:720–730. https://doi.org/10.1016/j.chom.2016.03.010.
25. Wen J, Elong Ngono A, Regla-Nava JA, Kim K, Gorman MJ, Diamond MS, Shresta S. 2017. Dengue virus-reactive CD8$^+$ T cells mediate cross-protection against subsequent Zika virus challenge. Nat Commun 8:1459. https://doi.org/10.1038/s41467-017-01669-z.
26. Regla-Nava JA, Elong Ngono A, Viramontes KM, Huynh A-T, Wang Y-T, Nguyen A-VT, Salgado R, Mamidi A, Kim K, Diamond MS, Shresta S. 2018. Cross-reactive dengue virus-specific CD8$^+$ T cells protect against Zika virus during pregnancy. Nat Commun 9:3042. https://doi.org/10.1038/s41467-018-05458-0.
27. Holbrook MR. 2017. Historical perspectives on flavivirus research. Viruses 9:97. https://doi.org/10.3390/v9050097.
28. Zambrana JV, Bustos Carrillo F, Burger-Calderon R, Collado D, Sanchez N, Ojeda S, Carey Monterrey J, Plazaola M, Lopez B, Arguello S, Elizondo D, Aviles W, Coloma J, Kuan G, Balmaseda A, Gordon A, Harris E. 2018. Seroprevalence, risk factor, and spatial analyses of Zika virus infection after the 2016 epidemic in Managua, Nicaragua. Proc Natl Acad Sci U S A 115:9294–9299. https://doi.org/10.1073/pnas.1804672115.
29. Gordon A, Gresh L, Ojeda S, Katzelnick LC, Sanchez N, Mercado JC, Chowell G, Lopez B, Elizondo D, Coloma J, Burger-Calderon R, Kuan G, Balmaseda A, Harris E. 2019. Prior dengue virus infection and risk of Zika: a pediatric cohort in Nicaragua. PLoS Med 16:e1002726. https://doi.org/10.1371/journal.pmed.1002726.
30. Blazevic J, Rouha H, Bradt V, Heinz FX, Stiasny K. 2016. The membrane anchors of the structural flavivirus proteins and their role in virus assembly. J Virol 90:6365–6378. https://doi.org/10.1128/JVI.00447-16.
31. De Góes Cavalcanti LP, Tauil PL, Alencar CH, Oliveira W, Teixeira MM, Heukelbach J. 2016. Zika virus infection, associated microcephaly, and low yellow fever vaccination coverage in Brazil: is there any causal link? J Infect Dev Ctries 10:563–566. https://doi.org/10.3855/jidc.8575.
32. Hassert M, Brien JD, Pinto AK. 2019. Mouse models of heterologous flavivirus immunity: a role for cross-reactive T cells. Front Immunol 10:1045. https://doi.org/10.3389/fimmu.2019.01045.
33. Rossi SL, Tesh RB, Azar SR, Muruato AE, Hanley KA, Auguste AJ, Langsjoen RM, Paessler S, Vasilakis N, Weaver SC. 2016. Characterization of a novel murine model to study Zika virus. Am J Trop Med Hyg 94:1362–1369. https://doi.org/10.4269/ajtmh.16-0111.
34. Nazerai L, Schøller AS, Rasmussen POS, Buus S, Stryhn A, Christensen JP, Thomsen AR. 2018. A new in vivo model to study protective immunity to Zika virus infection in mice with intact type I interferon signaling. Front Immunol 9:593. https://doi.org/10.3389/fimmu.2018.00593.
35. Shan C, Xie X, Luo H, Muruato AE, Liu Y, Wakamiya M, La J-H, Chung JM, Weaver SC, Wang T, Shi P-Y. 2019. Maternal vaccination and protective immunity against Zika virus vertical transmission. Nat Commun 10:5677. https://doi.org/10.1038/s41467-019-13589-1.
36. Liang H, Yang R, Liu Z, Li M, Liu H, Jin X. 2018. Recombinant Zika virus envelope protein elicited protective immunity against Zika virus in immunocompetent mice. PLoS One 13:e0194860. https://doi.org/10.1371/journal.pone.0194860.
37. Salvo MA, Kingstad-Bakke B, Salas-Quinchucua C, Camacho E, Osorio JE. 2018. Zika virus like particles elicit protective antibodies in mice. PLoS Negl Trop Dis 12:e0006210. https://doi.org/10.1371/journal.pntd.0006210.
38. Espinosa D, Mendy J, Manayani D, Vang L, Wang C, Richard T, Guenther B, Aruri J, Avanzini J, Garduno F, Farness P, Gurwith M, Smith J, Harris E, Alexander J. 2018. Passive transfer of immune sera induced by a Zika virus-like particle vaccine protects AG129 mice against lethal Zika virus challenge. EBioMedicine 27:61–70. https://doi.org/10.1016/j.ebiom.2017.12.010.
39. Magnani DM, Rogers TF, Beutler N, Ricciardi MJ, Bailey VK, Gonzalez-Nieto L, Briney B, Sok D, Le K, Strubel A, Gutman MJ, Pedreño-Lopez N, Grubaugh ND, Silveira CGT, Maxwell HS, Domingues A, Martins MA, Lee DE, Okwuazi EE, Jean S, Strobert EA, Chahroudi A, Silvestri G, Vanderford TH, Kallas EG, Desrosiers RC, Bonaldo MC, Whitehead SS, Burton DR, Watkins DI. 2017. Neutralizing human monoclonal antibodies prevent Zika virus infection in macaques. Sci Transl Med 9:aan8184. https://doi.org/10.1126/scitranslmed.aan8184.
40. Dejnirattisai W, Supasa P, Wongwiwat W, Rouvinski A, Barba-Spaeth G, Duangchinda T, Sakuntabhai A, Cao-Lormeau VM, Malasit P, Rey FA, Mongkolsapaya J, Screaton GR. 2016. Dengue virus sero-cross-reactivity drives antibody-dependent enhancement of infection with Zika virus. Nat Immunol 17:1102–1108. https://doi.org/10.1038/ni.3515.
41. Pantoja P, Perez-Guzman EX, Rodriguez IV, White LJ, Gonzalez O, Serrano C, Giavedoni L, Hodara V, Cruz L, Arana T, Martinez MI, Hassert MA, Brien JD, Pinto AK, de Silva A, Sariol CA. 2017. Zika virus pathogenesis in rhesus macaques is unaffected by pre-existing immunity to dengue virus. Nat Commun 8:15674. https://doi.org/10.1038/ncomms15674.
42. Rathore APS, St. John AL. 2020. Cross-reactive immunity among flaviviruses. Front Immunol 11:334. https://doi.org/10.3389/fimmu.2020.00334.
43. Jurado KA, Yockey LJ, Wong PW, Lee S, Huttner AJ, Iwasaki A. 2018. Antiviral CD8 T cells induce Zika-virus-associated paralysis in mice. Nat Microbiol 3:141–147. https://doi.org/10.1038/s41564-017-0060-z.
44. Manangeeswaran M, Ireland DD, Verthelyi D. 2016. Zika (PRVABC59) infection is associated with T cell infiltration and neurodegeneration in CNS of immunocompetent neonatal C57Bl/6 mice. PLoS Pathog 12:e1006004. https://doi.org/10.1371/journal.ppat.1006004.
45. Dudley DM, Aliota MT, Mohr EL, Weiler AM, Lehrer-Brey G, Weisgrau KL, Mohns MS, Breitbach ME, Rasheed MN, Newman CM, Gellerup DD, Moncla LH, Post J, Schultz-Darken N, Schotzko ML, Hayes JM, Eudailey JA, Moody MA, Permar SR, O'Connor SL, Rakasz EG, Simmons HA, Capuano S, Golos TG, Osorio JE, Friedrich TC, O'Connor DH. 2016. A rhesus macaque model of Asian-lineage Zika virus infection. Nat Commun 7:12204. https://doi.org/10.1038/ncomms12204.
46. Bell TM, Field EJ, Narang HK. 1971. Zika virus infection of the central nervous system of mice. Arch Gesamte Virusforsch 35:183–193. https://doi.org/10.1007/BF01249709.
47. Tripathi S, Balasubramaniam VRMT, Brown JA, Mena I, Grant A, Bardina SV, Maringer K, Schwarz MC, Maestre AM, Sourisseau M, Albrecht RA, Krammer F, Evans MJ, Fernandez-Sesma A, Lim JK, García-Sastre A. 2017. A novel Zika virus mouse model reveals strain specific differences in virus pathogenesis and host inflammatory immune responses. PLoS Pathog 13:e1006258. https://doi.org/10.1371/journal.ppat.1006258.
48. Ramos HJ, Lanteri MC, Blahnik G, Negash A, Suthar MS, Brassil MM, Sodhi K, Treuting PM, Busch MP, Norris PJ, Gale M, Jr. 2012. IL-1β signaling promotes CNS-intrinsic immune control of West Nile virus infection. PLoS Pathog 8:e1003039. https://doi.org/10.1371/journal.ppat.1003039.
49. Brien JD, Hassert M, Stone ET, Geerling E, Cruz-Orengo L, Pinto AK. 15 August 2019. Isolation and quantification of Zika virus from multiple organs in a mouse. J Vis Exp https://doi.org/10.3791/59632.
50. Wen J, Tang WW, Sheets N, Ellison J, Sette A, Kim K, Shresta S. 2017. Identification of Zika virus epitopes reveals immunodominant and protective roles for dengue virus cross-reactive CD8$^+$ T cells. Nat Microbiol 2:17036. https://doi.org/10.1038/nmicrobiol.2017.36.
51. Miner JJ, Sene A, Richner JM, Smith AM, Santeford A, Ban N, Weger-Lucarelli J, Manzella F, Ruckert C, Govero J, Noguchi KK, Ebel GD, Diamond MS, Apte RS. 2016. Zika virus infection in mice causes panuveitis with shedding of virus in tears. Cell Rep 16:3208–3218. https://doi.org/10.1016/j.celrep.2016.08.079.
52. Huang W-C, Abraham R, Shim B-S, Choe H, Page DT. 2016. Zika virus infection during the period of maximal brain growth causes microcephaly and corticospinal neuron apoptosis in wild type mice. Sci Rep 6:34793. https://doi.org/10.1038/srep34793.
53. Pierson TC, Diamond MS. 2020. The continued threat of emerging flaviviruses. Nat Microbiol 5:796–812. https://doi.org/10.1038/s41564-020-0714-0.
54. Akrami KM, de Nogueira BMF, do Rosário MS, de Moraes L, Cordeiro MT, Haddad R, Gomes LN, de Pádua Carvalho I, dos Reis Pimentel E, de Jesus Silva J, de Oliveira Francisco MVL, de Siqueira IC, Farias D, Barral-Netto M, Barral A, Boaventura V, Khouri R. 2020. The re-emergence of Zika in Brazil in 2020: a case of Guillain Barré syndrome during the low season for arboviral infections. J Travel Med 27:taaa165. https://doi.org/10.1093/jtm/taaa165.
55. Paixão ES, Teixeira MG, Rodrigues LC. 2018. Zika, chikungunya and dengue: the causes and threats of new and re-emerging arboviral diseases. BMJ Glob Health 3:e000530. https://doi.org/10.1136/bmjgh-2017-000530.
56. Pérez-Guzmán EX, Pantoja P, Serrano-Collazo C, Hassert MA, Ortiz-Rosa A, Rodríguez IV, Giavedoni L, Hodara V, Parodi L, Cruz L, Arana T, White LJ, Martínez MI, Weiskopf D, Brien JD, de Silva A, Pinto AK, Sariol CA. 2019. Time elapsed between Zika and dengue virus infections affects antibody and T cell responses. Nat Commun 10:4316. https://doi.org/10.1038/s41467-019-12295-2.
57. Anderson KB, Gibbons RV, Cummings DAT, Nisalak A, Green S, Libraty DH, Jarman RG, Srikiatkhachorn A, Mammen MP, Darunee B, Yoon I-K, Endy TP. 2014. A shorter time interval between first and second dengue infections is associated with protection from clinical illness in a school-based cohort in Thailand. J Infect Dis 209:360–368. https://doi.org/10.1093/infdis/jit436.

58. Bailey MJ, Duehr J, Dulin H, Broecker F, Brown JA, Arumemi FO, Bermúdez González MC, Leyva-Grado VH, Evans MJ, Simon V, Lim JK, Krammer F, Hai R, Palese P, Tan GS. 2018. Human antibodies targeting Zika virus NS1 provide protection against disease in a mouse model. Nat Commun 9:4560. https://doi.org/10.1038/s41467-018-07008-0.
59. Grifoni A, Pham J, Sidney J, O'Rourke PH, Paul S, Peters B, Martini SR, de Silva AD, Ricciardi MJ, Magnani DM, Silveira CGT, Maestri A, Costa PR, de-Oliveira-Pinto LM, de Azeredo EL, Damasco PV, Phillips E, Mallal S, de Silva AM, Collins M, Durbin A, Diehl SA, Cerpas C, Balmaseda A, Kuan G, Coloma J, Harris E, Crowe JE, Jr, Stone M, Norris PJ, Busch M, Vivanco-Cid H, Cox J, Graham BS, Ledgerwood JE, Turtle L, Solomon T, Kallas EG, Watkins DI, Weiskopf D, Sette A. 2017. Prior dengue virus exposure shapes T cell immunity to Zika virus in humans. J Virol 91:e01469-17. https://doi.org/10.1128/JVI.01469-17.
60. Makhluf H, Buck MD, King K, Perry ST, Henn MR, Shresta S. 2013. Tracking the evolution of dengue virus strains D2S10 and D2S20 by 454 pyrosequencing. PLoS One 8:e54220. https://doi.org/10.1371/journal.pone.0054220.
61. Li X, Anselin L, Koschinsky J. 2015. GeoDa web: enhancing web-based mapping with spatial analytics. Abstr 23rd SIGSPATIAL International Conference on Advances in Geographic Information Systems. Association for Computing Machinery, Seattle, Washington.
62. World Health Organization. 2020. Yellow fever: reported cases by country. World Health Organization, Geneva, Switzerland. https://apps.who.int/gho/data/view.main.1540_50?lang=en.
63. World Health Organization. 2020. Yellow fever vaccine: reported estimates of YFV coverage. World Health Organization, Geneva, Switzerland. https://apps.who.int/immunization_monitoring/globalsummary/timeseries/tscoverageyfv.html.
64. Pan American Health Organization. 2021. Cases of Zika virus disease by country or territory: cumulative cases. Pan American Health Organization, Washington, DC. https://www.paho.org/data/index.php/en/mnu-topics/zika/524-zika-weekly-en.html.
65. Pan American Health Organization. 2021. Reported cases of dengue fever in the Americas by country or territory: cumulative cases. Pan American Health Organization, Washington, DC. https://www.paho.org/data/index.php/en/mnu-topics/indicadores-dengue-en/dengue-nacional-en/252-dengue-pais-ano-en.html.

STAR Protocols

CellPress
OPEN ACCESS

Protocol

Titration and neutralizing antibody quantification by focus forming assay for Powassan virus

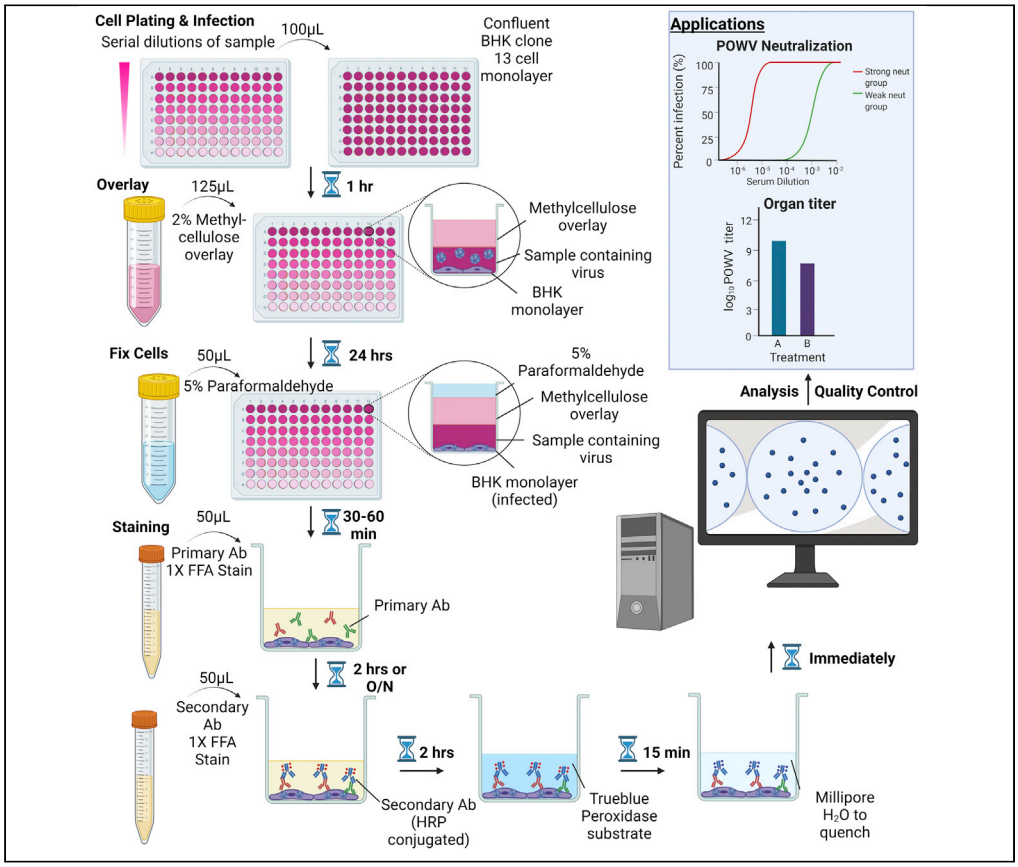

The development of high-throughput assays measuring Powassan virus (POWV) lineage I and II represents an important step in virological and immunological studies. By adapting focus-forming assays previously optimized for West Nile virus and Zika virus, this protocol is able to determine viral load, evaluate antivirals, and measure neutralizing antibodies. Although limited by its requirement of a detection antibody, this protocol includes a rapid and high-throughput assay for measuring viral titer. By utilizing a baby hamster kidney cell line and a 96-well plate format, this protocol allows for more sensitivity in the detection of POWV lineage I.

Publisher's note: Undertaking any experimental protocol requires adherence to local institutional guidelines for laboratory safety and ethics.

E. Taylor Stone, Alec J. Hirsch, Jessica L. Smith, James D. Brien, Amelia K. Pinto

amelia.pinto@health.slu.edu (A.K.P.)
taylor.t.stone@slu.edu (E.T.S.)

Highlights

Powassan virus focus forming assay for evaluation of antivirals

Antibody focus reduction neutralization assay (FRNT) for Powassan virus

Steps describing Powassan virus lineage I and II titration

Stone et al., STAR Protocols 3, 101473
September 16, 2022
https://doi.org/10.1016/j.xpro.2022.101473

STAR Protocols

CellPress
OPEN ACCESS

Protocol

Titration and neutralizing antibody quantification by focus forming assay for Powassan virus

E. Taylor Stone,[1,4,*] Alec J. Hirsch,[2,3] Jessica L. Smith,[2,3] James D. Brien,[1] and Amelia K. Pinto[1,5,*]

[1]Department of Molecular Microbiology and Immunology, Saint Louis University, St. Louis, MO 63104, USA

[2]The Vaccine & Gene Therapy Institute, Oregon Health & Science University, Beaverton, OR 97006, USA

[3]Division of Pathobiology & Immunology, Oregon National Primate Research Center, Oregon Health & Science University, Beaverton, OR 97006, USA

[4]Technical contact

[5]Lead contact

*Correspondence: amelia.pinto@health.slu.edu (A.K.P.), taylor.t.stone@slu.edu (E.T.S.)
https://doi.org/10.1016/j.xpro.2022.101473

SUMMARY

The development of high-throughput assays measuring Powassan virus (POWV) lineage I and II represents an important step in virological and immunological studies. By adapting focus-forming assays previously optimized for West Nile virus and Zika virus, this protocol is able to determine viral load, evaluate antivirals, and measure neutralizing antibodies. Although limited by its requirement of a detection antibody, this protocol includes a rapid and high-throughput assay for measuring viral titer. By utilizing a baby hamster kidney cell line and a 96-well plate format, this protocol allows for more sensitivity in the detection of POWV lineage I.

For complete details on the use and execution of this protocol, please refer to Stone et al. (2022).

BEFORE YOU BEGIN

1. Establish baby hamster kidney cells (BHK). It is well-established in literature describing POWV virus stock generation that BHK cells are a preferable choice for propagating virus, over the well-characterized African green monkey kidney Vero cell line (referred to as Vero or Vero WHO) (Leonova et al., 2009; Abdelwahab et al., 1964; Anderson and Armstrong, 2012). Although both cell lines are known to be type I interferon-deficient (Osada et al., 2014; Macpherson and Stoker, 1962) in our hands we have found that titration of identical serial dilutions of the POWV-LB lineage on the two cell types yields drastically different titers, with Vero WHO cells showing ~2 logs less virus than BHK-21 cells (Figure 1). For this reason, our assays are optimized with the use of BHK-21 clone 13 cells.
2. Determine desired application. This protocol describes the specific steps for titration of POWV by focus forming assay in a 96-well plate format. However, we have also used this protocol in 12-, and 24-well plate formats for titration of other flaviviruses (Brien et al., 2008, 2019; Hassert et al., 2018, 2019, 2021). This protocol can also be adapted for antiviral compound screening, determining organ titer, and neutralizing antibody quantification.
3. Determine dilution of virus stock for assay (if needed). For antiviral compound screening and neutralizing antibody quantifications, the researcher should determine the dilution of virus stock/sample that will yield a count of ~70–100 foci per well before proceeding to the next steps. For quantification of neutralizing antibody, serial dilutions of serum samples should be made in growth media (Dulbecco's Modified Eagle's Medium (DMEM) containing 5% fetal bovine serum (FBS and 1% HEPES, see materials and equipment) and incubated with the appropriate dilution of

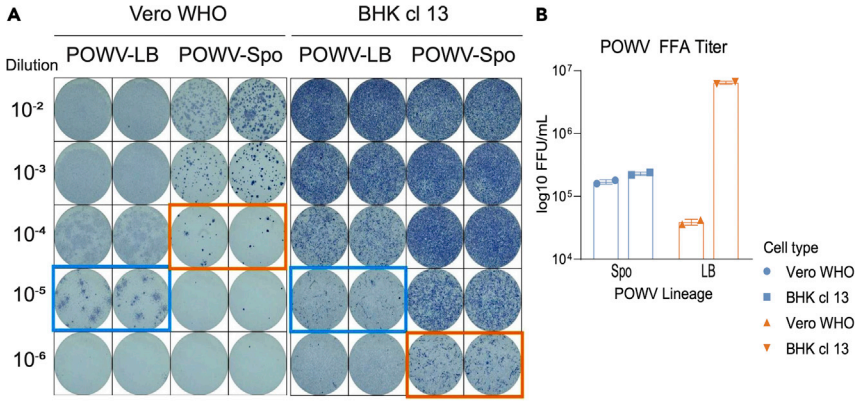

Figure 1. Baby hamster kidney cells should be used in Powassan virus titration

(A) A representative focus forming assay showing the results of plating identical ten-fold serial dilutions of Powassan virus Spooner lineage (Spo, blue) or Powassan virus LB lineage (LB, orange) on Vero WHO cells (left) or baby hamster kidney 21 clone 13 cells from the ATCC (right). Boxed in blue and orange are the serial dilutions that could be used to determine the viral titer.

(B) Quantification of POWV infectious viral titer images presented in (A). Data are reported as the mean foci for the two replicates.

virus (yielding 70–100 foci per well) for 1 h 37°C, 5% CO_2 to allow for immune complex formation. Mixture should then be applied to cell monolayer to allow for virus adsorption and handled identically to the focus forming assay (FFA) described below.

4. Determine method of spot counting. This protocol utilizes an ImmunoSpot S6 FluoroCore M2 analyzer, and outlines the parameters that produce the most rapid and accurate foci counts.

Institutional permissions

This protocol requires biosafety level 3 containment facilities. Standard operating procedures, protocols and disinfectants approved by the Institutional Biosafety Committee (IBC) or equivalent biosafety regulatory bodies should be used, and all work is performed inside Biosafety Cabinets (BSC) unless otherwise noted.

Culture cell lines

Timing: 4–10 days

The maintenance of a healthy cell culture is essential to achieve accurate and reproducible titration assays, drug screens, and neutralizing antibody quantifications.

5. Baby hamster kidney American Type Cell Culture clone 13 (referred to as BHK-21 clone-13 or BHKs) should be passaged 2–3 times in 5% DMEM (see materials and equipment) upon initial thawing from liquid N_2 prior to plating for focus forming assays. Cells may be carried in T150 flasks and split 1:20 every 2–3 days. Cells should be carried in 20 mL of 5% DMEM to 90%–95% confluency and washed two times with 10 mL Ca^{2+} Mg^{2+} free phosphate buffered saline (PBS) and lifted via incubation with 4 mL trypsin. Following trypsinization, 6 mL of 5% DMEM should be added to halt the trypsin reaction, resulting in a single cell suspension of ~10 mL. To the same T150 flask, 1 mL of this single cell suspension may be added, along with 19 mL of fresh 5% DMEM and returned to the incubator.

Prepare reagents

Timing: 6 h

6. Prepare 2% methylcellulose, 5× FFA Staining buffer, and 1× FFA Wash buffer (see tables for recipe):

Cell plating and titration by focus forming assay

Timing: Active time: 2–3 h, With incubations: 48–72 h

7. The day before the assay, plate BHK-21 clone-13 (ATCC CCL-10) cells in a tissue culture treated 96-well plate in growth media overnight.
   a. Before beginning the assay, cells should reach ~90% confluency; BHKs will not form an even monolayer with complete cell-to-cell contact as seen with Vero cells.
8. Prepare 10-fold serial dilutions of the sample of interest in duplicate or triplicate.
9. Remove media from 96-well flat bottom plate containing BHKs. Add 100 µL per well of serially diluted samples in growth media to BHK cell monolayer.
10. Incubate for 1 h to allow for virus adsorption.
11. During incubation, prepare methylcellulose overlay and warm to room temperature.
12. Add methylcellulose overlay to minimize lateral spread of viral infection.
13. Incubate 24 h.
14. Following incubation, fix cells in freshly made 5% paraformaldehyde (PFA) in PBS for 30–60 min.
15. Wash cells twice with 1× PBS and once with 1× FFA Wash buffer. Incubate 5–10 min at room temperature to permeabilize cells.
16. Remove plates from BSL-3 containment and proceed to immunostaining.

Immunostaining

Timing: Active time: 2–3 h, With incubations: 8–24 h

17. Prepare and add primary antibody (Monoclonal Anti-Langat Virus Envelope Glycoprotein) in 1× FFA Staining buffer.
18. Incubate at room temperature for 1.5–2 h or overnight at 4°C.
19. Wash three times with 1× FFA Wash buffer.
20. Prepare and add secondary antibody (goat anti-mouse conjugated to HRP) in 1× FFA Staining buffer.
21. Incubate at room temperature for 2–3 h.
22. Wash three times with 1× FFA Wash buffer.
23. Add Trueblue substrate and incubate 15–20 min or until spots are fully defined with minimal background.
24. Quench the reaction by removing substrate and rinsing with Millipore water.
25. Tap on a paper towel to remove water and image.

Imaging (optional)

Timing: Active time: 15–60 min, with computer/software run time: 30–120 min

26. A CTL Immunospot analyzer can be used for high-throughput quantification of foci using CTL Immunospot 'Scan', 'Count' and 'Quality Control' functions. Researchers who do not have access to an Elispot may elect to manually count wells under a dissecting microscope, however this will reduce the high-throughput nature of the assay.

⚠ CRITICAL: Prior to fixation step, all agents should be handled in appropriate biological containment.

KEY RESOURCES TABLE

REAGENT or RESOURCE	SOURCE	IDENTIFIER
Antibodies		
Anti-Mouse IgG (whole molecule)–Peroxidase antibody produced in goat, 1:5,000	Sigma-Aldrich	Cat# A8924, RRID: AB_258426
Monoclonal Anti-Langat Virus Envelope Glycoprotein (E), Clone 10F6, 3 :10,000	BEI Resources	NR-40316
Bacterial and virus strains		
POWV strain LB	Ebel laboratory	Mandl et al., 1993
POWV-DTV strain Spooner	Ebel laboratory	Ebel et al., 1999
Experimental models: Cell lines		
BHK-21 clone 13	ATCC	ATCC Cat# CCL-10, RRID: CVCL_1915
Other		
Dulbecco's Modified Eagle's Media	Sigma-Aldrich	Cat# D5796-500ML
1 M HEPES solution	Sigma-Aldrich	Cat# H3537-100ML
Fetal bovine serum	Sigma-Aldrich	Cat# F0926
Methylcellulose	Sigma-Aldrich	Cat# M0512-250G
20% Electron microscopy grade paraformaldehyde	EMS	Cat# 15713-S
Saponin	Sigma-Aldrich	Cat# 47036
KPL TrueBlue Substrate	SeraCare	Cat# 5510-0052
ImmunoSpot® S6 FluoroCore M2 Analyzer	ImmunoSpot®	N/A

MATERIALS AND EQUIPMENT

Growth Media (5% DMEM)		
Reagent	Final concentration	Amount
Dulbecco's Modified Eagle's Media	n/a	500 mL
1 M HEPES solution	1%	5 mL
Fetal Bovine Serum	5%	25 mL
Total	**n/a**	**530 mL**
Store at 4°C away from light. Handle aseptically.		

2% Methylcellulose		
Reagent	Final concentration	Amount
Methylcellulose	2%	10 grams
Millipore H_2O	n/a	500 mL
Total	**n/a**	**500 mL**
Store at 4°C. Handle aseptically.		

5% Paraformaldehyde (PFA)		
Reagent	Final concentration	Amount
20% EM Grade PFA	5%	2.5 mL
1× PBS	n/a	7.5 mL
Total	**n/a**	**10 mL**
Store at 4°C. Prepare fresh on day of fix.		

1× FFA Wash Buffer		
Reagent	Final concentration	Amount
10× PBS	1×	1 L
Millipore H_2O	n/a	9 L
Triton X-100	0.05%	5 mL
Total	**n/a**	**10 L**
Store at room temperature.		

5× FFA Staining Buffer		
Reagent	Final concentration	Amount
10× PBS	5×	250 mL
Millipore H_2O	n/a	250 mL
Saponin	1 mg/mL	2.5 grams
Total	**n/a**	**500 mL**
Store at 4°C. Handle aseptically.		

Primary Antibody in 1× FFA Staining Buffer		
Reagent	Final concentration	Amount
5× FFA Staining Buffer	1×	2 mL
Millipore H_2O	n/a	8 mL
Primary Antibody (α-LGTV, clone 10F6)	3:10,000	3 µL
Total	**n/a**	**10 mL**
Store at 4°C. Prepare fresh on day of immunostaining.		

Secondary Antibody in 1× FFA Staining Buffer		
Reagent	Final concentration	Amount
5× FFA Staining Buffer	1×	2 mL
Millipore H_2O	n/a	8 mL
Secondary Antibody (Goat α-mouse conjugated HRP IgG)	1:5,000	2 µL
Total	**n/a**	**10 mL**
Store at 4°C. Prepare fresh on day of immunostaining.		

Storage: Growth media, 2% methylcellulose and 5× FFA Staining buffer can be made in advance and should be stored at 4°C and handled aseptically. All other solutions should be prepared on the day of the assay and stored at 4°C until use.

⚠ CRITICAL: Paraformaldehyde is a respiratory hazard and should be handled and disposed of with appropriate precautions and PPE in place.

Alternatives: Polyclonal sera can be used in place of The LGTV mAb, clone 10F6 (NR-40316) for the primary (detection) antibody. FFA Staining buffer can be used as an alternative to FFA Wash buffer for all wash steps. However, due to increased likelihood of contamination associated with the use of Saponin not seen with Triton X-100 it is advised to use FFA Wash buffer for the steps indicated. FFA Wash buffer is not an alternative for FFA Staining buffer.

STEP-BY-STEP METHOD DETAILS

Prepare reagents

Timing: 6 h

Advance preparation of 2% methylcellulose, 5× FFA Staining buffer, and 1× FFA Wash buffer will expedite the assay and ensure visualization of individually discernable foci.

1. Prepare 2% methylcellulose:
   a. Autoclave the following prior to preparation:
      i. 1 L glass bottle, 10 g methylcellulose, and a large stir bar.
      ii. 1 L glass bottle with 500 mL of Millipore water.
   b. In a tissue culture hood, add the 500 mL hot autoclaved Millipore water to bottle containing methylcellulose and a large stir bar. If the autoclaved water has cooled, reheat in the microwave until the bottle is hot to the touch, but water should not boil.
   c. Partially cap bottle and stir on a hotplate set between medium/high until methylcellulose is in solution (1–4 h).
   d. In a tissue culture hood, aliquot cooled 2% methylcellulose into 50 mL conical tubes. Pipette slowly, as the mixture will be viscous. Store at 4°C until further use in the assay, which will require bringing the methylcellulose to room temperature.
2. Prepare 5× FFA Staining buffer according to tables found in materials and equipment:
   a. To 250 mL of 10× PBS, add:
      i. 250 mL of Millipore water.
      ii. 2.5 g of Saponin.
   b. Stir until dissolved, then sterile filter and store at 4°C until the day of the assay.
3. Prepare 1× FFA Wash buffer (1× PBS, 0.05% Triton X-100) according to table found in materials and equipment:
   a. To 9 L of Millipore water, add:
      i. 1 L 10× PBS.
      ii. 5 mL Triton X-100.
4. Prepare media for carrying BHK-ATCC clone-13 cells (hereafter referred to as growth media):
   a. To 500 mL 5% DMEM, add:
      i. 5 mL HEPES solution.
      ii. 25 mL Fetal Bovine Serum (FBS).
      iii. Store at 4°C until further use.

Cell plating and titration by focus forming assay

Timing: Active time: 2–3 h, With incubations: 48–72 h

Quantification of Powassan viral titer by focus forming assay relies on the addition of sample with an unknown quantity of virus to a monolayer of permissive cells (BHKs). This step outlines the plating conditions and titration schema that, in our hands, produces the most reproducible conditions for determining POWV titer. Researchers are encouraged to determine the appropriate cell density and culture conditions for their own cell lines before titrating precious samples. Additionally, this protocol details titration using a 10-fold dilution series, researcher may find it useful to increase or decrease the fold dilution series based on the need for sensitivity for the titration series. This step also outlines the process of adding sample to the cell monolayer, overlaying to minimize lateral spread of infection, and the process of fixing the cells for removal from biological containment.

5. The day before the assay: to a tissue culture treated 96-well plate, add 2.5×10^4 cells per well of BHK-21 ATCC clone-13 cells in 100 μL of growth media per well. Incubate overnight at 37°C, 5% CO_2.
   a. Before starting the assay, examine cells under a light microscope to ensure you have proper cell confluence the day of the assay (~90%); BHKs will not form an even monolayer with complete cell-to-cell contact as seen with Vero cells.
6. In a 96-well round bottom plate, prepare 10-fold serial dilutions of the sample containing virus by adding 20 μL of sample to 180 μL of growth media. Sample dilutions should be performed in duplicate or triplicate, and at least one column should include a 'mock' infected PBS control.

7. Remove media from 96-well flat bottom plate containing BHKs. Add 100 μL per well of serially diluted samples in growth media to the 96-well flat bottom plate containing BHKs.
8. Incubate at 37°C, 5% CO_2 for 1 h without shaking to allow for virus adsorption.
9. During incubation, prepare methylcellulose:
   a. Mix one part 2% methylcellulose (see prepare reagents) with one part growth media. Place on a rocker at room temperature with gentle agitation to mix methylcellulose and media.
10. Add 125 μL per well of diluted methylcellulose in growth media to the flat bottom plate containing BHKs and + serially diluted samples. This step will minimize lateral spread of viral infection.
11. Incubate 24 h without shaking at 37°C, 5% CO_2.
12. Following incubation, fix the 96-well flat bottom plates as follows:
    a. Prepare 5% paraformaldehyde (PFA) by diluting 20% electron microscopy grade PFA four-fold in 1× PBS.
    b. Fix cells with 5% paraformaldehyde by adding 50 μL per well and incubate at room temperature for 30–60 min.
    c. Wash cells gently three times with 150 μL per well of 1× PBS.
    d. Add 150 μL per well of 1× FFA Wash buffer and let sit for 5–10 min at room temperature.
    e. Remove plates from BSL-3 containment and proceed to immunostaining.

Immunostaining

Timing: Active time: 2–3 h, With incubations: 8–24 h

After cells have been fixed, individual foci must be visualized following an immunostaining protocol that relies on the detection of viral antigen in the cells. This step outlines the immunostaining protocol that, in our hands, allows the researcher to visualize foci with minimal background.

13. Prepare 1× FFA Staining buffer by diluting 5× FFA Staining buffer five-fold in Millipore water. 5× FFA Staining buffer should be handled aseptically.
14. Remove Wash buffer and add primary antibody (e.g., Monoclonal Anti-Langat Virus Envelope Glycoprotein (E), Clone 10F6) that has been diluted 3:10,000 in 1× FFA Staining buffer (50 μL per well).
15. Incubate at room temperature for 1.5–2 h with gentle agitation on an orbital shaker, or overnight at 4°C without shaking.
16. Wash three times with 1× FFA Wash buffer (150 μL per well).
17. Remove Wash buffer and add secondary antibody (goat anti-mouse conjugated to HRP) that has been diluted 1:5,000 in 1× FFA Staining buffer (50 μL per well).
18. Incubate at room temperature for 2–3 h.
19. Wash three times with 1× FFA Wash buffer (150 μL per well).
20. Remove Wash buffer; add Trueblue substrate (50 μL per well) and incubate 15–20 min without shaking, in the dark, or until spots are fully defined with minimal background.
21. Flick off substrate and wash twice with 200 μL/well of cool Millipore water to quench the reaction. The reaction should not be quenched with hot (>37°C) water.
22. Tap on a paper towel to remove water and count or image within 15–30 min of quenching for best counting results.

Imaging (optional)

Timing: Active time: 15–60 min, With computer/software run time: 30–120 min

After immunostaining, individual foci should be visible wells. While POWV titer can be calculated manually by counting under a dissecting microscope, we have found that the high-throughput nature of the 96-well plate format is more suitable for automated counting. For this purpose, we utilize

an ImmunoSpot S6 FluoroCore M2 analyzer, hereafter referred to as a CTL Elispot machine. The steps below outline the parameters on a CTL Immunospot analyzer that, in our hands, produce the most rapid and accurate foci counts.

23. Turn on both the computer and CTL machine.
24. Open the CTL Switchboard and select the 'Scan' function.
25. Select 'Full plate scan'.
26. Under 'Dashboard', ensure the correct filepath and plate setting.
    a. The '96 well BD Falcon' setting can be used for most FFAs.
27. Load and name the plate.
28. Start the scan, confirm that the CTL machine can correctly identify the A1, A12, and H1 wells, and allow the images to be collected.
29. After the scan has completed, return to the CTL Switchboard.
30. Select the 'Count' function.
31. Select 'SmartCount'.
32. Find the file folder containing the plate that was just scanned/imaged and load the plate(s) into the autocount queue.
33. Select a few wells with clear, distinct foci. Adjust the parameters of the spot count, giving special consideration to the appropriate gate size, background balance, and spot separation to yield an accurate count.
    a. It may be necessary to adjust parameters using a manually counted well or series of wells.
34. Once the appropriate parameters are selected, start the autocount.
35. After the autocount has completed, return to the CTL Switchboard.
36. Select the 'Quality Control' Function.
37. Find the file folder containing the plate that was just counted and load the plate(s) into the quality queue.
    a. Quality control functions of the CTL Elispot should be used to manually correct aberrant counts, remove false spots/hits, and, if necessary, re-count wells with different parameters.
    b. Parameters should be determined/adjusted in the same manner as the original autocount.
38. Titration should be based on wells with individually discernable foci.

EXPECTED OUTCOMES

Once a sample has been sufficiently diluted, individual foci should be visible and countable in the well. For determination of viral titer, the researcher should utilize the dilution that yields a suitable number (between 20–120) of distinct foci.

QUANTIFICATION AND STATISTICAL ANALYSIS

For quantification of neutralizing antibodies at a given serum dilution, use the following formula:

$$\left(\frac{(\#\ of\ foci\ rep\ 1 + \#\ of\ foci\ rep\ 2)}{2} \div \#\ of\ foci\ in\ PBS\ control\right) \times 100 = \%\ POWV\ inhibition$$

Alternatively, the reduction in foci can also be subtracted from 100 to give the '% POWV infection'. Serum serial dilutions should then be log transformed. In GraphPad Prism (v9), Python, R, etc., perform a nonlinear regression (curve fit) for a 'log(agonist) vs. response, variable slope (four parameters) analysis, with constraints set to top equal to 100 and bottom equal to 0. This analysis can also be used to find the EC_{50} and EC_{90} values, or the reciprocal dilution of serum required to obtain 50% or 90% neutralization, respectively.

LIMITATIONS

All focus forming assays rely on antibody binding for the detection of viral antigen within infected cells. The assay is therefore highly reliant on the quality and specificity of the antibody for the viral antigen being detected. Researchers should take care in selecting the primary antibody being

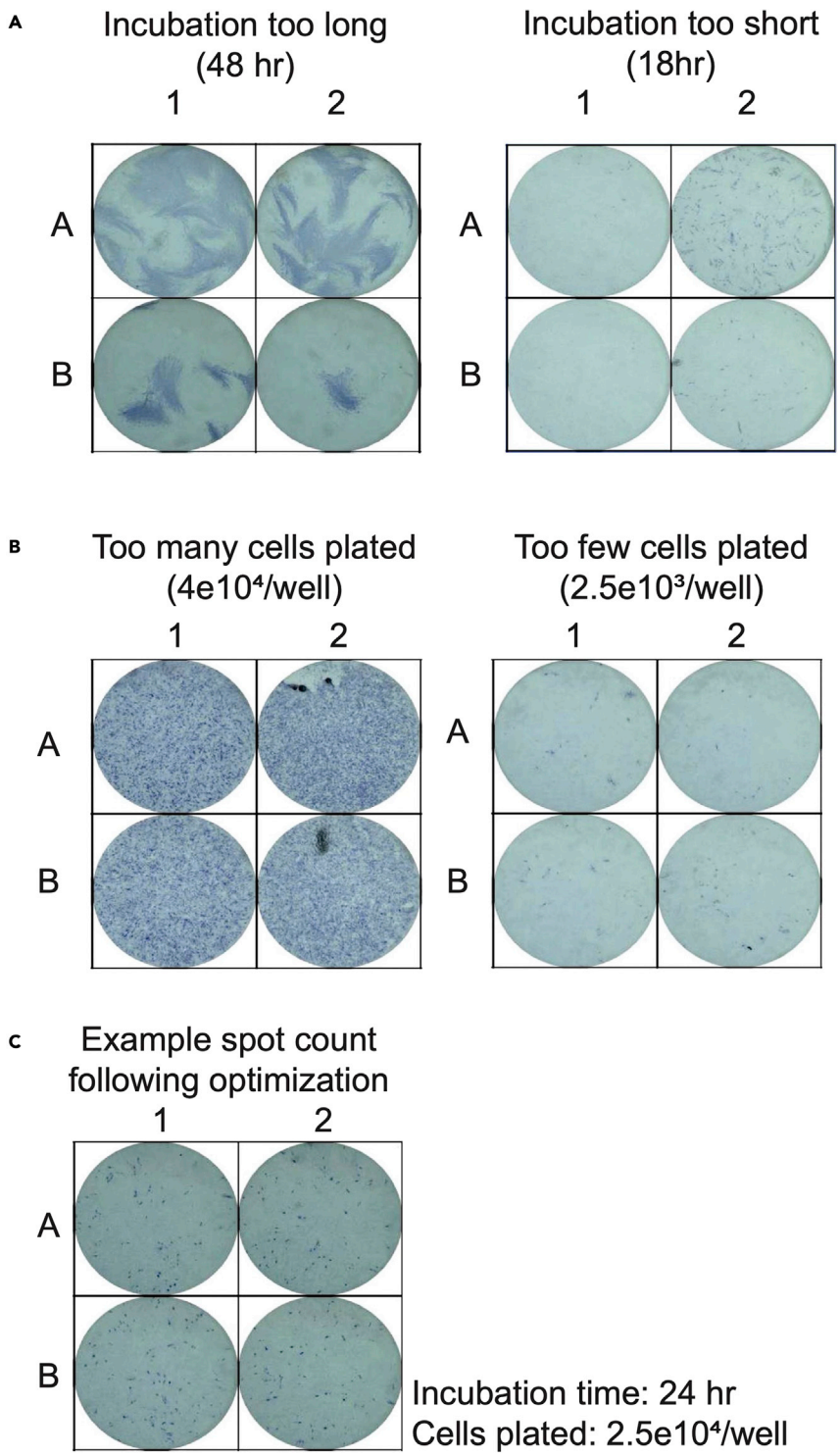

Figure 2. Common Powassan virus focus forming assay issues

Representative images of focus forming assays performed with lineage 1 Powassan virus LB in duplicate depicting some common issues.

(A) These images show the results of incubation times that are too long (48 h, left) or too short (18 h, right). For incubations that are too long, foci will run together and will not be individually discernable. For incubations that are too short, foci will appear too small for detection, or will not appear at all.

Figure 2. *Continued*
(B) These images show the results of plating cell densities that are too high (4×10^4 cells per well, left) or too low (2.5×10^3 cells per well, right). For plating an excess of cells, background staining or 'stacking' of cells vertically (i.e., not on the cell monolayer) is possible. An excess of cells also increases the likelihood of washes damaging the cell monolayer (well A2). For plating too few cells, gaps in the cell monolayer may be visible, and viral titer will likely appear lower than expected.
(C) Representative image showing a focus forming assay with a cell dilution of 2.5×10^4 cells and 24 h incubation, suitable for viral titer determination, as well as compound screening or neutralizing antibody quantification, resulting in distinct and individually discernible foci.

used. For those using polyclonal serum it is recommended that different dilutions of serum and incubation times and conditions are tested to minimize non-specific binding, which can greatly increase the background and make counting difficult.

TROUBLESHOOTING

Problem 1

Cell plating.

In the cell plating and titration by focus forming assay section step one the addition of an excess of cells, or too few cells, to the 96-well plate before the addition of POWV can result in highly variable or inaccurate titration. Examples of focus forming assays which were conducted on over-confluent or under-confluent plates are shown in Figure 2.

Potential solution

Researchers are encouraged to determine the appropriate cell density and culture conditions for their own cell lines before titrating precious or limited samples.

Problem 2

Organ toxicity.

When titrating by focus forming assay in the cell plating and titration by focus forming assay step, it is possible for organ homogenate to be cytotoxic to the cell monolayer. This may alter the sensitivity of the assay, decreasing the limit of detection, and causing inaccuracy in viral titer determination. This is often the case with organs such as lungs, salivary glands, and livers.

Potential solution

Organ toxicity can be overcome by diluting the organ homogenate (i.e., rather than applying 20 μL of organ homogenate diluted in 180 μL of media (final dilution 1:100), consider diluting 100-fold, then adding 20 μL of the 100-fold dilution to 180 μL of media (final dilution 1:1,000).It is, however, possible that in instances of low viral titer the dilution required to mitigate organ toxicity may exceed the sensitivity of the assay, thus preventing accurate recording of infectious virus.

Problem 3

Incubation times.

In the cell plating and titration by focus forming assay section step seven, the twenty-four-hour incubation step following the methylcellulose overlay is based on the amount of time needed for the POWV lineages to replicate to sufficient levels for foci to be detected. This timing is highly variable among different viruses or even among different strains of the same virus. Examples of focus forming assays which were conducted using excessively long or short incubation times are shown in Figure 2.

Potential solution

Researchers are encouraged to test many incubation times prior to the fixation step according to the cell type, strain, and doubling time of their own cell lines before titrating limited samples. Generally, 24–72 h is sufficient for POWV focus forming assays for either lineage I or lineage II.

Problem 4

Removal of monolayer.

In the cell plating and titration by focus forming assay section and the Immunostaining steps eight, two, four, five, seven and eight, vigorous pipetting or washing can remove the monolayer, leading to lost data or inaccurate reporting of titer results.

Potential solution

Care must be taken when liquid is added to the plates containing the monolayer so as not to scratch the monolayer with the pipet tip or agitate the monolayer too harshly. This will prevent dislodging the cells.

Problem 5

Fibers and hairs.

In the immunostaining and imaging sections, fibers and hairs present during the washing of the assay plates can remain associated with the monolayer and be carried through to the imaging step. The presence of hairs and fibers can cause significant errors if using an automated counting program.

Potential solution

Refrain from using absorbent materials which contain fibers that can be released into the assay and maintain a clean laboratory environment.

RESOURCE AVAILABILITY

Lead contact

Further information and requests for resources and reagents should be directed to and will be fulfilled by the lead contact, Amelia K. Pinto (amelia.pinto@health.slu.edu).

Materials availability

There are restrictions to the availability of the primary detection antibody (polyclonal mouse sera) due to limited supply. We will provide the serum to labs that request it, while our supply lasts. However, as these sera were generated in our lab, and we cannot guarantee that there will be no differences or batch-to-batch variation in different lots of POWV serum. We therefore recommend that researchers seeking a primary detection antibody utilize the cross-reactive Langat virus (LGTV) antibody (clone 10F6, Cat#: NR-40316) available from BEI Resources.

Data and code availability

This study did not generate or analyze neither datasets nor code.

ACKNOWLEDGMENTS

Thanks to M. Mai for edits and feedback. This research was supported in part by the National Institutes of Health, National Institute of Allergy and Infectious Diseases (NIAID): 5R01AI152192-02, 5R01AI137424-03, and F31AI152460-01, and in part by the Department of Defense (award no. PR192269). The funders had no role in study design, data collection and analysis, decision to publish, or preparation of the manuscript.

AUTHOR CONTRIBUTIONS

Experimental conceptualization: all authors; data curation: E.T.S. and A.K.P., formal analysis: E.T.S.; funding acquisition: A.K.P. and J.D.B.; investigation: A.K.P. and E.T.S.; methodology: A.K.P., J.D.B., and E.T.S.; project administration, A.K.P.; resources: all authors; software, A.K.P. and J.D.B.; supervision: A.K.P.; validation: A.K.P.; visualization: A.K.P. and E.T.S.; writing – original draft: A.K.P. and E.T.S.; writing – review & editing, all authors, who reviewed and approved the content and submission of the final manuscript.

DECLARATION OF INTERESTS

The authors declare no competing interests.

REFERENCES

Abdelwahab, K.S., Almeida, J.D., Doane, F.W., and Mclean, D.M. (1964). Powassan virus: morphology and cytopathology. Can. Med. Assoc. J. *90*, 1068–1072.

Anderson, J.F., and Armstrong, P.M. (2012). Prevalence and genetic characterization of Powassan virus strains infecting Ixodes scapularis in Connecticut. Am. J. Trop. Med. Hyg. *87*, 754–759. https://doi.org/10.4269/ajtmh.2012.12-0294.

Brien, J.D., Uhrlaub, J.L., and Nikolich-Žugich, J. (2008). West Nile virus-specific CD4 T cells exhibit direct antiviral cytokine secretion and cytotoxicity and are sufficient for antiviral protection. J. Immunol. *181*, 8568–8575. https://doi.org/10.4049/jimmunol.181.12.8568.

Brien, J.D., Hassert, M., Stone, E.T., Geerling, E., Cruz-Orengo, L., and Pinto, A.K. (2019). Isolation and quantification of Zika virus from multiple organs in a mouse. JoVE, e59632. https://doi.org/10.3791/59632.

Hassert, M., Wolf, K.J., Schwetye, K.E., DiPaolo, R.J., Brien, J.D., and Pinto, A.K. (2018). CD4+T cells mediate protection against Zika associated severe disease in a mouse model of infection. PLoS Pathog. *14*, e1007237. https://doi.org/10.1371/journal.ppat.1007237.

Ebel, G.D., Foppa, I., Spielman, A., and Telford, S.R., 2nd (1999). A focus of deer tick virus transmission in the northcentral United States. Emerg. Infect. Dis. *5*, 570–574. https://doi.org/10.3201/eid0504.990423.

Hassert, M., Harris, M.G., Brien, J.D., and Pinto, A.K. (2019). Identification of protective CD8 T cell responses in a mouse model of Zika virus infection. Front. Immunol. *10*, 1678. https://doi.org/10.3389/fimmu.2019.01678.

Hassert, M., Steffen, T.L., Scroggins, S., Coleman, A.K., Shacham, E., Brien, J.D., and Pinto, A.K. (2021). Prior heterologous flavivirus exposure results in reduced pathogenesis in a mouse model of Zika virus infection. J. Virol. *95*, e00573-21. https://doi.org/10.1128/jvi.00573-21.

Leonova, G.N., Kondratov, I.G., Ternovoi, V.A., Romanova, E.V., Protopopova, E.V., Chausov, E.V., Pavlenko, E.V., Ryabchikova, E.I., Belikov, S.I., and Loktev, V.B. (2009). Characterization of Powassan viruses from far eastern Russia. Arch. Virol. *154*, 811–820. https://doi.org/10.1007/s00705-009-0376-y.

Macpherson, I., and Stoker, M. (1962). Polyoma transformation of hamster cell clones–an investigation of genetic factors affecting cell competence. Virology *16*, 147–151. https://doi.org/10.1016/0042-6822(62)90290-8.

Mandl, C.W., Holzmann, H., Kunz, C., and Heinz, F.X. (1993). Complete genomic sequence of Powassan virus: evaluation of genetic elements in tick-borne versus mosquito-borne flaviviruses. Virology *194*, 173–184. https://doi.org/10.1006/viro.1993.1247.

Osada, N., Kohara, A., Yamaji, T., Hirayama, N., Kasai, F., Sekizuka, T., Kuroda, M., and Hanada, K. (2014). The genome landscape of the African green monkey kidney-derived Vero cell line. DNA Res. *21*, 673–683. https://doi.org/10.1093/dnares/dsu029.

Stone, E.T., Hassert, M., Geerling, E., Wagner, C., Brien, J.D., Ebel, G.D., Hirsch, A.J., German, C., Smith, J.L., and Pinto, A.k. (2022). Balanced T and B cell responses are required for immune protection against Powassan virus in virus-like particle vaccination. Cell Rep. *38*, 110388. https://doi.org/10.1016/j.celrep.2022.110388.

frontiers in Immunology

ORIGINAL RESEARCH
published: 31 August 2021
doi: 10.3389/fimmu.2021.739025

Obesity Enhances Disease Severity in Female Mice Following West Nile Virus Infection

Elizabeth Geerling, E. Taylor Stone, Tara L. Steffen, Mariah Hassert, James D. Brien and Amelia K. Pinto *

Department of Molecular Microbiology and Immunology, Saint Louis University, St. Louis, MO, United States

A rise in adiposity in the United States has resulted in more than 70% of adults being overweight or obese, and global obesity rates have tripled since 1975. Following the 2009 H1N1 pandemic, obesity was characterized as a risk factor that could predict severe infection outcomes to viral infection. Amidst the SARS-CoV-2 pandemic, obesity has remained a significant risk factor for severe viral disease as obese patients have a higher likelihood for developing severe symptoms and requiring hospitalization. However, the mechanism by which obesity enhances viral disease is unknown. In this study, we utilized a diet-induced obesity mouse model of West Nile virus (WNV) infection, a flavivirus that cycles between birds and mosquitoes and incidentally infects both humans and mice. Likelihood for severe WNV disease is associated with risk factors such as diabetes that are comorbidities also linked to obesity. Utilizing this model, we showed that obesity-associated chronic inflammation increased viral disease severity as obese female mice displayed higher mortality rates and elevated viral titers in the central nervous system. In addition, our studies highlighted that obesity also dysregulates host acute adaptive immune responses, as obese female mice displayed significant dysfunction in neutralizing antibody function. These studies highlight that obesity-induced immunological dysfunction begins at early time points post infection and is sustained through memory phase, thus illuminating a potential for obesity to alter the differentiation landscape of adaptive immune cells.

Keywords: obesity, chronic inflammation, viral infection, West Nile virus, neutralizing antibody, vaccination, sex difference

OPEN ACCESS

Edited by:
Michael H. Lehmann, Ludwig-Maximilians-Universität München, Germany

Reviewed by:
Miguel A. Martín-Acebes, Instituto Nacional de Investigación y Tecnología Agroalimentaria (INIA), Spain
Vijay Karkal Hegde, Texas Tech University, United States

***Correspondence:**
Amelia K. Pinto
amelia.pinto@health.slu.edu

Specialty section:
This article was submitted to Viral Immunology, a section of the journal Frontiers in Immunology

Received: *09 July 2021*
Accepted: *09 August 2021*
Published: *31 August 2021*

Citation:
Geerling E, Stone ET, Steffen TL, Hassert M, Brien JD and Pinto AK (2021) Obesity Enhances Disease Severity in Female Mice Following West Nile Virus Infection. Front. Immunol. 12:739025. doi: 10.3389/fimmu.2021.739025

INTRODUCTION

Following the 2009 H1N1 pandemic, a link between obesity and enhanced viral infection severity first came to light. Similarly, amidst the SARS-CoV-2 pandemic, obesity has been cited as a risk factor for SARS-CoV-2 patients to develop coronavirus disease 2019 (COVID-19) (1, 2). Obese COVID-19 patients also have a higher likelihood for requiring hospitalization due to severe symptoms, in addition to a higher mortality rate when compared to healthy weight patients (3, 4). While multiple studies have begun to address the link between obesity and severe disease (5–8), the mechanism by which obesity heightens the likelihood of severe disease outcome is still unclear.

Within the United States, ~72% of adults are overweight, while ~40% are characterized as obese based upon a body mass index greater than or equal to 30 kg/m^2 (9). Half of United States adults are predicted to be obese by 2030 (10). Globally, obesity rates have tripled since 1975 resulting in 1 out of 3 people being currently classified as overweight or obese (11, 12). Rising obesity rates are problematic due to obesity being linked to numerous comorbidities including nonalcoholic fatty liver disease, type 2 diabetes and respiratory distress, as well as being a risk factor for metabolic syndrome (13–15). Further, within the obese state, energy intake often exceeds energy expenditure, resulting in a positive energy balance that can result in fat accumulation. This accumulation can cause adipocyte enlargement, thus interfering with blood supply to adipocytes and inducing a hypoxic state. Hypoxia within adipose tissue can incite necrosis and result in macrophage infiltration, leading to the production of pro-inflammatory cytokines like interleukin-1β (IL-1β) and tumor necrosis factor-α (TNF-α) that contribute to a state of chronic inflammation seen in obese subjects (16, 17).

Retrospective analyses following the 2009 H1N1 pandemic classified obesity as an independent risk factor of severe H1N1 infection outcomes, as a large proportion of hospitalized patients who succumbed to H1N1 infection were obese (18–23). Since the 2009 H1N1 pandemic highlighted the susceptibility of the obese population to severe infection outcomes, numerous laboratories sought to determine if increasing vaccination rates of this high-risk population could mitigate the risk for severe disease. Such studies, predominately done utilizing respiratory viruses, have revealed that obese humans and mice displayed impaired immune responses to vaccination (8, 24–27) and classified obesity as a comorbidity that exacerbates viral disease severity (6, 7, 24, 25, 28–30). To explore the impact of obesity on immune responses over time, we utilized West Nile virus (WNV).

WNV is a positive-sense, single-stranded RNA member of the *Flaviviridae* family (31). WNV cycles between birds and mosquitoes with other infections, including those of humans and mice, being incidental. In humans, WNV infections are commonly asymptomatic but can cause severe illness resulting in encephalitis and meningitis (32). Protection against WNV infection is mediated by humoral and cellular immune responses (33–37). Elevated risk of severe WNV disease is associated with age, diabetes, hypertension, kidney disease and immune deficiencies. As WNV is a neurovirulent virus, severe disease in both humans and mice is associated with dissemination of the virus into the central nervous system (CNS) (33, 38–43).

Here, we show that obesity-associated chronic inflammation dysregulates host immune responses, increasing host susceptibility to severe WNV infection. We identified an early impact of obesity on viral control, where obese female mice have significantly higher viral loads in the CNS and die at a higher rate when compared to non-obese controls. Additionally, this study demonstrates that the impact of obesity on immune cell dysfunction is exacerbated in obese female mice when compared to obese male mice, as highlighted by significant defects in the ability of neutralizing antibodies primed in obese female mice to limit WNV infection. Overall, our data reveal that obesity has an impact early during the course of infection in inducing dysfunctional immunological responses to WNV infection.

MATERIALS AND METHODS

Ethics Statement

All animal studies were conducted in accordance with the National Institutes of Health Guide for Care and Use of Laboratory Animals and approved by the Saint Louis University Animal Care and Use Committee (IACUC protocol 2771).

Virus and Cells

WNV (strain New York 99) was passaged once in Vero cells (African green monkey kidney epithelial cells) purchased from American Type Culture Collection (ATCC CCL-81). Virus was titered *via* focus forming assay (FFA) on Vero cells as previously described (44).

Mice and Viral Infections

Wild type C57BL/6J mice were purchased commercially from Jackson Laboratories and housed in a pathogen-free mouse facility at the Saint Louis University School of Medicine. 3- to 12-week-old mice were fed either a control (wt) or high fat diet (HFD) (40% kcal fat, 20% kcal fructose and 2% cholesterol, Research Diets Inc.) for approximately 12 weeks. Once mice on the HFD weighed 25% more than wild type counterparts, they were considered to be obese (ob). 15- to 30-week-old male and female C57BL/6J mice were infected subcutaneously (SC) *via* footpad injection with 100 FFU of WNV.

Measurement of Liver Enzyme Levels

Serum was collected from naïve wild type and obese mice that had been fed their respective diets for 12 weeks. Serum was diluted 1:2 in PBS and loaded into a sample collection cup for analysis *via* an IDEXX Catalyst One Chemistry Analyzer. An NSAID clip was loaded into the analyzer to measure liver damage based on serum levels of alkaline phosphatase, alanine aminotransferase and aspartate aminotransferase.

Measurement of Circulating Inflammatory Cytokine Levels

Blood from naïve wild type and obese female and male mice that had been fed their respective diets for 12 weeks was collected into RNAzol BD (Molecular Research Center, Inc.: RB 192) and RNA was isolated according to the manufacturer's instructions. mRNA expression of TNF-α, IL-1β and IL-6 was determined through qRT-PCR using Taqman primer probe sets purchased from Integrated DNA Technologies (IDT) based on the following assay identifiers: Mm.PT.58.12575861 (TNF-α), Mm.PT.58.41616450 (IL-1β) and Mm.PT.58.10005566 (IL-6). Relative expression of each cytokine was determined by $2^{\Delta\Delta CT}$ with fold induction being relative to GAPDH (assay identifier: Mm.PT.39a.1) levels of the same samples.

Measurement of Viral Burden

15- to 17-week-old male and female C57BL/6J mice were infected SC *via* footpad injection with 100 FFU of WNV. At 3, 8 and

15 days-post-infection (DPI), intracardiac perfusion with 20 ml of PBS was performed and brains, kidneys, spleens, livers and fat were snap frozen in Sarstedt tubes. Organs were homogenized in DMEM supplemented with 5% FBS using a BeadMill 24 (Fisher Scientific). Infectious viral load was determined by incubating ten-fold serial dilutions of organ homogenate on Vero WHO cell monolayers in 96-well plates. Cells and organ homogenates were incubated for 1 hour at 37°C, then overlaid with 2% methylcellulose diluted in 5% DMEM to prevent indiscriminate viral spread. Cells were then incubated for 24 hours at 37°C prior to being fixed with 5% paraformaldehyde in PBS for 30 minutes at room temperature. Cells were then washed 3x with PBS and permeabilized for 10 minutes in focus forming assay permeability (FFA perm) wash (PBS, 0.05% Triton-X). Foci formed from infected cells were identified by incubating plates with anti-mouse 4G2 (D1-4G2-4-15) (BioXCell), a flavivirus group antibody that binds to the fusion loop of domain II on the envelope protein, at 1 μg/ml for 2 hours at room temperature. Cells were washed 3x with FFA perm wash and incubated for 1 hour at room temperature with a goat anti-mouse horseradish peroxidase-conjugated (HRP) secondary antibody (Sigma) at 5μg/ml. Cells were again washed 3x with FFA perm wash and TrueBlue detection reagent (KPL) was added for visualization of foci of infection. Foci were counted using a CTL Elispot as described in (45). For quantification of viral genome copies, RNA was extracted from organ homogenates using TriReagent RT (Molecular Research Center Inc.: RT111). Viral genome copies were quantified *via* qRT-PCR using Prime-Time primer-probe sets purchased from IDT with the following sequences: Forward: TCAGCGATCTCTCCACCAAAG, Reverse: GGGTCAGC ACGTTTGTCATTG, Probe: TGCCCGACCATGGGAGAAGCTC. Viral genome copies/μl were quantified based on a standard curve generated through dilutions of a flavivirus copy control.

Focus Reduction Neutralization Tests

Mouse serum was diluted 1:10 in PBS, serially diluted 3-fold and mixed with ~100 FFU of WNV. Serum:virus dilutions were incubated for 1 hr at 37°C to allow for immune complex formation. Complexes were then added to Vero WHO cell monolayers in 96-well plates and incubated for 1 hr at 37°C to allow for viral entry into cells. Cells were then overlaid with 2% methylcellulose, and plates were incubated 24 hr at 37°C. Plates were fixed with 5% paraformaldehyde for 30 minutes at room temperature. Plates were then rinsed with PBS and permeabilized for 10 minutes with FFA perm wash. Foci formed from infected cells were detected by incubating cells with α-mouse 4G2 (D1-4G2-4-15) at 1μg/ml for 2 hours at room temperature. Plates were washed 3 times with FFA perm wash and incubated for 1 hr at room temperature with goat α-mouse HRP-conjugated secondary (Sigma) at 5μg/ml. Plates were then washed 3 times with FFA perm wash and foci were visualized through the addition of TrueBlue detection reagent (KPL). Foci were counted using a CTL Elispot. Neutralization curves and $FRNT_{90}$ and $FRNT_{50}$ values were generated in GraphPad Prism 8 though x-axis logarithmic transformation followed by a non-linear curve fit regression analysis.

Statistical Analyses

All statistical analyses were performed using GraphPad Prism 8. Survival curve statistical differences were determined using Mantel-Cox tests. Statistical differences in weight gain, liver enzyme levels, viral burden and neutralizing antibody $FRNT_{90}$ and $FRNT_{50}$ values were determined by Mann-Whitney tests.

RESULTS

Diet-Induced Obese Mice Display Liver Damage and Elevated Inflammatory Cytokine Levels

To determine the impact of obesity on immune responses to WNV, we developed a mouse model of high fat diet induced obesity based on previously published studies (46, 47). Female and male 3-5-week-old C57BL/6J mice were fed either a regular chow diet (wild type) or high fat diet. Mice were considered obese (ob) when they weighed 25% more than wild type (wt) mice, which occurred approximately 12 weeks after initial high fat diet feeding ($p<0.0001$) (**Figure 1A**). As wild type and ob female mice weighed significantly less than their male counterparts ($p <0.0001$ for wild type mice and $p=0.0018$ for obese mice), we separated the mice based on sex. The significant elevation in weight observed in ob female and ob male mice compared to the wild type controls has been shown to be a reasonable surrogate for obesity as determined by elevated BMI in humans (48, 49).

Due to diet-induced obesity being linked to nonalcoholic fatty liver disease (50, 51), we sought to determine if liver-resident enzyme levels were increased in serum of obese mice. When wild type and obese mice had been fed their respective diets for 12 weeks, serum was collected to measure circulating levels of alkaline phosphatase, alanine aminotransferase and aspartate aminotransferase (**Figures 1B–D**). Obese mice displayed significantly increased alkaline phosphatase (female $p=0.0079$ and male $p=0.0127$), alanine aminotransferase (female $p=0.0079$ and male $p=0.0007$) and aspartate aminotransferase (female $p=0.0079$ and male $p=0.0080$) levels when compared to wild type mice. The elevated liver enzyme levels in the obese mice indicate hepatocyte death due to normally liver-resident enzymes being released into the bloodstream. Importantly, obese liver enzyme levels often fell outside of the normal range for mice as indicated by the dotted lines, suggesting that the high fat diet fed mice exhibited evidence of disease similar to nonalcoholic fatty liver disease seen in humans (52, 53).

Since human obesity is accompanied by chronic inflammation, we also sought to measure circulating inflammatory cytokine levels of the mice in our model. We noted that obese female mice displayed significantly higher TNF-α ($p=0.0043$), IL-6 ($p=0.0303$) and IL-1β ($p=0.0043$) levels when compared to female wild type counterparts (**Figures 1E–G**). Similarly, obese males also displayed significantly higher circulating levels of TNF-α ($p=0.0002$), IL-6 ($p=0.0019$) and IL-1β ($p=0.0499$) when compared to wild type male counterparts (**Figures 1E–G**). Interestingly, wild type females also displayed significantly higher levels of TNF-α ($p=0.0016$) and IL-6 ($p=0.0186$) when compared to wild type males, while obese females displayed significantly higher levels of TNF-α ($p=0.0200$) and IL-1β ($p=0.0127$) when compared to obese males (**Figures 1E–G**). These data highlight that inflammation is generally higher in females than in males, regardless of diet status. Taking together the sex differences

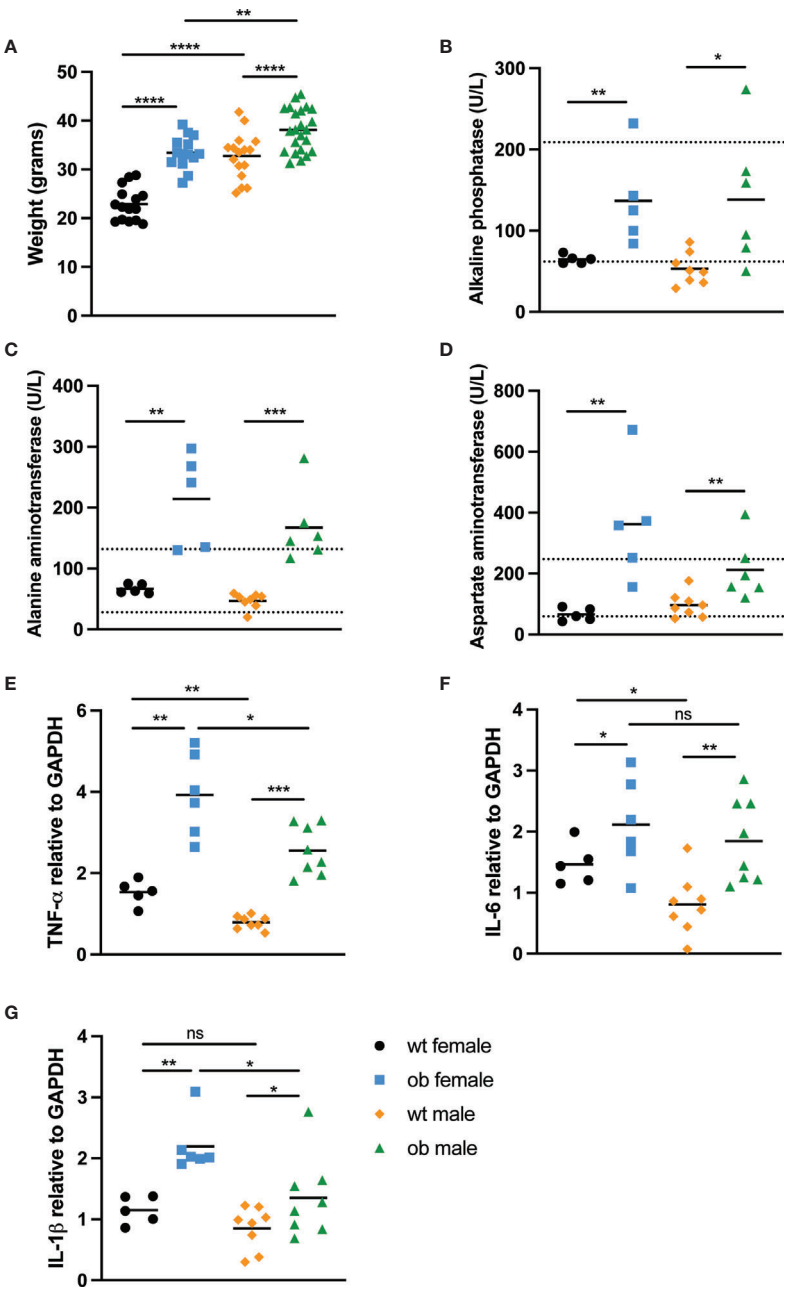

FIGURE 1 | Diet-induced obese mice experience liver damage and have elevated levels of circulating inflammatory cytokines. **(A)** Weights at time of infection. To ensure mice fed the high fat diet were obese prior to infection, female (wt n=28 and ob n=27) and male (wt n=20 and ob n=27) mice were weighed. Both female and male ob mice weighed significantly more than wt counterparts ($p<0.0001$). **(B–D)** Serum liver enzyme levels. Liver function was monitored by measuring serum levels of **(B)** alkaline phosphatase (ALKP), **(C)** alanine aminotransferase (ALT) and **(D)** aspartate aminotransferase (AST) in wt female (n=5), ob female (n=5), wt male (n=8) and ob male (n=6) mice. All liver enzyme levels tested were detected at significantly higher amounts in ob mice when compared to wt mice, and numerous ob mice displayed enzyme levels outside of the normal range for a mouse (as indicated by the dotted lines). When comparing ALKP levels in ob versus wt females, $p=0.0079$, while $p=0.0127$ for ob versus wt males. When comparing ALT levels, $p=0.0079$ for ob versus wt females, while $p=0.0007$ for ob versus wt males. When comparing AST levels, $p=0.0079$ for ob versus wt females, while $p=0.0080$ for ob versus wt males. **(E–G)** Circulating inflammatory cytokine levels. qRT-PCR was used to characterize expression of three inflammatory cytokines, tumor necrosis factor-α (TNF-α), interleukin-6 (IL-6) and interleukin-1β (IL-1β), in the blood of naïve wt and ob female (n=5 and n=6, respectively) and male (n=8 and n=8) mice. In each instance, inflammatory cytokine levels were significantly higher in ob mice when compared to wt counterparts. Additionally, overall, inflammation was higher in female mice when compared to male mice. **(E)** TNF-α expression: $p=0.0043$ for ob versus wt females, $p=0.0047$ for ob versus wt males, $p=0.0080$ for ob females versus ob males and $p=0.0109$ for wt female versus wt males. **(F)** IL-6 expression: $p=0.0303$ for ob versus wt females, $p=0.0045$ for ob versus wt males, $p=0.0533$ for ob females versus ob males and $p=0.0109$ for wt female versus wt males. **(G)** IL-1β expression: $p=0.0303$ for ob versus wt females, $p=0.0499$ for ob versus wt males, $p=0.0127$ for ob females versus ob males and $p=0.0109$ for wt female versus wt males. Statistical significance was determined by Mann-Whitney test. *$p < 0.05$, **$p < 0.01$, ***$P < 0.001$, ****$p < 0.0001$, ns, not significant.

in terms of weight change and inflammation levels, we decided to separate the female and male mice for the remainder of our studies.

Obesity Enhances the Mortality Rate of Female Mice Following WNV Infection

Following the establishment of our obesity mouse model, we sought to test our hypothesis that obese mice would be more susceptible to severe WNV infection. To test this, female and male obese and wild type mice were infected subcutaneously (SC) with 100 focus forming units (FFU) of WNV *via* hind footpad injection. Following infection, the mice were monitored for survival for 30 days. Wild type females exhibited a significantly higher survival rate when compared to obese females with ~73% of wild type females surviving, while only about ~26% of obese females survived (p=0.0132) (**Figure 2A**). The mean time to death (MTD) for the obese females was 10 days post infection (DPI). These findings are consistent with studies done using influenza viral infection models in obese mice (25, 28, 54, 55). However, no significant differences were noted in survival rates between wild type and obese male mice (**Figure 2B**). Wild type females also displayed a 10% greater survival rate than wild type males (**Figures 2A, B**). The disparity between the survival rate of male and female mice was somewhat surprising, although studies in humans have previously noted differences in WNV disease severity between sexes (56, 57).

Obesity Enhances WNV Load in the CNS of Female Mice

Due to the high mortality rate of obese females, we next sought to measure viral titers in various organs previously shown to harbor productive WNV replication (58) to determine if increased viral burden contributed to enhanced mortality rates or altered WNV tissue tropism. To this end, wild type and obese mice were infected SC with 100 FFU WNV. The following organs were collected at 3, 8 and 15 DPI: subcutaneous fat, liver, spleen, kidney and brain. As we noted a significant difference in the survival only with the female mice (**Figure 2**) we separated the analysis of the mice based on the sex of the animals. Virus was quantified both by focus forming assay to detect infectious virus (**Figure 3**), and qRT-PCR to detect WNV genome copies (**Supplementary Figure 1**).

In the periphery, obese females exhibited a slight but significantly higher level of infectious WNV in the liver at each time point post infection (3 DPI p=0.0433, 8 DPI p=0.0238, 15 DPI p=0.0286) (**Figure 3A**). Similarly, the female obese state displayed higher levels of infectious WNV in the spleen at 3 DPI (p=0.0152) when compared to wild type females, however, no differences in titer were noted at 8 or 15 DPI (**Figure 3B**). The infectious virus was not significantly different in other peripheral sites including fat and kidney at any time point post infection (**Figures 3C, D**). Examination of the WNV genome copies in the peripheral organs showed no differences between the obese and wild type female mice liver and fat titers (**Supplementary Figures 1A, C**), but a slight yet significantly lower amount of viral genome copies was observed in the obese mouse spleens (p=0.0315) and kidneys (p=0.0268) at eight days post infection (**Supplementary Figures 1B, D**). As expected, WNV viral titer data showed no differences in infectious virus or viral genome copies between male wild type and obese mice in any peripheral or CNS organ at any time point tested (**Supplementary Figures 2**, **3**). Overall, these data suggest that the obese state in female mice may contribute to modestly higher viral replication in some peripheral organs with the greatest impact occurring in the liver, but the slight differences in viral titer in the periphery do not appear to explain the stark differences in mortality between the obese and wild type female mice.

As WNV is predominately a CNS disease (59) we hypothesized that the higher mortality observed in the obese females would be associated with higher WNV titers in the brains of these animals. To determine if obesity impacted viral infection in the CNS, we examined WNV viral titer in the brains of the obese and wild type female mice at 3, 8 and 15 DPI (**Figure 4**). We were unable to

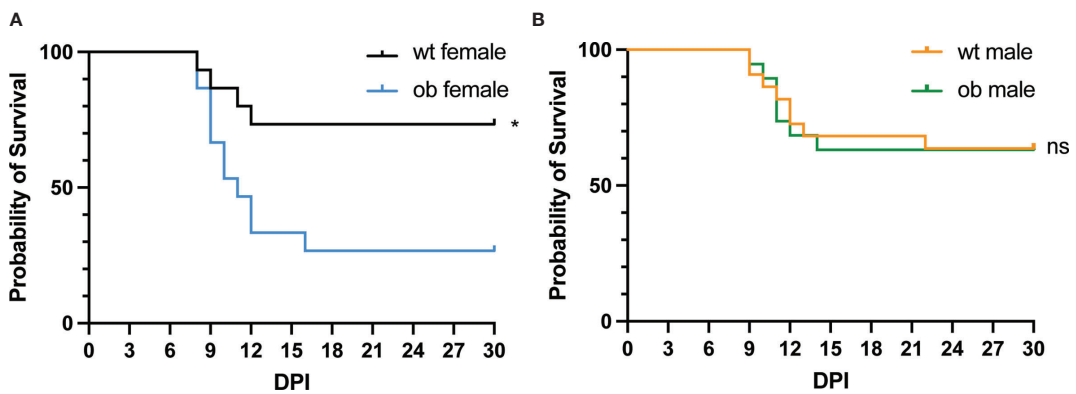

FIGURE 2 | Diet-induced obese mice have enhanced mortality following viral infection. **(A, B)** Survival of mice following WNV infection. Mice were infected with 100 FFU of WNV *via* subcutaneous foot pad injection. **(A)** Wt females (n = 15) displayed a significantly higher survival rate when compared to ob females (n = 15) (p = 0.0132). **(B)** No differences were noted in the survival rates between male wt and ob mice (n = 22 and n = 19, respectively) (p = 0.9559). Survival significance was determined *via* Mantel-Cox test. *p < 0.05, ns, not significant.

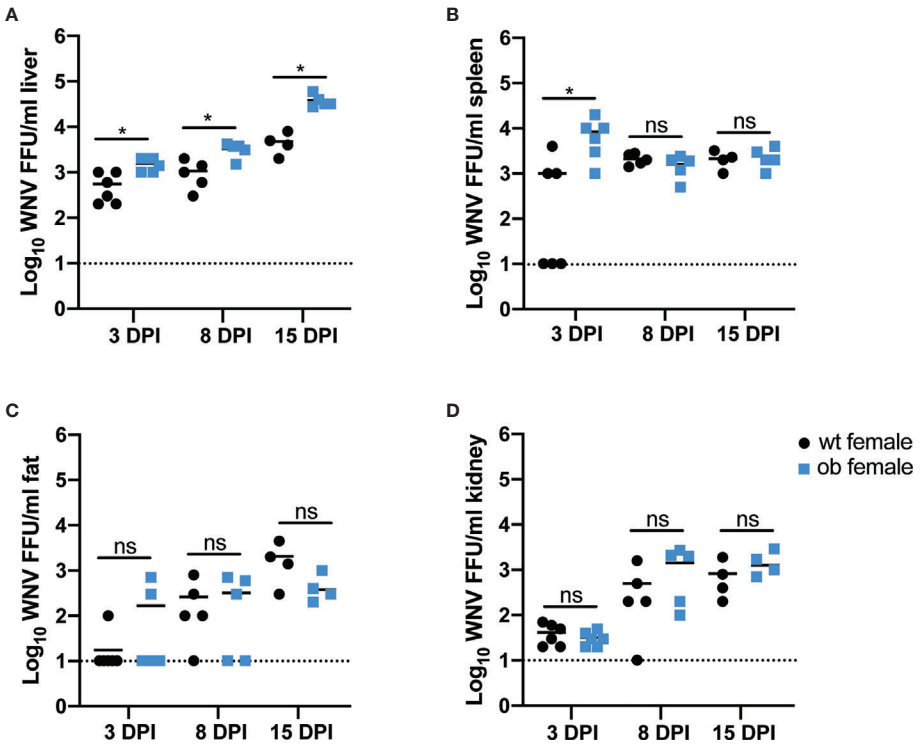

FIGURE 3 | The obese state in females promotes early WNV entry into peripheral organs. **(A–D)** Infectious viral titers in female mouse organs. Mice were infected with 100 FFU of WNV *via* subcutaneous foot pad injection. At 3 (wt n=6 and ob n=6), 8 (wt n=5 and ob n=5) or 15 (wt n=4 and ob n=4) days post infection, liver **(A)**, spleen **(B)**, fat **(C)** and kidney **(D)** were harvested, frozen and homogenized. Levels of infectious virus were measured *via* focus forming assay and reported as FFU/ml of organ homogenate. Asterisks indicate statistically significant values (*$p < 0.05$) as determined by Mann-Whitney test. ns, not significant.

detect infectious virus and saw no differences in the genome copy numbers between the wild type and obese females at 3 DPI (**Figure 4A**). However, by 8 DPI, obese females had approximately two logs more infectious virus in the brains as compared to the wild type control mice (p=0.0397) (**Figure 4B**). The obese female mice also displayed significantly higher WNV genome copies in the brain at this time point (p=0.0012) (**Figure 4B**). The obese female mice maintained a significantly higher infectious viral titer compared to the controls with a log difference between the two groups in the surviving mice at 15 DPI (p=0.0079) (**Figure 4C**), but there were no differences in the genome copy numbers of WNV in brains between these groups at this time point. Interestingly, the genome copy number in the brains of the wild type animals increased between day 8 and 15 post infection. Importantly, as the MTD for the obese mice is 10 DPI, viral titer in the surviving obese mice decreased suggesting some evidence of effective immune control in the surviving animals.

Obese Females Generate Poorly Functioning Neutralizing Antibodies to WNV

Previous studies have shown that obesity can lead to poor antibody responses following vaccination (25–27, 60–62). Therefore, we hypothesized that the increase in mortality and high viral loads seen in the obese female mice was due in part to defects in the antibody response in the obese WNV infected animals. To test this hypothesis, we analyzed the function of neutralizing antibodies in wild type and obese mice at 8, 15 and 30 DPI through focus reduction neutralization tests (FRNTs), as we described previously (63). Employing the use of FRNTs allowed us to determine the concentration of serum, as a by proxy of neutralizing antibody titer, required to neutralize 90% ($FRNT_{90}$) and 50% ($FRNT_{50}$) of WNV present in the assay. Between male obese and male wild type mice, the percentage of WNV infected cells was slightly elevated at low serum dilutions at 8 and 30 DPI, but as the serum dilution increased, nearly identical infection rates were noted between the two groups (**Supplementary Figures 4A, G**). In addition, both obese and wild type males display similar $FRNT_{90}$ and $FRNT_{50}$ values, suggesting that neutralizing antibodies primed in male obese mice are functional (**Supplementary Figures 4B, C, E, F, H, I**).

At 8, 15 and 30 DPI in the female mice, there is a higher percentage of WNV infected cells for each obese mouse serum dilution tested when compared to the serum dilutions of wild type females (**Figures 5A, D, G**), suggesting that the neutralizing antibodies primed in the female obese state fail to neutralize WNV as robustly as those antibodies primed in wild type females. Further, at each time point tested, $FRNT_{90}$ values are significantly lower in the obese females when compared to the wild type females (8 DPI p=0.0286, 15 DPI p=0.0079, 30 DPI p=0.0021), again highlighting a defect in the quality of

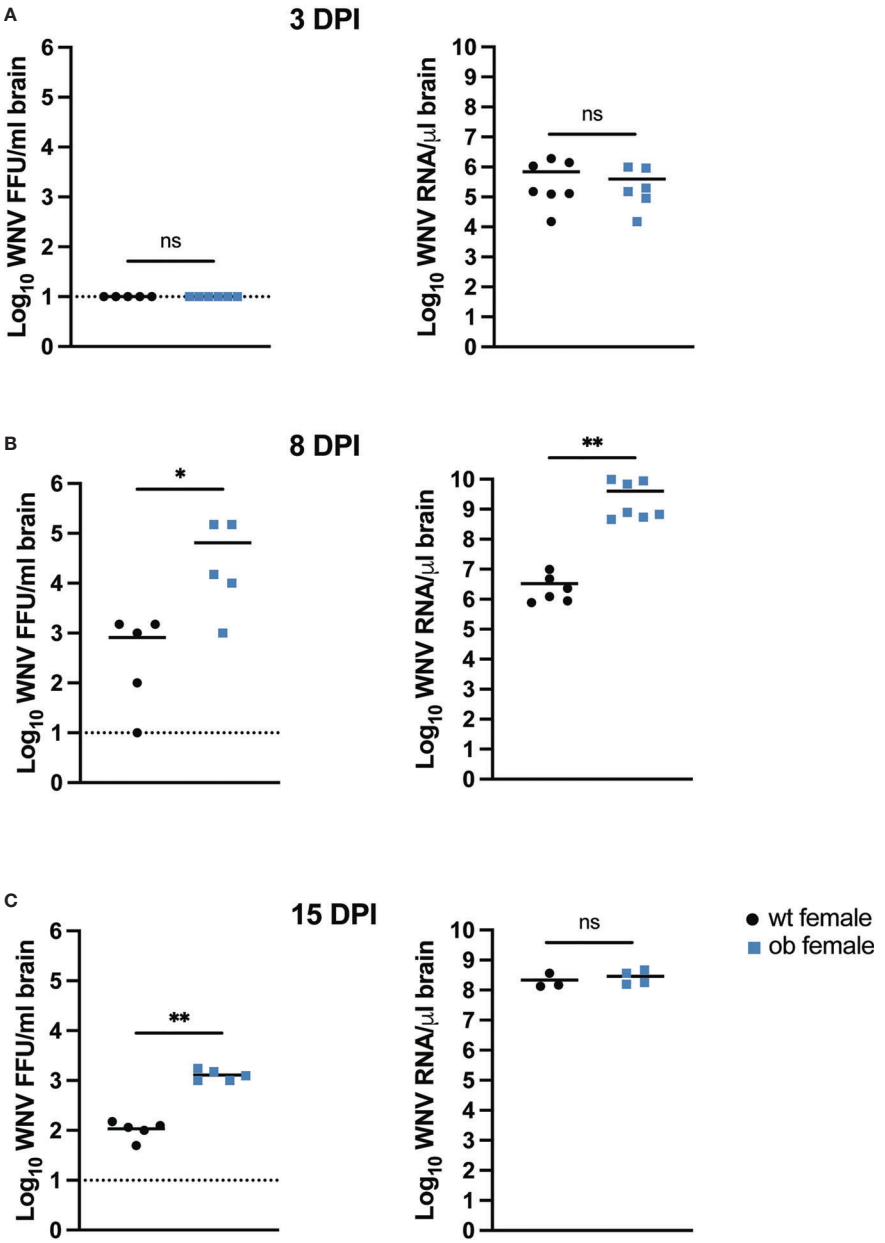

FIGURE 4 | The obese state in female mice promotes heightened viral titers in the brain. **(A–C)** Brain viral titers in female mice. Mice were infected with 100 FFU WNV *via* SC footpad injection and brains were harvested at 3 **(A)**, 8 **(B)** and 15 **(C)** DPI. Brains were homogenized and used to determine infectious titer *via* focus forming assay or RNA was isolated and used for qRT-PCR analysis to determine WNV genome copy numbers based off a copy control. Infectious titer data were reported as WNV FFU/ml and genome copy data were reported as WNV RNA/µl based off GAPDH expression. Asterisks indicate statistically significant values (*$p < 0.05$, **$p < 0.001$) as determined by Mann-Whitney test. ns, not significant.

neutralizing antibodies primed in obese female mice (**Figures 5C, F, I**). Similarly, $FRNT_{50}$ values trend toward being lower in obese females versus wild types at 8 DPI (**Figure 5B**), and these values are significantly lower in obese females at 15 and 30 DPI (15 DPI p=0.0079, 30 DPI p=0.0044) (**Figures 5E, H**). Thus, the neutralizing antibodies primed in the obese females display a reduced neutralization capacity when compared to those primed in the wild type females.

DISCUSSION

With obesity rates rising globally and having links to numerous pathophysiological conditions, we sought to determine if obesity conferred immunological dysfunction in a murine diet-induced obesity WNV infection model. Here we have shown that in female mice, high fat diet feeding induces an obese state that promotes increased mortality, heightened viral titers in the brain,

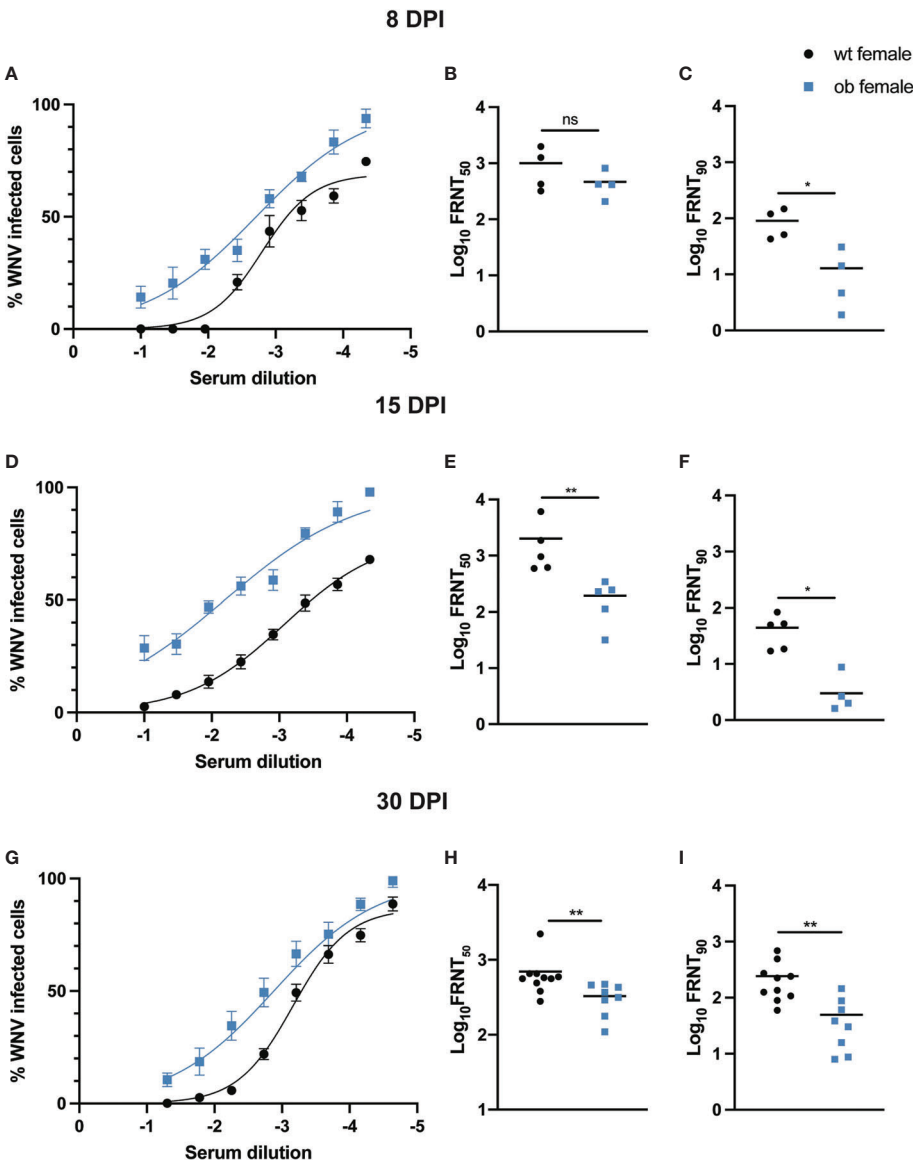

FIGURE 5 | Obese females have poorly neutralizing antibodies to WNV. At 8 (wt n = 4 and ob n = 4), 15 (wt n = 5 and ob n = 5) and 30 (wt n = 10 and ob n = 8) DPI, focus reduction neutralization tests were performed to assess neutralizing antibody function. Neutralization curves at each time point **(A, D, G)** show a higher frequency of infected cells when virus was incubated with serum derived from obese females. Although no differences are noted between FRNT50 values at 8 DPI between wild type and obese animals **(B)**, these values are significantly lower in obese females at 15 and 30 DPI when compared to wild type counterparts **(E, H)**, while FRNT90 values are significantly lower in obese females when compared to wild type at each time point tested **(C, F, I)**. Asterisks indicate statistically significant values (* $p<0.05$, ** $p<0.001$) as determined by Mann-Whitney test. ns, not significant.

and impaired function of neutralizing antibodies. In this report, we primarily focused on the female data as it highlights the most pronounced differences in disease, but current studies are underway in our laboratory to further investigate the interplay between chronic inflammation and sex in altering immune responses to viral pathogens. Interestingly, sex has been cited as a confounding factor in immune responses to viral pathogens with males generally having a higher risk of severe outcomes from respiratory infections at younger and older ages, while females are often at a higher risk for severe viral disease during reproductive years (reviewed in [64]).

We noted a stark difference in survival between wild type and obese females where obese females died at a significantly higher rate than wild type females (**Figure 2A**). The WNV titers in the peripheral organs revealed modest differences between the obese and wild type female mice with elevated titers in the livers and spleens of obese females at various earlier time points post infection (**Figures 3A, B**). These findings are consistent with

other studies exploring the impact of obesity on organ titer in the context of various viral infections (55, 65, 66). As WNV is known to be neuroinvasive (67, 68), we sought to explore a potential role of obesity in altering WNV pathogenesis. Notably, the obese females displayed significantly higher titers in the brains at 8 and 15 DPI when compared to wild type females (**Figures 4B, C**). As shown previously by Brien et al., elevated WNV titers in the brain significantly correlate with mortality from WNV (69). Based on our work and on previous studies in the literature, we can conclude that the significant increase in mortality in the obese mice is due to the elevated viral titers observed.

Numerous studies exploring the effect of diet-induced obesity on vaccination outcomes to various viruses and toxins, including influenza and hepatitis B viruses and tetanus toxin, have highlighted that the titer of neutralizing antibodies primed in the obese state is reduced when compared to the wild type state, and such antibodies wane rapidly (26, 27, 29, 62, 70, 71). These observations highlight a potential defect in the formation of memory B cells within the obese state, a phenomenon that could be detrimental in the context of WNV infection as neutralizing antibodies are essential in reducing viral load amidst WNV infection (33, 72, 73). Previous studies have also shown that WNV specific antibody responses are important for the control of WNV burden in the CNS (33). Thus, we sought to determine if the obese state impacted the function of neutralizing antibodies. As can be seen on the neutralization curves in **Figure 5**, we noted a higher frequency of WNV-infected cells at each dilution tested from female obese mouse-derived serum at all the time points observed. Similarly, when analyzing the $FRNT_{90}$ and $FRNT_{50}$ values, it is evident that a significantly higher amount of female obese mouse-derived serum is required to neutralize 90%, as well as half, of the virus present when compared to serum derived from wild type female mice (**Figures 5B, C, E, F, H, I**), implicating defects in sterilizing immunity within obese females.

Through these studies, we determined that obesity induces immunological dysfunction in a murine diet-induced obesity WNV infection model. We showed that high fat diet feeding in female mice induces an obese state that promotes altered viral pathogenesis, and a decreased neutralization capacity of neutralizing antibodies. The early time points studied throughout these experiments revealed that the obese state impacts the adaptive immune responses at early time points post infection, thus shedding light on the potential for obesity to induce epigenetic changes that alter the differentiation landscape within the obese state. This phenomenon could account for why obesity tends to induce impaired memory responses. Studies to further explore the sex differences noted within our model, as well as to investigate the impact of obesity on epigenetic modification of immune cells, are undergoing.

DATA AVAILABILITY STATEMENT

The original contributions presented in the study are included in the article/**Supplementary Material**. Further inquiries can be directed to the corresponding author.

ETHICS STATEMENT

The animal study was reviewed and approved by the Saint Louis University Animal Care and Use Committee and done in accordance with the Guide for Care and Use of Laboratory Animals.

AUTHOR CONTRIBUTIONS

EG and AP conceptualized the work, wrote and edited the manuscript. EG, AP, JB, ES, TS and MH aided in experimental design. TS and JB aided in FRNT data analysis. Execution of all experiments was performed by EG. AP was responsible for the support of experiments. All authors contributed to the article and approved the submitted version.

FUNDING

This research was supported by the National Institutes of Health grant R0112781495 from the NIAID (NIH.gov) and a Discovery award USAMRDCPR192269 from Department of Defense.

SUPPLEMENTARY MATERIAL

The Supplementary Material for this article can be found online at: https://www.frontiersin.org/articles/10.3389/fimmu.2021.739025/full#supplementary-material

Supplementary Figure 1 | The obese state in females promotes early WNV entry into peripheral organs. **(A–D)** Organ viral titers in female mice. Mice were infected with 100 FFU of WNV *via* subcutaneous foot pad injection. At 3, 8 or 15 days post infection, liver **(A)**, spleen **(B)**, fat **(C)** and kidney **(D)** were harvested, frozen and homogenized. RNA was isolated from organ homogenates and viral genome copies were quantified *via* qRT-PCR using a standard curve to interpolate values based off a copy control. Data were then normalized to GAPDH and reported as WNV genome copies/µl of organ homogenate. Asterisks indicate statistically significant values (*$p<0.05$) as determined by Mann-Whitney test. ns: not significant.

Supplementary Figure 2 | The obese state in males does not impact the timing or replication pattern of WNV in peripheral organs. **(A–D)** Infectious viral titers in male mouse organs. Mice were infected with 100 FFU of WNV *via* subcutaneous foot pad injection. At 3 (wt n=4, ob n=3), 8 (wt n=3, ob n=3) or 15 (wt n=3, ob n=3) days post infection, liver **(A)**, spleen **(B)**, fat **(C)** and kidney **(D)** were harvested, frozen and homogenized. Levels of infectious virus were measured *via* focus forming assay and reported as FFU/ml of organ homogenate. **(E–H)** Organ viral genome copies in male mice. RNA was isolated from organ homogenates of liver **(E)**, spleen **(F)**, fat **(G)** and kidney **(H)** and viral genome copies were quantified *via* qRT-PCR using a standard curve to interpolate values based off a copy control. Data were then normalized to GAPDH and reported as WNV genome copies/µl of organ homogenate. ns: not significant.

Supplementary Figure 3 | The obese state in males does not impact the timing or replication pattern of WNV in the CNS. **(A–C)** Infectious and genome copy viral titers in male mouse brain. Mice were infected with 100 FFU of WNV *via* subcutaneous foot pad injection. At 3 **(A)**, 8 **(B)** or 15 **(C)** days post infection, brains were harvested, frozen and homogenized. Levels of infectious virus were measured *via* focus forming assay and reported as FFU/ml of brain homogenate. To determine genome copy number, RNA was isolated from brain homogenates and viral genome copies were quantified *via* qRT-PCR using a standard curve to interpolate

values based off a copy control. Data were then normalized to GAPDH and reported as WNV genome copies/µl of organ homogenate. ns: not significant.

Supplementary Figure 4 | Obese males have no defects in neutralizing antibody function against WNV. At 8 (wt n=3 and ob n=4), 15 (wt n=4 and ob n=3) and 30 (wt n=11 and ob n=13) DPI, focus reduction neutralization tests were performed to assess neutralizing antibody function. Neutralization curves at 8 and 30 DPI **(A, G)** show a slightly higher frequency of infected cells when virus was incubated with low serum dilutions derived from obese males, but nearly identical levels of infection are ultimately reached as the serum becomes more dilute. $FRNT_{50}$ and $FRNT_{90}$ values are nearly identical at each time point tested between wild type and obese male mice **(B, C, E, F, H, I)**. ns: not significant.

REFERENCES

1. Richardson S, Hirsch JS, Narasimhan M, Crawford JM, McGinn T, Davidson KW, et al. Presenting Characteristics, Comorbidities, and Outcomes Among 5700 Patients Hospitalized With COVID-19 in the New York City Area. *JAMA* (2020) 323(20):2052–9. doi: 10.1001/jama.2020.6775
2. Popkin BM, Du S, Green WD, Beck MA, Algaith T, Herbst CH, et al. Individuals With Obesity and COVID-19: A Global Perspective on the Epidemiology and Biological Relationships. *Obes Rev* (2020) 21(11):e13128. doi: 10.1111/obr.13128
3. Simonnet A, Chetboun M, Poissy J, Raverdy V, Noulette J, Duhamel A, et al. High Prevalence of Obesity in Severe Acute Respiratory Syndrome Coronavirus-2 (SARS-CoV-2) Requiring Invasive Mechanical Ventilation. *Obes (Silver Spring)* (2020) 28(7):1195–9. doi: 10.1002/oby.22831
4. Lighter J, Phillips M, Hochman S, Sterling S, Johnson D, Francois F, et al. Obesity in Patients Younger Than 60 Years Is a Risk Factor for COVID-19 Hospital Admission. *Clin Infect Dis* (2020) 71(15):896–7. doi: 10.1093/cid/ciaa415
5. Smith M, Honce R, Schultz-Cherry S. Metabolic Syndrome and Viral Pathogenesis: Lessons From Influenza and Coronaviruses. *J Virol* (2020) 94 (18):e00665-20. doi: 10.1128/jvi.00665-20
6. Honce R, Schultz-Cherry S. Impact of Obesity on Influenza A Virus Pathogenesis, Immune Response, and Evolution. *Front Immunol* (2019) 10:1071. doi: 10.3389/fimmu.2019.01071
7. Honce R, Karlsson EA, Wohlgemuth N, Estrada LD, Meliopoulos VA, Yao J, et al. Obesity-Related Microenvironment Promotes Emergence of Virulent Influenza Virus Strains. *mBio* (2020) 11(2):e03341–19. doi: 10.1128/mBio.03341-19
8. Kosaraju R, Guesdon W, Crouch MJ, Teague HL, Sullivan EM, Karlsson EA, et al. B Cell Activity Is Impaired in Human and Mouse Obesity and Is Responsive to an Essential Fatty Acid Upon Murine Influenza Infection. *J Immunol* (2017) 198 (12):4738–52. doi: 10.4049/jimmunol.1601031
9. Centers for Disease Control and Prevention. *Obesity and Overweight*. (2020). Available at: CDC.gov.
10. Ward ZJ, Bleich SN, Cradock AL, Barrett JL, Giles CM, Flax C, et al. Projected U.S. State-Level Prevalence of Adult Obesity and Severe Obesity. *N Engl J Med* (2019) 381(25):2440–50. doi: 10.1056/NEJMsa1909301
11. *Global Nutrition Report: Action on Equity to End Malnutrition*. Bristol, UK: Development Initiatives (2020).
12. World Health Organization. *Obesity and Overweight*. (2020). Available at: WHO.int.
13. Pi-Sunyer FX. The Obesity Epidemic: Pathophysiology and Consequences of Obesity. *Obes Res* (2002) 10(S12):97S–104S. doi: 10.1038/oby.2002.202
14. Schelbert KB. Comorbidities of Obesity. *Prim Care* (2009) 36(2):271–85. doi: 10.1016/j.pop.2009.01.009
15. American Heart Association. *Metabolic Syndrome*. (2016). Available at: heart.org.
16. Ellulu MS, Patimah I, Khaza'ai H, Rahmat A, Abed Y. Obesity and Inflammation: The Linking Mechanism and the Complications. *Arch Med Sci AMS* (2017) 13(4):851–63. doi: 10.5114/aoms.2016.58928
17. Nijhuis J, Rensen SS, Slaats Y, van Dielen FMH, Buurman WA, Greve JWM. Neutrophil Activation in Morbid Obesity, Chronic Activation of Acute Inflammation. *Obesity* (2009) 17(11):2014–8. doi: 10.1038/oby.2009.113
18. Morgan OW, Bramley A, Fowlkes A, Freedman DS, Taylor TH, Gargiullo P, et al. Morbid Obesity as a Risk Factor for Hospitalization and Death Due to 2009 Pandemic Influenza A(H1N1) Disease. *PloS One* (2010) 5(3):e9694. doi: 10.1371/journal.pone.0009694
19. Van Kerkhove MD, Vandemaele KA, Shinde V, Jaramillo-Gutierrez G, Koukounari A, Donnelly CA, et al. Risk Factors for Severe Outcomes Following 2009 Influenza A (H1N1) Infection: A Global Pooled Analysis. *PloS Med* (2011) 8(7):e1001053. doi: 10.1371/journal.pmed.1001053
20. Sun Y, Wang Q, Yang G, Lin C, Zhang Y, Yang P. Weight and Prognosis for Influenza A(H1N1)pdm09 Infection During the Pandemic Period Between 2009 and 2011: A Systematic Review of Observational Studies With Meta-Analysis. *Infect Dis (Lond)* (2016) 48(11-12):813–22. doi: 10.1080/23744235.2016.1201721
21. Vaillant L, La Ruche G, Tarantola A, Barboza P, InVS fteita. Epidemiology of Fatal Cases Associated With Pandemic H1N1 Influenza 2009. *Eurosurveillance* (2009) 14(33):19309. doi: 10.2807/ese.14.33.19309-en
22. Thompson DL, Jungk J, Hancock E, Smelser C, Landen M, Nichols M, et al. Risk Factors for 2009 Pandemic Influenza A (H1N1)–Related Hospitalization and Death Among Racial/Ethnic Groups in New Mexico. *Am J Public Health* (2011) 101(9):1776–84. doi: 10.2105/AJPH.2011.300223
23. Venkata C, Sampathkumar P, Afessa B. Hospitalized Patients With 2009 H1N1 Influenza Infection: The Mayo Clinic Experience. *Mayo Clin Proc* (2010) 85(9):798–805. doi: 10.4065/mcp.2010.0166
24. Karlsson EA, Sheridan PA, Beck MA. Diet-Induced Obesity in Mice Reduces the Maintenance of Influenza-Specific CD8+ Memory T Cells. *J Nutr* (2010) 140(9):1691–7. doi: 10.3945/jn.110.123653
25. Karlsson EA, Hertz T, Johnson C, Mehle A, Krammer F, Schultz-Cherry S. Obesity Outweighs Protection Conferred by Adjuvanted Influenza Vaccination. *mBio* (2016) 7(4):e01144–16. doi: 10.1128/mBio.01144-16
26. Park H-L, Shim S-H, Lee E-Y, Cho W, Park S, Jeon H-J, et al. Obesity-Induced Chronic Inflammation Is Associated With the Reduced Efficacy of Influenza Vaccine. *Hum Vaccines Immunother* (2014) 10(5):1181–6. doi: 10.4161/hv.28332
27. Sheridan PA, Paich HA, Handy J, Karlsson EA, Hudgens MG, Sammon AB, et al. Obesity Is Associated With Impaired Immune Response to Influenza Vaccination in Humans. *Int J Obes* (2012) 36(8):1072–7. doi: 10.1038/ijo.2011.208
28. Karlsson EA, Sheridan PA, Beck MA. Diet-Induced Obesity Impairs the T Cell Memory Response to Influenza Virus Infection. *J Immunol* (2010) 184 (6):3127–33. doi: 10.4049/jimmunol.0903220
29. Milner JJ, Sheridan PA, Karlsson EA, Schultz-Cherry S, Shi Q, Beck MA. Diet-Induced Obese Mice Exhibit Altered Heterologous Immunity During a Secondary 2009 Pandemic H1N1 Infection. *J Immunol (Baltimore Md 1950)* (2013) 191(5):2474–85. doi: 10.4049/jimmunol.1202429
30. Gardner EM, Beli E, Clinthorne JF, Duriancik DM. Energy Intake and Response to Infection With Influenza. *Annu Rev Nutr* (2011) 31(1):353–67. doi: 10.1146/annurev-nutr-081810-160812
31. Suthar MS, Diamond MS, Gale M Jr. West Nile Virus Infection and Immunity. *Nat Rev Microbiol* (2013) 11(2):115–28. doi: 10.1038/nrmicro2950
32. Centers for Disease Control and Prevention. *West Nile Virus: Symptoms, Diagnosis, & Treatment*. (2020). Available at: CDC.gov.
33. Diamond MS, Shrestha B, Marri A, Mahan D, Engle M. B Cells and Antibody Play Critical Roles in the Immediate Defense of Disseminated Infection by West Nile Encephalitis Virus. *J Virol* (2003) 77(4):2578–86. doi: 10.1128/JVI.77.4.2578-2586.2003
34. Diamond MS, Sitati EM, Friend LD, Higgs S, Shrestha B, Engle M. A Critical Role for Induced IgM in the Protection Against West Nile Virus Infection. *J Exp Med* (2003) 198(12):1853–62. doi: 10.1084/jem.20031223
35. Shrestha B, Diamond MS. Role of CD8+ T Cells in Control of West Nile Virus Infection. *J Virol* (2004) 78(15):8312–21. doi: 10.1128/JVI.78.15.8312-8321.2004
36. Brien JD, Uhrlaub JL, Nikolich-Zugich J. Protective Capacity and Epitope Specificity of CD8(+) T Cells Responding to Lethal West Nile Virus Infection. *Eur J Immunol* (2007) 37(7):1855–63. doi: 10.1002/eji.200737196
37. Brien JD, Uhrlaub JL, Nikolich-Zugich J. West Nile Virus-Specific CD4 T Cells Exhibit Direct Antiviral Cytokine Secretion and Cytotoxicity and aAe Sufficient for Antiviral Protection. *J Immunol* (2008) 181(12):8568–75. doi: 10.4049/jimmunol.181.12.8568

38. Way JH, Bowen ET, Platt GS. Comparative Studies of Some African Arboviruses in Cell Culture and in Mice. *J Gen Virol* (1976) 30(1):123–30. doi: 10.1099/0022-1317-30-1-123
39. Lanciotti RS, Roehrig JT, Deubel V, Smith J, Parker M, Steele K, et al. Origin of the West Nile Virus Responsible for an Outbreak of Encephalitis in the Northeastern United States. *Science* (1999) 286(5448):2333–7. doi: 10.1126/science.286.5448.2333
40. Roehrig JT, Staudinger LA, Hunt AR, Mathews JH, Blair CD. Antibody Prophylaxis and Therapy for Flavivirus Encephalitis Infections. *Ann NY Acad Sci* (2001) 951:286–97. doi: 10.1111/j.1749-6632.2001.tb02704.x
41. Xiao SY, Guzman H, Zhang H, Travassos da Rosa AP, Tesh RB. West Nile Virus Infection in the Golden Hamster (Mesocricetus Auratus): A Model for West Nile Encephalitis. *Emerg Infect Dis* (2001) 7(4):714–21. doi: 10.3201/eid0704.017420
42. Kleinschmidt-DeMasters BK, Marder BA, Levi ME, Laird SP, McNutt JT, Escott EJ, et al. Naturally Acquired West Nile Virus Encephalomyelitis in Transplant Recipients: Clinical, Laboratory, Diagnostic, and Neuropathological Features. *Arch Neurol* (2004) 61(8):1210–20. doi: 10.1001/archneur.61.8.1210
43. Murray K, Baraniuk S, Resnick M, Arafat R, Kilborn C, Cain K, et al. Risk Factors for Encephalitis and Death From West Nile Virus Infection. *Epidemiol Infect* (2006) 134(6):1325–32. doi: 10.1017/S0950268806006339
44. Brien J, Lazear H, Diamond M. Propagation, Quantification, Detection, and Storage of West Nile Virus. *Curr Protoc Microbiol* (2013) 31:15D.3.1–15D.3.18. doi: 10.1002/9780471729259.mc15d03s31
45. Brien JD, Hassert M, Stone ET, Geerling E, Cruz-Orengo L, Pinto AK. Isolation and Quantification of Zika Virus From Multiple Organs in a Mouse. *J Vis Exp* (2019) (150). doi: 10.3791/59632
46. Kuehm LM, Khojandi N, Piening A, Klevorn LE, Geraud SC, McLaughlin NR, et al. Fructose Promotes Cytoprotection in Melanoma Tumors and Resistance to Immunotherapy. *Cancer Immunol Res* (2021) 9(2):227–38. doi: 10.1158/2326-6066.CIR-20-0396
47. Brockmann GA, Bevova MR. Using Mouse Models to Dissect the Genetics of Obesity. *Trends Genet* (2002) 18(7):367–76. doi: 10.1016/S0168-9525(02)02703-8
48. Parekh PI, Petro AE, Tiller JM, Feinglos MN, Surwit RS. Reversal of Diet-Induced Obesity and Diabetes in C57BL/6J Mice. *Metabolism* (1998) 47(9):1089–96. doi: 10.1016/S0026-0495(98)90283-9
49. Petro AE, Cotter J, Cooper DA, Peters JC, Surwit SJ, Surwit RS. Fat, Carbohydrate, and Calories in the Development of Diabetes and Obesity in the C57BL/6J Mouse. *Metabolism* (2004) 53(4):454–7. doi: 10.1016/j.metabol.2003.11.018
50. Fabbrini E, Sullivan S, Klein S. Obesity and Nonalcoholic Fatty Liver Disease: Biochemical, Metabolic, and Clinical Implications. *Hepatol (Baltimore Md)* (2010) 51(2):679–89. doi: 10.1002/hep.23280
51. Bayard M, Holt J, Boroughs E. Nonalcoholic Fatty Liver Disease. *Am Fam Physician* (2006) 73(11):1961–8.
52. Hariri N, Thibault L. High-Fat Diet-Induced Obesity in Animal Models. *Nutr Res Rev* (2010) 23(2):270–99. doi: 10.1017/S0954422410000168
53. Fock KM, Khoo J. Diet and Exercise in Management of Obesity and Overweight. *J Gastroenterol Hepatol* (2013) 28(Suppl 4):59–63. doi: 10.1111/jgh.12407
54. Milner JJ, Rebeles J, Dhungana S, Stewart DA, Sumner SCJ, Meyers MH, et al. Obesity Increases Mortality and Modulates the Lung Metabolome During Pandemic H1N1 Influenza Virus Infection in Mice. *J Immunol (Baltimore Md 1950)* (2015) 194(10):4846–59. doi: 10.4049/jimmunol.1402295
55. Smith AG, Sheridan PA, Harp JB, Beck MA. Diet-Induced Obese Mice Have Increased Mortality and Altered Immune Responses When Infected With Influenza Virus. *J Nutr* (2007) 137(5):1236–43. doi: 10.1093/jn/137.5.1236
56. Jean CM, Honarmand S, Louie JK, Glaser CA. Risk Factors for West Nile Virus Neuroinvasive Disease, California, 2005. *Emerg Infect Dis* (2007) 13(12):1918–20. doi: 10.3201/eid1312.061265
57. Gubler DJ. The Continuing Spread of West Nile Virus in the Western Hemisphere. *Clin Infect Dis* (2007) 45(8):1039–46. doi: 10.1086/521911
58. Samuel MA, Diamond MS. Pathogenesis of West Nile Virus Infection: A Balance Between Virulence, Innate and Adaptive Immunity, and Viral Evasion. *J Virol* (2006) 80(19):9349–60. doi: 10.1128/JVI.01122-06
59. Halevy M, Akov Y, Ben-Nathan D, Kobiler D, Lachmi B, Lustig S. Loss of Active Neuroinvasiveness in Attenuated Strains of West Nile Virus: Pathogenicity in Immunocompetent and SCID Mice. *Arch Virol* (1994) 137(3):355–70. doi: 10.1007/BF01309481
60. Pellini R, Venuti A, Pimpinelli F, Abril E, Blandino G, Campo F, et al. Obesity May Hamper SARS-CoV-2 Vaccine Immunogenicity. *medRxiv* (2021) 2021.02.24.21251664. doi: 10.1101/2021.02.24.21251664
61. Neidich SD, Green WD, Rebeles J, Karlsson EA, Schultz-Cherry S, Noah TL, et al. Increased Risk of Influenza Among Vaccinated Adults Who Are Obese. *Int J Obes (Lond)* (2017) 41(9):1324–30. doi: 10.1038/ijo.2017.131
62. Eliakim A, Schwindt C, Zaldivar F, Casali P, Cooper DM. Reduced Tetanus Antibody Titers in Overweight Children. *Autoimmunity* (2006) 39(2):137–41. doi: 10.1080/08916930600597326
63. Pinto AK, Richner JM, Poore EA, Patil PP, Amanna IJ, Slifka MK, et al. A Hydrogen Peroxide-Inactivated Virus Vaccine Elicits Humoral and Cellular Immunity and Protects Against Lethal West Nile Virus Infection in Aged Mice. *J Virol* (2013) 87(4):1926–36. doi: 10.1128/JVI.02903-12
64. Ursin RL, Klein SL. Sex Differences in Respiratory Viral Pathogenesis and Treatments. *Annu Rev Virol* (2021) 8(1). doi: 10.1146/annurev-virology-091919-092720
65. Weger-Lucarelli J, Carrau L, Levi LI, Rezelj V, Vallet T, Blanc H, et al. Host Nutritional Status Affects Alphavirus Virulence, Transmission, and Evolution. *PloS Pathog* (2019) 15(11):e1008089. doi: 10.1371/journal.ppat.1008089
66. Moorthy AN, Tan KB, Wang S, Narasaraju T, Chow VT. Effect of High-Fat Diet on the Formation of Pulmonary Neutrophil Extracellular Traps During Influenza Pneumonia in BALB/c Mice. *Front Immunol* (2016) 7:289. doi: 10.3389/fimmu.2016.00289
67. Asnis DS, Conetta R, Teixeira AA, Waldman G, Sampson BA. The West Nile Virus Outbreak of 1999 in New York: The Flushing Hospital Experience. *Clin Infect Dis* (2000) 30(3):413–8. doi: 10.1086/313737
68. Lazear HM, Daniels BP, Pinto AK, Huang AC, Vick SC, Doyle SE, et al. Interferon-Lambda Restricts West Nile Virus Neuroinvasion by Tightening the Blood-Brain Barrier. *Sci Transl Med* (2015) 7(284):284ra59. doi: 10.1126/scitranslmed.aaa4304
69. Brien JD, Uhrlaub JL, Hirsch A, Wiley CA, Nikolich-Zugich J. Key Role of T Cell Defects in Age-Related Vulnerability to West Nile Virus. *J Exp Med* (2009) 206(12):2735–45. doi: 10.1084/jem.20090222
70. Kim Y-H, Kim J-K, Kim D-J, Nam J-H, Shim S-M, Choi Y-K, et al. Diet-Induced Obesity Dramatically Reduces the Efficacy of a 2009 Pandemic H1N1 Vaccine in a Mouse Model. *J Infect Dis* (2011) 205(2):244–51. doi: 10.1093/infdis/jir731
71. Weber DJ, Rutala WA, Samsa GP, Santimaw JE, Lemon SM. Obesity as a Predictor of Poor Antibody Response to Hepatitis B Plasma Vaccine. *JAMA* (1985) 254(22):3187–9. doi: 10.1001/jama.1985.03360220053027
72. Ben-Nathan D, Lustig S, Tam G, Robinzon S, Segal S, Rager-Zisman B. Prophylactic and Therapeutic Efficacy of Human Intravenous Immunoglobulin in Treating West Nile Virus Infection in Mice. *J Infect Dis* (2003) 188(1):5–12. doi: 10.1086/376870
73. Engle MJ, Diamond MS. Antibody Prophylaxis and Therapy Against West Nile Virus Infection in Wild-Type and Immunodeficient Mice. *J Virol* (2003) 77(24):12941–9. doi: 10.1128/JVI.77.24.12941-12949.2003

Conflict of Interest: The authors declare that the research was conducted in the absence of any commercial or financial relationships that could be construed as a potential conflict of interest.

frontiers | Frontiers in Cell and Developmental Biology

ORIGINAL RESEARCH
published: 06 June 2022
doi: 10.3389/fcell.2022.912880

Plasmalogen Loss in Sepsis and SARS-CoV-2 Infection

*Daniel P. Pike[1,2], Reagan M. McGuffee[1,2], Elizabeth Geerling[3], Carolyn J. Albert[1,2], Daniel F. Hoft[3,4], Michael G. S. Shashaty[5,6], Nuala J. Meyer[5,6], Amelia K. Pinto[3] and David A. Ford[1,2]**

[1]Edward A. Doisy Department of Biochemistry and Molecular Biology, Saint Louis University School of Medicine, St. Louis, MO, United States, [2]Center for Cardiovascular Research, Saint Louis University School of Medicine, St. Louis, MO, United States, [3]Department of Molecular Microbiology and Immunology, Saint Louis University School of Medicine, St. Louis, MO, United States, [4]Department of Internal Medicine, Division of Infectious Diseases, Allergy and Immunology, Saint Louis University School of Medicine, St. Louis, MO, United States, [5]Pulmonary, Allergy, and Critical Care Division, University of Pennsylvania Perelman School of Medicine, Philadelphia, PA, United States, [6]Center for Translational Lung Biology, University of Pennsylvania Perelman School of Medicine, Philadelphia, PA, United States

Plasmalogens are plasma-borne antioxidant phospholipid species that provide protection as cellular lipid components during cellular oxidative stress. In this study we investigated plasma plasmalogen levels in human sepsis as well as in rodent models of infection. In humans, levels of multiple plasmenylethanolamine molecular species were decreased in septic patient plasma compared to control subject plasma as well as an age-aligned control subject cohort. Additionally, lysoplasmenylcholine levels were significantly decreased in septic patients compared to the control cohorts. In contrast, plasma diacyl phosphatidylethanolamine and phosphatidylcholine levels were elevated in septic patients. Lipid changes were also determined in rats subjected to cecal slurry sepsis. Plasma plasmenylcholine, plasmenylethanolamine, and lysoplasmenylcholine levels were decreased while diacyl phosphatidylethanolamine levels were increased in septic rats compared to control treated rats. Kidney levels of lysoplasmenylcholine as well as plasmenylethanolamine molecular species were decreased in septic rats. Interestingly, liver plasmenylcholine and plasmenylethanolamine levels were increased in septic rats. Since COVID-19 is associated with sepsis-like acute respiratory distress syndrome and oxidative stress, plasmalogen levels were also determined in a mouse model of COVID-19 (intranasal inoculation of K18 mice with SARS-CoV-2). 3 days following infection, lung infection was confirmed as well as cytokine expression in the lung. Multiple molecular species of lung plasmenylcholine and plasmenylethanolamine were decreased in infected mice. In contrast, the predominant lung phospholipid, dipalmitoyl phosphatidylcholine, was not decreased following SARS-CoV-2 infection. Additionally total plasmenylcholine levels were decreased in the plasma of SARS-CoV-2 infected mice. Collectively, these data demonstrate the loss of plasmalogens during both sepsis and SARS-CoV-2 infection. This study also indicates plasma plasmalogens should be considered in future studies as biomarkers of infection and as prognostic indicators for sepsis and COVID-19 outcomes.

Keywords: sepsis, SARS-CoV-2, plasmalogen, infection, inflammation, lipidomics

OPEN ACCESS

Edited by:
Fabian Dorninger, Medical University of Vienna, Austria

Reviewed by:
Christine Des Rosiers, Université de Montréal, Canada
Jesús Balsinde, Instituto de Biología y Genética Molecular (CSIC), Spain

****Correspondence:***
David A. Ford
david.ford@health.slu.edu

Specialty section:
This article was submitted to Cellular Biochemistry, a section of the journal Frontiers in Cell and Developmental Biology

Received: *05 April 2022*
Accepted: *23 May 2022*
Published: *06 June 2022*

Citation:
Pike DP, McGuffee RM, Geerling E, Albert CJ, Hoft DF, Shashaty MGS, Meyer NJ, Pinto AK and Ford DA (2022) Plasmalogen Loss in Sepsis and SARS-CoV-2 Infection. Front. Cell Dev. Biol. 10:912880. doi: 10.3389/fcell.2022.912880

INTRODUCTION

Sepsis has been a major threat to global health over the past several decades. In the United States, approximately one million individuals are diagnosed with sepsis annually, with mortality estimated between 12 and 25 percent (Mayr et al., 2014; Paoli et al., 2018). An estimated 20 percent of all deaths globally were attributed to sepsis (Rudd et al., 2020). The more severe septic shock has an estimated 38 percent mortality, and half of all Americans who die in the hospital are diagnosed with sepsis (Liu et al., 2014; Vincent et al., 2019). Sepsis occurs when an infection triggers a dysregulated host immune response, leading to systemic microcirculatory and immune dysfunction. This dysregulated inflammatory response in the microvasculature leads to direct damage of cells from reactive oxygen species and other inflammatory mediators, activation of the coagulation cascade, vasodilation, and tissue hypoxia with subsequent mitochondrial dysfunction. This complex system culminates in life-threatening organ injury and metabolic derangements (Chuang et al., 2006; Robertson and Coopersmith, 2006; Galley, 2011; Angus and van der Poll, 2013; Delano and Ward, 2016; Singer et al., 2016; Prauchner, 2017). Lipids and lipid-related signaling pathways have been investigated as mediators, potentially at the blood-endothelial interface during sepsis (Amunugama et al., 2021a). Specific lipids may also have prognostic value as biomarkers in sepsis (Meyer et al., 2017; Mecatti et al., 2018; Mecatti et al., 2020; Wang et al., 2020; Amunugama et al., 2021a). Additionally, a major cause of COVID-19 mortality is sepsis-associated acute respiratory distress syndrome (ARDS). Similar to sepsis, lipids have been investigated as important mediators and biomarkers in COVID-19 (Tanner et al., 2014; Aktepe et al., 2015; Villareal et al., 2015; Jean Beltran et al., 2018; Fernández-Oliva et al., 2019; Sviridov et al., 2020; Casari et al., 2021; Mesquita et al., 2021; Theken et al., 2021).

Plasmalogens comprise a significant fraction of the lipid content in the plasma, immune cells, and endothelium (Chilton and Murphy, 1986; Chilton and Connell, 1988; Kayganich and Murphy, 1992; Murphy et al., 1992; Bräutigam et al., 1996). There is considerable diversity in plasmalogen molecular species. In general, plasmalogens contain either phosphocholine or phosphoethanolamine at the *sn*-3 position of the glycerol backbone. The vinyl ether aliphatic group attached to the glycerol backbone predominantly contains sixteen and eighteen carbon groups. Recently we have also shown neutrophil plasmalogens contain vinyl ether groups that are greater than twenty carbons in length (Amunugama et al., 2021b). Plasmalogens have been suggested to have important roles in biological membranes, which are due, in part, to their unique packing in membranes compared to diacyl phospholipids (Han and Gross, 1990; Han and Gross, 1991). Plasmalogens have been shown to have roles in synaptic fusion, cholesterol efflux, lipid rafts, and transmembrane protein function (Glaser and Gross, 1994; Ford and Hale, 1996; Mandel et al., 1998; Pike et al., 2002). Plasmalogens likely have key roles in inflammation at several levels. Plasmalogens are plasma-borne antioxidants and have been shown to protect endothelium from oxidative stress (Vance, 1990; Zoeller et al., 1999). The vinyl ether bond of plasmalogens is susceptible to attack by reactive species, and this propensity suggests that these lipids can protect cells by scavenging reactive oxygen species (Zoeller et al., 1988; Reiss et al., 1997; Zoeller et al., 1999; Zoeller et al., 2002; Dean and Lodhi, 2018). Additionally, plasmalogens have been shown to have a key role in macrophage phagocytosis (Rubio et al., 2018). Furthermore, plasmalogens are enriched with arachidonic acid and docosahexaenoic acid at the *sn*-2 position, and their metabolism by phospholipases leads to the mobilization of these fatty acids and their subsequent oxidation to bioactive eicosanoids and resolvins (Paul et al., 2019). Collectively, the roles of plasmalogens in membrane molecular dynamics, as antioxidants, and as precursors of bioactive lipids indicate they may be important in inflammation associated with disease and infection.

Plasma plasmalogen levels have been shown to decrease during inflammation such as during endotoxemia (Ifuku et al., 2012), Parkinson's disease (Dragonas et al., 2009; Fabelo et al., 2011), and lupus (Hu et al., 2016). Several of these previous studies (Dragonas et al., 2009; Hu et al., 2016) have suggested the loss of plasmalogens during Parkinson's disease and lupus is due to the associated oxidative stress. Surprisingly only one study has investigated plasmalogen loss during human sepsis, which also attributed plasmalogen loss to oxidative stress (Brosche et al., 2013). This study was limited to measuring dimethyl acetals as a measure of plasmalogen levels and was performed in a limited number of geriatric septic patients. In addition to sepsis, several investigations have emerged over the past 2 years demonstrating plasma plasmalogen levels in humans with severe COVID-19 are decreased (Schwarz et al., 2021; Snider et al., 2021). The loss of plasmalogens and other phospholipids enriched with arachidonic acid and docosahexaenoic acid as well as increased secretory phospholipase A_2 (Snider et al., 2021) in COVID-19 patients support an important role for plasmalogens as precursors of oxylipids.

We have previously shown the plasmalogen vinyl ether bond is targeted by neutrophil-derived HOCl (a product of myeloperoxidase activity) resulting in 2-chlorofatty aldehyde and 2-chlorofatty acid production (Albert et al., 2001; Thukkani et al., 2002; Anbukumar et al., 2010). Furthermore, increased 2-chlorofatty acid plasma levels associate with ARDS-caused mortality in human sepsis (Meyer et al., 2017). 2-Chlorofatty acids are also elevated in the plasma and several organs in rats subjected to cecal slurry sepsis (Pike et al., 2020). Since plasmalogens are the precursors of chlorinated lipid production during sepsis and since limited molecular detail is known about human plasma plasmalogen loss during sepsis, in the present study we have investigated plasma plasmalogen levels in human sepsis patients. Furthermore, we have employed the rat cecal slurry sepsis model to identify both plasma plasmalogen loss as well as changes in liver and kidney plasmalogen levels during sepsis. Lastly, we examined changes in plasmalogen levels in plasma and lung in mice challenged with SARS-CoV-2. Collectively, these studies show the loss of plasmalogens during sepsis and SARS-CoV-2 infection with new detail into changes in plasma molecular species, as well as changes in organs in rodent models of sepsis and COVID-19.

MATERIALS AND METHODS

Human Plasma Specimens and Analysis

Sepsis plasma samples were obtained from subjects admitted to the intensive care unit (ICU) with suspected infection and acute organ dysfunction (sepsis) at day 7 in the ICU. The cohort has been previously described (Reilly et al., 2018). The cohort study is approved by the University of Pennsylvania institutional review board (IRB protocol #808542), and all subjects or their proxies provided informed consent to participate. Control healthy plasma samples were obtained at Saint Louis University under IRB protocol 26646. Plasma samples were stored in aliquots to minimize freeze thaw cycles to two times or less.

Rat Cecal Slurry Studies

Rats were supplied from Envigo (Harlan—Indianapolis, IN, United States). All rats were young adult male Sprague-Dawley weighing between 270–330 g (8–12 weeks old). All animals were maintained in a temperature and humidity-controlled room with a 12 h light/dark cycle and unrestricted access to chow and water. Upon arrival to Saint Louis University, rats were acclimated to the environment for at least a week prior to experiments. All animal experiments were conducted with the approval of the Institutional Animal Care and Use Committee at Saint Louis University. Cecal slurry (CS) was prepared from cecal contents of donor male Sprague-Dawley rats as previously detailed (Pike et al., 2020). Prior to ip CS administration for sepsis studies, aliquots of CS were thawed quickly in warm water. Rats were administered 15 ml/kg CS or 15% glycerol vehicle control (ip) in a total volume of 20 ml/kg, with the remaining 5 ml/kg being sterile saline (B Braun Medical, Bethlehem, PA, United States). At the time of CS administration, animals were administered a concurrent 30 ml/kg dose of subcutaneous sterile saline. Eight hours following CS treatment, 25 mg/kg ceftriaxone (Hospira) in sterile saline was administered intramuscularly in the hind limb in a 1 ml/kg volume. A second subcutaneous 30 ml/kg dose of sterile saline was administered concurrently with the ceftriaxone in order to simulate treatment of human sepsis with crystalloid and antibiotics. 20 h following CS injection, rats were euthanized, and organs were collected, which were immediately frozen on dry ice. Blood was collected *via* cardiac puncture, and plasma was immediately prepared and then stored at −80°C. Plasma preparation and storage was achieved within 30–45 min of the blood draw. Plasma samples were stored in aliquots to minimize freeze thaw cycles to two times or less. Rats were euthanized by injecting 0.5 ml Somnasol (390 mg/ml sodium pentobarbital and 50 mg/ml phenytoin sodium), ip followed by thoracotomy.

Mouse SARS-CoV-2 Infection Studies

K18 mice (JAX strain 034860, human angiotensin converting enzyme 2 (hACE2 transgenic)) were supplied from the Jackson Laboratory (Bar Harbor, MA, United States). All mice were young adult females weighing between 25–30 g (~9 weeks old). All animals were maintained in a temperature and humidity-controlled room with a 12 h light/dark cycle and unrestricted access to chow and water. Upon arrival to Saint Louis University, mice were acclimated to the ABSL-3 environment for at least a week prior to experiments. All animal experiments were conducted with the approval of the Institutional Animal Care and Use Committee at Saint Louis University. K18 mice were either mock infected or infected with 1×10^4 focus forming units (FFU) of the beta variant B.1.351 of SARS-CoV-2 intranasally (20 µl). The beta variant B.1.351 of SARS-CoV-2 was obtained from BEI Resources (#NR55282). Tissues and plasma were collected from euthanized mice three- or 4-days following infection. Tissue homogenates were prepared for analyses of either viral burden, cytokine mRNA, or lipids. SARS-CoV-2 viral burden was measured by focus forming assays (FFAs) using Vero E6 cells transfected with hACE2 and TMPRSS2 as we have previously described (Geerling et al., 2022). Inflammatory cytokine levels were measured *via* qRT-PCR using Taqman primer and probe sets from IDT as previously described (Geerling et al., 2021).

Lipid Analysis

Tissue and plasma lipids were extracted in the presence of internal standards (see **Supplementary Table S1**) by a modified Bligh-Dyer extraction as previously described (Bligh and Dyer, 1959; Maner-Smith et al., 2020; Pike et al., 2020; Amunugama et al., 2021b). Individual choline and ethanolamine glycerophosphospholipids were detected using selected reaction monitoring (see **Supplementary Table S1** for transitions) with an Altis TSQ mass spectrometer equipped with a Vanquish UHPLC System (Thermo Scientific) with isotopomer corrections for each target molecular species compared to the respective internal standard. Lipids were separated on an Accucore™ C30 column 2.1 mm × 150 mm (Thermo Scientific) with mobile phase A comprised of 60% acetonitrile, 40% water, 10 mM ammonium formate, and 0.1% formic acid and mobile phase B comprised of 90% isopropanol, 10% acetonitrile with 2 mM ammonium formate, and 0.02% formic acid. Initial conditions were 30% B with a discontinuous gradient to 100% B at a flow rate of 0.260 ml/min. Plasmalogen molecular species were identified by acid lability and fatty acid aliphatic group identification under identical conditions employed using the TSQ mass spectrometer but using a Q-Exactive mass spectrometer with choline glycerophospholipids detected in negative ion mode.

Statistics

Student's t-test was used to compare two groups in rat CS and K18 mouse SARS-CoV-2 infection studies. Plasma concentrations were compared between healthy control subjects and sepsis subjects by Wilcoxon rank sum test.

RESULTS

Alterations in Plasma Plasmalogen and Diacyl Phospholipids in Human Sepsis

Human geriatric septic patients have previously been shown to have decreased plasma plasmalogen levels as determined by assessing dimethyl acetals of plasmalogens by gas chromatography. These analyses did not identify the lipid class

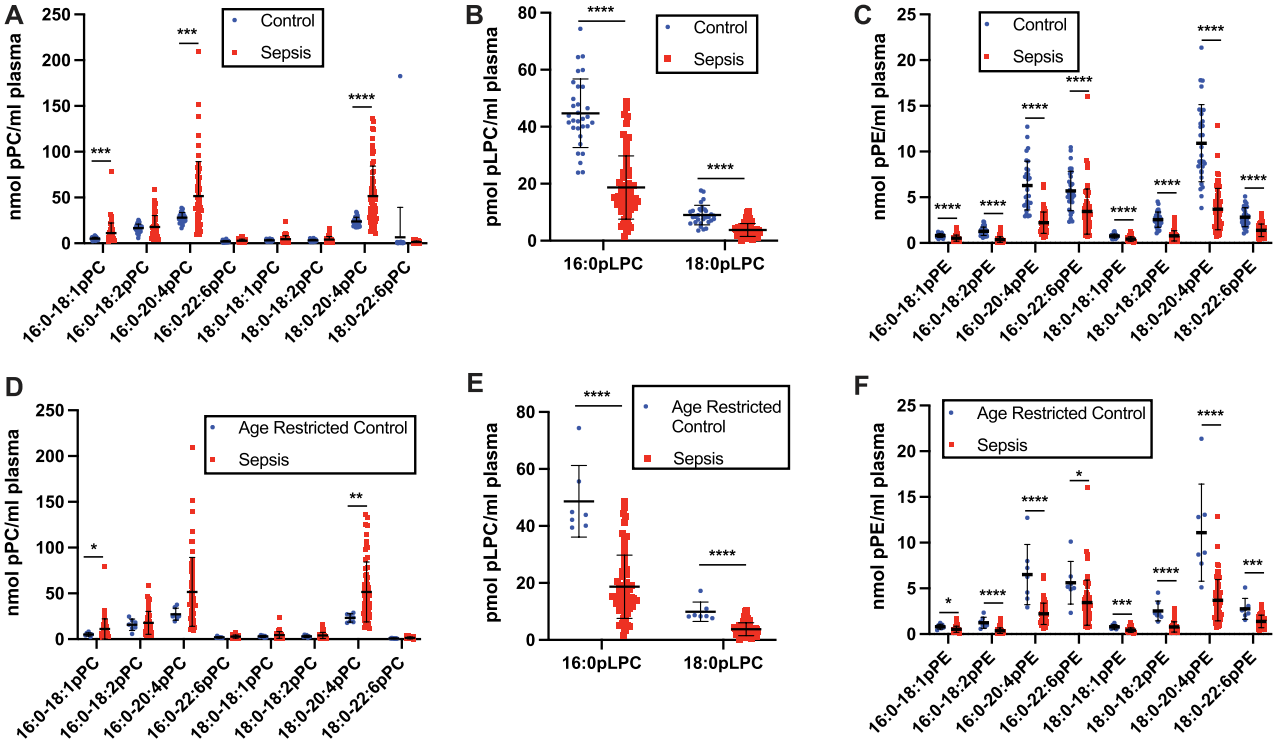

FIGURE 1 | Loss of plasma plasmenylethanolamine (pPE) and lysoplasmenylcholine (pLPC) in human sepsis. Plasma was collected from 31 healthy humans (control) and 63 ICU patients with sepsis following 7 days in the ICU. Lipids were extracted and plasmalogen levels were quantitated as described in "Materials and Methods." Plasma plasmenylcholine (pPC) **(A,D)**, pLPC **(B,E)**, and pPE **(C,F)** are compared between the control and sepsis cohorts **(A–C)** and an age restricted control and sepsis cohorts **(D–F)**. *, **, ***, and **** indicate $p < 0.05$, 0.01, 0.001, and 0.0001, respectively, for comparisons between cohorts. Mean and standard deviation values are indicated for each molecular species and condition.

TABLE 1 | Clinical characteristics of the sepsis and control population.

	Sepsis (*n* = 63)	Controls (*n* = 31)	Age restricted controls (*n* = 7)
Age, years	59.8 ± 12.7	38.2 ± 15.1	56.6 ± 8.4
Female sex (N, %)	25, 39.6%	Not available	Not available
APACHE III score[a]	85 (68, 107)	—	—
Diabetes (N, %)	19, 30.2%		
Solid organ malignancy (N, %)	12, 19%		
Hematologic malignancy (N, %)	20, 31.7%		
Mortality at 30 days (N, %)	17, 27%		

[a]*The acute physiology and chronic health examination (APACHE) III score is displayed as median (interquartile range) due to a skewed distribution.*

(choline or ethanolamine) of the plasmalogen pool or the molecular species that decrease during sepsis. Additionally, we have previously shown plasma 2-chloropalmitic acid levels are increased in human sepsis and associate with ARDS-caused mortality (Meyer et al., 2017). 2-Chloropalmitic acid is derived from 2-chloropalmitaldehyde produced by the action of HOCl targeting the vinyl ether bond of plasmalogens (Albert et al., 2001; Thukkani et al., 2002; Anbukumar et al., 2010). Accordingly, we performed a detailed study of plasma plasmalogens in septic humans. The plasma specimens of patients in this study are from septic patients collected following 7 days in the ICU. The average age of these patients is 59.8 years. Interestingly, data shown in **Figure 1A** show levels of plasma plasmenylcholine (pPC) molecular species either were unchanged or increased in septic patients compared to control subjects. Since the control cohort age was younger than the sepsis group (**Table 1**), we also compared changes in plasma pPC levels between the sepsis cohort and an age restricted subgroup of the control subjects to test a cohort that was more closely aligned in age with the sepsis cohort (**Figure 1D**). A similar pattern of either increased or unchanged levels of pPC was observed in the septic patients compared to the age restricted controls to sepsis. The two pPC

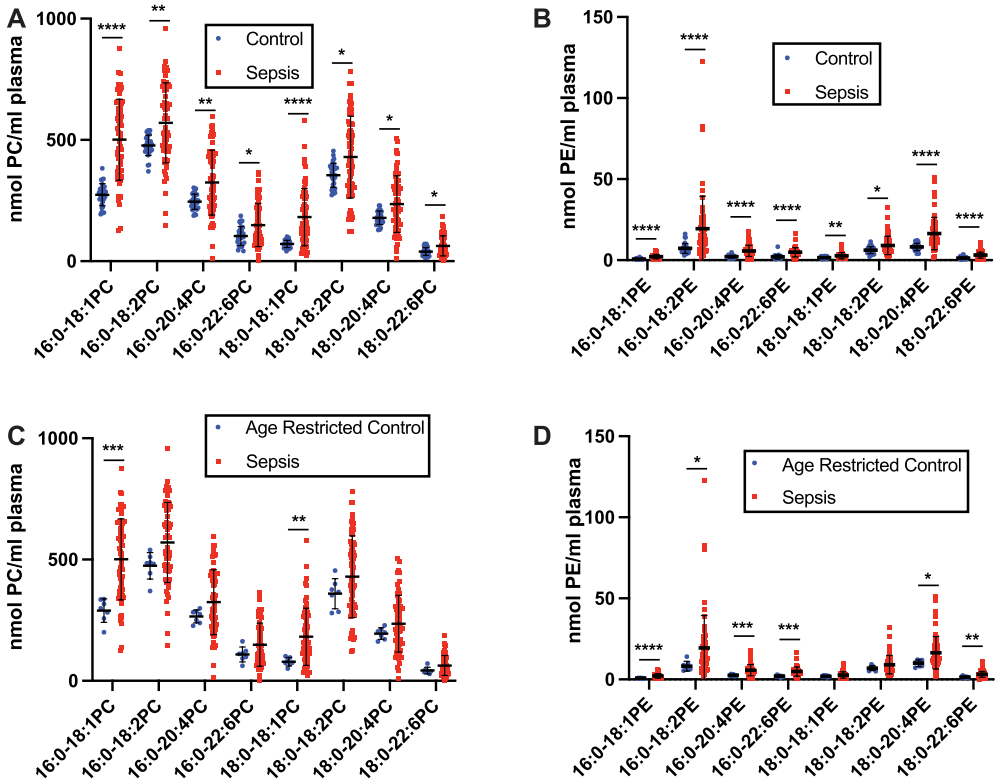

FIGURE 2 | Increases in plasma phosphatidylcholine (PC) and phosphatidylethanolamine (PE) in human sepsis. Plasma was collected from 31 healthy humans (control) and 63 ICU patients with sepsis following 7 days in the ICU. Lipids were extracted and plasmalogen levels were quantitated as described in "Materials and Methods." Plasma PC **(A,C)** and PE **(B,D)** are compared between the control and sepsis cohorts **(A,B)** and an age restricted control and sepsis cohorts **(C,D)**. *, **, ***, and **** indicate $p < 0.05$, 0.01, 0.001, and 0.0001, respectively, for comparisons between cohorts. Mean and standard deviation values are indicated for each molecular species and condition.

molecular species elevated in sepsis were 16:0-18:1 pPC and 18:0-20:4 pPC (x:y-x:y where x# of carbons and y# of double bonds in aliphatic groups at the *sn*-1 and *sn*-2 position, respectively). In contrast, significant decreases were observed with plasma 16:0 and 18:0 lysoplasmenylcholine (pLPC) in septic subjects with comparisons to both the unrestricted control group **(Figure 1B)**, as well as the age restricted control group (**Figure 1E**). Furthermore, all plasma plasmenylethanolamine (pPE) molecular species in our targeted analyses were significantly decreased in the septic patient cohort in comparison to both the unrestricted control group (**Figure 1C**), as well as the age restricted control group (**Figure 1F**). In contrast to pPE, plasma levels of diacyl phosphatidylethanolamine (PE), as well as phosphatidylcholine (PC), were increased in the sepsis cohort in comparisons to both the unrestricted and age restricted cohorts **(Figures 2A–D)**.

Alterations in Plasmalogen and Diacyl Phospholipids in Rodent Sepsis

To gain further insights into alterations in plasmalogens, as well as diacyl phospholipids, during sepsis we examined both plasma and tissue changes in these phospholipids in the cecal slurry (CS) rodent model of sepsis. Previous studies have demonstrated under the CS infection conditions followed by antibiotic treatment 8 h post infection employed in these studies, rats survive at least 20 h and have increased plasma 2-chlorofatty acid levels in comparison to vehicle treated rats (Pike et al., 2020). pPC was identified as the most abundant plasmalogen class in both control and sepsis rat plasma compared to pPE. (**Figures 3A,C**). Plasma plasmalogen loss was observed in CS treated rats compared to vehicle injected rats. Plasma 16:0-18:2, 18:0-18:2, and 18:0-18:1 pPC levels were decreased in septic rats 20 h post infection (**Figure 3A**). Similar to human sepsis, both 16:0 and 18:0 pLPC levels were decreased in septic rats in comparison to control vehicle-treated rats (**Figure 3B**). In contrast to human sepsis, the predominant species of plasma pPE levels were not significantly decreased in rat sepsis, however less abundant species such as 16:0-18:2, 18:0-18:2, and 18:0-18:1 pPE did significantly decrease (**Figure 3C**). For the diacyl species, sepsis resulted in a decrease of only 16:0-20:4 PC in rat plasma (**Figure 3D**). In stark contrast to the drop in plasma pPE levels, all diacyl PE levels were significantly increased (**Figure 3E**).

Previously in this rodent model we identified the kidney and liver as primary sites of organ failure based on loss of permeability barrier function as assessed by Evans blue extravasation (Pike et al., 2020). Additionally, both liver and kidney levels of 2-

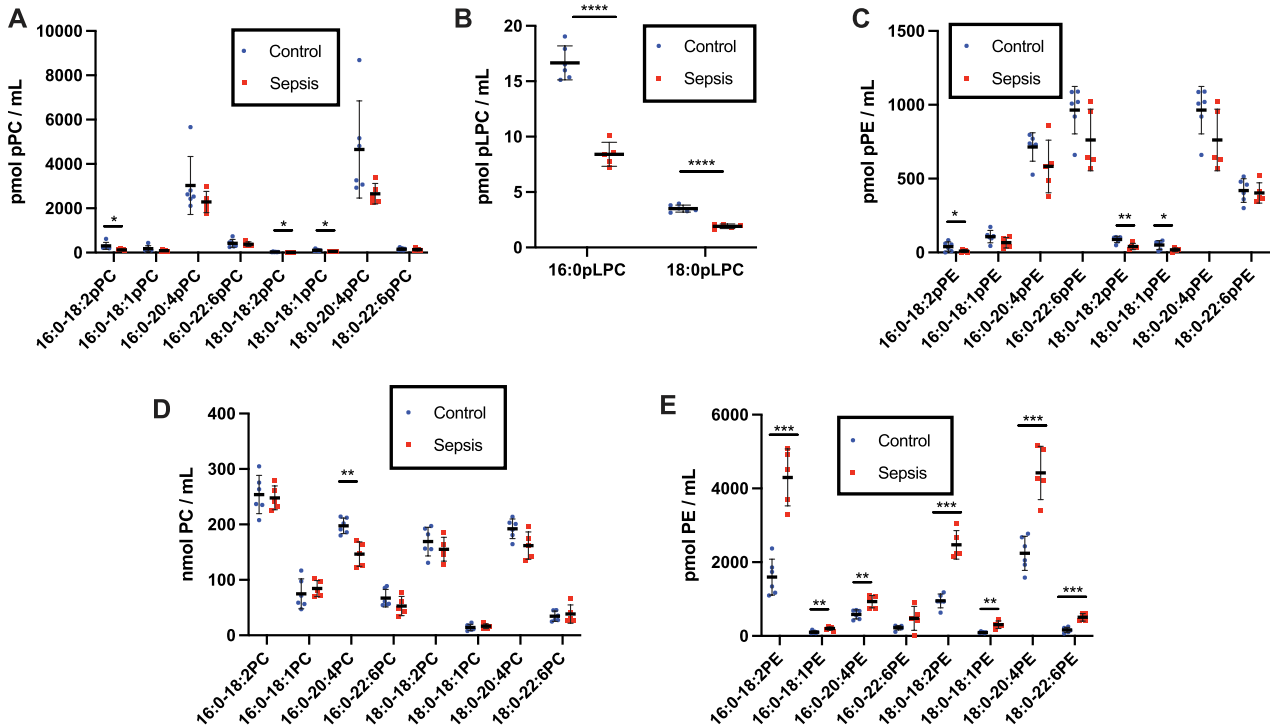

FIGURE 3 | Loss of plasma plasmalogens and increases in diacyl PC and PE in septic rats. Rats were injected with cecal slurry (sepsis) ($n = 5$) or vehicle (control) ($n = 6$) and were subsequently treated with fluid replacement and ceftriaxone 8 h following cecal slurry injection as described in "Materials and Methods." Plasma was collected 20 h following cecal slurry or vehicle treatment, and lipids were extracted. Plasmalogen levels were quantitated as described in "Materials and Methods." Plasma pPC, pLPC, pPE, PC, and PE are shown in **(A–E)**, respectively. *, **, ***, and **** indicate $p < 0.05$, 0.01, 0.001, and 0.0001, respectively, for comparisons between control and septic rats. Mean and standard deviation values are indicated for each molecular species and condition.

chlorofatty acids were previously shown to be increased in this sepsis model (Pike et al., 2020). 2-Chlorofatty acids are produced as a result of neutrophil-derived HOCl targeting plasmalogens (Thukkani et al., 2002; Anbukumar et al., 2010). Accordingly, we examined plasmalogen levels in the kidney and liver of CS infected rats. In contrast to plasma, pPE is the predominant plasmalogen class in both rat kidney and liver compared to pPC (**Figures 4**, **5**). Multiple pPE molecular species in the rat kidney were significantly decreased in septic rats, including the predominant 16:0-20:4 and 18:0-20:4 pPE species (**Figure 4C**). Renal 16:0 pLPC was also significantly decreased in sepsis (**Figure 4B**). Meanwhile, some less predominant renal pPC levels were increased (**Figure 4A**). In contrast to changes in rat plasma and kidney plasmalogens, as well as in human plasma, several liver plasmalogens increased during rat sepsis. All pPC species significantly increased, including the predominant 16:0-20:4 pPC and 18:0-20:4 pPC species, in livers of CS elicited septic rats (**Figure 5A**). 16:0-20:4 pPE and 18:0-20:4 pPE, among others, also were significantly increased in livers from septic rats compared to control rats (**Figure 5C**). Further in contrast to changes in the plasma and kidney, there was no significant difference in pLPC levels in livers from septic rats compared to those of control rats (**Figure 5B**). Diacyl species were measured in the kidney and liver as well. In the kidney, multiple species of diacyl PC and PE were significantly decreased (**Figures 4D,E**). While in the liver, CS-elicited sepsis resulted in increases in both diacyl PC and PE (**Figures 5D,E**).

Plasmalogens in SARS-CoV-2 Infected K18 Mice

Since plasmalogens have been shown to decrease in the plasma of humans with severe COVID-19 (Schwarz et al., 2021; Snider et al., 2021) and SARS-CoV-2 infection leads to a form of sepsis-associated ARDS, we investigated the role of airway infection with SARS-CoV-2 in K18-hACE2 transgenic mice. The human keratin 18 promoter (K18) in K18 mice directs human ACE2 expression in the epithelium, which is important as SARS-CoV-2 infections tend to begin in airway epithelia. Three days following nasal inoculation with SARS-CoV-2 a robust viral burden was observed in the lung (**Figure 6A**), which is similar to findings by others (Zheng et al., 2021). The associated cytokine storm of SARS-CoV-2 infection was confirmed with increases in interleukin-1β (IL-1B), interleukin-6 (IL-6) and tumor necrosis factor-α (TNF-α) mRNA expression in lung tissue (**Figure 6B**). These cytokine mRNAs were not detected in mock-infected lung (data not shown). 16:0-20:4 pPC and 18:0-20:4 pPC levels in the lung were selectively decreased in SARS-CoV-2 infected K18 mice (**Figure 6C**). Additionally, both 16:0-20:4 pPE and 18:0-20:4 pPE, as well as 18:0-22:6 pPE, were decreased in the lung of SARS-

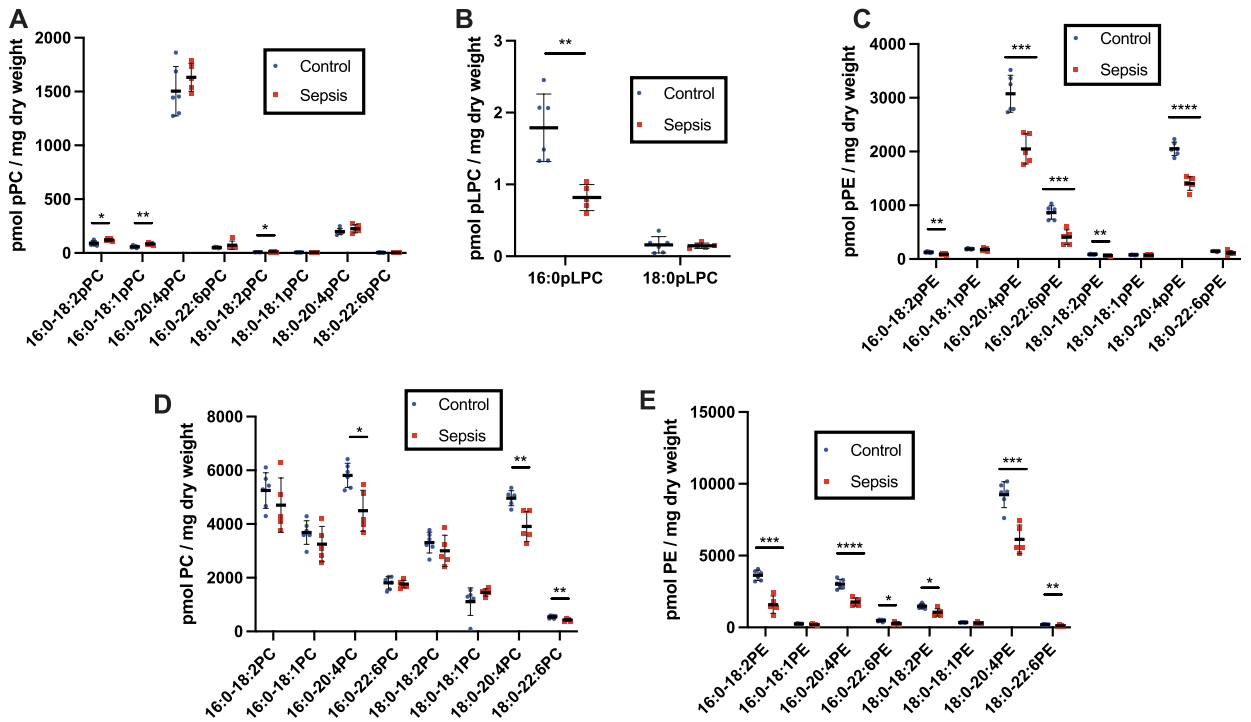

FIGURE 4 | Alterations in kidney diacyl and plasmalogen phospholipids during rat sepsis. Rats were injected with cecal slurry (sepsis) (n = 5) or vehicle (control) (n = 6) as described in **Figure 3**. Kidneys were collected 20 h following cecal slurry or vehicle treatment, and lipids were extracted. Plasmalogen levels were quantitated as described in "Materials and Methods." Kidney pPC, pLPC, pPE, PC, and PE are shown in **(A–E)**, respectively. *, **, ***, and **** indicate $p < 0.05$, 0.01, 0.001, and 0.0001, respectively, for comparisons between control and septic rats. Mean and standard deviation values are indicated for each molecular species and condition.

CoV-2 mice (**Figure 6D**). As in rat tissues, pPE levels were higher than that of pPC in the mouse lung. We also assessed the major lung lipid, 1,2-dipalmitoyl-*sn*-glycero-3-phosphocholine (DPPC) in the lungs, which is the major phospholipid component of surfactant. Lung DPPC levels were not altered in SARS-CoV-2 infected mice (**Figure 6E**). Changes in plasma plasmalogen levels were only modestly decreased in SARS-CoV-2 infected mice (**Figure 6F**).

DISCUSSION

Plasmalogens are a lipid subclass characterized by a vinyl ether linked aliphatic group attached to the *sn*-1 position of glycerol, a fatty acid esterified at the *sn*-2 position and, in general, either phosphoethanolamine or phosphocholine at the *sn*-3 position. The *sn*-2 fatty acid of plasmalogens is enriched with arachidonic acid in many mammalian tissues and thus one role of plasmalogens has been described as a storage depot for arachidonic acid that is released during inflammation (Chilton and Connell, 1988; Ford and Gross, 1989; Braverman and Moser, 2012). The *sn*-1 vinyl ether is a target for reactive oxygen species leading to the release of free fatty aldehydes that subsequently can be metabolized to free fatty acids (Khaselev and Murphy, 1999; Stadelmann-Ingrand et al., 2001). The reaction of reactive oxygen species with the vinyl ether is a terminal event for ROS and thus is considered an antioxidant activity. Multiple studies have shown plasmalogens protect tissues and cells from reactive oxygen species and oxidative stress. Cells deficient in plasmalogens are susceptible to free radical-mediated toxicity (Morand et al., 1988; Zoeller et al., 1988). Furthermore, supplementing cells with precursors to plasmalogens has been shown to protect cells from reactive oxygen species including during hypoxic damage to endothelial cells (Zoeller et al., 1999). Collectively, the abundance of arachidonic acid esterified to plasmalogens that can be mobilized for eicosanoid production and the susceptibility of the vinyl ether to oxidative stress suggest plasmalogens may have important roles in infection and inflammation. Plasma plasmalogen depletion has also been demonstrated in humans with Parkinson's disease, Alzheimer's disease, lupus and endotoxemia (Dragonas et al., 2009; Fabelo et al., 2011; Ifuku et al., 2012; Hu et al., 2016; Su et al., 2019). In the present study we provide further support for the involvement of plasmalogens in inflammation by providing molecular detail to changes in plasmalogen levels both in plasma and in organs during sepsis as well as SARS-CoV-2 infection.

Previous studies showed the 16:0 dimethyl acetal derivative of plasmalogens containing a sixteen-carbon vinyl ether aliphatic group bound to the glycerol backbone are decreased 55% in plasma of twenty geriatric septic patients compared to age-matched healthy subjects (Brosche et al., 2013). In this previous study, data for 18:0 dimethyl acetals were not reported and changes in 16:0 dimethyl acetal were from patient plasma collected within 24 h of severe sepsis diagnosis.

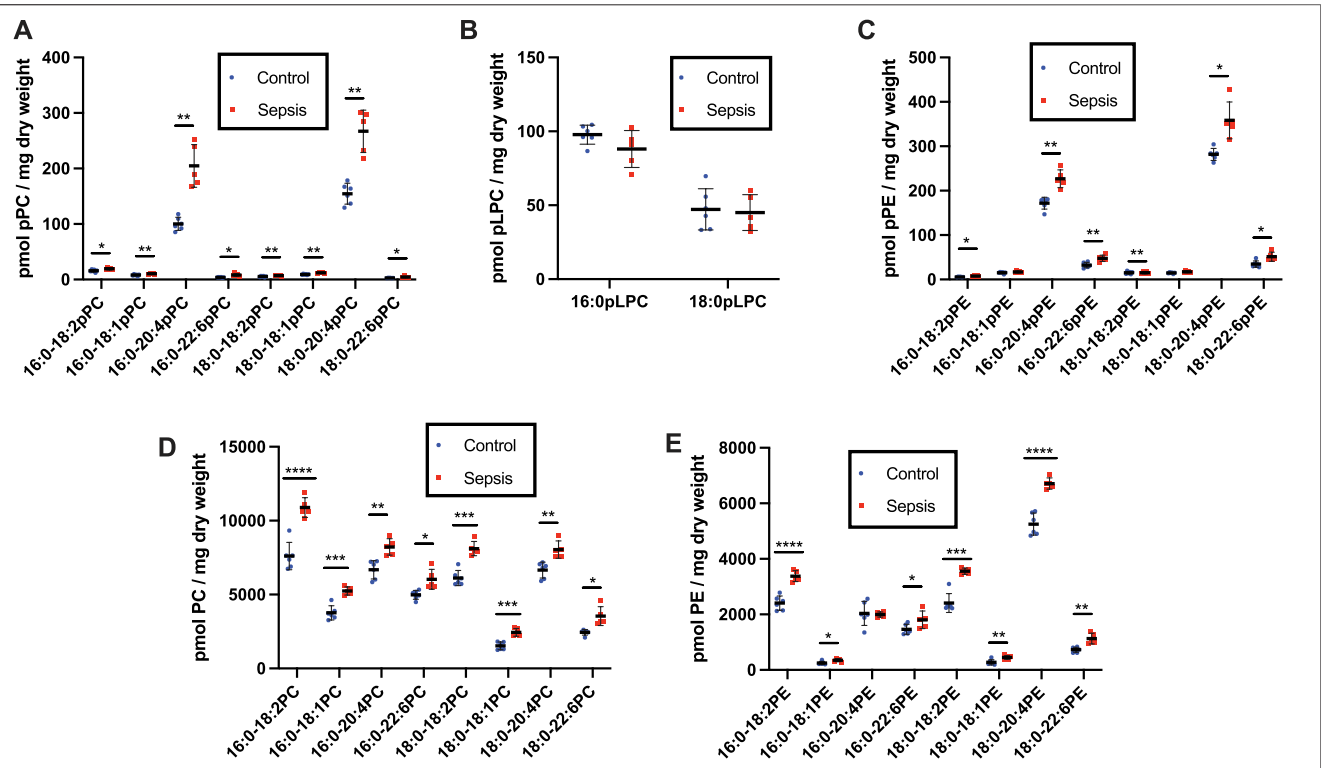

FIGURE 5 | Alterations in liver diacyl and plasmalogen phospholipids during rat sepsis. Rats were injected with cecal slurry (sepsis) ($n = 5$) or vehicle (control) ($n = 6$) as described in **Figure 3**. Liver was collected 20 h following cecal slurry or vehicle treatment, and lipids were extracted. Plasmalogen levels were quantitated as described in "Materials and Methods." Liver pPC, pLPC, pPE, PC, and PE are shown in **(A–E)**, respectively. *, **, ***, and **** indicate $p < 0.05$, 0.01, 0.001, and 0.0001, respectively, for comparisons between control and septic rats. Mean and standard deviation values are indicated for each molecular species and condition.

Human plasma pPC levels are ~8–10 fold greater than pPE levels, and pPC is highly enriched in molecular species containing a sixteen-carbon vinyl ether aliphatic group bound to the glycerol backbone, suggesting the plasma plasmalogens that decreased in geriatric sepsis patients (Brosche et al., 2013) are from pPC pools. In contrast to this previous study, our findings from the MESSI cohort were from patient plasma collected 7d following ICU admission for sepsis. This difference in time for plasma collection prevents direct comparisons to the previously reported study (Brosche et al., 2013). However, in the present studies pPE molecular species containing 16:0 vinyl ether groups, as well as 16:0 pLPC, were decreased in the human sepsis cohort. Plasma pPE species containing 18:0 vinyl ether groups were also significantly decreased in septic subjects investigated in our study. Future studies should be directed at determining details of plasmalogen loss at 24 h and examine longitudinal changes in plasmalogen loss. It will also be interesting to compare changes in human plasmalogen molecular species at 24 h to the changes we observed in the rat plasma plasmalogen molecular species that changed 20 h post CS injection. Interestingly with rat sepsis, plasma plasmalogen loss at 20 h decreased in several pPC and pPE species as well as pLPC. A summary of levels of plasmalogen and diacyl species shows a general downward trend in plasmalogen levels in sepsis, excluding livers from of septic rats (**Figure 7**). In particular, this summary highlights the many differences in changes elicited during sepsis between plasmalogen and diacyl phospholipid levels depending on the tissue and particular phospholipid class. One of the more striking observations is the loss of pPE in plasma in contrast to increases in diacyl PE during sepsis in both humans and rats.

The mechanisms responsible for plasma pLPC and pPE loss during sepsis are not known, but several mechanisms seem likely. One mechanism is that loss of plasmalogen is due to oxidative stress during sepsis. We have previously shown plasma 2-chlorofatty acid levels are elevated in human sepsis (Meyer et al., 2017; Amunugama et al., 2021b). Furthermore, in this rat sepsis model there are increased levels of 2-chlorofatty acid levels (Pike et al., 2020), which is derived from plasmalogens (Albert et al., 2001; Thukkani et al., 2002; Amunugama et al., 2021b). During sepsis the tissue plasmalogen pool or the specific plasmalogen molecular species targeted by HOCl has not been determined. In this respect it could be speculated that the impressive loss of plasma pLPC, which is overall a small pool of the total plasmalogen, could be responsible for the nanomolar levels of 2-chlorofatty acid observed during sepsis. It is also possible that the loss of plasmalogens is due to the activation of phospholipases. It has been suggested that phospholipase A_2-mediated release of arachidonic acid from plasmalogens is important in the production of oxylipids in COVID-19

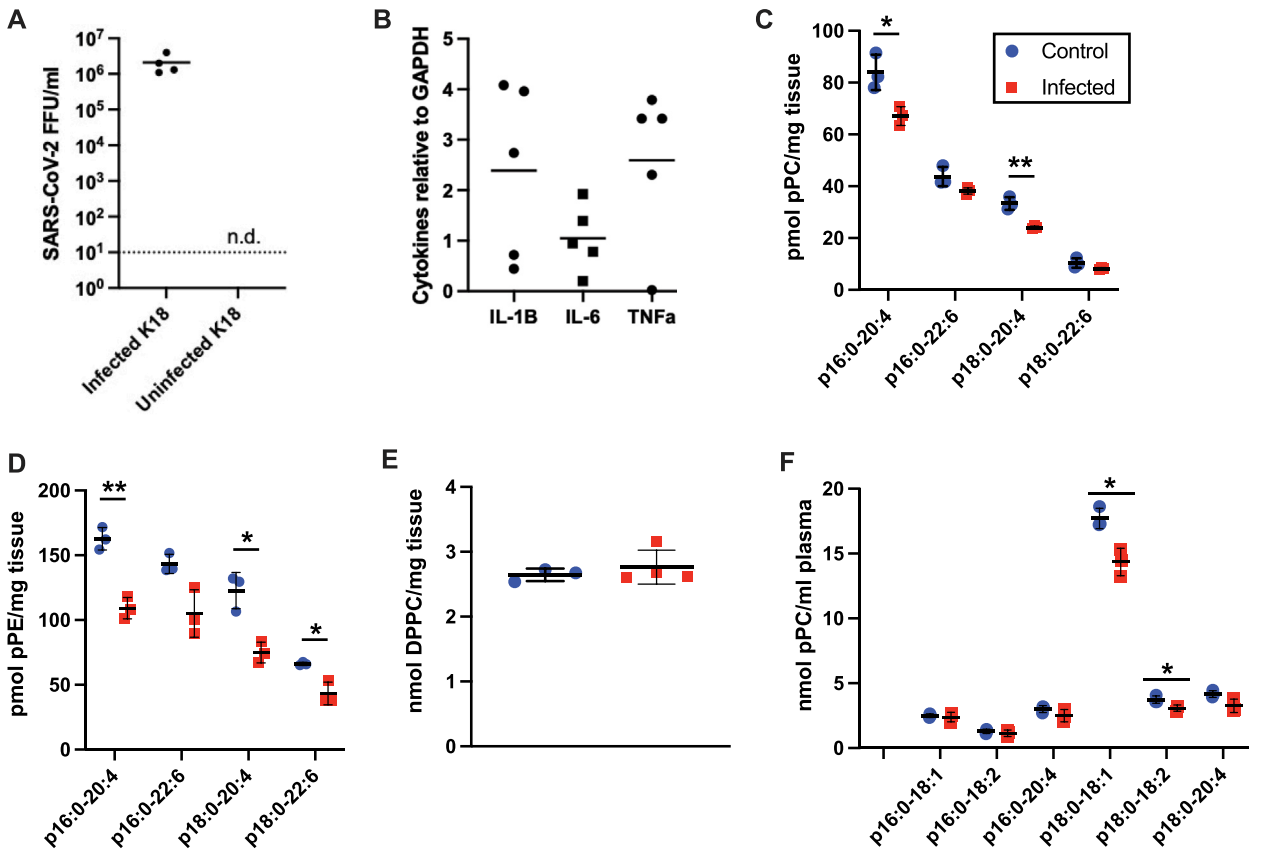

FIGURE 6 | Plasmalogen changes in K18 mice infected with the beta B.1.351 SARS-CoV-2 variant. K18 mice were either mock infected (blue circles) or infected (red squares) with 10^4 FFU of SARS-CoV-2, 20 ul, IN. 3 days post infection, lungs **(C–E)** and plasma **(F)** were collected for lipidomics analyses ($n = 3$ for both conditions). *, **, and *** indicate $p < 0.05$, 0.01, and 0.001, respectively, for comparisons between mock and virus infected mice. **(A)** SARS-CoV-2 titers in lungs of infected ($n = 4$) and uninfected ($n = 4$) mice from this study. N.d. indicates titers were not observed in the uninfected lungs. **(B)** Pro-inflammatory cytokine mRNA was detected in the infected lungs ($n = 4$ or 5) but were not detected in the uninfected lungs. Mean and standard deviation values are indicated for each molecular species and condition.

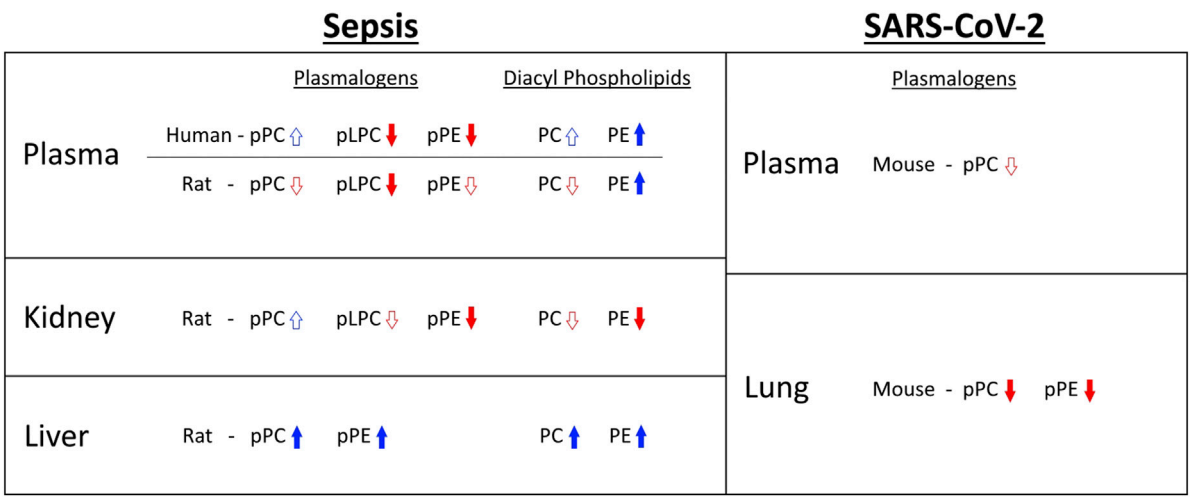

FIGURE 7 | Summary of plasmalogen and diacyl phospholipid changes observed in sepsis and SARS-CoV-2 infection. Arrow outlines indicate that fewer than half of reported species show statistically significant increase or decrease. Solid arrows indicate that at least half of reported species show statistically significant increase or decrease. For human sepsis, only trends in age restricted data are shown.

(Schwarz et al., 2021; Snider et al., 2021). The phospholipase A_2 mechanisms may be directly responsible for pPE loss. It is also possible pLPC loss is due to either accelerated use as an acceptor by acyltransferases leading to conserved levels of pPC despite putative oxidative loss or tissue uptake during sepsis. Another possibility is pPE and pLPC decrease as a result of reduced release from the liver and vascular endothelium. In human sepsis, HDL-cholesterol decreases (Vavrova et al., 2016; Tanaka et al., 2019), which may also be due to decreased secretion from the liver. Decreased plasma plasmalogens and increased liver plasmalogens during sepsis are similar to plasmalogen changes in *H-Lrpprc* mice, a mouse model of the monogenic form of the mitochondrial disease, Leigh syndrome (Ruiz et al., 2019). In *H-Lrpprc* mice, hepatic *Far1* and *Agps* are also elevated suggesting decreased plasma plasmalogen levels mediate a feedback system to increase liver plasmalogen biosynthesis. Such a feedback system may also be responsible for elevated liver plasmalogen levels in livers during sepsis. It will be interesting in future studies to examine *Agps* and *Far1* as well as differences in the levels of the plasmalogen precursors, alkyl ether lipids, in the livers from septic and control rats.

The possibility that pLPC is a circulating precursor to enrich plasmalogens in endothelium is intriguing. Plasmalogen enhancement in isolated cell studies protects cells from oxidative stress (Zoeller et al., 1999). Additionally, several studies have investigated plasmalogen precursors as a potential treatment in inflammatory diseases (Bozelli and Epand, 2021; Paul et al., 2021). Enhancing plasmalogen levels is difficult since dietary consumption of plasmalogens is reduced due to the acidic environment of the gastrointestinal tract. Using acid-stable precursors such as alkyl ether lipids will raise plasmalogen levels over time following desaturation of the alkyl ether bond to the vinyl ether. However, under acute conditions such as sepsis, the conversion of an alkyl ether to plasmalogens likely will be very slow. On the other hand, circulating pLPC already has the vinyl ether bond and lysolipids are rapidly incorporated into cells. It will be important in the future to determine the source of circulating pLPC under physiological conditions as well as during sepsis. It could be envisaged that pLPC is a product of lipoprotein-associated pPC hydrolysis by either secretory phospholipase A_2 or lipoprotein lipase. During sepsis pLPC levels potentially are dependent on a combination of oxidation of pPC or pLPC and pPC hydrolysis. Finally, the role of pLPC during sepsis needs to be further considered as a biomarker of outcomes. Similarly, the role of other plasmalogens, as well as the relationship of plasma plasmalogen levels with changes in plasma 2-chlorofatty acid levels, need to be considered as outcome predictors. The relationship of plasmalogen and chlorinated lipid levels may also allow distinction of changes in these lipids with greater specificity to infection compared to other disease states associated with only decreased plasma plasmalogen levels with the exception of lupus (Dragonas et al., 2009; Fabelo et al., 2011; Ifuku et al., 2012; Mahieu et al., 2014; Hu et al., 2016; Paul et al., 2019; Su et al., 2019).

The studies herein show plasmalogen loss during sepsis. However, there are several limitations to these studies. In the human studies we analyzed differences between septic humans and healthy control humans. Our healthy cohort average age was thirty-eight while the sepsis group was sixty. To overcome this limitation, we selected the oldest individuals ($n = 7$) in the healthy group and assessed differences in this control subset compared to the larger group of septic subjects (**Figures 1D–F**, **2**; **Table 1**). These additional analyses indicated plasma pLPC and pPE levels were reduced in the sepsis cohort when compared to this age-aligned control subgroup. Another limitation is that we have no data on the sex of individuals in our healthy cohort, while our sepsis cohort was comprised of 40% females. Our rat studies focused on changes occurring only in male rats and 20 h following cecal slurry injection. Thus, comparisons of rat specimens to human specimens were collected at different times and sex differences were not a parameter in the rat studies. It should also be appreciated that plasma levels of plasmalogens were considerably different in healthy controls due to the inherent differences in plasmalogen levels in man versus rat. Nevertheless, both human and rat sepsis led to decreases in plasma plasmalogen levels, and the rat studies afforded the opportunity to investigate changes in plasmalogen levels in the liver and kidney during sepsis. There were also limitations to the SARS-CoV-2 infection studies when comparisons are made to the rat and human sepsis studies. The SARS-CoV-2 infection studies were a viral infection elicited by airway inoculation to transgenic mice expressing the hACE2 receptor in all epithelial cells. Humans do not express ACE2 in all epithelial cells. Furthermore, these studies were performed only in female mice due to availability of genotyped mice for this study. Future studies are needed to consider sex as a parameter in both SARS-CoV-2 infected mice and rat cecal slurry sepsis. Compared to the unknown time for human sepsis beginning and the known time for CS injection, mouse infections with SARS-CoV-2 leading to pulmonary inflammation require time for viral replication to elicit injury which is typically 3–5 days. While our human and rat sepsis studies involved systemic infection, SARS-CoV-2 infection of K18 mice initially was primarily localized to infection of the respiratory tree. Infection led to robust increases in the expression of pro-inflammatory cytokines. The loss of plasmalogen in the lung during SARS-CoV-2 infection likely is the result of oxidative stress. We did not observe a loss in DPPC in the lung of infected mice. The chemical makeup of plasmalogens compared to DPPC provides a contrast in susceptibility to oxidative stress. The plasmalogen vinyl ether bond is a target for oxidation while the saturated fatty acids of DPPC are very stable under oxidative stress. Similar to findings with severe COVID-19 patients (Schwarz et al., 2021; Snider et al., 2021) we detected decreases in plasma plasmalogens in infected K18 mice.

This is the first demonstration of the loss of plasmalogens at a molecular species level in human sepsis. Furthermore, we show pLPC loss in both human and rodent sepsis. It is possible that plasma pLPC is a critical lipid to maintain endothelial plasmalogen levels under oxidative stress associated with sepsis. The demonstration of plasmalogen loss during SARS-CoV-2 further highlights the nature of plasmalogen loss during oxidative stress associated with infectious disease. The role of plasmalogens as biomarkers of outcomes in

sepsis and COVID-19 need to be explored as well as the potential protective role of plasmalogens during infectious disease.

DATA AVAILABILITY STATEMENT

The original contributions presented in the study are included in the article/**Supplementary Material**, further inquiries can be directed to the corresponding author.

ETHICS STATEMENT

The studies involving human participants were reviewed and approved by the University of Pennsylvania institutional review board and Saint Louis University institutional review board. The patients/participants provided their written informed consent to participate in this study. The animal study was reviewed and approved by the Institutional Animal Care and Use Committee at Saint Louis University.

AUTHOR CONTRIBUTIONS

DP performed experimental studies and data analysis and prepared the manuscript. RM performed experimental studies and data analysis and contributed to final manuscript preparation. EG performed experimental studies and data analysis and contributed to final manuscript preparation. CA performed experimental studies and data analysis and contributed to final manuscript preparation. DH contributed specimen collection and final manuscript preparation. MS contributed clinical study data collection, statistical analyses, and final manuscript preparation. NM contributed clinical study data collection, statistical analyses, and final manuscript preparation. AP performed data analysis and contributed to final manuscript preparation. DF was responsible for oversight of all aspects of studies, manuscript preparation, and final manuscript.

FUNDING

This study was supported (in part) by research funding from the National Institutes of Health R01 GM-115553 and S10OD025246 to DF. Clinical samples and patient phenotyping were funded by NIH HL137006 and HL137915 to NM.

SUPPLEMENTARY MATERIAL

The Supplementary Material for this article can be found online at: https://www.frontiersin.org/articles/10.3389/fcell.2022.912880/full#supplementary-material

REFERENCES

Aktepe, T. E., Pham, H., and Mackenzie, J. M. (2015). Differential Utilisation of Ceramide during Replication of the Flaviviruses West Nile and Dengue Virus. *Virology* 484, 241–250. doi:10.1016/j.virol.2015.06.015

Albert, C. J., Crowley, J. R., Hsu, F.-F., Thukkani, A. K., and Ford, D. A. (2001). Reactive Chlorinating Species Produced by Myeloperoxidase Target the Vinyl Ether Bond of Plasmalogens: Identification of 2-chlorohexadecanal. *J. Biol. Chem.* 276 (26), 23733–23741. doi:10.1074/jbc.m101447200

Amunugama, K., Jellinek, M. J., Kilroy, M. P., Albert, C. J., Rasi, V., Hoft, D. F., et al. (2021). Identification of Novel Neutrophil Very Long Chain Plasmalogen Molecular Species and Their Myeloperoxidase Mediated Oxidation Products in Human Sepsis. *Redox Biol.* 48, 102208. doi:10.1016/j.redox.2021.102208

Amunugama, K., Pike, D. P., and Ford, D. A. (2021). The Lipid Biology of Sepsis. *J. Lipid Res.* 62, 100090. doi:10.1016/j.jlr.2021.100090

Anbukumar, D. S., Shornick, L. P., Albert, C. J., Steward, M. M., Zoeller, R. A., Neumann, W. L., et al. (2010). Chlorinated Lipid Species in Activated Human Neutrophils: Lipid Metabolites of 2-chlorohexadecanal. *J. Lipid Res.* 51 (5), 1085–1092. doi:10.1194/jlr.m003673

Angus, D. C., and van der Poll, T. (2013). Severe Sepsis and Septic Shock. *N. Engl. J. Med.* 369 (9), 840–851. doi:10.1056/nejmra1208623

Bligh, E. G., and Dyer, W. J. (1959). A Rapid Method of Total Lipid Extraction and Purification. *Can. J. Biochem. Physiol.* 37, 911–917. doi:10.1139/o59-099

Bozelli, J. C., Jr., and Epand, R. M. (2021). Plasmalogen Replacement Therapy. *Membr. (Basel)* 11 (11), 838. doi:10.3390/membranes11110838

Bräutigam, C., Engelmann, B., Reiss, D., Reinhardt, U., Thiery, J., Richter, W. O., et al. (1996). Plasmalogen Phospholipids in Plasma Lipoproteins of Normolipidemic Donors and Patients with Hypercholesterolemia Treated by LDL Apheresis. *Atherosclerosis* 119 (1), 77–88. doi:10.1016/0021-9150(95)05632-7

Braverman, N. E., and Moser, A. B. (2012). Functions of Plasmalogen Lipids in Health and Disease. *Biochimica Biophysica Acta (BBA) - Mol. Basis Dis.* 1822 (9), 1442–1452. doi:10.1016/j.bbadis.2012.05.008

Brosche, T., Bertsch, T., Sieber, C. C., and Hoffmann, U. (2013). Reduced Plasmalogen Concentration as a Surrogate Marker of Oxidative Stress in Elderly Septic Patients. *Archives gerontology geriatrics* 57, 66–69. doi:10.1016/j.archger.2013.02.007

Casari, I., Manfredi, M., Metharom, P., and Falasca, M. (2021). Dissecting Lipid Metabolism Alterations in SARS-CoV-2. *Prog. Lipid Res.* 82, 101092. doi:10.1016/j.plipres.2021.101092

Chilton, F. H., and Connell, T. R. (1988). 1-ether-linked Phosphoglycerides. Major Endogenous Sources of Arachidonate in the Human Neutrophil. *J. Biol. Chem.* 263 (11), 5260–5265. doi:10.1016/s0021-9258(18)60709-4

Chilton, F. H., and Murphy, R. C. (1986). Remodeling of Arachidonate-Containing Phosphoglycerides within the Human Neutrophil. *J. Biol. Chem.* 261 (17), 7771–7777. doi:10.1016/s0021-9258(19)57467-1

Chuang, C.-C., Shiesh, S.-C., Chi, C.-H., Tu, Y.-F., Hor, L.-I., Shieh, C.-C., et al. (2006). Serum Total Antioxidant Capacity Reflects Severity of Illness in Patients with Severe Sepsis. *Crit. Care* 10 (1), R36. doi:10.1186/cc4826

Dean, J. M., and Lodhi, I. J. (2018). Structural and Functional Roles of Ether Lipids. *Protein Cell* 9 (2), 196–206. doi:10.1007/s13238-017-0423-5

Delano, M. J., and Ward, P. A. (2016). The Immune System's Role in Sepsis Progression, Resolution, and Long-Term Outcome. *Immunol. Rev.* 274 (1), 330–353. doi:10.1111/imr.12499

Dragonas, C., Bertsch, T., Sieber, C. C., and Brosche, T. (2009). Plasmalogens as a Marker of Elevated Systemic Oxidative Stress in Parkinson's Disease. *Clin. Chem. Lab. Med.* 47 (7), 894–897. doi:10.1515/CCLM.2009.205

Fabelo, N., Martín, V., Santpere, G., Marín, R., Torrent, L., Ferrer, I., et al. (2011). Severe Alterations in Lipid Composition of Frontal Cortex Lipid Rafts from Parkinson's Disease and Incidental Parkinson's Disease. *Mol. Med.* 17 (9-10), 1107–1118. doi:10.2119/molmed.2011.00119

Fernández-Oliva, A., Ortega-González, P., and Risco, C. (2019). Targeting Host Lipid Flows: Exploring New Antiviral and Antibiotic Strategies. *Cell. Microbiol.* 21 (3), e12996. doi:10.1111/cmi.12996

Ford, D. A., and Gross, R. W. (1989). Plasmenylethanolamine Is the Major Storage Depot for Arachidonic Acid in Rabbit Vascular Smooth Muscle and Is Rapidly

Hydrolyzed after Angiotensin II Stimulation. *Proc. Natl. Acad. Sci. U.S.A.* 86 (10), 3479–3483. doi:10.1073/pnas.86.10.3479

Ford, D. A., and Hale, C. C. (1996). Plasmalogen and Anionic Phospholipid Dependence of the Cardiac Sarcolemmal Sodium-Calcium Exchanger. *FEBS Lett.* 394 (1), 99–102. doi:10.1016/0014-5793(96)00930-1

Galley, H. F. (2011). Oxidative Stress and Mitochondrial Dysfunction in Sepsis. *Br. J. Anaesth.* 107 (1), 57–64. doi:10.1093/bja/aer093

Geerling, E., Pinski, A. N., Stone, T. E., DiPaolo, R. J., Zulu, M. Z., Maroney, K. J., et al. (2022). Roles of Antiviral Sensing and Type I Interferon Signaling in the Restriction of SARS-CoV-2 Replication. *iScience* 25 (1), 103553. doi:10.1016/j.isci.2021.103553

Geerling, E., Stone, E. T., Steffen, T. L., Hassert, M., Brien, J. D., and Pinto, A. K. (2021). Obesity Enhances Disease Severity in Female Mice Following West Nile Virus Infection. *Front. Immunol.* 12, 739025. doi:10.3389/fimmu.2021.739025

Glaser, P. E., and Gross, R. W. (1994). Plasmenylethanolamine Facilitates Rapid Membrane Fusion: a Stopped-Flow Kinetic Investigation Correlating the Propensity of a Major Plasma Membrane Constituent to Adopt an HII Phase with its Ability to Promote Membrane Fusion. *Biochemistry* 33 (19), 5805–5812. doi:10.1021/bi00185a019

Han, X., and Gross, R. W. (1990). Plasmenylcholine and Phosphatidylcholine Membrane Bilayers Possess Distinct Conformational Motifs. *Biochemistry* 29 (20), 4992–4996. doi:10.1021/bi00472a032

Han, X., and Gross, R. W. (1991). Proton Nuclear Magnetic Resonance Studies on the Molecular Dynamics of Plasmenylcholine/cholesterol and Phosphatidylcholine/cholesterol Bilayers. *Biochimica Biophysica Acta (BBA) - Biomembr.* 1063 (1), 129–136. doi:10.1016/0005-2736(91)90362-c

Hu, C., Zhou, J., Yang, S., Li, H., Wang, C., Fang, X., et al. (2016). Oxidative Stress Leads to Reduction of Plasmalogen Serving as a Novel Biomarker for Systemic Lupus Erythematosus. *Free Radic. Biol. Med.* 101, 475–481. doi:10.1016/j.freeradbiomed.2016.11.006

Ifuku, M., Katafuchi, T., Mawatari, S., Noda, M., Miake, K., Sugiyama, M., et al. (2012). Anti-inflammatory/anti-amyloidogenic Effects of Plasmalogens in Lipopolysaccharide-Induced Neuroinflammation in Adult Mice. *J. Neuroinflammation* 9, 197. doi:10.1186/1742-2094-9-197

Jean Beltran, P. M., Cook, K. C., Hashimoto, Y., Galitzine, C., Murray, L. A., Vitek, O., et al. (2018). Infection-Induced Peroxisome Biogenesis Is a Metabolic Strategy for Herpesvirus Replication. *Cell Host Microbe* 24 (4), 526–541. doi:10.1016/j.chom.2018.09.002

Kayganich, K. A., and Murphy, R. C. (1992). Fast Atom Bombardment Tandem Mass Spectrometric Identification of Diacyl, Alkylacyl, and Alk-1-Enylacyl Molecular Species of Glycerophosphoethanolamine in Human Polymorphonuclear Leukocytes. *Anal. Chem.* 64 (23), 2965–2971. doi:10.1021/ac00047a015

Khaselev, N., and Murphy, R. C. (1999). Susceptibility of Plasmenyl Glycerophosphoethanolamine Lipids Containing Arachidonate to Oxidative Degradation. *Free Radic. Biol. Med.* 26 (3-4), 275–284. doi:10.1016/s0891-5849(98)00211-1

Liu, V., Escobar, G. J., Greene, J. D., Soule, J., Whippy, A., Angus, D. C., et al. (2014). Hospital Deaths in Patients with Sepsis from 2 Independent Cohorts. *Jama* 312 (1), 90–92. doi:10.1001/jama.2014.5804

Mahieu, M. A., Guild, C. P., Albert, C. J., Kondos, G. T., Carr, J. J., Edmundowicz, D., et al. (2014). Alpha-chlorofatty Acid and Coronary Artery or Aorta Calcium Scores in Women with Systemic Lupus Erythematosus. A Pilot Study. *J. Rheumatol.* 41 (9), 1834–1842. doi:10.3899/jrheum.131361

Mandel, H., Sharf, R., Berant, M., Wanders, R. J. A., Vreken, P., and Aviram, M. (1998). Plasmalogen Phospholipids Are Involved in HDL-Mediated Cholesterol Efflux: Insights from Investigations with Plasmalogen-Deficient Cells. *Biochem. Biophysical Res. Commun.* 250 (2), 369–373. doi:10.1006/bbrc.1998.9321

Maner-Smith, K. M., Goll, J. B., Khadka, M., Jensen, T. L., Colucci, J. K., Gelber, C. E., et al. (2020). Alterations in the Human Plasma Lipidome in Response to Tularemia Vaccination. *Vaccines* 8 (3), 414. doi:10.3390/vaccines8030414

Mayr, F. B., Yende, S., and Angus, D. C. (2014). Epidemiology of Severe Sepsis. *Virulence* 5 (1), 4–11. doi:10.4161/viru.27372

Mecatti, G. C., Fernandes Messias, M. C., Sant'Anna Paiola, R. M., Figueiredo Angolini, C. F., da Silva Cunha, I. B., Eberlin, M. N., et al. (2018). Lipidomic Profiling of Plasma and Erythrocytes from Septic Patients Reveals Potential Biomarker Candidates. *Biomark. Insights* 13, 1177271918765137. doi:10.1177/1177271918765137

Mecatti, G. C., Messias, M. C. F., and de Oliveira Carvalho, P. (2020). Lipidomic Profile and Candidate Biomarkers in Septic Patients. *Lipids Health Dis.* 19 (1), 68. doi:10.1186/s12944-020-01246-2

Mesquita, F. S., Abrami, L., Sergeeva, O., Turelli, P., Kunz, B., Raclot, C., et al. (2021). S-acylation Controls ARS-Cov-2 Membrane Lipid Organization and Enhances Infectivity. *Dev Cell* 56, 2790. doi:10.1016/j.devcel.2021.09.016

Meyer, N. J., Reilly, J. P., Feng, R., Christie, J. D., Hazen, S. L., Albert, C. J., et al. (2017). Myeloperoxidase-derived 2-chlorofatty Acids Contribute to Human Sepsis Mortality via Acute Respiratory Distress Syndrome. *JCI Insight* 2. e96432. doi:10.1172/jci.insight.96432

Morand, O. H., Zoeller, R. A., and Raetz, C. R. (1988). Disappearance of Plasmalogens from Membranes of Animal Cells Subjected to Photosensitized Oxidation. *J. Biol. Chem.* 263 (23), 11597–11606. doi:10.1016/s0021-9258(18)38001-3

Murphy, E. J., Joseph, L., Stephens, R., and Horrocks, L. A. (1992). Phospholipid Composition of Cultured Human Endothelial Cells. *Lipids* 27 (2), 150–153. doi:10.1007/bf02535816

Paoli, C. J., Reynolds, M. A., Sinha, M., Gitlin, M., and Crouser, E. (2018). Epidemiology and Costs of Sepsis in the United States-An Analysis Based on Timing of Diagnosis and Severity Level*. *Crit. care Med.* 46 (12), 1889–1897. doi:10.1097/ccm.0000000000003342

Paul, S., Lancaster, G. I., and Meikle, P. J. (2019). Plasmalogens: A Potential Therapeutic Target for Neurodegenerative and Cardiometabolic Disease. *Prog. Lipid Res.* 74, 186–195. doi:10.1016/j.plipres.2019.04.003

Paul, S., Smith, A. A. T., Culham, K., Gunawan, K. A., Weir, J. M., Cinel, M. A., et al. (2021). Shark Liver Oil Supplementation Enriches Endogenous Plasmalogens and Reduces Markers of Dyslipidemia and Inflammation. *J. Lipid Res.* 62, 100092. doi:10.1016/j.jlr.2021.100092

Pike, D. P., Vogel, M. J., McHowat, J., Mikuzis, P. A., Schulte, K. A., and Ford, D. A. (2020). 2-Chlorofatty Acids Are Biomarkers of Sepsis Mortality and Mediators of Barrier Dysfunction in Rats. *J. Lipid Res.* 61 (7), 1115–1127. doi:10.1194/jlr.ra120000829

Pike, L. J., Han, X., Chung, K.-N., and Gross, R. W. (2002). Lipid Rafts Are Enriched in Arachidonic Acid and Plasmenylethanolamine and Their Composition Is Independent of Caveolin-1 Expression: a Quantitative Electrospray Ionization/mass Spectrometric Analysis. *Biochemistry* 41, 2075–2088. doi:10.1021/bi0156557

Prauchner, C. A. (2017). Oxidative Stress in Sepsis: Pathophysiological Implications Justifying Antioxidant Co-therapy. *Burns* 43 (3), 471–485. doi:10.1016/j.burns.2016.09.023

Reilly, J. P., Wang, F., Jones, T. K., Palakshappa, J. A., Anderson, B. J., Shashaty, M. G. S., et al. (2018). Plasma Angiopoietin-2 as a Potential Causal Marker in Sepsis-Associated ARDS Development: Evidence from Mendelian Randomization and Mediation Analysis. *Intensive Care Med.* 44 (11), 1849–1858. doi:10.1007/s00134-018-5328-0

Reiss, D., Beyer, K., and Engelmann, B. (1997). Delayed Oxidative Degradation of Polyunsaturated Diacyl Phospholipids in the Presence of Plasmalogen Phospholipids *In Vitro*. *Biochem. J.* 323 (Pt 3Pt 3), 807–14. doi:10.1042/bj3230807

Robertson, C. M., and Coopersmith, C. M. (2006). The Systemic Inflammatory Response Syndrome. *Microbes Infect.* 8 (5), 1382–1389. doi:10.1016/j.micinf.2005.12.016

Rubio, J. M., Astudillo, A. M., Casas, J., Balboa, M. A., and Balsinde, J. (2018). Regulation of Phagocytosis in Macrophages by Membrane Ethanolamine Plasmalogens. *Front. Immunol.* 9, 1723. doi:10.3389/fimmu.2018.01723

Rudd, K. E., Johnson, S. C., Agesa, K. M., Shackelford, K. A., Tsoi, D., Kievlan, D. R., et al. (2020). Global, Regional, and National Sepsis Incidence and Mortality, 1990-2017: Analysis for the Global Burden of Disease Study. *Lancet* 395 (10219), 200–211. doi:10.1016/s0140-6736(19)32989-7

Ruiz, M., Cuillerier, A., Daneault, C., Deschênes, S., Frayne, I. R., Bouchard, B., et al. (2019). Lipidomics Unveils Lipid Dyshomeostasis and Low Circulating Plasmalogens as Biomarkers in a Monogenic Mitochondrial Disorder. *JCI Insight* 4 (14), e123231. doi:10.1172/jci.insight.123231

Schwarz, B., Sharma, L., Roberts, L., Peng, X., Bermejo, S., Leighton, I., et al. (2021). Cutting Edge: Severe SARS-CoV-2 Infection in Humans Is Defined by a Shift in the Serum Lipidome, Resulting in Dysregulation of Eicosanoid Immune Mediators. *J. Immunol.* 206 (2), 329–334. doi:10.4049/jimmunol.2001025

Singer, M., Deutschman, C. S., Seymour, C. W., Shankar-Hari, M., Annane, D., Bauer, M., et al. (2016). The Third International Consensus Definitions for Sepsis and Septic Shock (Sepsis-3). *JAMA* 315 (8), 801–10. doi:10.1001/jama.2016.0287

Snider, J. M., You, J. K., Wang, X., Snider, A. J., Hallmark, B., Zec, M. M., et al. (2021). Group IIA Secreted Phospholipase A2 Is Associated with the Pathobiology Leading to COVID-19 Mortality. *J. Clin. Invest.* 131 (19), e149236. doi:10.1172/JCI149236

Stadelmann-Ingrand, S., Favreliere, S., Fauconneau, B., Mauco, G., and Tallineau, C. (2001). Plasmalogen Degradation by Oxidative Stress: Production and Disappearance of Specific Fatty Aldehydes and Fatty α-hydroxyaldehydes. *Free Radic. Biol. Med.* 31, 1263–1271. doi:10.1016/s0891-5849(01)00720-1

Su, X. Q., Wang, J., and Sinclair, A. J. (2019). Plasmalogens and Alzheimer's Disease: a Review. *Lipids Health Dis.* 18 (1), 100. doi:10.1186/s12944-019-1044-1

Sviridov, D., Miller, Y. I., Ballout, R. A., Remaley, A. T., and Bukrinsky, M. (2020). Targeting Lipid Rafts-A Potential Therapy for COVID-19. *Front. Immunol.* 11, 574508. doi:10.3389/fimmu.2020.574508

Tanaka, S., Diallo, D., Delbosc, S., Genève, C., Zappella, N., Yong-Sang, J., et al. (2019). High-density Lipoprotein (HDL) Particle Size and Concentration Changes in Septic Shock Patients. *Ann. Intensive Care* 9 (1), 68. doi:10.1186/s13613-019-0541-8

Tanner, L. B., Chng, C., Guan, X. L., Lei, Z., Rozen, S. G., and Wenk, M. R. (2014). Lipidomics Identifies a Requirement for Peroxisomal Function during Influenza Virus Replication. *J. Lipid Res.* 55 (7), 1357–1365. doi:10.1194/jlr.m049148

Theken, K. N., Tang, S. Y., Sengupta, S., and FitzGerald, G. A. (2021). The Roles of Lipids in SARS-CoV-2 Viral Replication and the Host Immune Response. *J. Lipid Res.* 62, 100129. doi:10.1016/j.jlr.2021.100129

Thukkani, A. K., Hsu, F.-F., Crowley, J. R., Wysolmerski, R. B., Albert, C. J., and Ford, D. A. (2002). Reactive Chlorinating Species Produced during Neutrophil Activation Target Tissue Plasmalogens: Production of the Chemoattractant, 2-chlorohexadecanal. *J. Biol. Chem.* 277 (6), 3842–3849. doi:10.1074/jbc.m109489200

Vance, J. E. (1990). Lipoproteins Secreted by Cultured Rat Hepatocytes Contain the Antioxidant 1-Alk-1-Enyl-2-Acylglycerophosphoethanolamine. *Biochimica Biophysica Acta (BBA) - Lipids Lipid Metabolism* 1045 (2), 128–134. doi:10.1016/0005-2760(90)90141-j

Vavrova, L., Rychlikova, J., Mrackova, M., Novakova, O., Zak, A., and Novak, F. (2016). Increased Inflammatory Markers with Altered Antioxidant Status Persist after Clinical Recovery from Severe Sepsis: a Correlation with Low HDL Cholesterol and Albumin. *Clin. Exp. Med.* 16 (4), 557–569. doi:10.1007/s10238-015-0390-1

Villareal, V. A., Rodgers, M. A., Costello, D. A., and Yang, P. L. (2015). Targeting Host Lipid Synthesis and Metabolism to Inhibit Dengue and Hepatitis C Viruses. *Antivir. Res.* 124, 110–121. doi:10.1016/j.antiviral.2015.10.013

Vincent, J.-L., Jones, G., David, S., Olariu, E., and Cadwell, K. K. (2019). Frequency and Mortality of Septic Shock in Europe and North America: a Systematic Review and Meta-Analysis. *Crit. Care* 23 (1), 196. doi:10.1186/s13054-019-2478-6

Wang, J., Sun, Y., Teng, S., and Li, K. (2020). Prediction of Sepsis Mortality Using Metabolite Biomarkers in the Blood: a Meta-Analysis of Death-Related Pathways and Prospective Validation. *BMC Med.* 18 (1), 83. doi:10.1186/s12916-020-01546-5

Zheng, J., Wong, L.-Y. R., Li, K., Verma, A. K., Ortiz, M. E., Wohlford-Lenane, C., et al. (2021). COVID-19 Treatments and Pathogenesis Including Anosmia in K18-hACE2 Mice. *Nature* 589 (7843), 603–607. doi:10.1038/s41586-020-2943-z

Zoeller, R. A., Lake, A. C., Nagan, N., Gaposchkin, D. P., Legner, M. A., and Lieberthal, W. (1999). Plasmalogens as Endogenous Antioxidants: Somatic Cell Mutants Reveal the Importance of the Vinyl Ether. *Biochem. J.* 338 (Pt 3), 769–76. doi:10.1042/bj3380769

Zoeller, R. A., Grazia, T. J., LaCamera, P., Park, J., Gaposchkin, D. P., and Farber, H. W. (2002). Increasing Plasmalogen Levels Protects Human Endothelial Cells during Hypoxia. *Am. J. Physiology-Heart Circulatory Physiology* 283 (2), H671–H679. doi:10.1152/ajpheart.00524.2001

Zoeller, R. A., Morand, O. H., and Raetz, C. R. (1988). A Possible Role for Plasmalogens in Protecting Animal Cells against Photosensitized Killing. *J. Biol. Chem.* 263 (23), 11590–11596. doi:10.1016/s0021-9258(18)38000-1

Author's Disclaimer: The content is solely the responsibility of the authors and does not necessarily represent the official views of the National Institutes of Health.

Conflict of Interest: The authors declare that the research was conducted in the absence of any commercial or financial relationships that could be construed as a potential conflict of interest.

Publisher's Note: All claims expressed in this article are solely those of the authors and do not necessarily represent those of their affiliated organizations, or those of the publisher, the editors and the reviewers. Any product that may be evaluated in this article, or claim that may be made by its manufacturer, is not guaranteed or endorsed by the publisher.